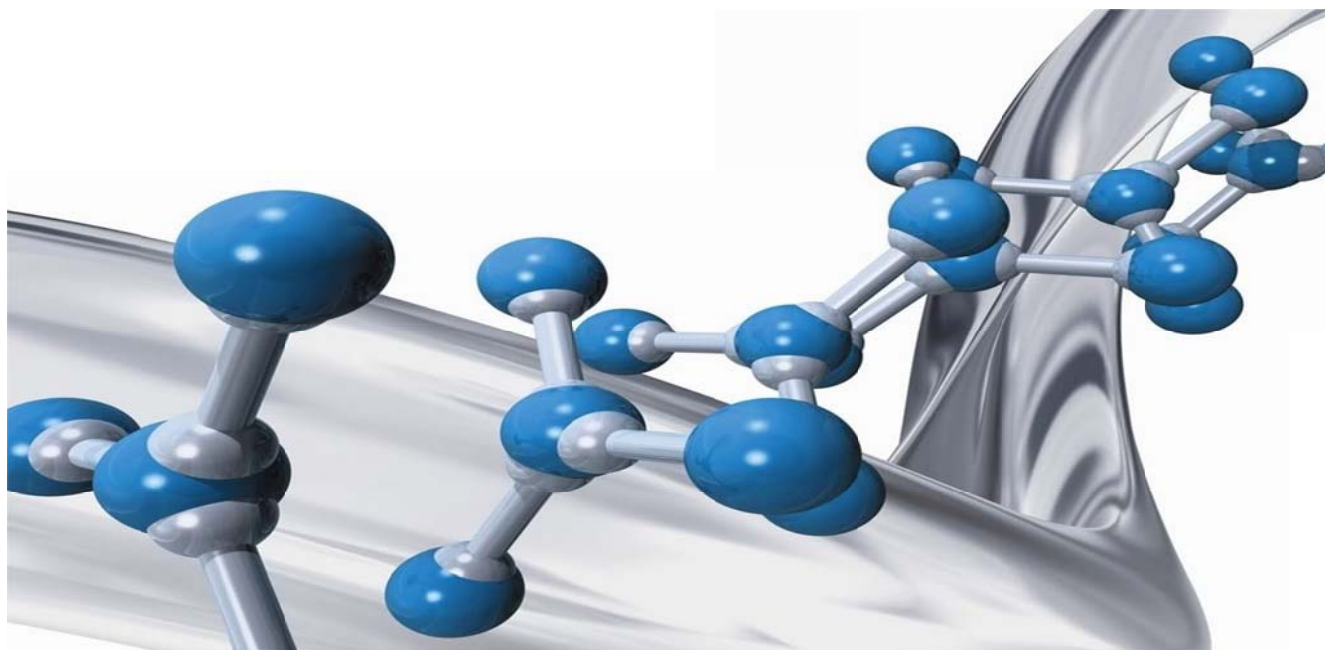


Structural and Magnetic Investigation of hybrid compounds of saturated primary, secondary and tertiary organic amines and metal halides

by
Shalene Natalia Bothma



This dissertation is presented in partial fulfilment of the requirements for the degree of Masters of Science
at
The University of Pretoria

Department of Chemistry
Faculty of Natural and Agricultural Sciences
Supervisor: Dr Melanie Rademeyer

May 2014

Declaration

Declaration of Originality University of Pretoria

The Department of Chemistry places great emphasis upon integrity and ethical conduct in the preparation of all written work submitted for academic evaluation.

While academic staff teaches you about referencing techniques and how to avoid plagiarism, you too have a responsibility in this regard. If you are at any stage uncertain as to what is required, you should speak to your lecturer before any work is submitted.

You are guilty of plagiarism if you copy something from another author's work (e.g. A book, an article, or a website) without acknowledging the source and pass it off as your own. In effect you are stealing something that belongs to somebody else. This is not only the case when you copy work word-for-word (verbatim), but also when you submit someone else's work in a slightly altered form (paraphrase) or use a line of argument without acknowledging it. You are not allowed to use work previously produced by another student. You are also not allowed to let anybody copy your work with the intention of passing it off as his/her work.

Students who commit plagiarism will not be given any credit for plagiarised work. The matter may also be referred to the Student Disciplinary Committee for ruling. Plagiarism is regarded as a serious contravention of the University's rules and can lead to expulsion from the University.

The declaration which follows must accompany all written work submitted while you are a student of the Department of Chemistry. No written work will be accepted unless the declaration has been completed and attached.

I declare that this dissertation, which I hereby submit for the degree of Masters of Science at The University of Pretoria, is my own work and has not previously been submitted by me for a degree at another university. Where secondary material is used, this has been carefully acknowledged and referenced in accordance with university requirements. I am aware of university policy and implications regarding plagiarism.

Full names of student: **Shalene Natalia Bothma**

Student number: **26239222**

Topic of work: **Structural and Magnetic Investigation of hybrid compounds of saturated primary, secondary and tertiary organic amines and metal halides.**

Signature:

.....

Date: 23 May 2014

Acknowledgements

“I was captured for life by chemistry and by crystals”

— Dorothy Crowfoot Hodgkin

Oxford Dictionary of Quotations, 6th ed.

To my dad, Victor and my mom, Beryl, you steered me in the right direction and knew what was best for me, with your on-going love and support you helped me to achieve my goals. To my sister, Renee and brother, Charl, thank you for your continuous support during tough times and to my nephews Connor and Trent, for being the sunshine in my life. I hope this dissertation makes all of you proud.

I would also like to thank the following people for the valuable support and assistance during the completion of this my MSc degree.

- I would like to extend my gratitude to my supervisor, Dr Melanie Rademeyer for all her guidance and support during the course of my work, and for giving me the opportunity to conduct research visits and exposing me to new theory and techniques.
- To Dave Liles for the single crystal data collection on the materials discussed in this dissertation.
- To Prof Mark Turnbull and Prof Christopher Landee from Clark University, Massachusetts, USA, for specialised training on the SQUID instrument, as well as for their insightful advice on magnetic data collection and interpretation.
- To Sasol for their generous funding and specifically to Dr Lodya, Dr Anderson and Dr van Helden for useful discussions and assistance in magnetic theory and magnetic data interpretation.
- To the faculty of the department of chemistry for their continuous support and encouragement.
- I would like to extend my gratitude, those who form part of my chemistry family, to Cara Slabbert, Parveen Beebeejaun and Stefan Coetzee for all the great chats and fun times.
- And lastly, to my cousin, Ray, you will live on forever in our hearts and I will always miss you, our pilot boy, rest in peace, till we meet again.

Conferences

- Indaba 7 Conference, Skukuza, Kruger National Park, South Africa (2nd - 7th September 2013), Poster Presentation: The structural study of organic-inorganic hybrid materials.
- Introductory Chemical Crystallography School, University of the Witwatersrand, South Africa (8th - 9th September 2013).
- Southern African Powder Diffraction Conference and Workshop, University of the Witwatersrand, South Africa (27rd - 31st January 2014), Poster presentation: The structural study of organic-inorganic hybrid materials.

Research Visit

- Clark University, Worcester, MA, USA for training on the SQUID instrument, to collect magnetic data and to receive help with data interpretation. (8th May - 9th June 2013).

Abstract

Organic-inorganic hybrid materials combine an inorganic component with an organic component at the nano-scale, while potentially retaining the properties of both components. In the current study the structural characteristics and magnetic properties of hybrid materials combining cations of saturated primary, secondary and tertiary amines with perchloridocuprate(II) and perbromidocuprate(II) anions, were studied.

The saturated cations of cyclopentylamine, cyclohexylamine, cycloheptylamine, piperazine and 1,4-diazoniabicyclo[2.2.2]octane were chosen since the series allows for the study of the effect of the cation size, charge and saturation on the hybrid structure and also due to the scarcity of hybrid structures containing these types of saturated cations in the literature.

Perhalocuprate(II) containing hybrid materials exhibit magnetic properties due to the presence of an unpaired electron on the Cu^{2+} ion. At low temperatures magnetic ordering may occur *via* magnetic exchange pathways involving the halogeno ligands, forming ferromagnetic or antiferromagnetic materials. Identification of the magnetic exchange pathways by consideration of the crystal structure allows for the selection of a suitable theoretical quantum mechanical model to which the experimental magnetic data can be modelled, to obtain parameters like the exchange constant.

A part of the work describes the preparation of crystals of the family of hybrid materials under investigation, and the experimental techniques employed to study the structural and magnetic characteristics of the materials. The crystal structures of six novel materials are discussed in detail and compared to related structures characterised in this study, or to structures previously reported in the literature, where possible. Magnetic susceptibility data is analysed for four compounds, two of which are novel and two for structures reported previously in the literature.

By considering the novel structures characterised in this study, as well as structures previously reported in the literature, structural trends are identified. The role of saturation of the cation on the structure, as well as the effect of cation charge, is highlighted for related compounds. Robust hydrogen bonding motifs are identified for two sub-families of structures, namely those containing isolated tetrahalocuprate(II) anions and those containing related polymeric perhalocuprate(II) anions. In addition, the magnetic properties of the family containing polymeric anions are compared.

List of Schematics

Chapter One: Introduction

- Scheme 1.2.1.** The various forms of hydrogen bonding that may exist in materials. (a) Classic, charge assisted, (b) bifurcated charge assisted, and (c) trifurcated hydrogen bonding
- Scheme 1.4.1.** The organic components used in this study
- Scheme 1.6.1.** Orbital energy level diagrams for Cu^{2+} ions in (a) square pyramidal, (b) trigonal bipyramidal and (c) octahedral geometries
- Scheme 1.6.2.** The schematic representation of the possible spin interactions
- Scheme 1.6.3.** The various types of magnetic exchange pathways relevant to the current study
- Scheme 1.6.4.** The schematic representation of linear exchange between magnetic metal ion orbitals and a ligand orbital
- Scheme 1.6.5.** The schematic representation of the exchange process for orthogonal M-L-M overlap of magnetic ion orbitals and ligand orbitals

Chapter Four: Discussion

- Scheme 4.7.1.** The schematic representation of the hydrogen bonding motif found in compounds containing secondary cations and (a) square pyramidal anions or (b) tetrahedral anionic units.
- Scheme 4.7.2.** The schematic representation of the two types of hydrogen bonding motifs present in primary cation containing compounds. (a) Type one and (b) type two
- Scheme 4.7.3.** The schematic representation of the hydrogen bonded motif that forms between cations and polymeric anions

List of Figures

Chapter One: Introduction

- Figure 1.3.1.** The operational OLED device (Mitzi *et al.* 2001)
- Figure 1.3.2.** Zero-dimensional anionic units
- Figure 1.3.3.** One- and two-dimensional anionic units
- Figure 1.4.1.** Selected geometries of perhalocuprate anions (Smith. 1976)
- Figure 1.5.1.** The asymmetric unit of (a) NABNEK01 and (b) NABNEK
- Figure 1.5.2.** The hydrogen-bonded unit of (a) NABNEK01 and (b) NABNEK respectively. The hydrogen bonding network of (c) NABNEK01 and (d) NABNEK as viewed down the b-axis.
- Figure 1.5.3.** The arrangement of the CuBr_4^{2-} anions in NABNEK
- Figure 1.5.4.** The asymmetric unit of NUTDUB
- Figure 1.5.5.** (a) The hydrogen-bonded unit of NUTDUB. (b) The hydrogen bonding network of NUTDUB as viewed down the b-axis.
- Figure 1.5.6.** The asymmetric unit of NUTDOV
- Figure 1.5.7.** (a) The hydrogen-bonded unit of NUTDOV. (b) The three-dimensional hydrogen-bonded network of NUTDOV.
- Figure 1.5.8.** The asymmetric unit of (a) AGAWIO and (b) LURTAT
- Figure 1.5.9.** The hydrogen-bonded units of (a) AGAWIO and (b) LURTAT, respectively. The hydrogen bonding network in (c) AGAWIO and (d) LURTAT, respectively
- Figure 1.5.10.** The asymmetric unit of ULAVAF
- Figure 1.5.11.** (a) The hydrogen-bonded unit of ULAVAF. (b) The three-dimensional hydrogen bonding network in ULAVAF
- Figure 1.5.12.** The asymmetric unit of the (a) room temperature, TOAFAP03, and (b) the low temperature, TOZFAP02 structures
- Figure 1.5.13.** (a) The hydrogen-bonded unit of TOZFAP02. (b). The three-dimensional hydrogen bonding

network that is present in both the room and low temperature structures as viewed down the *a*-axis.

- Figure 1.5.14.** The asymmetric unit of FAWDAI
Figure 1.5.15. (a) The hydrogen-bonded unit of FAWDAI
Figure 1.5.15. (b) The polymer chain of FAWDAI
Figure 1.5.15. (c) The hydrogen bonding network of FAWDAI as viewed down the *a*-axis
Figure 1.5.16. The asymmetric unit of FUTBUR
Figure 1.5.17. (a) The hydrogen-bonded unit of FUTBUR
Figure 1.5.17. (b) The polymer component of FUTBUR
Figure 1.5.17. (c) The one-dimensional hydrogen bonded network present in the FUTBUR structure as viewed down the *b*-axis
Figure 1.5.18. The asymmetric unit of the BAPYUM structure
Figure 1.5.19. (a) The hydrogen bonded unit of BAPYUM.
Figure 1.5.19. (b) The polymer chain of BAPYUM
Figure 1.5.19. (c) The one-dimensional hydrogen bonded network of the BAPYUM structure as viewed down the *b*-axis
Figure 1.5.20. The asymmetric unit of COPDOA01
Figure 1.5.21. The hydrogen-bonded unit of COPDOA01
Figure 1.5.22. The hydrogen bonding network of COPDOA01 as viewed down the *b*-axis
Figure 1.5.23. The asymmetric unit of YATYUP
Figure 1.5.24. (a) The hydrogen-bonded unit of YATYUP. (b) The one-dimensional hydrogen bonding network of YATYUP as viewed down the *b*-axis.
Figure 1.6.1. The graphical representation of the Curie Law for paramagnetic interactions
Figure 1.6.2. The plots of (a) χ , (b) χT and (c) χ^{-1} vs T that are governed by the Curie-Weiss Law for paramagnetic (black), ferromagnetic (red) and antiferromagnetic (blue)

Chapter Two: Experimental Techniques

- Figure 2.2.1.** The conditions required by the Bragg's equation for diffraction to occur
Figure 2.2.2. (a) The components comprising a SXR
Figure 2.2.2. (b) An example of a diffraction pattern
Figure 2.2.3. The Bruker D2 Phaser instrument used in PXRD analysis of the compounds

Chapter Three: Experimental Results

- Figure 3.1.1.** The asymmetric unit of PENCuCl
Figure 3.1.2. (a) The anionic moiety of PENCuCl
Figure 3.1.2. (b) The positions of the Cu²⁺ ion centers within the unit cell
Figure 3.1.3. (a) The packing diagram of PENCuCl as viewed down the *c*-axis
Figure 3.1.3. (b) The two-dimensional perovskite sheet showing long semi-coordinate bonds between Cu1...Cl1
Figure 3.1.4. (a) Classic, charge assisted hydrogen bonding interactions that exist between the anionic and cationic moieties
Figure 3.1.4. (b) The hydrogen bonding network of PENCuCl
Figure 3.2.1. The asymmetric unit of PENCuBr
Figure 3.2.2. The polymeric perbromidocuprate (II) anionic chain formed in PENCuBr
Figure 3.2.3. (a) The packing diagram of PENCuBr as viewed down the *b*-axis
Figure 3.2.3. (b) The packing diagram of PENCuBr as viewed down the *c*-axis
Figure 3.2.4. (a) The hydrogen bonding between the anionic and cationic units
Figure 3.2.4. (b) Hydrogen bonding network of PENCuBr
Figure 3.2.5. The M (emu/mol) vs H (Oe) plot of PENCuBr
Figure 3.2.6. The graph of χT (emu.K/Oe.mol) vs T (K) for PENCuBr
Figure 3.2.7. The magnetic exchange pathway that exist *via* $d_{x^2-y^2}$ orbitals of Cu²⁺ ions and the *s* orbitals of the halogeno ligands
Figure 3.2.8. The distance between neighbouring polymers
Figure 3.2.9. The fit of experimental magnetic susceptibility data (χ) to a one dimensional FM model with CW correction

- Figure 3.3.1.** The asymmetric unit of HEPCuCl
- Figure 3.3.2. (a)** The complete copper (II) chlorido trimeric unit
- Figure 3.3.2. (b)** The positions of the copper (II) chlorido trimers in the unit cell
- Figure 3.3.3. (a)** The packing diagram of cationic and anionic units as viewed down the *b*-axis
- Figure 3.3.3. (b)** The packing diagram of cationic and anionic units as viewed down the *c*-axis
- Figure 3.3.4.** The hydrogen bonded unit
- Figure 3.3.5.** The one-dimensional hydrogen bonding network between neighbouring cationic and anionic species
- Figure 3.4.1.** The asymmetric unit of HEPCuBr
- Figure 3.4.2. (a)** The copper (II) bromido trimer
- Figure 3.4.2. (b)** The unit cell showing only the trimer anions as viewed down the *c*-axis
- Figure 3.4.3.** The packing diagram of cationic and anionic species as viewed down the *b*-axis
- Figure 3.4.4.** The hydrogen bonded motif
- Figure 3.4.5.** The one-dimensional hydrogen bonded ribbon
- Figure 3.5.1.** The asymmetric unit of HEPBr
- Figure 3.5.2.** The packing diagram of HEPBr as viewed down the *a*-axis
- Figure 3.5.3. (a)** The hydrogen bonded unit
- Figure 3.5.3. (b)** The two-dimensional hydrogen bonded sheet
- Figure 3.6.1.** The asymmetric unit of PIPCuCl
- Figure 3.6.2.** The cationic and anionic units comprising the PIPCuCl structure
- Figure 3.6.3.** The packing diagram of PIPCuCl as viewed down the *b*-axis
- Figure 3.6.4. (a)** The hydrogen bonding interactions between a dication and four different anions
- Figure 3.6.4. (b)** The hydrogen bonding network formed between anions and dications
- Figure 3.6.5.** The plot of χ (emu/Oe.mol) vs T (K)
- Figure 3.6.6.** The plot of χT (emu.K/Oe.mol) vs T (K)
- Figure 3.6.7.** The double-halide exchange pathway that links anions to form a three-dimensional network
- Figure 3.7.1.** The χT (emu.K/Oe.mol) vs T (K) plot of TOZFAP02 in a 1 kOe field
- Figure 3.7.2.** The χ (emu/Oe.mol) vs T (K) plot of TOZFAP02 in a 1 kOe field
- Figure 3.7.3. (a)** The double-halide exchange pathway that links anions to form a one-dimensional chain
- Figure 3.7.3. (b)** The distance between magnetic atoms in the one-dimensional chain
- Figure 3.7.4. (a)** The χT (emu.K/Oe.mol) vs T (K) data fit to the one-dimensional AFM chain model
- Figure 3.7.4. (b)** The χ (emu/Oe.mol) vs T (K) data fit to the one-dimensional AFM chain model with CW correction
- Figure 3.8.1.** The plot of χT (emu.K/Oe.mol) vs T (K) for the ULAVAF structure
- Figure 3.8.2.** The double-halide exchange pathway that links anions to form a three-dimensional network

Chapter Four: Discussion

- Figure 4.2.1.** The packing diagrams of (a) NABNEK01 and (b) HEPCuCl
- Figure 4.2.2.** The packing diagrams of (a) AGAWIO and (b) YATYUP
- Figure 4.3.1.** The packing diagrams of aromatic systems such as (a) HUPVIX, (b) BACHIX, and saturated systems (c) PNCLCU01 and (d) PAFYUR
- Figure 4.3.2.** Monolayer type packing of secondary/tertiary cations observed in (a) AGAWIO, (b) LURTAT, (c) ULAVAF, (d) PIPCuCl/BICPEK
- Figure 4.3.3.** Layered packing of cations and anions in (a) NABNEK01, (b) PAFYUR, (c) PNCLCU01, (d) FAWDAI, (e) YATYUP and (f) PENCuCl
- Figure 4.4.1.** The hydrogen bonded tube in (a) HEPCuCl and (b) HEPCuBr
- Figure 4.4.2.** The packing of the hydrogen bonding tubes in (a) HEPCuCl and (b) HEPCuBr
- Figure 4.5.1.** Layered packing in (a) PENCuCl, (b) YATYUP, and (c) ANILCP as viewed down the *b*-axis
- Figure 4.5.2.** The packing diagrams in (a) PENCuCl, (b) YATYUP, and (c) ANILCP as viewed down the *a*-axis
- Figure 4.5.3.** The hydrogen bonding interactions of (a) ANILCP, (b) YATYUP and (c) PENCuCl.
- Figure 4.6.1.** The packing diagrams of (a) FAWDAI, (b) BAPYUM, (c) FUTBUR and (d) PENCuBr respectively.
- Figure 4.6.2.** The dihedral angle, δ , measured between the X-Cu-X planes, in this example, X=Br⁻
- Figure 4.6.3.** The hydrogen bonding network formed in (a) FAWDAI, (b) FUTBUR and (c) PENCuBr structures, and (d) The side-view of the hydrogen bonding ladders in FAWDAI, FUTBUR and PENCuBr respectively.

- Figure 4.6.4.** The arrangement of the hydrogen bonded sheets (grey highlight), and the orientation of the polymer units in FAWDAI, as viewed down the b-axis.
- Figure 4.6.5.** The arrangement of the hydrogen bonded sheets (grey highlight), and the orientation of the polymer units in FUTBUR as viewed down the c-axis.
- Figure 4.6.6.** The arrangement of the hydrogen bonded sheets (grey highlight), and the orientation of the polymer units in PENCuBr as viewed down the b-axis.
- Figure 4.7.1.** The bifurcated, one-dimensional hydrogen bonding capability of AGAWIO
- Figure 4.7.2.** The hydrogen bonded motif present in the BICPEK structure
- Figure 4.7.3. (a)** The hydrogen bonded motif of BICPEK
- Figure 4.7.3. (b)** The two-dimensional hydrogen bonding network of BICPEK
- Figure 4.7.4.** The hydrogen bonded motifs in (a) FAWDAI, (b) FUTBUR and (c) PENCuBr
- Figure 4.8.1.** The double-halide exchange pathways in (a) LURTAT and (b) ULAVAF
- Figure 4.8.2.** The double-halide exchange pathways in the TOZFAP structure

Appendix One

- Figure 1.** The experimental and calculated powder patterns of PENCuBr
- Figure 2.** The experimental and calculated powder patterns of PIPCuCl
- Figure 3.** The experimental and calculated powder patterns of TOZFAP03
- Figure 4.** The experimental and calculated powder patterns of ULAVAF

Appendix Two

Compact disc containing the crystallographic information files as well as cif check reports of the novel structures.

List of Tables

Chapter One: Introduction

- Table 1.5.1.** Related zero-dimensional structures reported in the literature. The CSD refcodes and components comprising the structures are indicated
- Table 1.5.2.** The hydrogen bonding parameters of NABNEK01 and NABNEK
- Table 1.5.3.** The hydrogen bonding parameters of NUTDUB
- Table 1.5.4.** The hydrogen bonding parameters of NUTDOV
- Table 1.5.5.** The hydrogen bonding parameters for AGAWIO and LURTAT
- Table 1.5.6.** The hydrogen bonding parameters ULAVAF
- Table 1.5.7.** The hydrogen bonding parameters for TOZFAP02.
- Table 1.5.8.** Related one-dimensional structures reported in the literature. The CSD refcodes and components comprising the structures are indicated
- Table 1.5.9.** The hydrogen bonding parameters for FAWDAI.
- Table 1.5.10.** The hydrogen bonding parameters for FUTBUR.
- Table 1.5.11.** The hydrogen bonding parameters for BAPYUM.
- Table 1.5.12.** The hydrogen bonding parameters for COPDOA01.
- Table 1.5.13.** A related two-dimensional structure reported in the literature. The CSD refcodes and components comprising the structure are indicated
- Table 1.5.14.** The hydrogen bonding parameters for YATYUP

Chapter Two: Experimental Techniques

- Table 2.1.** The novel compounds successfully synthesised and characterised in this study, as well as those reported in literature.

Chapter Three: Experimental Results

- Table 3.0.1.** The schematic representations of the novel and published structures discussed.
- Table 3.0.2.** The crystallographic parameters of the novel structures determined in this study

Table 3.1.	Hydrogen bonding parameters of PENCuCl
Table 3.2.	Hydrogen bonding parameters of PENCuBr
Table 3.3.	Hydrogen bonding parameters of HEPCuCl
Table 3.4.	Hydrogen bonding parameters of HEPCuBr
Table 3.5.	Hydrogen bonding parameters of HEPBr
Table 3.6.	Hydrogen bonding parameters of PIPCuCl
Table 3.7.	The parameters obtained for the AFM chain and AFM chain with CW models employed.

Chapter Four: Discussion

Table 4.1.	The structures containing CuX_4^{2-} anions and saturated or aromatic cations used in the current study.
Table 4.2.	The hydrogen bonding parameters of ANILCP, YATYUP and PENCuCl.
Table 4.3.	The average intrachain parameters of the polymer containing compounds.
Table 4.4.	The average interchain parameters of polymeric containing structures

List of Abbreviations

δ	Angle between planes formed by CuX_4^{2-} units
Å	Angstroms
AFM	Antiferromagnet
H	Applied magnetic field
PENCuCl	Bis(cyclopentylammonium) tetrachloridocuprate (II)
CSD	Cambridge Structural Database
cm	centimetre
θ_w	Characteristic magnetisation temperature
Cu^{2+}	Copper (II)
cm^3	Cubic centimetre
CC	Curie constant
T_c	Curie temperature
CW	Curie-Weiss constant
HEPBr	Cycloheptylammonium Bromide
PENCuBr	Cyclopentylammonium catena (μ_2 -bromido) bromidocuprate (II)
°	Degrees
°C	Degrees Celsius
DFT	Density Function Theory
ρ	Density of material
DIA	Diamagnetic correction
DABCO	1,4-diazoniabicyclo[2.2.2]octane
DCM	Dichloromethane
DSC	Differential Scanning Calorimetry
DC	Direct current
eV	Electron volts
EPR	Electron Paramagnetic Resonance spectroscopy
<i>et al</i>	et alia
FM	Ferromagnet
g	gram
X	Halogeno ligand/ halide ion, X= Cl^- or Br^-
HEPCuBr	Hexa(cycloheptylammonium)(μ_2 -bromido)(μ -bromido) ₂ hexabromido tricuprate(II)
HEPCuCl	Hexa(cycloheptylammonium)(μ_2 -chlorido)(μ -chlorido) ₂ hexachlorido tricuprate(II) dichloride
HCl	Hydrogen chloride
HBr	Hydrogen bromide
K	Kelvin
kOe	kilooersted
kV	kilovolts
θ	Linear bond angle
L.T	Low temperature
M	Magnetisation
J	Magnetic exchange constant
χ	Magnetic susceptibility
χ_{mol}	Magnetic susceptibility per mole
M1	Metal centre one
M2	Metal centre two
mA	milliampre
ml	millilitre
mmol	millimol
M_r	Molar mass

T_N	Neél temperature
Oe	Oersted
L	Orbital angular momentum
\hat{H}_x	Pair-wise Hamiltonian
PIPCuCl	Piperazinium tetrachloridocuprate(II)
PXRD	Powder X-ray diffraction
R.T	Room temperature
SXRD	Single crystal X-ray diffraction
S	Spin angular momentum
C_6	Six membered carbon cyclic ring
SQUID	Super quantum interference device
T	Temperature
TIP	Temperature independence parameter
C_3	Three membered carbon cyclic ring
μ_0	Vacuum permeability
r	van der Waals radius
Ψ	Wavefunction

Table of Contents

Declaration	i
Acknowledgments	ii
Conferences	iii
Research Visit	iii
Abstract	iv
List of Schematics	v
List of Figures	v
List of Tables	viii
List of Abbreviations	x

Chapter One: Introduction

1.1. Material Science	1
1.2. Crystal Engineering	1
1.3. Aspects of the Current Study	2
1.3.1. Hybrid Materials	2
1.3.2. Properties and Application of Hybrid Materials	3
1.3.3. Structure Dimensionality	3
1.4. Specific Aspects of the Current Study	4
1.4.1. Materials Selected for this Study	4
1.4.2. Copper (II)	5
1.5. Literature Survey	5
1.5.1. Zero-dimensional Structures	6
1.5.2. One-dimensional Polymeric Structures	16
1.5.3. Two-dimensional Structures	23
1.6. Magnetochemistry	24
1.6.1. Magnetism	24
1.6.2. Magnetostructural Relationships	25
1.6.3. Magnetic Structure vs Crystal Structure	26
1.6.4. Magnetism of Cu ²⁺ Ions	26
1.6.4.1. Jahn-Teller Distortion	26
1.6.5. Magnetic Exchange Coupling	27
1.6.6. Paramagnetism	27
1.6.7. Ferromagnetism (FM) and Antiferromagnetism (AFM)	28
1.6.7.1. Ferromagnetic Ordering	28

1.6.7.2. Antiferromagnetic Ordering	28
1.6.7.3. Metamagnetic Ordering	29
1.6.8. Curie-Weiss Law	29
1.6.9. Exchange Parameter.....	29
1.6.10. Superexchange	30
1.6.11. Orbital Models.....	30
1.6.11.1. Through-bond Exchange	30
1.6.11.2. Through-space Exchange.....	31
1.7. Research Aims and Objectives	32
1.8. References	32

Chapter Two: Experimental Techniques

2.1. Synthetic Procedures	35
2.1.1. Materials.....	35
2.1.2. Synthesis.....	35
2.1.2.1. Slow Evaporation at Room Temperature	36
2.1.2.2. Slow Cooling of Saturated Acid Solutions.....	36
2.1.2.3. Compounds Prepared.....	36
2.2. Structural Characterisation.....	37
2.2.1. X-ray Diffraction	38
2.2.1.1. Single Crystal X-ray Diffraction (SXRD)	39
2.2.1.2. Powder X-ray Diffraction (PXRD).....	40
2.3. Magnetic Characterisation	40
2.3.1. Sample Preparation.....	40
2.3.2. Instrumentation	41
2.3.3. Data Collection.....	41
2.3.4. Data Processing.....	42
2.3.5. Data Fitting to Quantum Models	42
2.4. Computer Software Programs	42
2.4.1. Cambridge Structural Database (CSD)	42
2.4.2. Diffract. Suite. Eva.....	43
2.4.3. Powdercell for Windows.....	43
2.4.4. Mercury CSD	43
2.4.5. Origin.....	43
2.5. References	43

Chapter Three: Experimental Results

3.1. Bis(cyclopentylammonium) tetrachloridocuprate(II)	48
3.1.1. Structure Analysis	48
3.1.2. Magnetic Characterisation	50
3.2. Cyclopentylammonium catena (μ_2 -bromido) bromidocuprate(II).....	51
3.2.1. Structure Analysis	51
3.2.2. Magnetic Characterisation	53
3.3. Hexa(cycloheptylammonium) (μ_2 -chlorido) (μ -chlorido) ₂ hexachlorido tricuprate(II) dichloride	56
3.3.1. Structure Analysis	56
3.3.2. Magnetic Characterisation	59
3.4. Hexa(cycloheptylammonium) (μ_2 -bromido) (μ -bromido) ₂ hexabromido tricuprate(II) dibromide	60
3.4.1. Structure Analysis	60
3.4.2. Magnetic Characterisation	63
3.5. Cycloheptylammonium bromide	64
3.5.1. Structure Analysis	64
3.6. Piperazinium tetrachloridocuprate(II)	67
3.6.1. Structure Analysis	67
3.6.2. Magnetic Property Analysis	69
3.7. Bis (1,4-diazoniabicyclo[2.2.2]octane) trichloride diaqua trichloridocuprate(II) monohydrate.....	71
3.7.1. Structure Description	71
3.7.2. Magnetic Characterisation	71
3.8. 1,4-diazoniabicyclo[2.2.2]octane tetrabromidocuprate(II) monohydrate	74
3.8.1. Structure Description	74
3.8.2. Magnetic Property Analysis	74
3.9. References	75

Chapter Four: Discussion

4.1. Structural Comparisons.....	77
4.1.1. Perhalometallate Anion Diversity	77
4.2. Layered Structures	78
4.3. Cation Effects	79
4.3.1. Aromatic vs Saturated Cations	79
4.3.2. Monocations vs Dications	81

4.4. Comparison of Families of Structures.....	83
4.4.1. Cycloheptylammonium (HEP) Clusters.....	83
4.5. Comparison of Perovskite Compounds.....	85
4.6. Polymeric Structure and Magnetic Comparison.....	88
4.7. Crystal Engineering Synthons.....	94
4.7.1. Zero-dimensional Systems (DABCO vs Piperazinium Cations)	95
4.7.2. One-dimensional Systems	96
4.8. Diversity and Trends in Magnetic Behaviour	96
4.9. References	98

Chapter Five: Conclusion and Future Work

5.1. Conclusion.....	100
5.2. Future Work.....	101

Appendix One	102
Appendix Two	107

Chapter One: Introduction

“The art and science of asking questions is the source of all knowledge”

– Thomas Berger

1.1. Material Science

In recent years there has been significant interest in and focus on the tailoring of materials to manifest desired properties for specific applications and this field of study is known as material science. Material science is one of the oldest forms of applied science and involves elements of applied physics and chemistry.

The need and want for technological improvements and revolutionary materials such as semi-conductors and biomaterials has become a top priority for various industries. The reason for failures in materials has also impacted hugely on the drive for improvement of materials, as the understanding of the behaviour of materials is necessary to improve the materials used.

Material science focuses on structure-property relationships in materials through characterisation. The ability to design materials for specific applications *via* structure control is the main aim of many researchers in this field. This may be achieved in crystalline materials by applying crystal engineering theory and principles.

1.2. Crystal Engineering

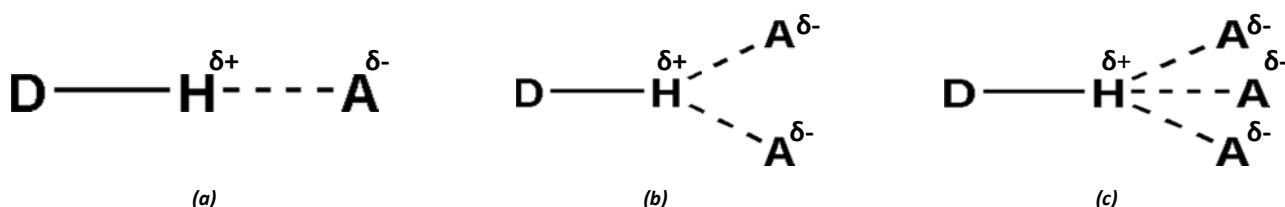
The term “crystal engineering” was implemented by Schmidt in 1971 (Schmidt. 1971), after realising that a more formal theoretical approach was required to describe the interactions that exist within the structure of solid-state materials. Crystal engineering is a field which aims to aid in the prediction of structure assembly in crystalline materials through covalent and non-covalent interactions, by the identification of molecular building blocks and synthons that pack to form the crystal structure of crystalline materials. The way in which building blocks pack is due to the balance between intermolecular forces that exist between molecular or ionic constituents, as well as the shape of the building block. These intermolecular interactions can be further explained by the concepts of supramolecular chemistry.

Supramolecular chemistry aids in the understanding of intermolecular interactions of solid-state materials and goes hand-in-hand with crystal engineering which utilises the understanding of intermolecular interactions for the design of new materials with desired physical and chemical properties (Desiraju. 1989). The intermolecular interactions are defined as repulsive or attractive forces, caused by electrostatic interactions that include ionic interactions, van de Waals forces, π - π interactions and hydrogen bonding interactions. Hydrogen bonding is the most robust non-covalent interaction (Brammer. 2004) and can be seen as a recognition motif between building blocks. The recognition motif or supramolecular synthon is used to direct structure assembly and networks (Desiraju. 1995).

Hydrogen bonding: After the discovery of hydrogen bonding interactions about a century ago, it has since been identified as the most important interaction of all directional molecular interactions and often acts as the “glue” holding the structure together. The classic definition of a hydrogen bond is an electrostatic interaction existing between the donor hydrogen atom, which is covalently bonded to a donor atom D and an electronegative acceptor atom denoted as A. The donor atom creates a partial positive charge on the hydrogen atom. The partially positively charged hydrogen atom is electrostatically attracted to the electronegative acceptor species, as shown in Scheme 1.2.1 (a). If the donor atom, D, or the acceptor atom, A,

are charged species, a charge assisted hydrogen bond is formed, which is typically stronger than the analogous neutral hydrogen bond.

As illustrated in Scheme 1.2.1 (b) and (c), electrostatic interactions can also exist between two or three electronegative acceptor species and a single donor hydrogen atom. If two acceptor species are shared between a single donor hydrogen atom, the interaction is known as bifurcated hydrogen bonding, if three acceptor atoms are shared then trifurcated hydrogen bonding occurs between the donor hydrogen atom and acceptor species, A (Steiner. 2002).



Scheme 1.2.1. The various forms of hydrogen bonding that may exist in materials. (a) Classic, charge assisted, (b) bifurcated charge assisted and (c) trifurcated charge assisted hydrogen bonding.

Typical classic hydrogen atom to acceptor hydrogen bond distances fall in the range of 1.80 Å to 2.00 Å and the linear bond angle, θ , of classic D-H \cdots A interactions range from 150° to 180° (Desiraju. 1995).

Compounds containing anionic units consisting of halogeno ligands coordinated to a metal centre have been reported to be good hydrogen bond acceptors (Aullón *et al.* 1998 and Brammer *et al.* 2001). Studies performed by Brammer revealed hydrogen bonding geometry preferences for terminal halide acceptor groups, such as a $^+D-H\cdots X$ angle of 90° to 130° for X = Cl⁻, Br⁻, I⁻ (Mareque and Brammer. 1998).

1.3. Aspects of the Current Study

1.3.1. Hybrid Materials

The term hybrid material is used to describe compounds that comprise both organic and inorganic components. For the purpose of the current study a hybrid compound is defined as a composite material formed through the combination of an inorganic metal(II) halide, with an organic component, which often contains an amine group. Due to the intermolecular interactions present between the units that make up these hybrid compounds, the organic and inorganic moieties self-assemble into ordered hybrid structures. Two types of hybrid materials may be formed, namely coordination and ionic hybrid materials. The ionic hybrid materials exist as cations and anions, while the organic units are coordinated to the metal ions of the inorganic units in coordination hybrid materials. The formation of these two types is based on the environment in which the organic and inorganic components are reacted. Coordination compounds form in the absence of acid, whereas the ionic compound is formed in the presence of acid. In this study only ionic compounds are considered, which consist of organic cations and perhalometallate anions.

Hybrid materials often have the ability to retain the desired properties of both the organic and inorganic components. The inorganic component may contribute to the mechanical hardness of the material and provide thermal stability, magnetic properties and electronic properties, which determine conductor, semiconductor or insulation behaviour (Knutson *et al.* 2005 and Guha *et al.* 1997). On the other hand, the organic component may impart structural diversity, templating effects and optical properties including fluorescence and luminescence (Mitzi *et al.* 2001). The various properties exhibited by hybrid materials have sparked interest in the application and understanding of these materials.

1.3.2. Properties and Applications of Hybrid Materials

Interesting optical, electronic and magnetic properties have been reported for organic-inorganic hybrid materials and a selection of examples of reported properties is given in this section. This list is by no means exhaustive and serves to illustrate the range of possible properties in these materials.

Unique electronic and optical properties have been reported for organic-inorganic hybrid materials. In a study conducted by Knutson and Martin (Knutson and Martin. 2005), who explored the possibility of tuning the band gaps of perovskite tin(II) iodide hybrid compounds, it was found that the experimental excitation energies correlated with the calculated band gaps. Furthermore, Sn-I-Sn bond angles were found to influence the tin(II) iodide hybrid band gaps and it was possible to tune the band gap by as much as 1 eV using the templating influence of organic ammonium cations (Mitzi. 1999).

Mitzi (2004) showed that perovskite-type hybrid materials are semi-conductors and exhibit a semiconductor-metal transition as the perovskite layer thickness increases.

An example of an application of a hybrid material has been reported by Mitzi (Mitzi *et al.* 2001). A PbCl_4^{2-} based hybrid was employed to construct an organic-inorganic light emitting diode (OLED), as shown in Figure 1.3.1. The $(\text{H}_2\text{AEQT})\text{PbCl}_4^{2-}$, where AEQT = 5, 5'''-bis(aminoethyl)-2,2':5', 2'': 5'', 2'''- quaterthiophene, hybrid material employed exhibited a perovskite-type structure.

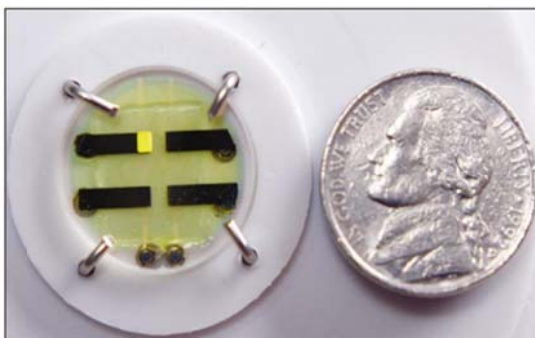


Figure 1.3.1. The operational OLED device. On the right a nickel coin is used as a scale comparison (Mitzi *et al.* 2001).

Another example of an application of a hybrid material is the use of these materials in photovoltaic cells. Lead(II) halide perovskite hybrids containing CH_3NH_3^+ cations have been used as visible-light sensitizers in photoelectrochemical cells by self-organising the material on TiO_2 (Kojima *et al.* 2009).

Numerous papers have reported the magnetic properties of hybrid materials. These materials typically contain a magnetic metal ion, for example Cu^{2+} , which is also relevant to the current study. Depending on the type of inorganic anion present in the structure, these perhalocuprate containing hybrids can exhibit diverse magnetic properties, for example ferromagnetism, antiferromagnetism or paramagnetism (Turnbull *et al.* 2005, Landee and Turnbull. 2013). The origin of magnetism in these materials will be discussed in more detail in section 1.6.

1.3.3. Structure Dimensionality

The dimensionality of the structure of a hybrid material is often dependent on the dimensionality of the inorganic component. The type of perhalometallate anion formed is dependent on the reaction conditions employed, the organic component used, as well as the metal atom used. The organic component offers a templating effect to the structure and this was proven by Brammer, who showed that by identifying different hydrogen bond acceptor sites on anions, selective population of these sites through hydrogen bond donors may offer dimensional control of the structure (Brammer *et al.* 2002).

The anionic units can exist as zero-, one-, two- or three-dimensional perhalometallate anions, as illustrated in Figures 1.3.2 and 1.3.3. Zero-dimensional anions are isolated units and do not share terminal ligands. Bridging of metal centres can occur when halogeno ligands are shared between metal centres. Corner-sharing, edge-sharing or face-sharing of halogeno ligands can result in the formation of one-dimensional perhalometallate chains or ribbons, two-dimensional sheets or three-dimensional structures.

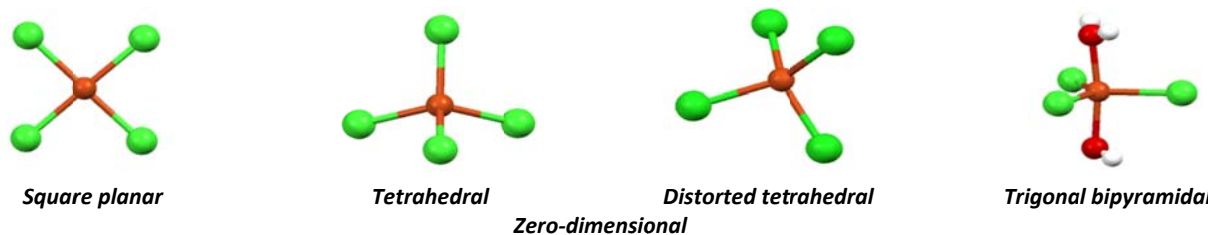


Figure 1.3.2. Zero-dimensional anionic units. (Green balls signify halogeno ligands, red balls signify oxygen atoms of H₂O molecules and orange spheres indicates metal ions)

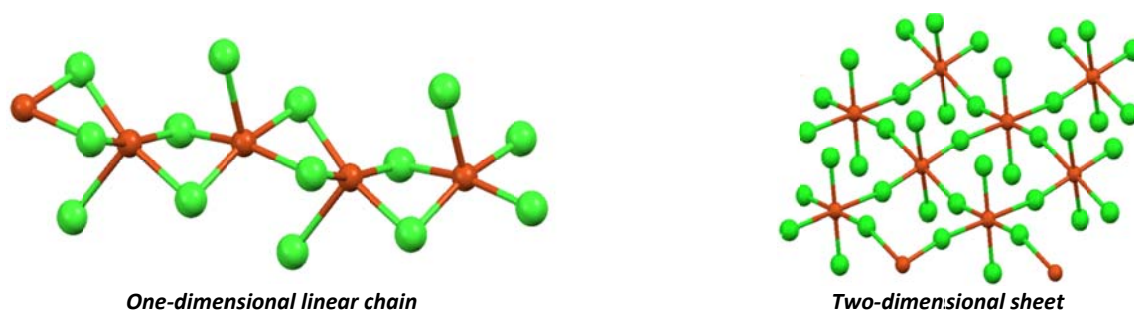


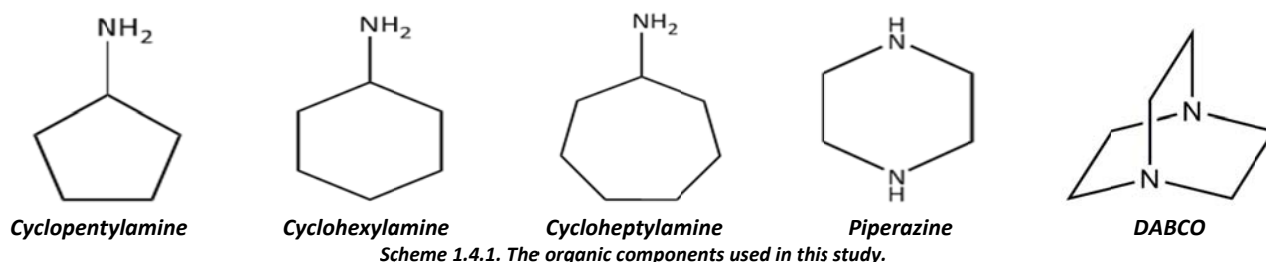
Figure 1.3.3. One- and two-dimensional anionic units (Green balls signify halogeno ligands and orange spheres indicates metal ions).

1.4. Specific Aspects of the Current Study

1.4.1. Materials Selected for this Study

In this study the ionic hybrid compounds formed by the combination of a chlorido or bromido salt of Cu²⁺ and a saturated organic cycloalkylamine component, which may be cyclopentylamine, cyclohexylamine, cycloheptylamine, piperazine or 1,4-diazoniabicyclo[2.2.2]octane (DABCO), were studied. All materials were prepared in the presence of acid, which resulted in the protonation of the amine and the formation of ionic structures comprising organic cationic and inorganic anionic units.

Organic components selected: Due to the fact that not many hybrid structures containing saturated organic components have been reported in the literature, as will be shown in section 1.5, this study focusses specifically on the investigation of the structures and magnetic properties of hybrids containing saturated cycloalkylammonium organic cations. The series: cyclopentylamine, cyclohexylamine and cycloheptylamine offer the opportunity to study the effect of an increase in the saturated ring size on the structural characteristics of the hybrid materials and the indirect effect on magnetic properties, while comparison of the saturated piperazine and DABCO organic components allows for the study of the effect of the geometry of the cation (the flexibility of piperazine versus the ridged cage-like structure of DABCO) and the indirect influence this may have on the magnetic properties. The schematic representations of the unprotonated amine organic components used in this study are illustrated in Scheme 1.4.1.



Inorganic components selected: The metal chlorido and bromido salts of Cu^{2+} (d^9) were selected specifically to impart magnetic properties to the materials, since this metal ion contains an unpaired electron. Cu^{2+} is the preferred oxidation state for this study, as Cu^+ offers no magnetic properties. CuI_2 is known to form CuI and I_2 on addition of I^- (Housecroft and Sharp, 2008) and therefore iodido containing materials were excluded from this study.

1.4.2. Copper (II)

The d^9 transition Cu^{2+} metal ion has a flexible coordination sphere, leading to a diverse range of coordination geometries. Perhalocuprate anions may exist as isolated $[\text{Cu}_x\text{X}_y]^{m-}$ ($\text{X} = \text{Cl}^-$ or Br^-) units that may adopt coordination geometries such as distorted tetrahedral or square planar for four coordinate species, distorted square pyramidal for five coordinate species and octahedral for six coordinate species, with Jahn-Teller distortion (discussed in full in section 1.6.4.1) occurring along the z-axis.

These anionic units can link *via* edge-, face- or corner- sharing of halogeno ligands to form one- or two-dimensional perhalometallate coordination polymers. $[\text{CuCl}_3]$ units may link *via* coordination bonds to form $[\text{Cu}_2\text{Cl}_6]^{2-}$ dimers, which may stack in various ways. Figure 1.4.1 shows a selection of perhalocuprate geometries.

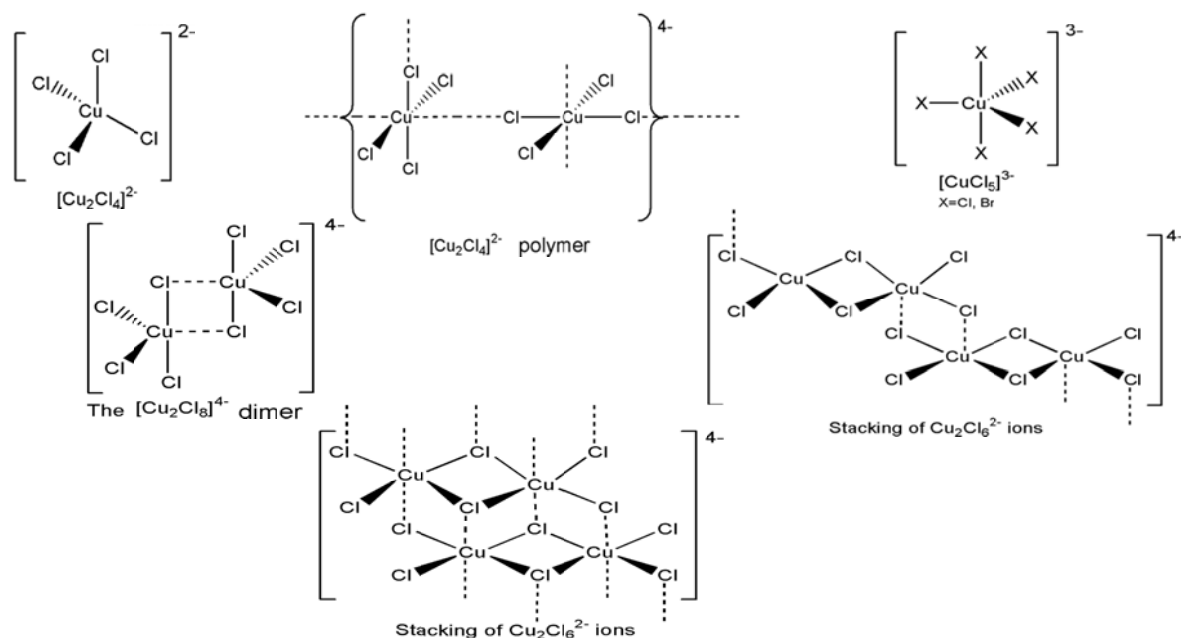


Figure 1.4.1. Selected geometries of perhalocuprate anions (Smith, 1976).

1.5. Literature Survey

The Cambridge Structural Database (CSD), version 5.34, May 2013 update (Allen, 2002) is a database containing a number of hybrid materials related to the compounds of interest that have been reported in the literature. The search for related structures was defined to include the cations of interest combined with a MX unit, where $\text{M} = \text{Cu}^{2+}$ and $\text{X} = \text{Cl}^-$ or Br^- . Water inclusion was allowed but structures containing other solvents were rejected. The structures containing free halide ions were retained. In this section, all figures were drawn from cif files of CSD entries, hence ellipsoids plots cannot be shown and the standard deviations of parameters may not be available.

A total of 12 related structures were located in the CSD, three of which contain cyclopentylammonium and perhalocuprate(II) components (**FAWDAL**, **NABNEK** and **NABNEK01**). Three structures contain cyclohexylammonium cations and perhalocuprate(II) anions (**BAPYUM**, **FUTBUR** and **YATYUP**). No structures

containing cycloheptylammonium cations and the perhalometallate anions of interest were found, in fact only three cycloheptylammonium hybrid structures have been reported, namely the hybrids with PbX , $X = Cl^-$, Br^- and I^- (Billing *et al.* 2007 and Billing *et al.* 2009). Three piperazinium perhalocuprate(II) structures of interest were found (**COPDOA01**, **NUTDUB** and **NUTDOV**), while three DABCO perhalocuprate(II) compounds have been reported (**AGAWIO**, **LURTAT** and **ULAVAF**).

From the literature survey it was evident that the combination of a specific organic amine with a metal halide salt under acidic conditions can result in the formation of more than one structure combining the components, with different chemical formulas, because of the ability to form different perhalometallate anions. Due to this tendency, it was decided to categorise the structures reported in the literature according to the specific perhalometallate anion present in the structure, as well as the dimensionality of the anions.

The related literature structures are summarised below and are referred to by their CSD refcodes.

1.5.1. Zero-dimensional Structures

The zero-dimensional structures consist of isolated MX_4^{2-} ($X = Cl^-$ or Br^-) or $MX_3L_2^-$ ($X = Cl^-$ and $L = H_2O$) anionic units and isolated cycloalkylammonium cationic units. In some of the structures isolated water molecules or isolated halide ions, or both, are present in the structure. Table 1.5 lists the zero-dimensional hybrid structures reported in the literature.

Table 1.5.1. Related zero-dimensional structures reported in the literature. The CSD refcodes and components comprising the structures are indicated.

CSD Refcode	Organic cation	Inorganic anion	Free water molecule present	Isolated halide ion present
NABNEK & NABNEK01	cyclopentylammonium	$CuBr_4^{2-}$	-	-
NUTDUB	piperazinium	$CuCl_4^{2-}$	Yes	-
NUTDOV	piperazinium	$CuCl_4^{2-}$	Yes	Yes
AGAWIO	DABCO	$CuCl_4^{2-}$	-	-
LURTAT	DABCO	$CuCl_4^{2-}$	Yes	-
ULAVAF	DABCO	$CuBr_4^{2-}$	Yes	-
TOZFAP	DABCO	$CuCl_3^-(H_2O)_2$	Yes	Yes

NABNEK & NABNEK 01 (Willet. 2004)

Bis(cyclopentylammonium) tetrabromidocuprate(II)

Formula: $2(C_5H_{12}N^+) CuBr_4^{2-}$

Synthesis: Cyclopentylamine and $CuBr_2$ were dissolved in an aqueous solution in a 2:1 ratio. To the solution a few drops of HBr were added to prevent hydrolysis of Cu^{2+} . Slow evaporation of all the solvent lead to the formation of black crystals.

Structure: Two phases of the bis(cyclopentylammonium) tetrabromidocuprate(II) compound exist. The structures of the phases were determined at room temperature (R.T), **NABNEK01** and at a low temperature (L.T), **NABNEK**, of $-70^\circ C$. According to DSC studies, a first order structure phase transition occurs at $-13^\circ C$ from the room temperature structure to the low temperature structure. Magnetic analysis was done on the low temperature phase.

The room temperature and low temperature structures crystallise in the orthorhombic space groups $Pn2_1a$ and $Pna2_1$ respectively. The asymmetric units of both phases are shown in Figure 1.5.1 (a) and (b). In the asymmetric unit of **NABNEK01**, two singly protonated isolated cyclopentylammonium cations are present, as

well as a distorted tetrahedral CuBr_4^{2-} anion. The asymmetric unit of **NABNEK** comprises four singly protonated cyclopentylammonium cations, with disorder occurring in one of the cationic rings and two isolated distorted tetrahedral CuBr_4^{2-} anionic units. The **NABNEK** and **NABNEK01** compounds exhibit the same organic cation to inorganic anion ratio of 2:1.

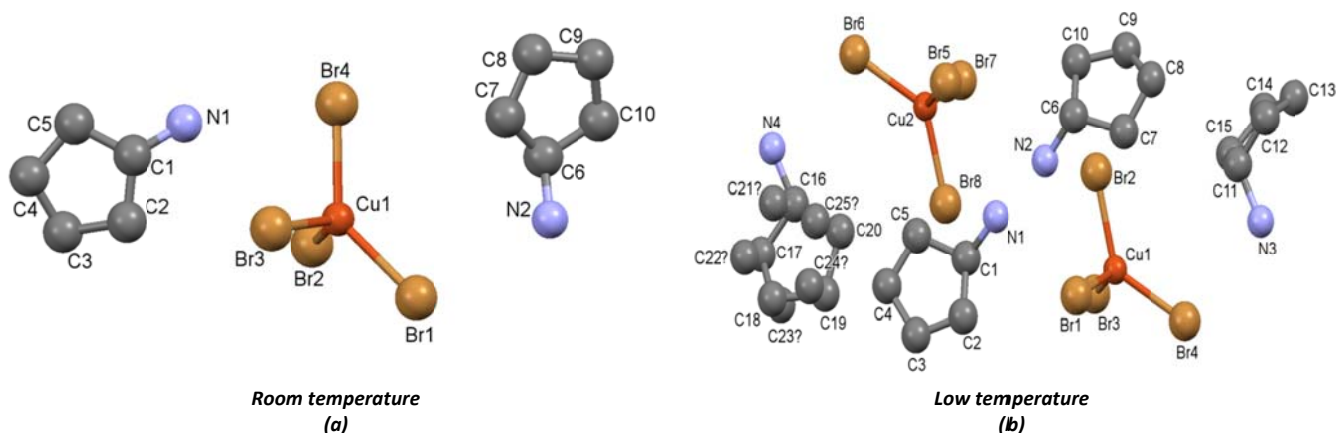


Figure 1.5.1. The asymmetric unit of (a) **NABNEK01** and (b) **NABNEK**. The hydrogen atoms are omitted for clarity.

The slight structural differences between **NABNEK** and **NABNEK01** can be seen in the orientation of the cationic rings, as well as the displacement of the anionic moieties. In both structures, the anionic units pack in a sheet that extends down the *ac*-plane and alternates with sheets of cations.

In the **NABNEK01** compound (Figure 1.5.2 (a)) classic charge assisted, $^+\text{N}-\text{H}\cdots\text{Br}^--\text{Cu}$ hydrogen bonding interactions occur between the hydrogen atom on the donor nitrogen atom to a single bromido ligand comprising a CuBr_4^{2-} unit. The **NABNEK** compound contains a single cation that is hydrogen-bonded to two individual anions. Both bifurcated, as well as classic charge assisted, $^+\text{N}-\text{H}\cdots\text{Br}^--\text{Cu}$, hydrogen bonds exist, as shown in Figure 1.5.2 (b). The positions of the anions and cations allow for the formation of a one-dimensional hydrogen bonded network, as shown in Figure 1.5.2 (c) and (d) for **NABNEK01** and **NABNEK** respectively. Hydrogen bonding parameters are listed in Table 1.5.2.

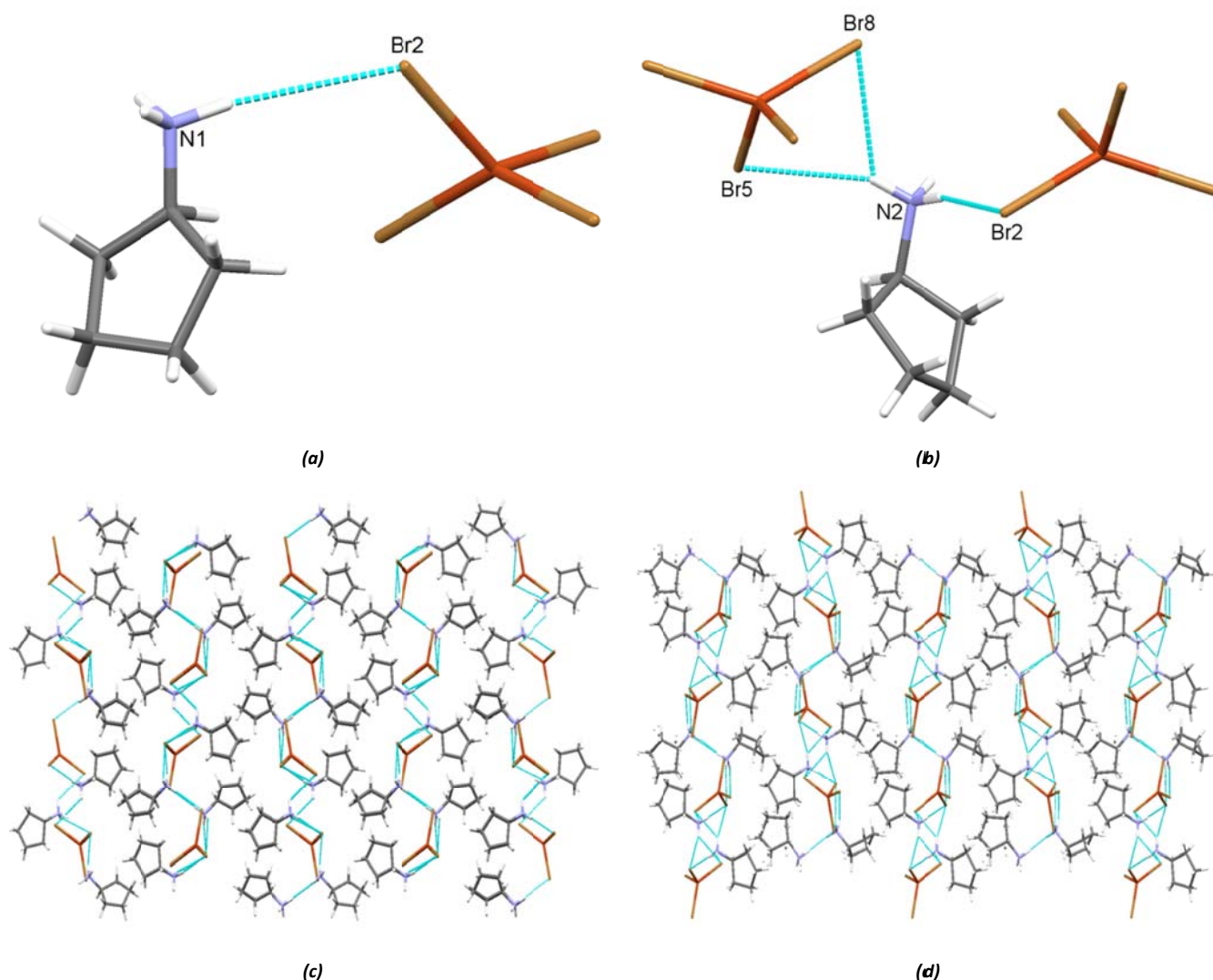


Figure 1.5.2. The hydrogen-bonded unit of (a) NABNEK01 and (b) NABNEK respectively. The hydrogen bonding network of (c) NABNEK01 and (d) NABNEK as viewed down the *b*-axis.

Table 1.5.2. The hydrogen bonding parameters of NABNEK01 and NABNEK.

NABNEK01		
D-H	$d(\text{H}\cdots\text{A})$ (Å)	A
N1-H2	2.731	Br2 $[-x, \frac{1}{2}+y, 1-z]$
NABNEK		
D-H	$d(\text{H}\cdots\text{A})$ (Å)	A
N2-H5	2.660	Br2
N2-H6	2.779	Br5
N2-H6	2.725	Br8

The magnetic behaviour of the L.T compound was analysed and found to be an antiferromagnetic (AFM) spin-ladder system at 8 K. The maximum at 8 K in the χ vs *T* plot is typical for AFM behaviour. The low temperature structure shows a ladder motif between CuBr_4^{2-} units, as shown in Figure 1.5.3, with rung distances of 4.396 Å and 4.519 Å. The shortest $\text{Br}^- \cdots \text{Br}^-$ distance for the two independent rails for the low temperature structure are 3.893 Å and 3.881 Å and the shortest interladder distances for the low temperature structure is 4.996 Å.

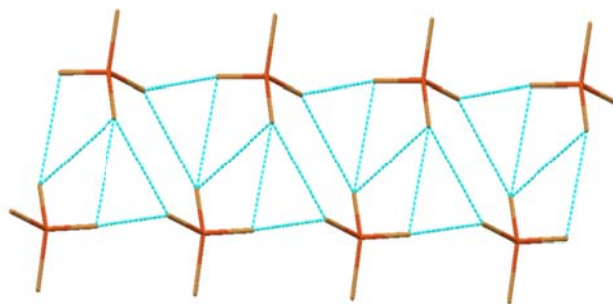


Figure 1.5.3. The arrangement of the CuBr_4^{2-} anions in NABNEK.

NUTDUB (Riley *et al.* 1998)

Piperazinium tetrachloridocuprate(II) dihydrate

Formula: $\text{C}_4\text{H}_{12}\text{N}_2^{2+} \text{CuCl}_4^{2-} \cdot 2(\text{H}_2\text{O})$

Synthesis: The cationic salt was prepared and precipitated by the addition of concentrated HCl to a solution of piperazine in ethanol. The hydrated CuCl_2 salt was dissolved in ethanol and added to the piperazinium salt solution forming a light green powder. The compound was recrystallised using dilute HCl, resulting in a mixture of yellow and green crystals. The yellow crystals of **NUTDUB** were isolated and analysed.

Structure: The **NUTDUB** structure belongs to the monoclinic space group $C2/c$. The asymmetric unit of the **NUTDUB** structure contains a $\text{NH}_2(\text{CH}_2)_2$ unit that is a fragment of a diprotonated piperazinium cation, a CuCl_2 unit that forms part of a distorted tetrahedral CuCl_4^{2-} anionic moiety, as well as a free water molecule, as shown in Figure 1.5.4. Thermochromism studies were conducted on the **NUTDUB** and **NUTDOV** structures.

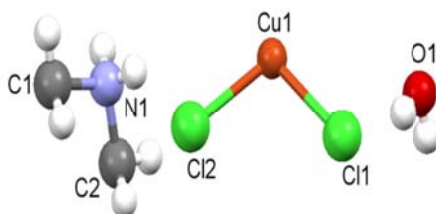


Figure 1.5.4. The asymmetric unit of **NUTDUB**.

The piperazinium cations adopt chair conformations. The piperazinium cation forms bifurcated hydrogen bonds to two chlorido ligands that are part of a CuCl_4^{2-} anion, this same anion contains a third chlorido ligand that is hydrogen-bonded *via* classic, charge assisted, $^+\text{N}-\text{H}\cdots\text{Cl}-\text{Cu}$ hydrogen bonding interactions to a water molecule, as shown in Figure 1.5.5 (a) The hydrogen bonding interactions present between cations, anions and free water molecules form a three-dimensional hydrogen-bonded network, as shown in Figure 1.5.5 (b). The hydrogen bonding parameters are given in Table 1.5.3.

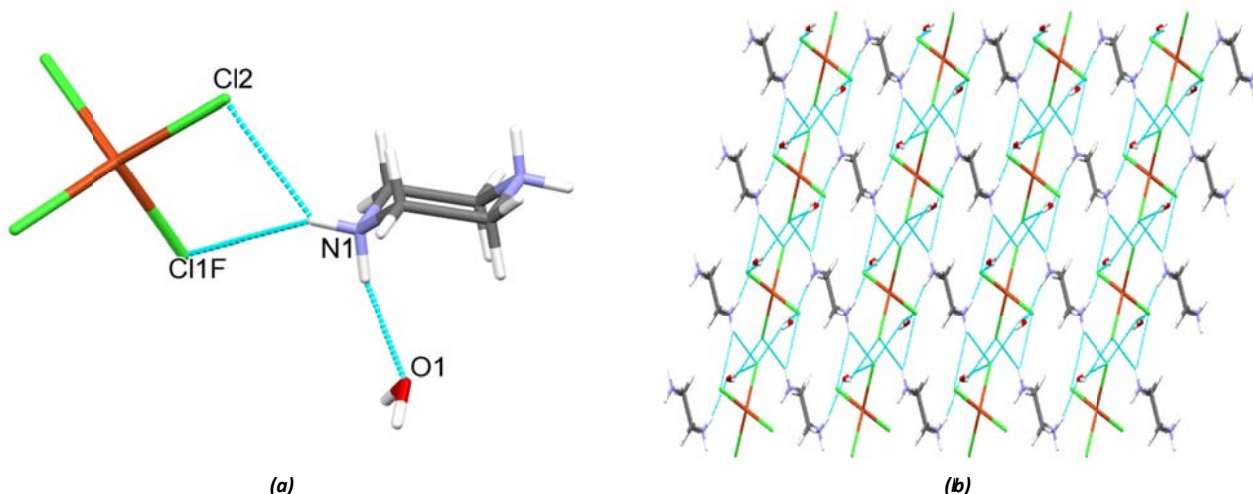


Figure 1.5.5. (a) The hydrogen-bonded unit of **NUTDUB**. (b) The hydrogen bonding network of **NUTDUB** as viewed down the b -axis.

Table 1.5.3. The hydrogen bonding parameters of NUTDUB.

D-H	d(H...A) (Å)	A
N1-H2	2.660	O1 [1.5-x, -½+y, ½-z]
N1-H1	2.779	Cl2
N1-H1	2.725	Cl1F [1-x, y, ½-z]

NUTDOV (Riley *et al.* 1998)

Bis(piperazinium) tetrachloridocuprate(II) trichloride trihydrate Formula: $2(\text{C}_4\text{H}_{12}\text{N}_2^{2+}) \text{CuCl}_4^{2-} \cdot 2\text{Cl}^- \cdot 3(\text{H}_2\text{O})$

Synthesis: The cationic salt was first prepared and precipitated by the addition of concentrated HCl to a solution of piperazine in ethanol. The hydrated CuCl_2 salt was dissolved in ethanol and added to the piperazinium salt solution, forming a light green powder. The compound was recrystallised using dilute HCl resulting in a mixture of yellow and green crystals. Recrystallisation in a minimum amount of acid resulted in an increase of the formation of the green **NUTDOV** crystals.

Structure: The **NUTDOV** structure crystallises in the triclinic $P\bar{1}$ space group. The asymmetric unit of **NUTDOV**, as shown in Figure 1.5.6, comprises two $\text{NH}_2(\text{CH}_2)_2$ units that are fragments of two isolated piperazinium cations, a diprotonated piperazinium cation that adopts a chair conformation, two CuCl_2 units that are fragments of two individual square planar CuCl_4^{2-} anionic moieties, two free chloride ions and three free water molecules. Upon heating the **NUTDOV** structure by laser irradiation the colour changes from green (**NUTDOV**) to yellow (**NUTDUB**).

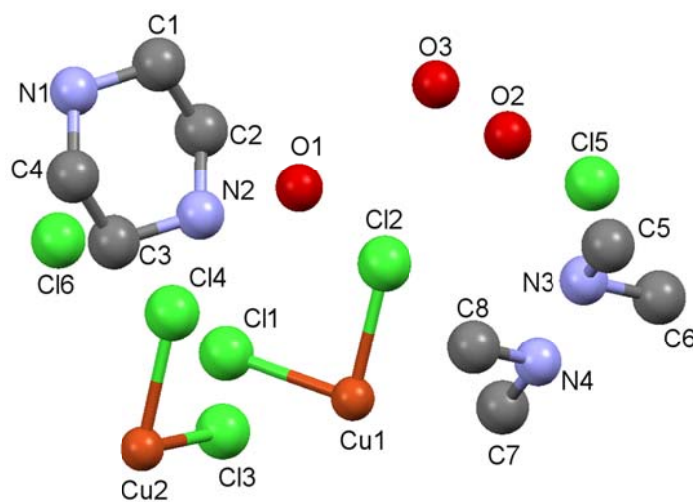


Figure 1.5.6. The asymmetric unit of NUTDOV. The hydrogen atoms are omitted for clarity.

Hydrogen bonding interactions occur on both sides of the piperazinium dication. The hydrogen atom on nitrogen, N1, is hydrogen-bonded to a single free chloride ion and a second hydrogen atom on nitrogen, N1, forms trifurcated hydrogen bonds to two chlorido ligands that form part of a single CuCl_4^{2-} anion. The hydrogen bonding interactions on nitrogen atom, N2, is formed between a hydrogen atom and two chlorido ligands that form part of a single CuCl_4^{2-} anion to form bifurcated hydrogen bonding interactions. A third classic, charge assisted, $^+\text{N}-\text{H}\cdots\text{O}-\text{H}_2$ hydrogen bonding interaction is formed between the hydrogen atom on a donor nitrogen atom to an oxygen atom of a free water molecule, as shown in Figure 1.5.7 (a) The hydrogen bonding interactions that are present between the cations, anions, chloride ions and free water molecules, form a three-dimensional hydrogen bonding network, as shown in Figure 1.5.7 (b). The hydrogen bonding parameters are given in Table 1.5.4.

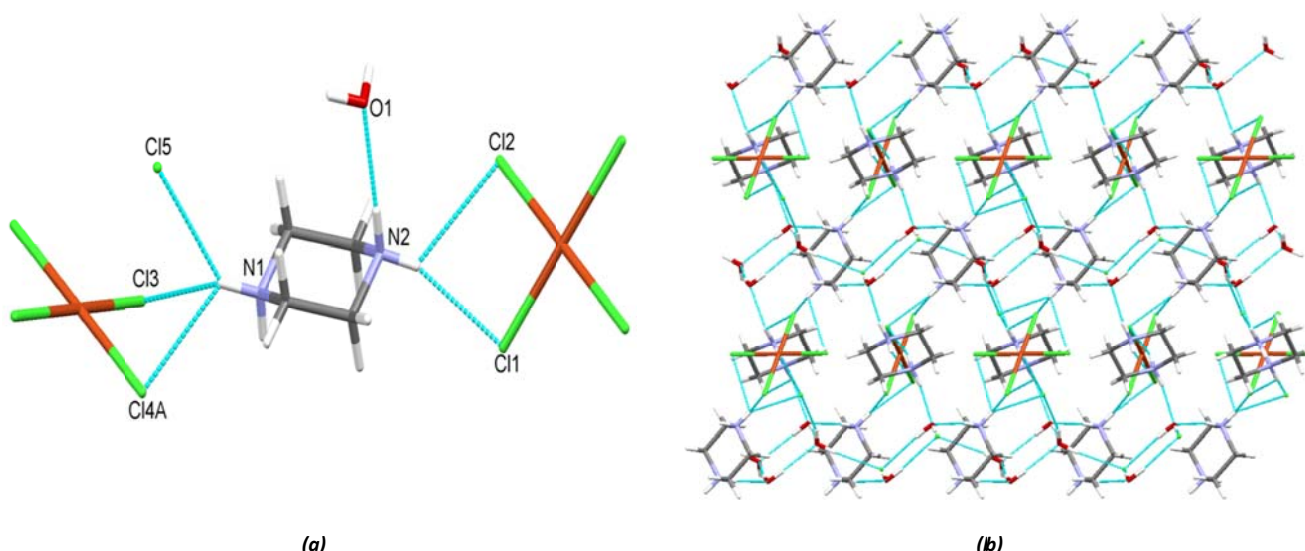


Figure 1.5.7. (a) The hydrogen-bonded unit of NUTDOV. (b) The three-dimensional hydrogen-bonded network of NUTDOV.

Table 1.5.4. The hydrogen bonding parameters of NUTDOV.

D-H	d(H...A) (Å)	A
N2-H8	2.420	Cl1
N2-H8	2.696	Cl2
N2-H7	2.563	O1
N1-H1	2.684	Cl4A [-x, -y, 2-x]
N1-H1	2.795	Cl3 [-1+x, y, z]
N1-H1	2.563	Cl5 [-x, 1-y, 2-z]

AGAWIO (Brammer *et al.* 2002) and LURTAT (Wei and Willet. 2002)

AGAWIO: 1,4-Diazoniabicyclo[2.2.2]octane tetrachloridocuprate(II)

AGAWIO Formula: $C_6H_{14}N_2^{2+} CuCl_4^{2-}$

LURTAT: 1,4-Diazoniabicyclo[2.2.2]octane tetrachloridocuprate(II) monohydrate

LURTAT Formula: $C_6H_{14}N_2^{2+} CuCl_4^{2-} \cdot H_2O$

Synthesis: 1:1 molar equivalents of DABCO and hydrated $CuCl_2$ were added to a concentrated HCl solution and left to slowly evaporate at R.T. which yielded the hydrated structure (**LURTAT**), whereas elevated temperatures gave the anhydrous structure (**AGAWIO**).

Two reports of the 1,4-diazoniabicyclo[2.2.2]octane tetrachloridocuprate(II) structure can be found in the literature, **AGAWIO** (Brammer *et al.* 2002) and **AGAWIO01** (Wei and Willet. 2002) that were structurally determined at 203 K and R.T, respectively and in this study the structure determined at the lowest temperature (**AGAWIO**) will be discussed.

Structure: The **AGAWIO** structure is the anhydrous form of the **LURTAT** structure. The asymmetric unit of **AGAWIO** comprises one DABCO cation and a distorted tetrahedral $CuCl_4^{2-}$ anion, whereas the **LURTAT** asymmetric unit contains the same organic and inorganic units but also includes one water molecule, as shown in Figure 1.5.8. Crystal structure determination revealed that both forms crystallise in the monoclinic space group $P2_1/c$. Wei and Willet (2002) compared the crystal structures of the anhydrous to the monohydrate form in detail.

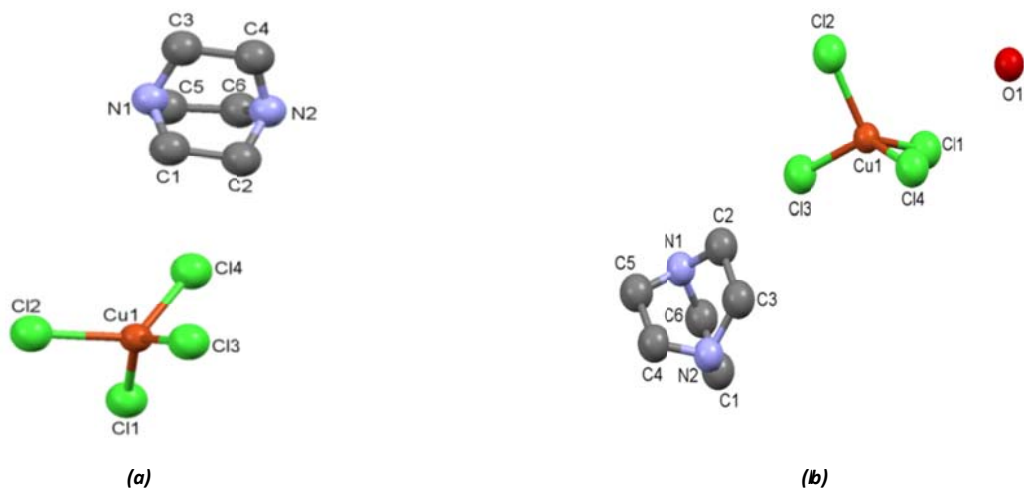


Figure 1.5.8. The asymmetric unit of (a) AGAWIO and (b) LURTAT. The hydrogen atoms are omitted for clarity.

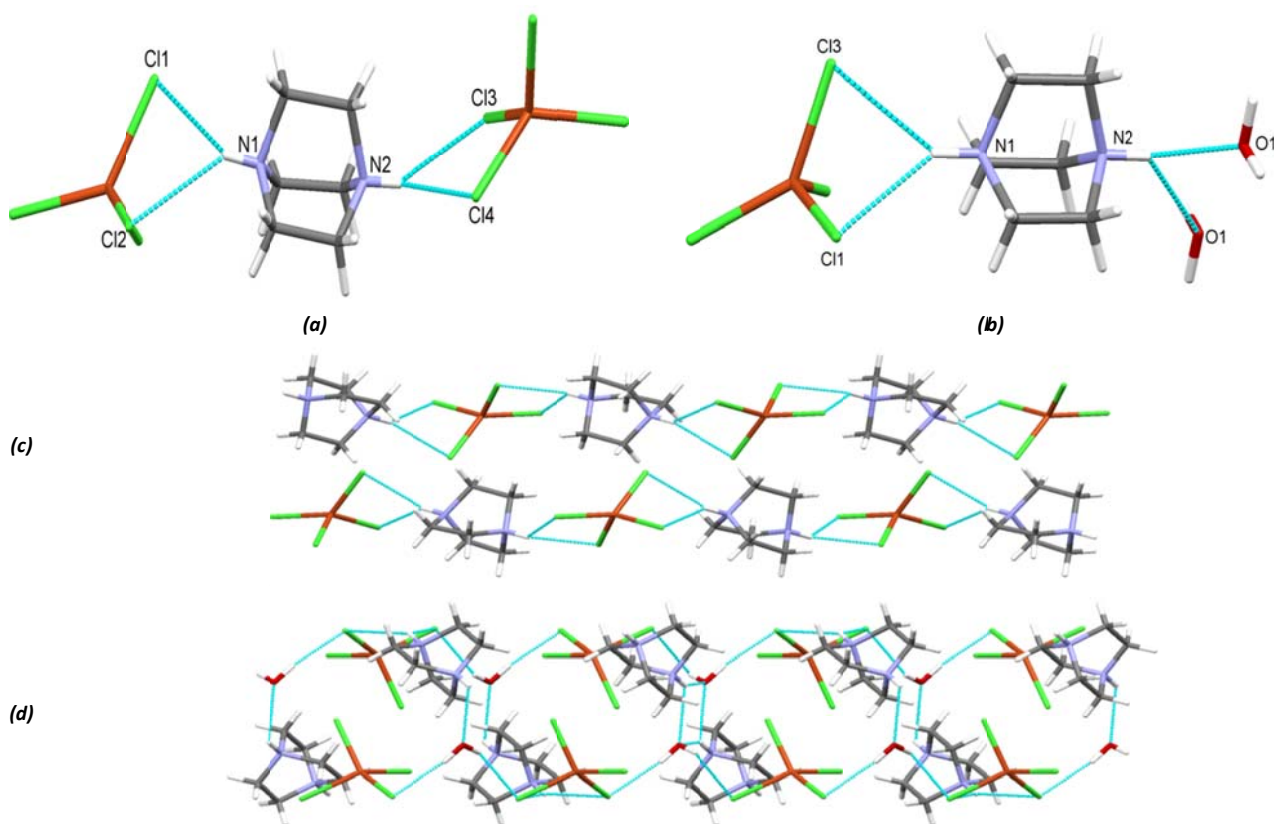


Figure 1.5.9. The hydrogen-bonded units of (a) AGAWIO and (b) LURTAT, respectively. The hydrogen bonding network in (c) AGAWIO and (d) LURTAT, respectively.

In the **AGAWIO** compound, the dication is bifurcately hydrogen-bonded on both sides, with each side forming bifurcated hydrogen bonds between a hydrogen atom on a nitrogen donor atom to two chlorido ligands that are part of individual CuCl_4^{2-} anions, as shown in Figure 1.5.9 (a). In the **LURTAT** compound, the dication is involved in bifurcated hydrogen bonding on both sides of the dication. On the one end, the hydrogen atoms on the donor nitrogen atom forms bifurcated hydrogen bonds to two chlorido atoms that form part of a single CuCl_4^{2-} anion. On the opposite end of the dication, bifurcated hydrogen bonding interactions exist between the hydrogen atom on the donor nitrogen to two oxygen atoms, each oxygen atom are from two individual water molecules, as shown in Figure 1.5.9 (b). The hydrogen bonding parameters are listed in Table 1.5.5.

Table 1.5.5. The hydrogen bonding parameters for AGAWIO and LURTAT.

AGAWIO		
D-H	d(H...A) (Å)	A
N2-H14	2.749	Cl3 [-x, 2-y, 1-y]
N2-H14	2.506	Cl4 [-x, 2-y, 1-z]
N1-H1	2.638	Cl1 [-x, ½+y, ½-z]
N1-H1	2.690	Cl2 [-x, ½+y, ½-z]
LURTAT		
D-H	d(H...A) (Å)	A
N1-H3	2.441	Cl1 [1-x, 1-y, 1-z]
N1-H3	2.811	Cl3 [1-x, 1-y, 1-z]
N2-H4	2.502	O1 [1+x, ½-y, 1.5-z]
N2-H4	1.966	O1 [1-x, -½+y, 1.5-z]

The hydrogen bonding network in **AGAWIO** consists of bifurcated hydrogen bonds between cations and anionic units, forming one-dimensional hydrogen-bonded chains, as shown in Figure 1.5.9 (c). The **LURTAT** structure forms a two-dimensional hydrogen-bonded network, as the water molecule is positioned between the bifurcated hydrogen bonding interactions that exist between the cationic and anionic species, forming ${}^+\text{N}-\text{H}\cdots\text{O}-\text{H}^+\cdots\text{Cl}-\text{Cu}$ links, instead of ${}^+\text{N}-\text{H}\cdots\text{Cl}-\text{Cu}$ as in the **AGAWIO** structure. Additional hydrogen bonding interactions, *via* $\text{O}-\text{H}^+\cdots\text{Cl}-\text{Cu}$ pathways, form a three-dimensional hydrogen-bonded network (Figure 1.5.9 (c)) and cause the CuCl_4^{2-} unit to become more distorted from tetrahedral geometry. The average *trans* Cl-Cu-Cl angles increase from 127.7° in the anhydrous form to 133.7° in the hydrated form. This distortion in the anionic units is in agreement with the study performed by Halvorson who showed that the distortion of the anion from tetrahedral to square planar is a direct result of the strength of the hydrogen bonding interactions to the anion (Halvorson *et al.* 1990). The hydrogen bonding holds the anions more rigidly in the hydrated form, with Cu-Cl distances of the anionic units averaging 2.238 Å to 2.249 Å.

The study done by Brammer (2002), which shows the tailoring of hybrid perhalometallate structures by the identification of hydrogen bonding sites, was done using the **AGAWIO** structure, amongst others.

ULAVAF (Zhang and Wang. 2011)

1,4-Diazoniabicyclo[2.2.2]octane tetrabromidocuprate(II) monohydrate

Formula: $\text{C}_6\text{H}_{14}\text{N}_2^{2+} \text{CuBr}_4^{2-} \cdot \text{H}_2\text{O}$

Synthesis: A 1:1 ratio of DABCO and CuBr_2 was added to a dilute solution of HBr and left to slowly evaporate, producing brown single crystals.

Structure: The **ULAVAF** structure is isostructural to the **LURTAT** structure and also crystallises in the monoclinic space group $P2_1/c$. The asymmetric unit comprises a distorted tetrahedral CuBr_4^{2-} anion, a diprotonated DABCO cation and a water molecule, as shown in Figure 1.5.10. The anionic unit exhibits Cu-Br bond lengths ranging from 2.3598(12) Å to 2.4070(12) Å and Br-Cu-Br angles ranging from 96.75° to 133.92° .

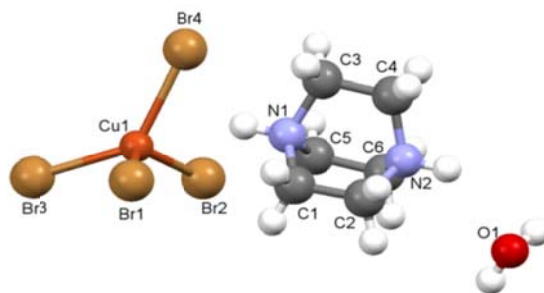


Figure 1.5.10. The asymmetric unit of ULAVAF.

The hydrogen-bonded unit of **ULAVAF** (Figure 1.5.11 (a)) contains the same hydrogen bonding interactions as the **LURTAT** compound mentioned previously. The anions and cations are linked by ${}^+\text{N}-\text{H}\cdots\text{Br}$, ${}^+\text{N}-\text{H}\cdots\text{O}$ and $\text{O}-\text{H}\cdots\text{Br}$ hydrogen bonds, forming one-dimensional chains along the *b*-axis. The chains are further linked by hydrogen bonds involving water molecules and the bromido ligands coordinated to the Cu^{2+} metal centres, to form a three-dimensional hydrogen-bonded network, as shown in Figure 1.5.11 (b). The hydrogen bonding parameters are given in Table 1.5.6.

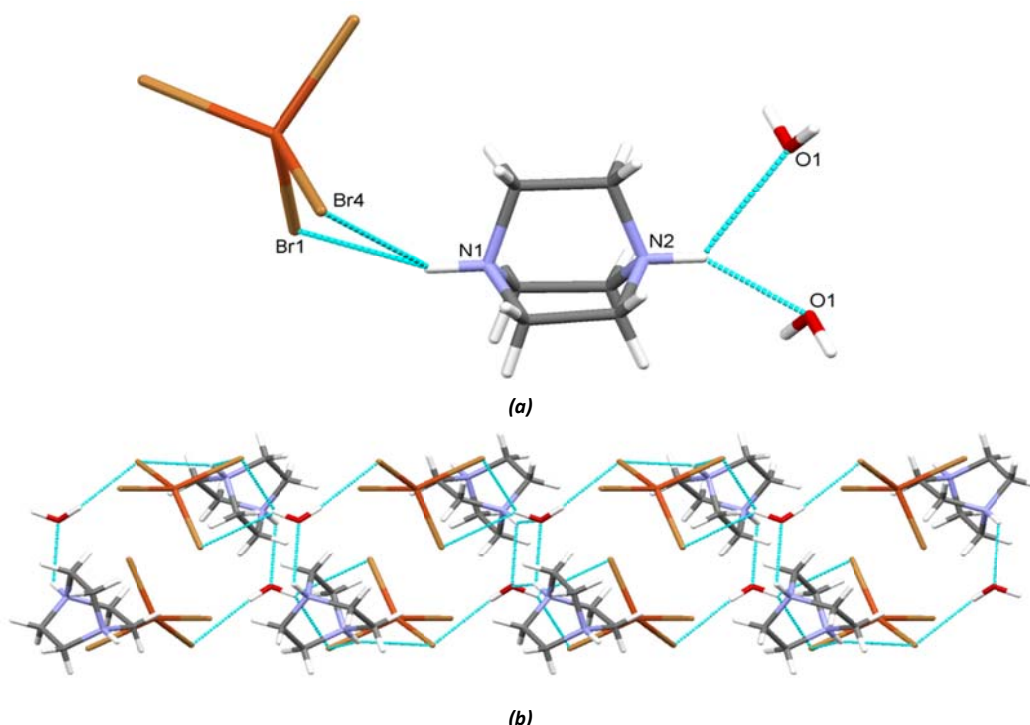


Figure 1.5.11. (a) The hydrogen-bonded unit of ULAVAF. (b) The three-dimensional hydrogen bonding network in ULAVAF.

Table 1.5.6. The hydrogen bonding parameters ULAVAF.

D-H	d(H \cdots A) (Å)	A
N1-H13	2.612	Br1
N1-H13	2.921	Br4
N2-H14	2.491	O1
N2-H14	1.983	O1 [1-x, 1-y, -z]

TOZFAP (Wei and Willet *et al.* 1996 & Zhang *et al.* 2010)

Bis(1,4-diazoniabicyclo[2.2.2]octane) diaqua trichloridocuprate(II) trichloride monohydrate

Formula: $2(\text{C}_6\text{H}_{14}\text{N}_2^{2+}) \text{CuCl}_3(\text{H}_2\text{O})_2 \cdot 3\text{Cl}^- \cdot \text{H}_2\text{O}$

Synthesis: A 2:1 ratio of DABCO and hydrated CuCl_2 was dissolved in dilute HCl solution and left to slowly evaporate at R.T, after which green crystals filtered and air-dried.

In the ferroelectric study conducted by Zhang (Zhang *et al.* 2010) it was seen from DSC studies that the bis(1,4-diazoniabicyclo[2.2.2]octane) diaqua trichloridocuprate(II) trichloride monohydrate structure undergoes a phase transition. The two different phases of the **TOZFAP** compound have been reported, one form occurs at room temperature, while a second form occurs below 230 K. The room temperature structure was reported twice in the literature, namely **TOZFAP** and **TOZFAP03** by Wei (1996) and Zhang (2010), respectively. Zhang (2010) also reported the low temperature structure, **TOZFAP01** and **TOZFAP02** that were determined at 193 K and 93 K respectively. For the purpose of this section the room temperature, **TOZFAP03** and low temperature **TOZFAP02** will be used. The room temperature structure crystallises in the orthorhombic space group $Pnma$ and the low temperature structure in the orthorhombic space group $Pna2_1$.

Structure: The asymmetric unit of the room temperature structure consists of a $\text{CuCl}_3(\text{H}_2\text{O})^-$ anionic unit, one diprotonated DABCO cation, a $\text{NH}_2(\text{CH}_2)_3$ unit, which is part of another diprotonated DABCO cation, with disorder occurring in one of the DABCO cations, three isolated chloride ions and a water molecule, as shown in Figure 1.5.12 (a). In the low temperature structure two diprotonated DABCO cations, one distorted trigonal bipyramidal $\text{CuCl}_3(\text{H}_2\text{O})_2^-$ anionic moiety, three isolated chloride ions and a water molecule are present in the asymmetric unit, as seen in Figure 1.5.12 (b), with the cation no longer being disordered.

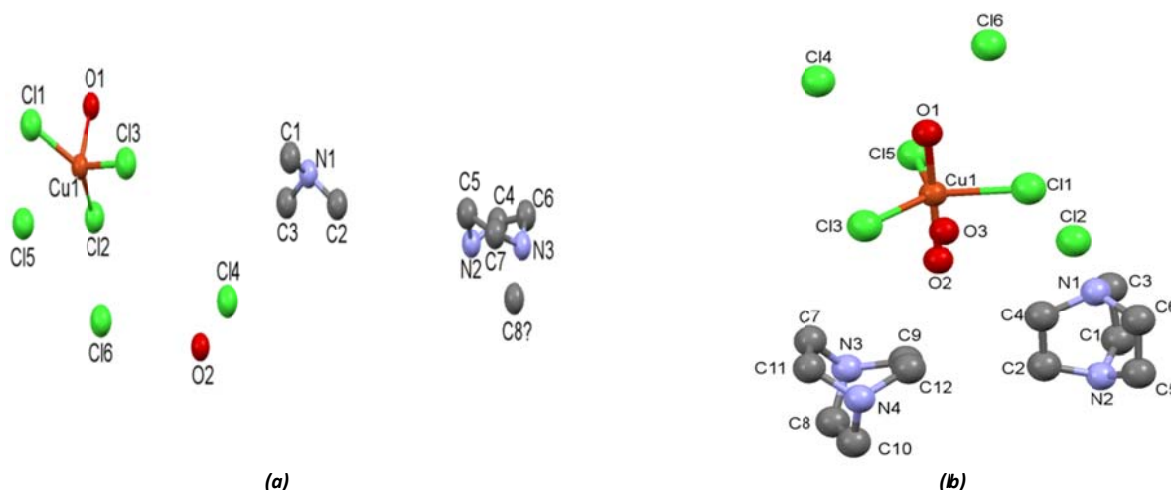


Figure 1.5.12. The asymmetric unit of the (a) room temperature, **TOZFAP03** and (b) the low temperature, **TOZFAP02** structures. Hydrogen atoms are omitted for clarity.

The anionic unit comprises three basal chlorido ligands and two water molecules in the axial position on the Cu^{2+} metal centre. The Cl-Cu-Cl equatorial bond angles are $132.45(6)^\circ$, $122.20(7)^\circ$ and $105.34(7)^\circ$, with average Cu-Cl equatorial bond lengths and Cu-O axial bond lengths of $2.376(2) \text{ \AA}$ and $1.967(3) \text{ \AA}$ respectively in **TOZFAP02**.

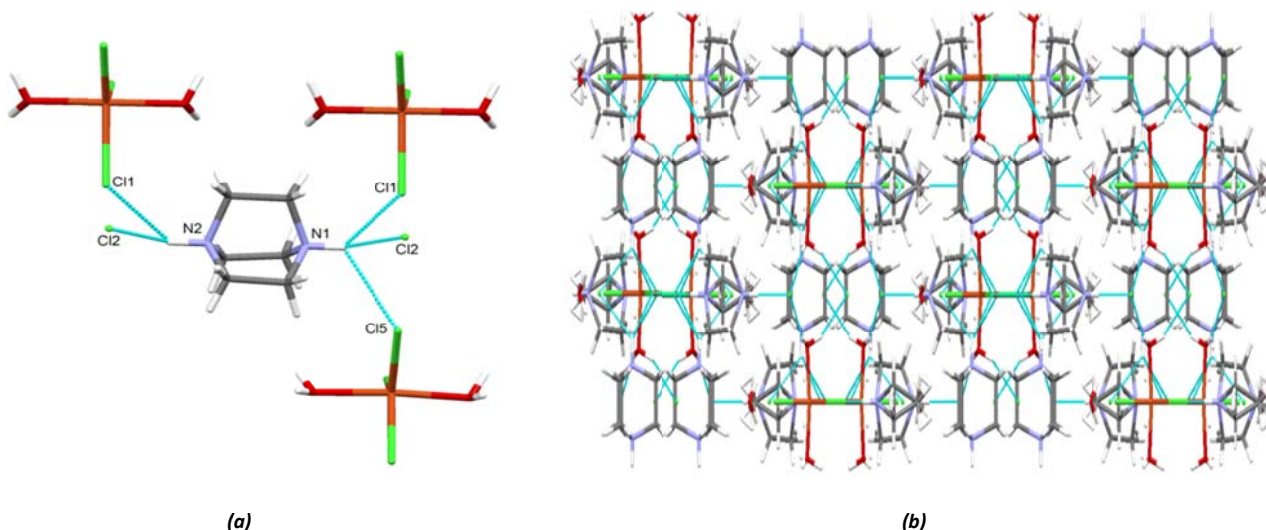


Figure 1.5.13. (a) The hydrogen-bonded unit of **TOZFAP02**. (b) The three-dimensional hydrogen bonding network that is present in both the room and low temperature structures as viewed down the a -axis.

The hydrogen bonding unit, as illustrated in Figure 1.5.13 (a) shows bifurcated and trifurcated hydrogen bonding interactions. On the one end of the dication, bifurcated hydrogen bonding interactions occur from a hydrogen atom to one acceptor chlorido ligand of a $\text{CuCl}_3(\text{H}_2\text{O})_2^-$ anion and also to a free chloride ion. On the opposite side of the dication, trifurcated hydrogen bonding interactions exist, as the hydrogen atom on the donor nitrogen atom forms hydrogen bonds to two individual chlorido ligands of two individual anions and also to a free chloride ion. The hydrogen bonding network that is formed is three-dimensional, as shown in Figure 1.5.13 (b) and includes classic, bifurcated and trifurcated hydrogen bonding. The equatorial chlorido ligands and coordinated water molecules partake in hydrogen bonding. The hydrogen bonding parameters are given in Table 1.5.5.

Table 1.5.7. The hydrogen bonding parameters for TOZFAP02.

D-H	d(H...A) (Å)	A
N2-H5	2.718	Cl1
N2-H5	2.547	Cl2
N1-H6	2.935	Cl1 [x, y, -1+z]
N1-H5	2.851	Cl5 [$\frac{1}{2}+x$, 1.5-y, z]
N1-H6	2.396	Cl2 [x, y, -1+z]

1.5.2. One-dimensional Polymeric Structures

The structures discussed in this section contain one-dimensional polymeric anionic moieties that form by the sharing of halogeno ligands between metal centres. The structures reported in the literature that fall within this category are listed in Table 1.5.2.

Table 1.5.8. Related one-dimensional structures reported in the literature. The CSD refcodes and components comprising the structures are indicated.

CSD refcode	Organic cation	Inorganic anion
FAWDAI	cyclopentylammonium	$(\text{Cu}_2\text{Cl}_6^{2-})_n$
FUTBUR	cyclohexylammonium	$(\text{Cu}_2\text{Br}_6^{2-})_n$
BAPYUM	cyclohexylammonium	$(\text{Cu}_2\text{Cl}_6^{2-})_n$
COPDOA01	piperazinium	$(\text{Cu}_2\text{Cl}_6^{2-})_n$

FAWDAI (Geiser *et al.* 1986)

Catena (cyclopentylammonium) bis(μ_2 -chlorido) chloridocuprate(II)

**Formula: $(\text{C}_5\text{H}_{12}\text{N}^+)_n$
 $0.5n(\text{Cu}_2\text{Cl}_6^{2-})$**

Synthesis: Cyclopentylamine and $\text{CuBr}_2 \cdot 2\text{H}_2\text{O}$ was dissolved in a mixture of dilute HCl and ethanol and left to slowly evaporate at R.T. Red platelets were isolated. The reagent ratio was not reported.

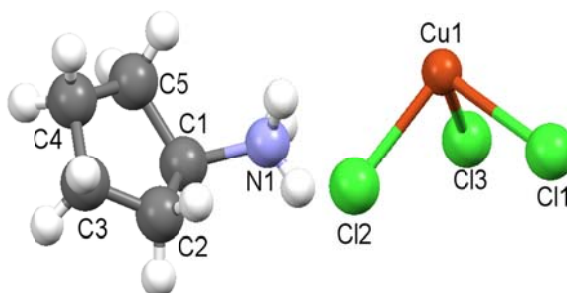


Figure 1.5.14. The asymmetric unit of FAWDAI.

Structure: The crystal structure was determined in the monoclinic space group $P2_1/n$. The asymmetric unit of **FAWDAI** comprises a protonated cyclopentylammonium cation and a CuCl_3^- unit, as shown in Figure 1.5.14. The CuCl_3^- units are linked *via* sharing of the halogeno ligands coordinated to the Cu^{2+} metal centres to form uniform bibriged chains. In the chain, each Cu^{2+} ion adopts a distorted square pyramidal geometry, with the Cu-X_{ax} bonds longer than the Cu-X_{eq} . Figure 1.5.15 (b) illustrates the polymeric anion, as well as the alternating terminal chlorido ligands along the polymer.

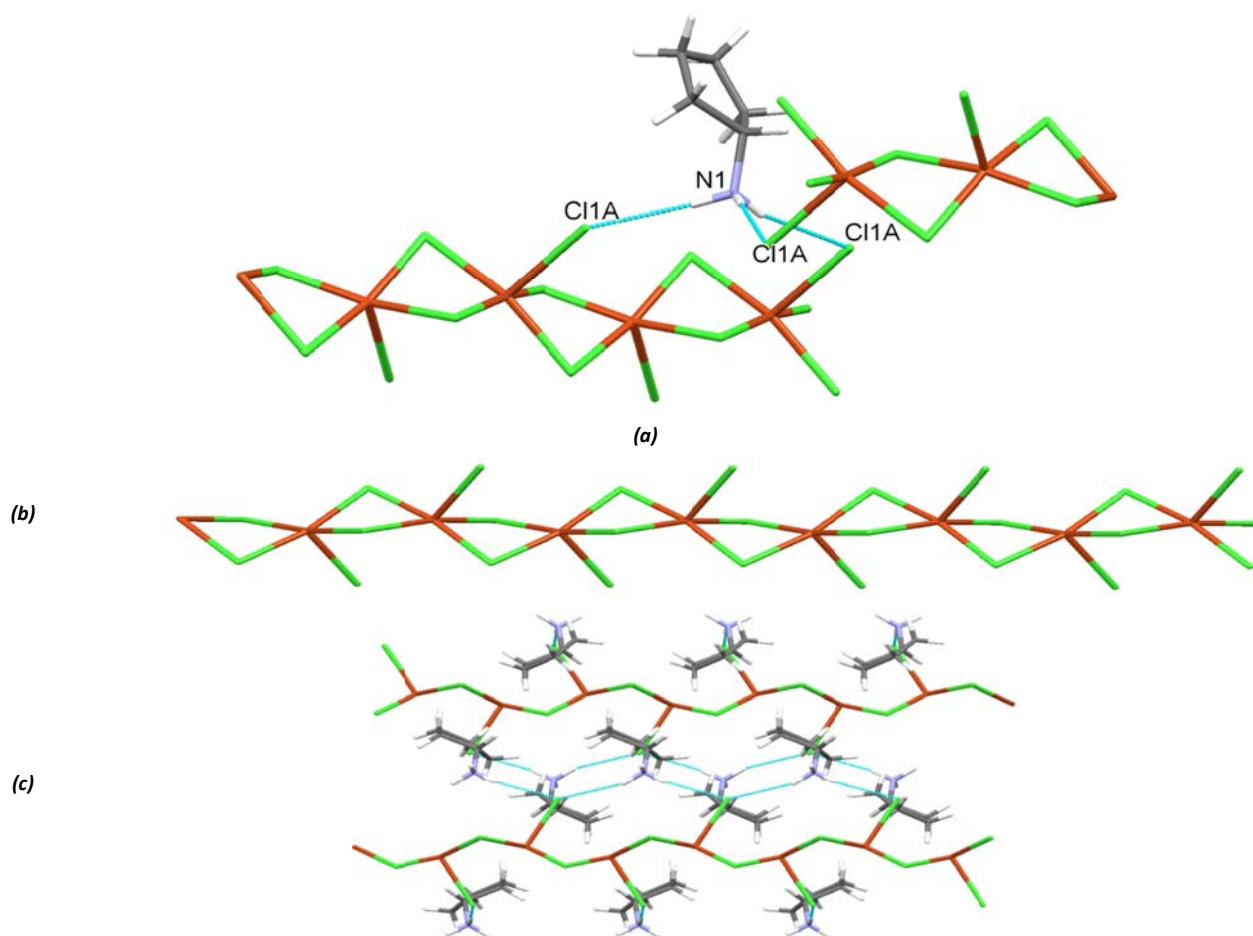


Figure 1.5.15 (a) The hydrogen-bonded unit of **FAWDAI**. (b) The polymer chain of **FAWDAI**. (c) The hydrogen bonding network of **FAWDAI** as viewed down the *a*-axis.

In Figure 1.5.15 (a), the hydrogen-bonded unit of **FAWDAI** is illustrated. The hydrogen bonding capability of the cation is fully satisfied, as classic, charge, assisted $^+\text{N-H}\cdots\text{Cl}^-\text{Cu}$ hydrogen bonding interactions form between the three hydrogen atoms on the donor nitrogen atom to two axial chlorido ligands on one polymer chain and a third interaction is formed to the axial chlorido ligand of a separate polymer chain. Bilayers of cations alternate with layers of polymers, with hydrogen bonding interactions linking cations to the terminal chlorido ligands of polymer chains. The packing of polymeric anionic chains and cations are shown in Figure 1.5.15 (c) The hydrogen bonding parameters are listed in Figure 1.5.9.

Table 1.5.9. The hydrogen bonding parameters for **FAWDAI**.

D-H	$d(\text{H}\cdots\text{A})$ (Å)	A
N1-H12	2.471	Cl1A [$\frac{1}{2}-x, \frac{1}{2}+y, 1.5-z$]
N1-H11	2.455	Cl1A [$\frac{1}{2}-x, \frac{1}{2}+y, 1.5-z$]
N1-H10	2.444	Cl1A [$-\frac{1}{2}+x, \frac{1}{2}-y, -\frac{1}{2}+z$]

The magnetic behaviour of **FAWDAI** was studied and three exchange constants were used to describe the magnetic behaviour, J , the intrachain exchange, J_c , the interchain interaction within sheets of neighbouring chains and J_a the interaction between sheets of chains. The strongest exchange coupling, J , occurs in the polymeric chain with a J value of +45 K, indicating ferromagnetic (FM) behaviour in the polymer chain. The

anionic component of **FAWDAI** is virtually identical to that of **BAPYUM**, resulting in an estimation of J_a and J_c values of -3×10^{-2} K and approximately 0.5 K respectively, these values are analogous to the magnetic data collected for **BAPYUM**.

FUTBUR (de Vries et al. 1987)

Catena(cyclohexylammonium) bis(μ_2 -bromido) bromidocuprate(II)

Formula: $(C_6H_{14}N^+)_n n(CuBr_3^-)_n$

Synthesis: The cyclohexylammonium salt was synthesised by the addition of concentrated HBr to cyclohexylamine. A 1:1 molar equivalent of the cationic salt and $CuBr_2$ was dissolved in a solution of partially deuterated n-propanol. On evaporation, black crystals were obtained.

Structure: The compound crystallises in the orthorhombic space group $P2_12_12_1$ and is isostructural to the chlorido analogue, **BAPYUM** discussed in the next section.

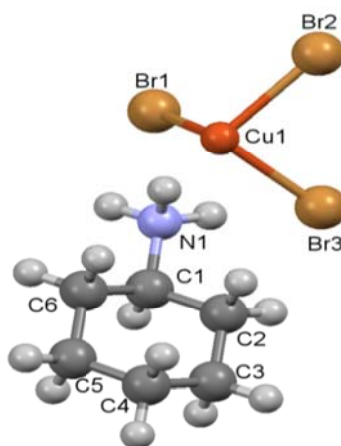


Figure 1.5.16. The asymmetric unit of FUTBUR. The hydrogen atoms were replaced by deuterium atoms.

The asymmetric unit of **FUTBUR** is made up of a singly protonated cyclohexylammonium cation that adopts a chair conformation and a $CuCl_3^-$ anion, as shown in Figure 1.5.16. The anionic units are linked together through edge-sharing of the halogeno ligands to form bridged Cu-Br-Cu angles of 82.31° and 83.49° , to form one-dimensional polymers that extend along the c -direction, with the Cu^{2+} metal centres adopting distorted square pyramidal geometries, as shown in Figure 1.5.17 (b). The polymers formed in **FAWDAI** are geometrically equivalent to the polymers of the **FUTBUR** structure, differing only in the halogeno component, where **FAWDAI** contains chlorido ligands and **FUTBUR** contains bromido ligands comprising the polymers.

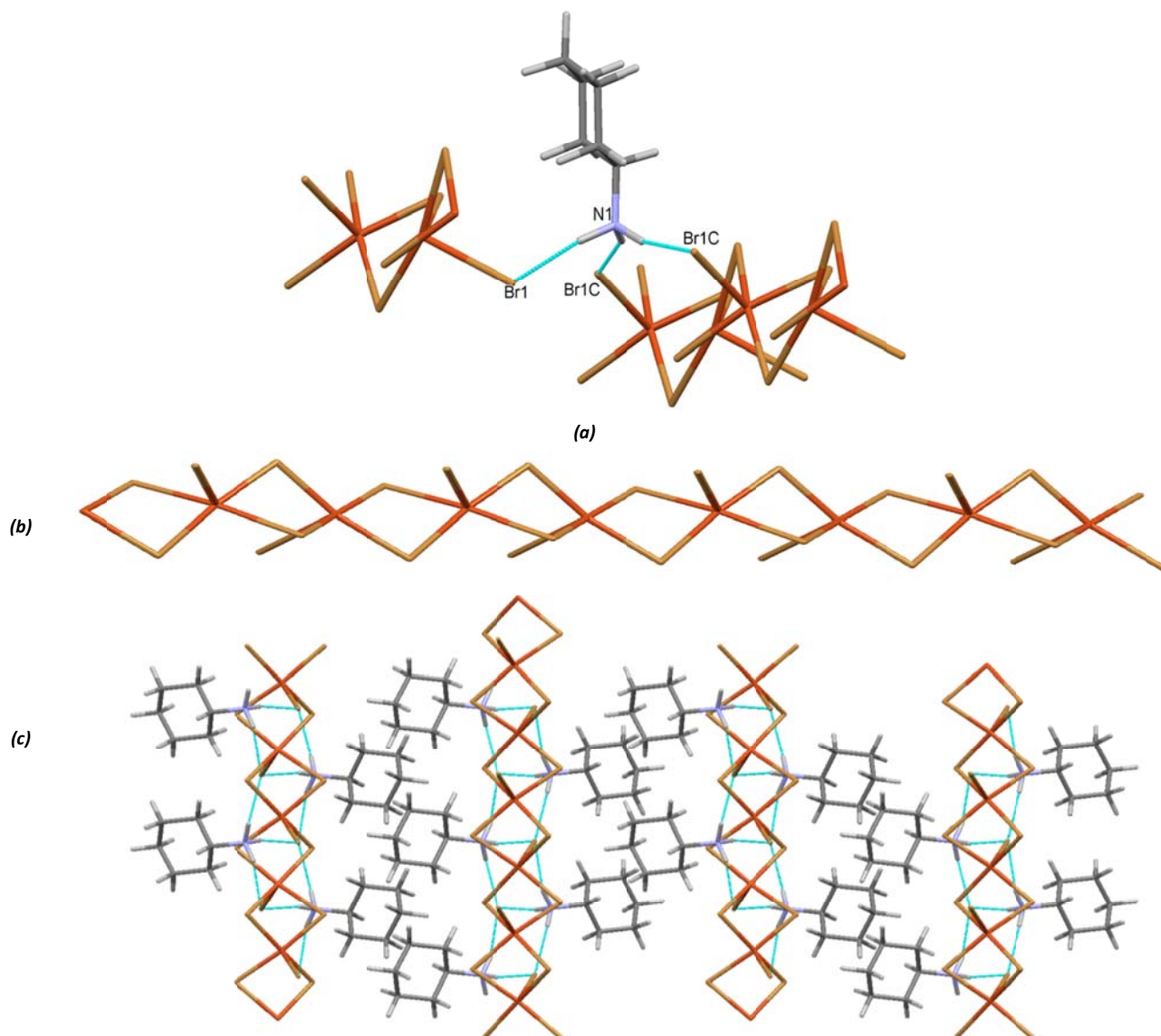


Figure 1.5.17 (a) The hydrogen-bonded unit of FUTBUR. (b) The polymer component of FUTBUR. (c) The one-dimensional hydrogen-bonded network present in the FUTBUR structure as viewed down the *b*-axis.

The hydrogen-bonded unit illustrated in Figure 1.5.17 (a) contains the same hydrogen bonding interactions as **FAWDAI** mentioned previously. In the structure bilayers of cations alternate with layers of polymers and hydrogen bonds link the cations to the terminal bromido ligands of the polymeric anions, to form one-dimensional hydrogen-bonded ladders, as illustrated in Figure 1.5.17 (c). The hydrogen bonding parameters are listed in Table 1.5.10.

Table 1.5.10. The hydrogen bonding parameters for FUTBUR.

D-H	$d(\text{H}\cdots\text{A})$ (Å)	A
N1-D3	2.435	Br1C [$\frac{1}{2}-x, 1-y, -\frac{1}{2}+z$]
N1-D2	2.444	Br1C [$\frac{1}{2}-x, 1-y, \frac{1}{2}+z$]
N1-D1	2.326	Br1C

In the polymeric chain, the symmetric Cu-X-Cu bridges have angles less than 90° and this allows for FM interactions between Cu^{2+} ions, in the chain (Willet and Landee. 1981). The **FUTBUR** compound is a good one-dimensional FM system with an exchange strength, $J = +55\text{K}$, with a Néel temperature, $T_N = 1.50\text{K}$ (Kopinga *et al.* 1982 and Phaff *et al.* 1984). By using neutron diffraction experiments, three-dimensional antiferromagnetic ordering was found to occur at an ordering temperature of $T_N = 1.56\text{K}$ (de Vries *et al.* 1987).

BAPYUM (Groenendijk *et al.* 1981)

Catena(cyclohexylammonium) bis(μ_2 -chlorido)chloridocuprate(II)

Formula: $(C_6H_{14}N^+)_n 0.5n(Cu_2Cl_6^{2-})$

Synthesis: The synthetic procedure is the same as that of the **FUTBUR** structure.

Structure: The structure of **BAPYUM** crystallises in the orthorhombic space group $P2_12_12_1$. The asymmetric unit of the **BAPYUM** structure consists of an isolated cyclohexylammonium cation and one $CuCl_3^-$ anionic unit, as illustrated in Figure 1.5.18. The **BAPYUM** structure is isostructural to the **FUTBUR** structure and therefore packs in the same manner as **FUTBUR**, as described previously. The asymmetric unit of **BAPYUM** contains the same cationic component as **FUTBUR** and a perchloridocuprate(II) anionic component.

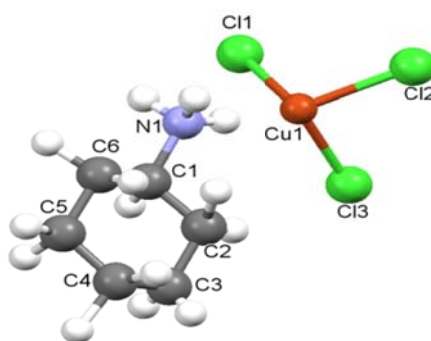


Figure 1.5.18. The asymmetric unit of the BAPYUM structure.

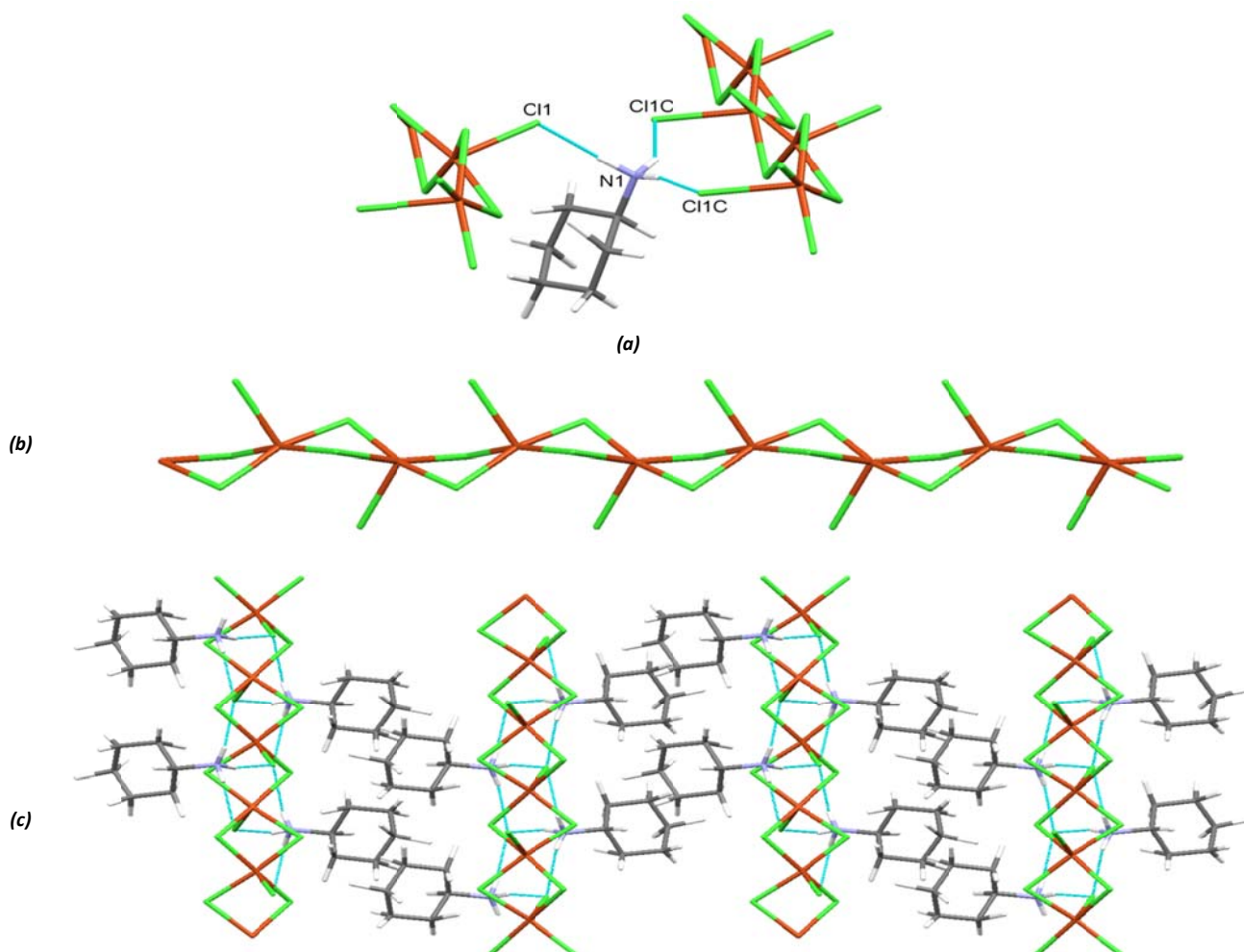


Figure 1.5.19. (a) The hydrogen bonded unit of BAPYUM. (b) The polymer chain of BAPYUM. (c) The one-dimensional hydrogen-bonded network of the BAPYUM structure as viewed down the *b*-axis.

The hydrogen-bonded unit comprises the same hydrogen bonding interactions as **FUTBUR**, as shown in Figure 1.5.19 (a). The polymeric component, as shown in Figure 1.5.19 (b) that make up the inorganic layer is separated by a bilayer of organic cationic units, as shown in Figure 1.5.19 (c). One-dimensional hydrogen-bonded ladders are formed between cations and anions, with the $^+\text{NH}_3$ groups of the cations pointing towards the inorganic moieties. The hydrogen bonding parameters are listed in Table 1.5.11.

Table 1.5.11. The hydrogen bonding parameters for BAPYUM.

D-H	d(H...A) (Å)	A
N1-H3	2.414	Cl1C [$\frac{1}{2}-x, 1-y, \frac{1}{2}+z$]
N1-H2	2.418	Cl1C [$\frac{1}{2}-x, 1-y, -\frac{1}{2}+z$]
N1-H1	2.144	Cl1

A FM intrachain exchange value, J , of +50 K was obtained for the **BAPYUM** compound by heat capacity measurements.

COPDOA01 (Battaglia *et al.*1988)

Catena(piperazinium) (μ_2 -chlorido) dichloridocuprate(II)

Formula: $(\text{C}_4\text{H}_{12}\text{N}_2^{2+})_n n(\text{Cu}_2\text{Cl}_6^{2-})$

Synthesis: A piperazinium salt solution was prepared by bubbling gaseous HCl through, or by the addition of concentrated HCl, to a solution of piperazine dissolved in diethyl ether. The piperazinium chloride salt was precipitated by evaporation of the solvent, washed with anhydrous ether and vacuum dried. A 2:1 ratio of piperazinium chloride and anhydrous CuCl_2 was dissolved in ethanol and left to slowly evaporate after which crystals of **COPDOA01** formed.

Structure: Three occurrences of catena(piperazinium) (μ_2 -chlorido) dichloridocuprate(II) were located in the literature, namely, **COPDOA** (Daoud and Qui. 1984), **COPDOA01** (Battaglia *et al.* 1988) and **COPDOA10** (Daoud *et al.* 1986). The **COPDOA** entry contains no coordinates and **COPDOA10** was reported with a suggested space group of $P\bar{1}$. Since **COPDOA01** is the most recent structure, it will be used in this discussion.

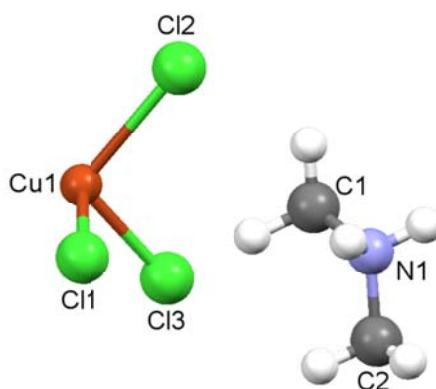


Figure 1.5.20. The asymmetric unit of COPDOA01.

Figure 1.5.20 illustrates the asymmetric unit of the **COPDOA01** structure, which contains a $\text{NH}_2(\text{CH}_2)_2$ fragment that forms part of the piperazinium dication, which adopts a chair conformation, as well as a CuCl_3^- unit that is part of a $\text{Cu}_2\text{Cl}_6^{2-}$ dimer unit. The coordination spheres around the Cu^{2+} ions adopt a distorted trigonal bipyramidal arrangement. The average Cu-Cl distances range from 2.265 Å to 2.321 Å, with longer Cu-Cl_{ax} bond lengths. The dimers are linked *via* edge-sharing of the halogeno ligands to form one-dimensional polymers. Each polymer chain is separated by a layer of cationic species, as seen in Figure 1.5.22.

The hydrogen-bonded unit of the **COPDOA01** structure consists of hydrogen bonding interactions on both ends of the dication. One hydrogen atom of the nitrogen atom, N1, partake in bifurcated hydrogen bonding to

two chlorido ligands (axial and equatorial) on the polymer anion, while the second hydrogen atom on nitrogen, N1, forms a hydrogen bonding interactions to the axial chlorido ligand of the same polymer. The hydrogen atom on nitrogen atom, N1A, forms bifurcated hydrogen bonding interactions to both the equatorial and axial chlorido ligands on the polymer, the second hydrogen atom on the nitrogen atom, N1A forms bifurcated hydrogen bonds to two chlorido ligands of two individual polymers, as shown in Figure 1.5.21. The packing occurs due to the interaction between the axial chlorido ligand and the $^+\text{NH}_2$ group of the piperazinium dication to form two-dimensional hydrogen-bonded sheets, as shown in Figure 1.5.22. The hydrogen bonding parameters are listed in Table 1.5.12.

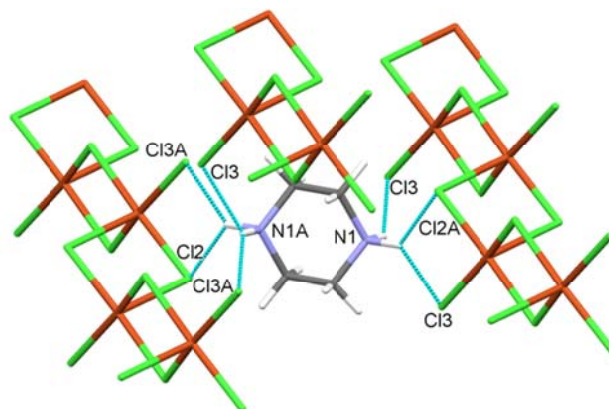


Figure 1.5.21. The hydrogen-bonded unit of COPDOA01.

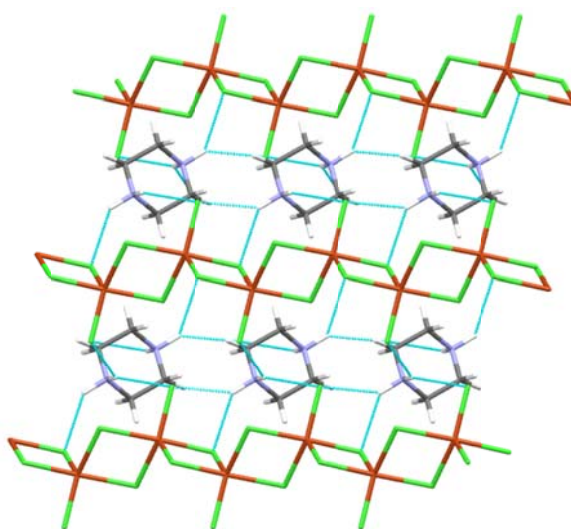


Figure 1.5.22. The hydrogen bonding network in COPDOA01 as viewed down the *b*-axis

Table 1.5.12. The hydrogen bonding parameters for COPDOA01.

D-H	d(H...A) (Å)	A
N1-H2A	2.647	Cl3
N1-H1	2.725	Cl2A [-x, 1-y, 1-z]
N1A-H2A	2.647	Cl3A [1-x, 1-y, 1-z]
N1A-H1A	2.363	Cl3A [1-x, -y, -z]
N1A-H1A	2.725	Cl2 [1+x, y, z]
N1A-H2	2.647	Cl3 [x, 1+y, z]
N1A-H1	2.363	Cl3 [x, 1+y, 1+z]

The magnetic behaviour of the compound has been studied by Battaglia (1988) and Daoud (1986). The χ vs T magnetic susceptibility data shows a maximum at T = 15 K and then decreases to zero. This is typical of an S = $\frac{1}{2}$ alternating AFM chain and the exchange parameters in the chain, J and J' were determined to be -13.35(7) K

and -7.6(3) K. AFM interactions also exist between chains making this a strong two-dimensional AFM system. Stone (2006) described the system as a two-dimensional AFM system.

1.5.3. Two-dimensional Structures

Only one two-dimensional structure of interest was located in the literature and is listed in Table 1.5.3. The perovskite structure, **YATYUP**, contains semi-coordinate bonds linking the CuCl_4^{2-} anionic components into a perovskite sheet.

Table 1.5.13. A related two-dimensional structure reported in the literature. The CSD refcode and components comprising the structure are indicated.

CSD refcode	Organic cation	Inorganic anion
YATYUP	cyclohexylammonium	CuBr_4^{2-}

YATYUP (Han. 2012)

Bis(cyclohexylammonium) tetrabromidocuprate(II)

Formula: $2(\text{C}_6\text{H}_{14}\text{N}^+) \text{CuBr}_4^{2-}$

Synthesis: Slow evaporation of an aqueous solution of 2:1 cyclohexylamine and CuBr_2 , containing a few drops of HBr to avoid hydrolysis of Cu^{2+} (Willet. 2004), yielded black crystals of the compound.

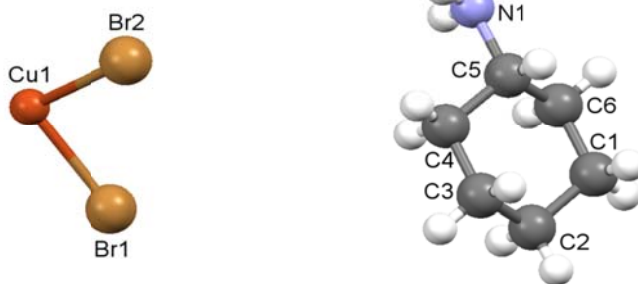


Figure 1.5.23. The asymmetric unit of YATYUP.

Structure: The asymmetric unit of **YATYUP**, as shown in Figure 1.5.23, comprises an isolated protonated cyclohexylammonium cation and a CuBr_2^- unit, which is part of a square planar CuBr_4^{2-} anionic unit. The cyclohexylammonium cations adopt a chair conformation and anions and cations pack in sheets that extend along the *ac*-plane, with the anionic layers separated by a bilayer of cations.

In the hydrogen-bonded unit of YATYUP, the hydrogen bonding capability of the donor nitrogen atom is satisfied, as all three hydrogen atoms partake in classic, charge assisted $^+\text{N}-\text{H}\cdots\text{Br}^--\text{Cu}$ bonds to three individual chlorido acceptor ligands of three separate CuBr_4^{2-} anions, as shown in Figure 1.5.24 (a). A hydrogen bonding network consisting of one-dimensional ribbons is formed. The ribbons are linked by classic, charge assisted $^+\text{N}-\text{H}\cdots\text{Br}^--\text{Cu}$ hydrogen bonds to form a two-dimensional hydrogen-bonded sheet, as shown in Figure 1.5.24 (b). The hydrogen bonding parameters are given in Table 1.5.14.

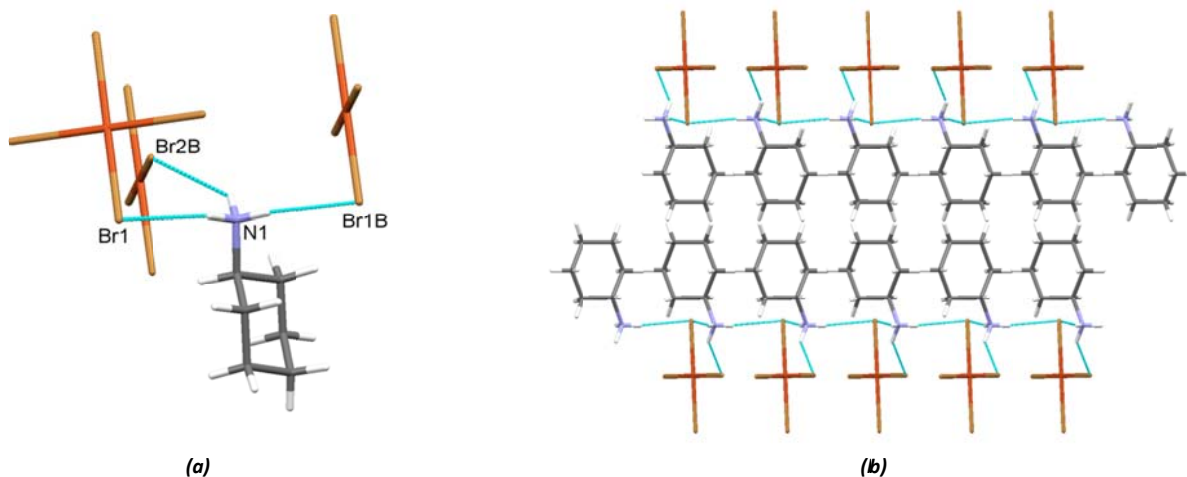


Figure 1.5.24. (a) The hydrogen-bonded unit of YATYUP. (b) The one-dimensional hydrogen bonding network of YATYUP as viewed down the b-axis.

Table 1.5.14. The hydrogen bonding parameters for YATYUP.

D-H	d(H...A) (Å)	A
N1-H3	2.604	Br1 [x, 1+y, -1+z]
N1-H2	2.559	Br1B [x, ½-y, -½+z]
N1-H1	2.623	Br2B [x, 1.5-y, -½+z]

1.6. Magnetochemistry

In recent years there has been considerable interest in the design of molecule-based magnetic materials in the field of material science due to the potential applications of these materials, including memory storage units of molecular size (Parthenopolous and Tentzepis. 1989) and carriers of quantum bits of information in quantum computers (Cavallini *et al.* 2005).

A molecule-based magnet can be described as a magnetic material in which the magnetism is due to a species that is molecular in nature, in contrast to conventional magnetic materials, which are typically metallic or metal oxides. Molecule-based magnets include organic systems, metal-based systems, heterobimetallic assemblies or mixed organic-inorganic systems (Yakhmi. 2009) and it is envisaged that their properties will allow for the development of new technologies in magnetic devices.

For the purposes of this study, molecule-based magnets are defined as molecular materials consisting of organic cycloalkylamines and inorganic copper(II) halide components. These types of materials have become of interest to scientists due to their ability to exhibit characteristics of both the organic and inorganic components. New magnetic materials can be designed by changing the organic component thereby tuning physicochemical properties of these materials (Konieczny *et al.* 2013). These compounds are expected to show low-dimensional structures and exhibit low-dimensional magnetic properties due to the tendency of the organic and inorganic compounds to pack in separate layers. The origin of magnetism in these materials, as well as the theoretical description of these possible magnetic characteristics is discussed in the following sections.

1.6.1. Magnetism

Materials that contain unpaired electrons, such as organic radicals or metal ions, are called paramagnetic materials. Paramagnetic centres carry magnetic moments or spins that are incorporated into the material, but a magnetic material also requires exchange between paramagnetic centres. In the materials of interest, the unpaired electrons are present on the Cu^{2+} metal ion. Each such paramagnetic centre has an associated magnetic dipole moment or spin, with associated spin angular momentum, S . In addition, the unpaired

electron also possesses orbital angular momentum, L. Both types of angular momenta are vectors and they interact through “spin-orbit coupling”. The resulting magnetic moment depends on the specific relative orientation of the spin and orbital components and this depends on the identity of the magnetic species. These magnetic moments may be measured as a function of temperature, when an applied magnetic field is set.

The magnetic moments or magnetisation, M, of materials is the magnetic dipole moment per unit volume when the material is exposed to an applied magnetic field, H, as given in equation 1.

$$M = \mu_0 \chi_m H \dots \dots \dots (1)$$

μ_0 is the vacuum permeability and χ_m is the magnetic susceptibility, which indicates the magnetisation induced by a unit applied magnetic field and H is the strength of the applied magnetic field, which is measured in Oersted (Oe).

In order to obtain the molar susceptibility of a material, the term χ_{mol} is substituted for χ_m , with $\chi_{mol} = \chi_m (M_r/10^3 \rho)$, where M_r is the molecular mass and ρ is the density of the material.

1.6.2. Magnetostructural Relationships

A fundamental understanding of the relationship between the magnetic behaviour and the structural characteristics of a material is one of the first steps in the design of magnetic materials. In the current study the specific arrangement of Cu^{2+} ions in a specific hybrid structure, as well as the covalent interactions, intermolecular interactions or close contacts in the structure may directly or indirectly influence the magnetic properties of the hybrid material. Hence the focus is on understanding the relationship between the structure and the magnetic properties of the material, also called magnetostructural relationships. The identification of the structure-property relationships requires the systematic synthesis of hybrid materials, the study of their structural characteristics and measurement of their magnetic properties.

Even though the magnetic moment carriers in all the materials in this study are the same, i.e. Cu^{2+} ions, the structural richness exhibited by perhalocuprate moieties result in different magnetic properties, because the magnetic properties are strongly correlated with the crystal structure of the material. In the hybrid materials the stereochemical flexibility of Cu^{2+} ions, as discussed previously, is combined with the bridging capability of the halogeno ligand and the templating effect of the organic cation. Even though no covalent interactions are present between the “magnetic” inorganic components and the cations in the hybrid structures, the cations have a templating role on the structure (Brammer *et al.* 2002), thereby indirectly influencing the magnetic properties of the material (Jeter and Hatfield. 1972). Thus the choice of the cation can determine the magnetic dimensionality and result in a magnetic dimensionality greater than zero, thus one- or two-dimensional.

The ultimate aim is the design of Cu^{2+} hybrid materials with specific magnetic properties through control of the structure using the principles of crystal engineering. This approach requires the systematic synthesis of magnetic materials, the study of their structural characteristics and measurement of their magnetic properties. The identification of structural trends and the correlation of these trends with their magnetic characteristics will, in the long term, allow for the prediction of magnetic properties.

1.6.3. Magnetic Structure vs Crystal Structure

In the ionic perhalocuprates studied, the inorganic component of the structure contains the magnetic moment carriers, as well as the inorganic ligands responsible for magnetic exchange between the metal ions, namely the halogeno ligands. The magnetic behavior of the hybrid material may be a function of the dimensionality of this inorganic sub-structure and the tendency of hybrid materials to form low-dimensional structures with one- or two-dimensional inorganic sub-structures make them ideal candidates for magnetic studies. In the inorganic units exchange occurs *via* the halogeno ligands that link the metal centers through coordination or semi-coordinate bonds.

A distinction should be made between the magnetic structure and crystal structure of a compound. The magnetic structure considers only the magnetic centers and considers possible exchange pathways between centers and the magnetic dimensionality refers to the dimensionality of the magnetic structure and is often different from the overall dimensionality of the structure. The magnetic dimensionality of the structure is determined by the exchange pathway present.

1.6.4. Magnetism of Cu²⁺ Ions

The current study focusses on the investigation of the magnetic properties of Cu²⁺ containing hybrid materials, specifically, the magnetic ordering of Cu²⁺ spins and the magnetic exchange that occurs between the d⁹ Cu²⁺ ions. The reasons for selecting Cu²⁺ are two-fold, firstly due to the Cu²⁺ ions forming a simple magnetic system and secondly, due to the structural richness offered by Cu²⁺ ions.

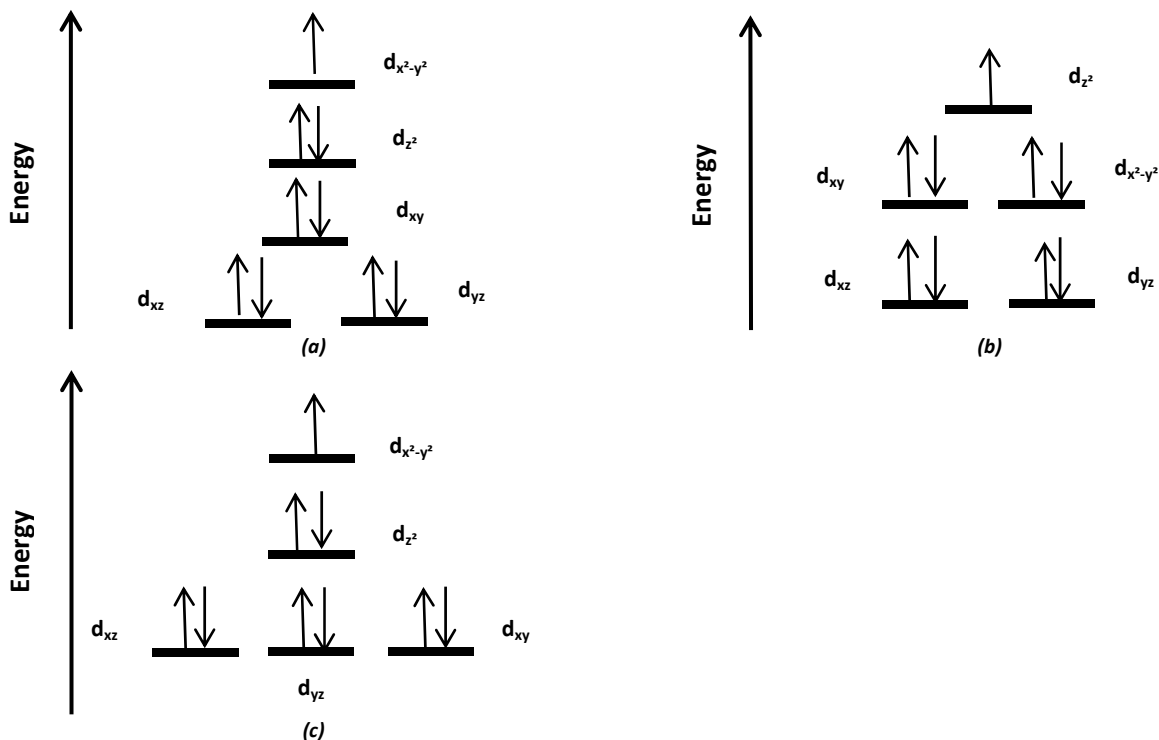
The orbital angular momentum contribution of Cu²⁺ is quenched. This and other factors¹ make it a simple magnetic system, with $S = \frac{1}{2}$ and therefore it is described by $S = \frac{1}{2}$ Heisenberg quantum models. The Cu²⁺ unpaired electron reside in either the d_{x²-y²} or d_{z²} orbitals depending on the geometry of the Cu²⁺ coordination species and these orbitals do not contribute to orbital angular momentum and are quenched.

1.6.4.1. Jahn-Teller Distortion

The theory of Jahn-Teller states that the energy in non-linear molecules is minimised when distortion occur to remove orbital degeneracy. Cu²⁺ complexes are often influenced by this effect. The distortion that occurs in the z-direction causes splitting of the t_{2g} and e_g energy levels.

The orbital of a metal ion containing the unpaired electron is called the magnetic orbital. Using the crystal field model, the half-filled vacant d orbitals may be either the d_{x²-y²} or d_{z²} orbitals in Cu²⁺ species. Distribution of the nine d electrons of Cu²⁺ places the unpaired electrons in the d_{x²-y²} orbital, which is the magnetic orbital for both square pyramidal and octahedral Cu²⁺ species, as shown in Scheme 1.6.1 (a) and (c), respectively, whereas the placement of the unpaired electron for trigonal bipyramidal geometries occurs in the d_{z²} orbital, as illustrated in Scheme 1.6.1 (b). Since Jahn-Teller distortion occurs along the z-axis, the orientation of the orbitals in the Cu²⁺ species can be identified. The orientation of the magnetic orbitals in the structure relative to the orbitals of ligands bonded to the magnetic ions, play an important role in the exchange interactions between magnetic ions in the structure.

¹ Cu²⁺ ions does not display any zero-field splitting and the g-value anisotropy is small (Carlin, 1986). A detailed discussion of these concepts is beyond the scope of this dissertation.



Scheme 1.6.1. Orbital energy level diagrams for Cu^{2+} ions in (a) square pyramidal, (b) trigonal bipyramidal and (c) octahedral geometries.

1.6.5. Magnetic Exchange Coupling

Magnetic exchange is a quantum mechanical phenomenon that is due to spin-spin correlations between paramagnetic centres.

The exchange interactions can be described as both electrostatic and quantum mechanic in nature and this was rationalised by Heisenberg and Dirac in 1926 (Heisenberg. 1928 and Dirac. 1926).

The coupling between magnetic ions can be described quantum mechanically by the pair-wise Hamiltonian (equation 2), as suggested by Heisenberg, Dirac and van Vleck (Dirac. 1926)

$$\hat{H}_X = -2J S_A \cdot S_B \dots \dots \dots (2)$$

where J is called the exchange parameter and S_A and S_B are the spins of two different sites. The energy of the exchange interaction depends on the relative orientations of the magnetic moments. Other forms of this Hamiltonian are also possible (Landee and Turnbull. 2014) and the form used should always be stated. The distribution among the energy states can be obtained using statistical thermodynamics, which allows for the calculation of bulk properties like magnetic susceptibility.

1.6.6. Paramagnetism

When a crystalline material contains a source of disordered unpaired electrons, for example an open shell metal ion and no exchange occurs between paramagnetic centres, a paramagnet is obtained. Each paramagnetic centre has a permanent magnetic dipole moment, m . When paramagnetic materials are placed in an applied magnetic field, the unpaired electrons begin to align with the field. The Curie Law, given in equation 3, explains this paramagnetic behaviour,

$$\chi_m = \frac{C}{T} \dots \dots \dots (3)$$

where C is called the Curie constant, which is measured in Kelvin and is unique for a specific material. T represents temperature, measured in Kelvin. A graphical representation of the Curie Law is given in Figure 1.6.1.

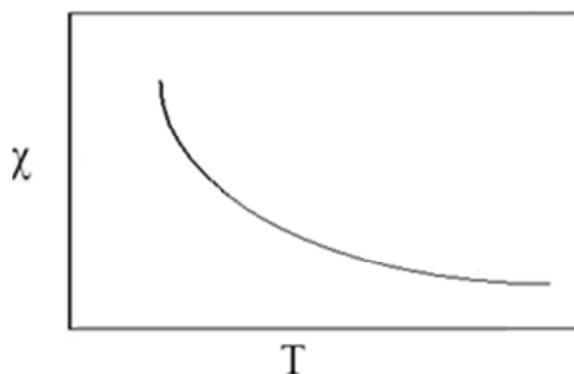


Figure 1.6.1. The graphical representation of the Curie law for paramagnetic interactions.

This law indicates that the susceptibility, χ , of paramagnetic materials in a field H is inversely proportional to temperature, i.e. the materials become more magnetised at lower temperatures in a field H , as thermal disorder decreases.

1.6.7. Ferromagnetism (FM) and Antiferromagnetism (AFM)

When exchange interactions occur between the magnetic dipoles of magnetic species, ordered magnetic materials may be obtained when paramagnetic materials are cooled in an applied magnetic field to sufficiently low temperatures. The temperature at which this ordering occurs is characteristic of a specific material. Two types of ordering may occur, namely antiferromagnetic (AFM) and ferromagnetic (FM) ordering.

1.6.7.1. Ferromagnetic Ordering

Ferromagnetic ordering occurs due to parallel coupling of magnetic dipoles in materials. Magnetic dipoles may order spontaneously when cooled down and the temperature at which this magnetic ordering occurs is known as the Curie temperature, T_c , named after Pierre Curie (1859-1906). If the material is cooled down in a magnetic field, when $T \rightarrow 0$ the ferromagnetic ordering is enhanced by the magnetic field. Above this temperature the material is paramagnetic and below this temperature the material exhibits FM behavior.

The limiting saturation, called the saturation magnetisation, may be reached if the magnetic field is strong enough. FM materials are not very common, but technologically important.

1.6.7.2. Antiferromagnetic Ordering

If spontaneous ordering of magnetic moments in an antiparallel fashion occurs during cooling, the material exhibits AFM ordering. When an AFM material is cooled in a magnetic field, the AFM ordering is opposed by the magnetic field, in contrast to what happens in the case of a FM material. In this case all the magnetic dipoles would tend to orient with the magnetic field, while a small percentage would be orientated opposite to the magnetic field, due to exchange coupling.

The temperature at which the material achieves an AFM ordered state is known as the Néel temperature, T_N and was named after Louis Néel (1904-2004). Above this temperature the material is paramagnetic implying that the thermal energy becomes large enough to dominate the magnetic ordering within the material and below this temperature AFM interactions dominate.

1.6.7.3. Metamagnetic Ordering

Both FM and AFM interactions may be present in the same crystalline material. It is possible to override the AFM interactions in a system that orders antiferromagnetically, to a FM ordered state by applying a strong magnetic field. A magnetic phase transition occurs, which is characteristic of a metamagnet.

1.6.8. Curie-Weiss Law

Analogous to the ideal gas law, the Curie Law is used to describe ideal magnetic behavior of paramagnetic systems. The Curie Law is expressed in terms of variables of H (applied magnetic field), M (magnetisation per mole) and T (temperature). Just as deviations from ideal gas behavior can be explained by means of the van der Waals equation, so can the deviations from ideal magnetic behavior be explained by the Curie-Weiss Law. These deviations occur due to the presence of an energy level whose population changes substantially over the measured temperature range, or due to magnetic interactions that occur between paramagnetic ions. These deviations can be taken into account by modifying the Curie Law into the Curie-Weiss Law given in equation 4.

$$\chi = \frac{C}{T - \theta} \dots\dots\dots (4)$$

A correction term, θ , is introduced into the equation and has units of temperature. The θ value can be obtained from the χ^{-1} vs T plot where the intercept does not pass through the origin for FM or AFM, as shown in Figure 1.6.2 (c). For $\theta < 0$ AFM interactions are indicated and FM interactions for $\theta > 0$. For a paramagnet, $\theta = 0$.

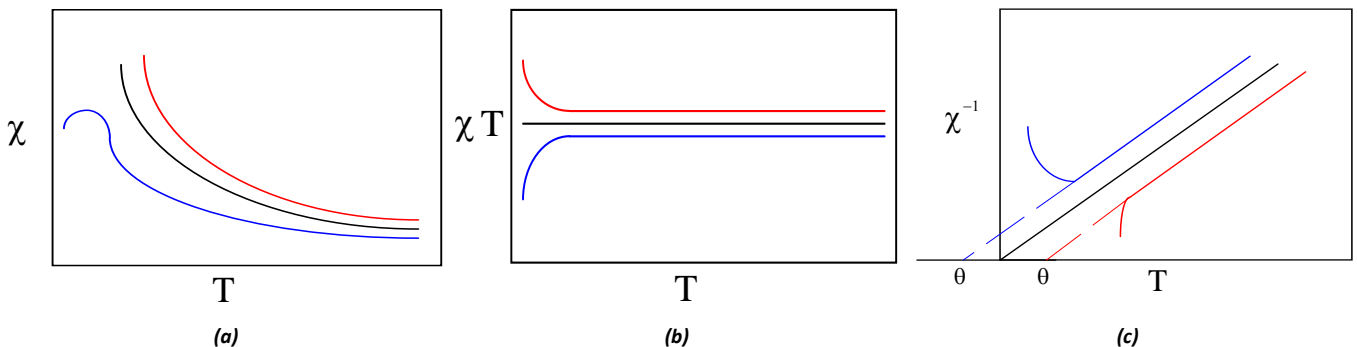


Figure 1.6.2. The plots of (a) χ , (b) χT and (c) χ^{-1} vs T that are governed by the Curie-Weiss law for paramagnetic (black), ferromagnetic (red) and antiferromagnetic (blue) materials. (Courtesy of Prof M. M Turnbull)

Schematic representations of different forms of the Curie-Weiss law for a PM, FM and AFM are shown in Figure 1.6.2. These figures allows for the distinction between these magnetic behaviours, based on the shape of the plot.

1.6.9. Exchange Parameter

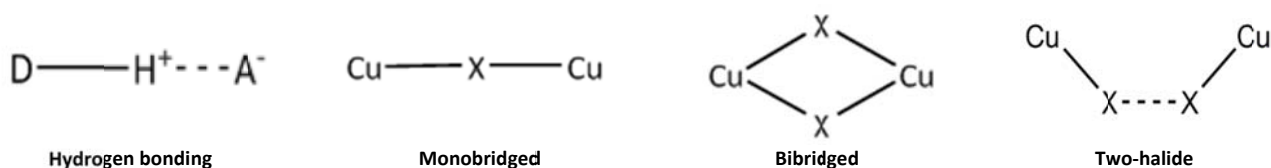
The exchange parameter, J, is a measure of the strength of the exchange between magnetic centres and the sign of J is important. In the ferromagnetic state all the spins are parallel, with $J > 0$ and only one ferromagnetic spin configuration is possible in a material. When coupling between the spins is anti-parallel, an AFM material is formed and $J < 0$ in these materials. More than one spin configuration may be present in an antiferromagnetic material. Ferrimagnets contain two different magnetic ions. Most ferrimagnets occur in oxides of transition metals such as spinels and garnets. The different types of magnetic spin ordering, which may occur in magnetic materials, are illustrated schematically in Scheme 1.6.2.



Scheme 1.6.2. The schematic representation of the possible spin interactions.

1.6.10. Superexchange

Magnetic exchange may occur through different mechanisms, one of which is relevant to the current study and is known as superexchange. The superexchange pathways possible in the hybrid materials investigated in this study include hydrogen bonding, although very weak and the stronger monobridged, bibridged and two-halide exchange, also known as the double-exchange pathway (Landee and Turnbull. 2013). These pathways are illustrated schematically in Scheme 1.6.3.



Scheme 1.6.3. The various types of magnetic exchange pathways relevant to the current study.

The superexchange pathway is an exchange coupling that exists between electron spin centres that require the orbitals of an intermediate species, for example a ligand bridging two paramagnetic centres, for the process to occur and is also known as indirect exchange. The magnetic coupling depends on the number and type of atoms between the spin carriers, as well as the geometric parameters of the bridging units (Turnbull *et al.* 2005). Exchange interactions between paramagnetic centres may result in long range magnetic ordering, a cooperative interaction between ions, which results in the formation of FM or AFM materials, as discussed previously. The monobridged pathway forms when two metal centres are linked by one halogeno ligand and the bibridged pathway when two halogeno ligands bridge two metal centres and is generally asymmetric as opposite Cu-X bonds differ in length (Landee and Turnbull. 2013). The monobromido bridging complexes are less common than monochlorido bridged complexes (Landee and Turnbull. 2013). Simple orbital models can be used to explain the magnetic exchange interactions as discussed below.

1.6.11. Orbital Models

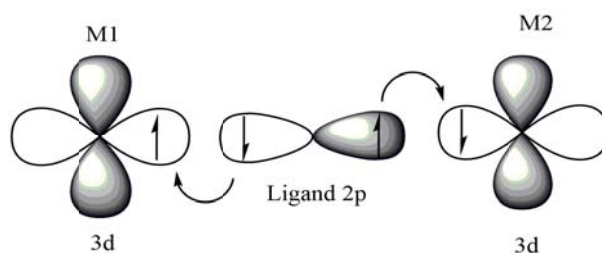
1.6.11.1. Through-bond Exchange

This superexchange pathway is based on orbital overlap between the metal orbitals and the orbitals of a non-magnetic ligand. In the case of this study the non-magnetic ligands are either chlorido or bromido ligands. For now we assume each metal atom has only one unpaired electron, as is the case with Cu²⁺ ions.

Through-bond exchange, also known as superexchange, refers to the scenario where two magnetic ions interact through mono- or bibridging ligands. This interaction may occur when metal ion and ligand orbitals overlap linearly or perpendicularly to each other.

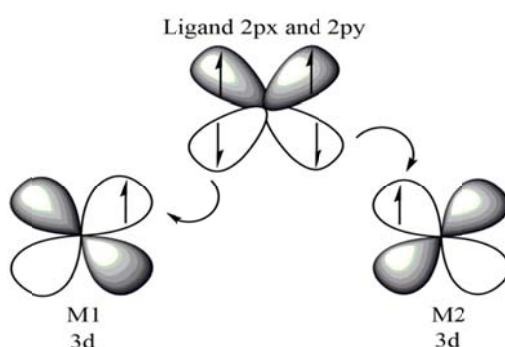
The scenario for linear (180°) overlap in an M-L-M bond is illustrated in Scheme 1.6.4. In this case AFM interactions result between the two metal centres M1 and M2 and this can be explained as follows. Consider M1 to contain an unpaired electron in its $d_{x^2-y^2}$ orbital with an “up” spin orientation. The electron density which is donated from the ligand to M1 would adopt spin “down” due to Pauli’s Exclusion Principle. Since the ligand also donates electron density to the second metal, M2, this electron density donated from the ligand would

have spin “up” and the unpaired electron on M2 will have a spin “down” orientation. The effect is that the two metals have opposite spins, thus AFM.



Scheme 1.6.4. The schematic representation of linear exchange between magnetic metal ion orbitals and a ligand orbital.

When the M-L-M bond is orthogonal (90°), the interaction between the metals is ferromagnetic. Considering Scheme 1.6.5, electron density from the ligand $2p_x$ or $2p_y$ orbitals is transferred to both metal atoms. When the transfer occurs to the $d_{x^2-y^2}$ orbital on metal M1, with spin “up”, the ligand will have a “down” spin orientation. The donation of the ligand to metal M2 also results in spin “up” on M2, hence a FM interaction is formed between M1 and M2.



Scheme 1.6.5. The schematic representation of the exchange process for orthogonal M-L-M overlap of magnetic ion orbitals and ligand orbitals.

1.6.11.2. Through-space Exchange

The double-halide superexchange pathway can be represented as an $M-X\cdots X-M$ interaction, where M represents a magnetic metal ion and X a halogeno ligand. The exchange pathway is typically AFM (Snively *et al.* 1979) and often occurs between isolated anions. This exchange occurs by the non-binding overlap of the orbitals of the two halogeno ligands through space and results in weaker exchange interactions for chlorido compounds than bromido compounds, if the compounds are isostructural (Lande and Turnbull. 2013). DFT spin density calculations (Awwadi *et al.* 2013) show that a significant spin density is present on the halogeno ligands bonded to a Cu^{2+} ion and it was shown that a spin end-cap is present along the Cu-X bond, which explains the antiferromagnetic double-halide exchange pathway. The spin end-cap results in a less negative electrostatic potential on the halogeno ligand end and less repulsion between the negatively charged halogeno ligands. The calculated spin density on a bromido anion is larger than that of a chlorido ligand bonded to a Cu^{2+} ion, which explains why the double bromido exchange, $Cu-Br\cdots Br-Cu$, is stronger than the double chlorido exchange $Cu-Cl\cdots Cl-Cu$.

The interhalide distance, the Cu-X \cdots X angle and the Cu-X \cdots X-Cu torsion angle (Turnbull *et al.* 2005) are the predominant factors in determining the strength of the exchange and not the inter-copper distance (Li *et al.* 2007). The exchange is the strongest when the Cu-X \cdots X angle is 180° .

M-X \cdots X-M contacts in crystal structure are not as common as halogen bonding interactions of the type C-X \cdots X-M (Awwadi *et al.* 2013). These M-X \cdots X-M contacts are, however, important because they provide a magnetic exchange pathway and hence play an important role in the magnetic properties of the material. This exchange may be very strong and in the order of -234 K (Butcher *et al.* 2009).

1.7. Research Aims and Objectives

The perchlorido/bromidocuprate(II) compounds of interest will be synthesised using existing and new synthetic techniques. The strategy of synthetic techniques needs to be adjusted accordingly by varying stoichiometric ratios of the reagents, as well as the environmental reaction conditions.

Single crystal X-ray diffraction (SXRD) will be employed to structurally characterise the materials. Powder X-ray diffraction (PXRD) will be used as a finger printing technique. The purity of samples used for magnetic characterisation will be confirmed by the comparison of the experimental powder patterns and the powder patterns calculated from known structures.

A Super Quantum Interference Device (SQUID) will be used to measure the magnetic susceptibility of selected materials used in this study, specifically to obtain information with regards to magnetic interactions at low temperatures. The magnetic data obtained will be fitted to the quantum mechanical models in order to obtain the exchange constants of the compounds. The magnetic characteristics obtained for these compounds will be correlated to their structure properties and superexchange pathways will be noted and trends identified.

1.8. References

Allen, F. R. (2002). *Acta Cryst.* B58, 380-388.

Aullón, G., Bellamy, D., Brammer, L., Bruton, E.A. and Orpen, A.G. (1998). *Chem. Commun*, 653-654.

Awwadi, F.F., Taher, D., Maabreh, A., Alwedian, F.Z., Al-Ebaisat, H., Rüffer, T. and Lang, H. (2013). *Struct. Chem.* 24, 401-408.

Battaglia, L.P., Corradi, A.B., Geiser, U., Willet, R.D., Motori, A., Sandrolini, F., Antolini, L., Manfredini, T., Menabue, L. and Pellacani, G.C. (1988). *J. Chem. Soc. Dalton Trans*, 265-271.

Billing, D.G. and Lemmerer, A. (2007). *CrystEngComm.* 9, 236-244.

Billing, D.G. and Lemmerer, A. (2009). *CrystEngComm.* 11, 1549-1562.

Bleaney, B. and Bowers, K.D. (1952). *Proc. R. Soc. London, Ser. A.* 214, 451-465.

Brammer, L., Bruton, E.A. and Sherwood, P. (2001). *Cryst. Growth Des.* 1, 277-290.

Brammer, L., Swearingen, J.K., Bruton, E.A. and Sherwood, P. (2002). *PNAS.* 99. 8, 4956-4961.

Brammer, L. (2004). *Chem. Soc. Rev.*, 33. 476-489.

Butcher, R.T., Novoa, J.J., Ribas-Ariño J., Sandvik, A.W., Turnbull, M.M., Landee, C.P., Wells, B.M. and Awwadi, F.F. (2009). *Chem. Commun*, 1359-1361.

Carlin, R.L. (1986). *Magnetochemistry*. Springer-Verlag. Berlin, 68.

Cavallini, M., Gomez-Segura, J., Ruiz-Molina, D., Massi, M., Albonetti, C., Rovira, C., Veciana, J. and Biscarini, F. (2005). *Angew. Chem, Int. Ed.* 44, 888-892.

Daoud, A. and Qui, D.T. (1984). *Acta Cryst., Sect A: Found Cryst.* 40, C234.

Daoud, A., Salah, A.B., Chappert, C., Renard, J.P., Cheikhrouhou, A., Duc, T. and Verdagner, M. (1986). *Phys. Rev. B, Condens. Mat.* 33, 6253-6260.

- Desiraju, G.R. (1989). *Crystal Engineering: The Design of Organic Solids*, Elsevier, Amsterdam.
- Desiraju, G.R. (1995). *Angew. Chem. Int. Ed. Engl.* 34, 2311-2327.
- de Vries, G.C., Helmholdt, R.B., Frikkee, E., Kopinga, K., de Jonge, W.J.M. and Godefroi, E.F. (1987). *J. Phys. Chem. Solids.* 48, 803-811.
- Dirac, P.A.M. (1926). *Proc. R. Soc. London. Ser. A.* 112, 661-677.
- Geiser, U., Gaura, R.M., Willet, R.D. and West, D.X. (1986). *Inorg. Chem.* 25, 4203-4212.
- Groenendijk, H.A., Blote, H.W.J., van Duyneveldt, A.J., Gaura, R.M., Landee, C.P. and Willett, R.D. (1981). *Physica, Pays-Bas.* 106, 47-58.
- Guha, S., Haight, R.A., Bojarczuk, N.A. and Kisker, D.W. (1997). *J. Appl. Phys.* 82, 4126-4128.
- Halvorson, K., Patterson, C. and Willett, R.D. (1990). *Acta Cryst. Sect. B.* 46, 508-519.
- Han, M.T. (2012). *Acta Cryst. Sect E: Struct. Rep. Online.* 68, m448.
- Heisenberg, W. (1928). *Z. Phys.* 38, 411-426.
- Housecroft, C.G. and Sharp, A.G. (2008). *'Inorganic Chemistry'*. Pearson Education Ltd., Essex, 3rd edn, 737.
- Jeter, D.T. and Hatfield, W.E. (1972). *J. Inorg. Nucl. Chem.* 34, 3055-3060.
- Johnston, D.C., Kremer, R.K., Troyer, M., Wang, X., Klümper, A., Bud'ko, S.L., Panchula, A.F. and Canfield, P.C. (2000). *Phys. Rev. B.* 61, 9558-9606.
- Knutson, J.L. and Martin, J.D. (2005). *Inorg. Chem.* 44, 4699-4705.
- Kojima, A., Teshima, K., Shirai, Y. and Miyasaka, T. (2009). *J. Am. Chem. Soc.* 131, 6050-6051.
- Konieczny, P., Pelka, R., Zieliński, P.M, Wasiutyński, T, Pinkowicz, D. and Sieklucka, B. (2013). *EPJ Web of Conferences.* 40, 14002.
- Kopinga, K., Tinus, A.M.C. and de Jonge, W.J.M. (1982). *Phys. Rev. B.* 25, 4685-4690.
- Landee, C.P. and Turnbull, M.M. (2013). *Eur. J. Inorg. Chem.* 2266-2285.
- Landee, C.P. and Turnbull, M.M. (2014). *Review: A gentle introduction to magnetism: units, fields, theory and experiments, Journal of Coordination Chemistry.* 63:3, 375-439.
- Li, L., Turnbull, M.M., Landee, C.P., Jornet, J., Deumal, M., Novoa, J.J. and Wikaira, J.L. (2007). *Inorg. Chem.* 46, 11254-11265.
- Mareque Rivas, J.C. and Brammer, L. (1998). *Inorg. Chem.* 37, 4756-4757.
- Mitzi, D. B. (1999). *Prog. Inorg. Chem.* 48, 1-12.
- Mitzi, D.B., Chondroudis, K. and Kagan, .C.R. (2001). *IBM J. Res. & Dev.* N1. 45, 29-38.
- Mitzi, D.B. (2004). *J. Mater. Chem.* 14, 2355-2365.
- Parthenopolous, D.A. and Tentzepis, P.M. (1989). *Science.* 245, 843-845.

- Phaff, A.C., Swüste, C.H.W., de Jonge, W.J.M., Hoogerbeets, R. and van Duyneveld, A.J. (1984). *J. Phys. C: Solid State Phys.* 17, 2583-2594.
- Riley, M.J., Neill, D., Berhardt, P.V., Byriel, K.A. and Kennard, C.H.L. (1998). *Inorg. Chem.* 37, 3635-3639.
- Schmidt, G.M. (1971). *Pure. Appl. Chem.* 27, 647-678.
- Smith, D.W. (1976). *Coord. Chem. Rev.* 21, 93-158.
- Snively, L.O., Seifert, P.L., Emerson, K. and Drumheller, J.E. (1979). *Phys. Rev. B: Condens. Mat.* 20, 2101-2104.
- Steiner, T. (2002). *Angew. Chem. Int. Ed.* 41, 48-76.
- Stone, M.B., Broholm, C., Reich, D.H., Tchernyshyov, O., Vorderwisch, P. and Harrison, N. (2006). *Phys. Rev. Lett.* 96, 257203.
- Turnbull, M.M., Landee, C.P. and Wells, B.M. (2005). *Coord. Chem. Rev.* 249., 2567-2576.
- Wei, M. and Willett, R.D. (1996). *Inorg. Chem.* 35, 6381-6385.
- Wei, M. and Willett, R.D. (2002). *J. Chem. Cryst.* 32, 439-445.
- Willett, R.D. and Landee, C.P. (1981). *J Appl. Phys.* 52, 2004-2009.
- Willett, R.D. (2004). *Inorg. Chem.* 43, 3804-3811.
- Yakhmi, J.V. (2009). *Bull. Mater. Sci.* 32, 217-225.
- Zhang, W., Ye, H-Y., Cai, H-L., Ge, J-Z., Xiong, R-G. and Huang, S.D. (2010). *J. Am. Chem. Soc.* 132, 7300-7302.
- Zhang, Y. and Wang, B. (2011). *Acta. Cryst. Sect E: Struct. Rep. Online.* 67, m371.

Chapter Two: Experimental Techniques

The experimental procedures employed to prepare the materials of interest will be highlighted in the current chapter. The percentage yield of each compound was not reported specifically, due to the fact that not all compounds could be obtained in a pure enough form for an accurate determination of the yield. In addition, the theory underpinning the experimental techniques and methods employed for structural and magnetic property characterisation will be discussed in this chapter.

2.1. Synthetic Procedures

2.1.1. Materials

All starting materials used were of reagent quality and were used as purchased, as no further purification was deemed necessary.


2.1.2. Synthesis

Table 2.1. The novel compounds successfully synthesised and characterised in this study, as well as those reported in literature. The reported compounds resynthesised in this study are highlighted below.

Cycloalkylamine component	CuCl ₂		CuBr ₂	
	Novel	Literature	Novel	Literature
cyclopentylamine	X	FAWDAI	XX	
cyclohexylamine	-	BAPYUM	-	FUTBUR
cycloheptylamine	XX	-	X Bromide salt, X	-
piperazine	XX	NUTDUB NUTDOV	-	
DABCO	-	TOZFAP	-	ULAVAF

Key: X- synthesised and structural characterization

XX-synthesised, structural and magnetic characterization

 Re-synthesised and magnetic characterization

A matrix of the ionic hybrid materials that may be obtained through the combination of the selected organic cycloalkylamines (cyclopentylamine, cyclohexylamine, cycloheptylamine, piperazine and DABCO) and metal(II) halides (CuCl₂ and CuBr₂) was constructed, as shown in Table 2.1. All the materials in the matrix were synthesised and compounds reported in literature were excluded, except the **TOZFAP** and **ULAVAF** compounds. A range of different preparation methods were tested in an attempt to obtain good quality single crystals of the materials, as well as pure bulk powder samples for magnetic studies. In addition, the different ratios of organic to inorganic component of 1:1, 1:2 and 2:1 were employed. For tertiary and secondary amines concentrated HX or 2 molar equivalents of 0.5 M HX was used and for primary amines concentrated HX or 1.5 molar equivalents of 0.5 M HX was employed.

Even though a large number of reactions, employing a range of experimental conditions, including variation of temperature and solvents, were carried out, two saturation methods of crystallisation proved successful and these are discussed in more detail below. Crystals were obtained for six novel compounds, of which four were used for magnetic analysis and two materials for which the structures have already been reported in the literature, were resynthesised and prepared for magnetic analysis.

2.1.2.1. Slow Evaporation at Room Temperature

Slow evaporation of the solvent employed, namely water, ethanol or a combination of the two, at room temperature, gave good quality single crystals, suitable for single crystal X-ray diffraction. In this procedure the organic cycloalkylamine was first dissolved in either 1.5 eq. or 2 eq. dilute 0.5 M HX acid depending on the cycloalkylamine employed, as mentioned previously. The metal(II) halide (anhydrous CuCl_2 or CuBr_2) was dissolved separately in ethanol and was added to the solution of the protonated cycloalkylamine solution, in some cases the metal(II) halide was added undissolved to the cycloalkylammonium solution. The reagents were added together in a number six vial and stirred on a magnetic stirrer for ten minutes at room temperature, resulting in a clear coloured solution. The CuCl_2 and the protonated amine produce a light blue solution and CuBr_2 and the protonated amine produce a dark purple solution. The stirrer magnet was removed from the solution and the solution was left to slowly evaporate at room temperature. Good quality single crystals were isolated for analysis.

2.1.2.2. Slow cooling of Saturated Acid Solutions

A slow cooling method reported by Billing (Billing and Lemmerer. 2007, Billing and Lemmerer. 2009) was used successfully to obtain good quality single crystals. The slow cooling method involves preparing a solution of the metal(II) halide and the organic cycloalkylamine in a small excess of concentrated acid. The cycloalkylamine was added to 2 ml of concentrated HX in a size six vial. The metal(II) halide was added to the acidic solution of the amine and the vial sealed. The sealed vial was lowered into an oil bath at a temperature of approximately 70 °C. The meniscus of the solution in the vial was placed just below the level of the oil bath, since this allows for evaporation and condensation of the solvent in the vial and the sealed container allows for an increase of pressure within the reaction vessel. The solution was left unstirred in the oil bath for 5 hours, with the reagents dissolving with an increase in temperature of the solution and pressure in the vial. By slowly increasing the solution temperature to just below boiling point of the solvent, all the components were dissolved in the acid. The now clear solution was left in the oil bath and the hot plate switched off, resulting in the slow cooling of the oil bath and solution. Good quality single crystals typically formed upon cooling to room temperature. The crystals were washed using dichloromethane (DCM), vacuum dried and stored in a closed vial.

A more detailed synthetic outline of each compound studied by single crystal X-ray diffraction or SQUID magnetometry is reported below. The IUPAC names, as well as abbreviations are given for each compound. The first part of the abbreviation indicates the amine component and the second part the metal(II) halide component.

2.1.2.3. Compounds Prepared

Bis(cyclopentylammonium) tetrachloridocuprate(II), PENCuCl

0.2550 g (2.99 mmol) of $\text{C}_5\text{H}_{11}\text{N}$ was dissolved in 9 ml 0.5 M HCl and left to stir for 10 minutes. To this 0.1959 g (1.45 mmol) of anhydrous CuCl_2 was added and left to stir for a further 10 minutes. The solution was left open to the air, at room temperature, to allow for slow evaporation of all the solvent. Green block shaped crystals were isolated after a week.

Cyclopentylammonium catena (μ_2 -bromido) bromidocuprate(II), PENCuBr

0.5019 g (5.89 mmol) of $\text{C}_5\text{H}_{11}\text{N}$ was dissolved in 18 ml 0.5 M HBr and left to stir for 10 minutes. To this 1.3022 g (5.83 mmol) of CuBr_2 was added and the solution was left to stir for a further 10 minutes. The solution was left open to the air, at room temperature, to allow for slow evaporation of all the solvent. Dark purple needle shaped crystals were isolated after a week.

Hexa(cycloheptylammonium) (μ_2 -chlorido) (μ -chlorido)₂ hexachlorido tricuprate(II) dichloride, HEPCuCl

0.2003 g (1.77 mmol) of $C_7H_{15}N$ and 0.1168 g (0.868 mmol) of $CuCl_2$ were added to 2 ml concentrated 32% HCl in a number six vial. The vial was sealed and placed in an oil bath at a temperature of approximately 70°C and left for 5 hours. The reagents dissolved as the temperature of the solution increased, after which the sample was slowly cooled, as described previously. The emerald green, needle shaped crystals were removed from the mother liquor at room temperature and washed using DCM, vacuumed dried and stored in a closed vial.

Hexa(cycloheptylammonium) (μ_2 -bromido) (μ -bromido)₂ hexabromido tricuprate(II) dibromide, HEPcubr

0.2063 g (1.82 mmol) of $C_7H_{15}N$ and 0.1948 g (0.872 mmol) of $CuBr_2$ were added to 2 ml concentrated 48% HBr in a number six vial. The vial was sealed and placed in an oil bath at a temperature of approximately 70°C and left for 5 hours. The reagents dissolved as the temperature of the solution increased, after which the sample was slowly cooled, as described previously. The dark purple, needle shaped crystals were isolated and washed using DCM, vacuumed dried and stored in a closed vial.

Cycloheptylammonium bromide, HEPBr

0.2571 g (2.30 mmol) of $C_7H_{15}N$ was dissolved in 7 ml 0.5 M HBr and stirred for 10 minutes. To this 0.2473 g (1.11 mmol) of anhydrous $CuBr_2$ was added and the solution was stirred for a further 10 minutes. The solution was left open to the air at room temperature to allow for slow evaporation of all the solvent. Black, block shaped and colourless needle shaped crystals formed. This was an indication that the reaction was not successful and the reagents did not react with each other as expected. The $CuBr_2$ crystal structure is known, however the cycloheptylammonium bromide salt structure has not been reported in literature. The colourless needle shaped crystals of cycloheptylammonium bromide were isolated, washed using DCM and left open to the air, to allow for slow evaporation until completely dry.

Piperazinium tetrachloridocuprate(II), PIPCuCl

0.0257 g (3.00 mmol) of $C_4H_{10}N_2$ and 0.0785 g (5.80 mmol) of anhydrous $CuCl_2$ were added to 2 ml concentrated 32% HCl in a number six vial. The vial was sealed and was placed in an oil bath at a temperature of approximately 70°C and left unstirred for 5 hours. The reagents dissolved as the temperature increased, after which the sample was slowly cooled, as described previously. Yellow, block-shaped crystals were isolated and washed using DCM, vacuumed dried and stored in a closed vial.

Bis(1,4-diazoniabicyclo[2.2.2]octane) trichloride diaqua-trichloridocuprate (II) monohydrate, TOZFAP

0.4180 g (3.73 mmol) of $C_6H_{14}N_2^{2+}$ was dissolved in 19 ml 0.5 M HBr and left to stir for 10 minutes. To this solution, 0.2516 g (1.87 mmol) of anhydrous $CuCl_2$ was added and left to stir for a further 10 minutes. The solution was then left open to the air, at room temperature. A yellow powder formed and was recrystallised by dissolving the powder in a minimum of hot ethanol. The solution was left to cool and left open to the air. Lime green, needle shaped crystals were isolated after a week.

1,4-Diazoniabicyclo[2.2.2]octane tetrabromidocuprate(II) monohydrate, ULAVAF

0.5057 g (4.51 mmol) of $C_5H_{11}N$ was dissolved in 22 ml 0.5 M HBr and left to stir for 10 minutes. To this 1.2746 g (5.71 mmol) of anhydrous $CuBr_2$ was added and left to stir for a further 10 minutes. Slow evaporation of the solvent yielded black needle shaped crystals, which were harvested after a week.

2.2. Structural Characterisation

The novel single crystals prepared were structurally characterised by single crystal X-ray diffraction, while the purity of the powder samples employed in the magnetic characterisation was confirmed by powder X-ray diffraction. The theoretical background of these techniques is discussed below.

2.2.1. X-ray Diffraction

The development of X-ray Crystallography has come a long way since the first structure discovery of a hexagonal snowflake crystal, by Kepler in the early seventeenth century (Kepler, 1611). Since then the discovery of X-rays and their ability to diffract, when a non-destructive monochromatic X-ray beam interacts with electrons in the crystal lattice, (Röntgen, 1895 & 1912), the implementation of the Miller Indices and Bragg's Law (Bragg, 1913) developed by Sir William Henry Bragg and his son Sir William Lawrence Bragg, all contributed to modern X-ray Crystallography.

The fundamentals of X-ray diffraction are based on Bragg's Law (Figure 2.2.1), whereby the scattering of X-rays by the electron density of single atoms can be represented as reflections off successive planes of atoms, separated by a distance, d , in the crystal lattice. The constructive or destructive interference of scattered X-rays can occur, as determined by conditions given by Bragg's Law. The incident X-ray beam is reflected off the electron density clouds of atoms. The amount of X-rays diffracted is a direct result of the amount of electron density around atomic nuclei. The larger the electron cloud, the more intense the diffraction of the X-rays at that position. Hence heavy atoms can be distinguished from light atoms. An electron density map of the atomic nuclei offers information with regards to the atomic positions and arrangements of atoms in the crystal lattice.

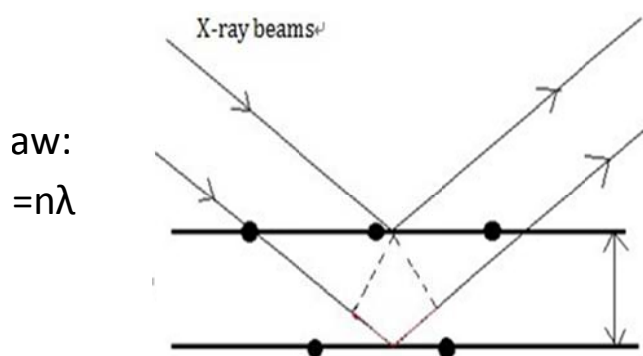


Figure 2.2.1. The conditions required by the Bragg's equation for diffraction to occur

- Wavelength of incident X-ray, λ .
- The angle between the incident rays and the surface, θ .
- The distance between layers of atoms d_{hkl} .

Two common X-ray diffraction techniques, namely single crystal X-ray diffraction (SXRD) and powder X-ray diffraction (PXRD), were employed in this study. SXRD allows for the determination of the structure of the compound, i.e. the position of the atoms in the unit cell and this provides information on bond lengths, bond angles, the packing of the units in the solid state, non-covalent interactions and symmetry. It is arguably one of the most definitive structural characterisation techniques used today. PXRD was used as a tool for fingerprinting and purity checks. The experimental powder patterns were compared against powder patterns calculated for known structures and purity checks were necessary to ensure the materials employed in the magnetic studies were pure and contained only one phase. Brief overviews of the implementation of the two techniques are given below.

2.2.1.1. Single Crystal X-ray Diffraction (SXRD)

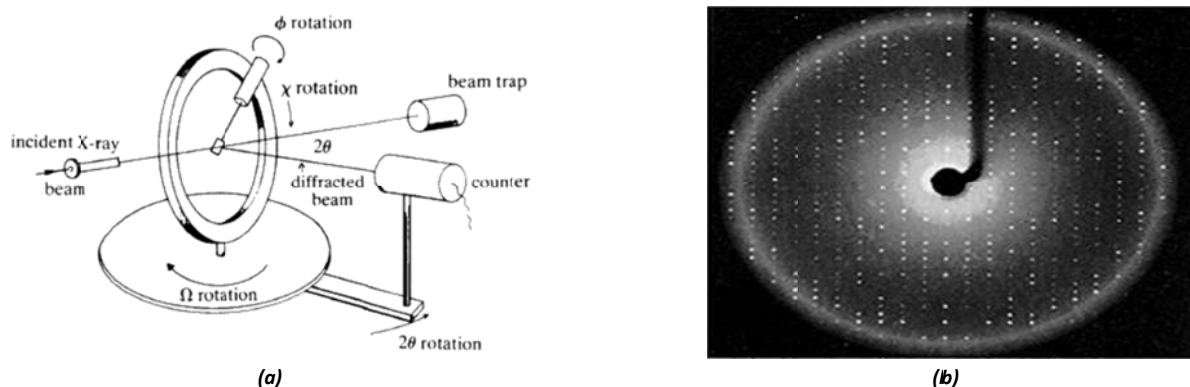


Figure 2.2.2 (a). The components comprising a SXRD diffractometer and (b) An example of a diffraction pattern.

The analysis of single crystals is a three-step process:

1. **Mounting of the crystal:** Possibly the most crucial step, as the crystal needs to be of good quality and are not twinned or contain defects. A suitable crystal was identified under a stereo microscope, with a typical crystal size of 0.25 mm^3 . Epoxy resin glue was used to affix the crystal to a single glass fibre, which was inserted into a brass sample mount.
2. **Data collection:** The X-ray diffraction data were collected using a Bruker D8 Venture diffractometer, with a Photon 100 CMOS detector, at 150 (2) K, employing a combination of ϕ and Ω scans. Cooling was achieved using an Oxford Cryogenics Cryostat and monochromatic MoK- α radiation of wavelength, λ of 0.71073 \AA , from an I μ s source, was employed to irradiate the crystal. Data reduction and absorption corrections were performed using SAINT+ and SADABS as part of the APEX II suite (2013).
3. **Structure determination:** The structures were solved by direct methods using SHELXS-97 (Sheldrick, 2008), as part of the WinGX (Farrugia, 2012) suite. Structure refinements were done using SHELXL-2013 (Sheldrick, 2013) in WinGX (Farrugia, 2012). Nitrogen atoms were distinguished from carbon atoms in the piperazinium structures through visual inspection of the thermal ellipsoids and by considering bond lengths. The non-hydrogen atoms were refined anisotropically, except if stated otherwise. Hydrogen atoms on carbon atoms were placed geometrically using a riding model, with a C-H distance of 0.970 \AA . Hydrogen atoms on nitrogen atoms were placed employing a riding model and electron density in the difference map, with a N-H distance of 0.890 \AA . Hydrogen atoms of water molecules were placed as observed or on the vector between the donor oxygen atom to a suitable hydrogen bonding acceptor, at a distance of 0.950 \AA from the oxygen atom. All hydrogen atoms were refined isotropically. Disorder was observed in one structure and was treated as described in section 3.5.

Single crystal X-ray diffraction is one of the most effective structure determination techniques, however, a single crystal is required and it is not always possible to obtain a good quality crystal. In this case PXRD is the characterisation technique of choice.

2.2.1.2. Powder X-ray Diffraction (PXRD)

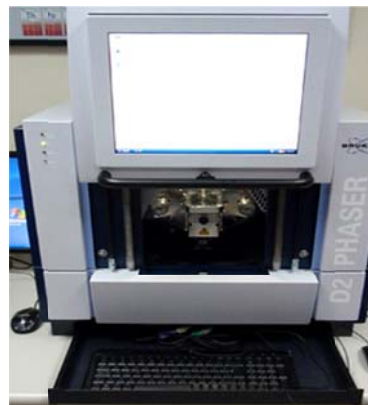
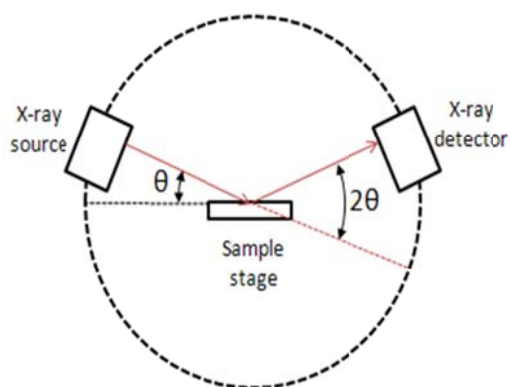


Figure 2.2.3. The Bruker D2 Phaser instrument used in PXRD analysis of the compounds.

Powder X-ray diffraction (PXRD) is a well-known characterisation technique, used in industry and also in this study, as a quick and cost effective method of characterising solid state materials.

The sample preparation is of importance in producing good quality powder patterns. All the samples analysed in this study were gently ground using a mortar and pestle. For small samples analysed, the sample was sifted using a sieve, to ensure uniform particle sizes and sprinkled on a low background silicon quartz sample holder. For larger samples a flat plate sample holder was employed and the sample was levelled using a microscope slide. All powder X-ray diffraction patterns were collected on a Bruker D2 Phaser powder X-ray diffractometer at room temperature, as shown in Figure 2.2.3 and CuK- α radiation was generated at 30 kV and 10 mA, with a wavelength, $\lambda = 1.54 \text{ \AA}$. Diffraction patterns were collected in the range of 5° to 45° 2θ , with a step size of 0.1° and a counting time of one second per step, when necessary a counting time of three seconds per step was implemented.

The advantage of this technique is that a single crystal is not required as the sample is ground into a powder and then analysed. A disadvantage is that not all materials can be analysed, materials such as those classified as amorphous, will not produce a diffraction pattern.

PXRD and SXRD are well known techniques and a detailed theoretical description is beyond the scope of this study.

2.3. Magnetic Characterisation

SQUID magnetometry was employed to study the magnetic characteristics of selected hybrid materials prepared in this investigation. All SQUID data were collected during a study visit conducted to the laboratory of Prof M. M. Turnbull at Clark University, Worcester, MA, USA.

2.3.1. Sample Preparation

The purity of each sample employed in the magnetic studies was confirmed by PXRD analysis. The sample was gently ground into a fine powder with the use of an agate mortar and pestle. An empty size three gelatine capsule was weighed and the mass recorded. The sample was loaded into one half of the gelatine capsule and the mass weighed and recorded. The capsule was sealed by inserting the other half of the gel capsule into the loaded capsule, such that the rounded end of the empty capsule is inserted into the loaded half of the capsule.

The sample was then inserted approximately 9.5 cm to 10 cm into a clear plastic straw. The straw was screwed onto a rod and inserted into the SQUID instrument under positive He pressure.

2.3.2. Instrumentation

A Superconducting Quantum Interference Device (SQUID) magnetometer is a very sensitive magnetometer allowing for the measurement of small magnetic moments in samples. A detailed description of the instrument and its operation is beyond the scope of this dissertation. However, a short introduction to the instrument is included.

Certain materials undergo a transition to a superconducting state at temperatures approaching absolute zero and in this superconducting state the material shows no electrical resistance. Above the transition temperature electrical resistance occurs as a result of the scattering of electrons, but in the superconducting state electrons associate in Cooper pairs which travel without scattering (Fagaly. 2006).

If a material is placed in a magnetic field, the magnetic flux lines penetrate the material. However, when a superconductor is placed in a magnetic field, the magnetic field is excluded from the superconductor and this is known as the Meissner effect (Gramm *et al.* 1976). If the superconductor is shaped in the form of a ring and placed in a magnetic field at a temperature above the superconducting transition temperature, T_c and then cooled down to below T_c , the flux inside the ring is trapped. When the magnetic field is switched off, a current is induced in the ring. This current keeps the magnetic flux in the ring constant. Because there is no resistance in the superconducting ring, the current will continue to circulate in the ring as long as the temperature is below T_c . Josephson (Josephson. 1962) predicted in 1962 that if a small section of the ring is replaced by a resistive material Cooper pairs can tunnel through the resistive section, thus tunnelling from one superconductive section to another and this is known as the Josephson effect (Josephson. 1974).

In a dc SQUID magnetometer, measurement of the change in voltage in the ring, *via* two Josephson junctions, allows for the determination of the change in magnetic flux coupled to the superconducting ring in the SQUID magnetometer. Input, feedback and modulation superconducting coils are coupled to the SQUID loop, to form a superconducting circuit. The sample is moved in a linear motion through the input coils, which causes a change in the magnetic flux in these coils. In the constant flux mode, the current in the feedback coil is changed to compensate for the flux change in the pickup coil and the signal measured by the magnetometer is proportional to this current (Czichos *et al.* 2006)

The magnetic susceptibility data was collected on powder samples employing a Quantum Design MPMS XL SQUID magnetometer, due to its high sensitivity. The instrument measures the magnetic moment or magnetisation, M , which is related to susceptibility as the degree of magnetisation of a response to an applied magnetic field. The SQUID instrument can typically reach low temperatures (1.8 K), where magnetic interactions can be measured in applied magnetic fields up to 7 Tesla.

2.3.3. Data Collection

The data collection was carried out in two steps. In the first step the magnetisation (M) of the sample was measured over a field (H) range of 0 Oe to 50 000 Oe at a constant temperature of 1.8 K. In the second step, the magnetisation was measured at a constant field of 1 kOe from 1.8 K to 310 K. For strongly FM samples the magnetic data was collected over a temperature range of 1.8 K to 294 K at a constant magnetic field of 0.5 kOe.

2.3.4. Data Processing

Once the experimental data was obtained, parameters such as sample mass and molar mass were taken into account to obtain the molar susceptibility. For accurate data interpretation, certain corrections to the data need to be subtracted from the original data. Two of the types of corrections that were carried out are given below.

Temperature independence parameter (TIP): The temperature independence parameter (TIP) is a correction term that is needed for systems that are expected to show diamagnetic behavior due to the singlet spin ground states. The interactions are actually weakly paramagnetic and are independent of temperature. The TIP arises from the mixing into the ground state wavefunction and the wavefunction of the excited states that aren't thermally populated. This is necessary for high temperature data as the TIP is large enough to be significant.

Diamagnetic correction (DIA): The paramagnetic susceptibility is associated with unpaired electrons whereas the diamagnetic susceptibility is associated with paired electrons. The diamagnetic correction is used to correct for paramagnetic materials with underlying diamagnetism. The DIA is calculated based on the sum of Pascal's constants (Pascal, 1910), which sums the contributions from components of the molecule. The Pascal's constants assume that the contributions are identical in all molecules. The magnitude of Pascal's constant correlates with the number of electrons in the groups.

Once corrected, the data collected is plotted as three separate plots of χ , χT and χ^{-1} versus temperature (K). From these plots the magnetic behaviour of the systems can be identified, as discussed in Chapter One.

Possible magnetic exchange pathways in the compounds can be identified by considering close M-X...X-M contacts by utilising the program Mercury (Macrae *et al.* 2006), with actual X...X distance shorter than 4.5 Å for chlorido ligands and 5.0 Å for bromido ligands.

2.3.5. Data Fitting to Quantum Mechanical Models

Once the possible exchange pathways have been identified, suitable quantum mechanical models are selected, based on the type of exchange pathway. It should be noted that quantum mechanical models are available for low-dimensional systems but not for three-dimensional systems due to their complexity.

The experimental data is fitted to the equation of the quantum mechanical model to obtain the values of the different parameters in the model using Origin software (OriginLab, Northampton, MA). The models are obtained from literature and the fitting is done iteratively. One parameter was initially allowed to refine independently, as the fit improved more parameters were released to run independently. The parameters defined are determined by the quantum magnetic models employed. In the case where more than one model is deemed suitable, the model providing the best fit between the experimental data and theoretical model is selected.

2.4. Computer Software Programs

2.4.1. Cambridge Structural Database, CSD version 5.34 (Allen, 2002)

The Cambridge Structural Database (CSD) contains 651 348 organic, inorganic and hybrid published structures. The database allows for structural searches of related materials, as well as structural comparison by powder

pattern analysis, cell parameters and structure compositions. Journal articles from various accredited journals for individual structures are also available. The CSD v 5.34 (May 2013) was used in this study for all CSD searches.

2.4.2. Diffrac. Suite. Eva version 2.0 copyright © BrukerAXS 2010, 2011

Diffrac. Eva is a licenced program used in the analysis of powder patterns. The software is also used for comparison of experimental and calculated powder patterns from the CSD for phase identification and quantitative analysis. The PDF database, linked to Eva, allows for purity checks of samples analysed.

2.4.3. Powdercell for Windows version 2.4 (Kraus and Nolze. 1996)

Powdercell (Kraus and Nolze. 1996) is a basic software package used for the analysis of powder patterns, an alternative to Diffrac. Suite. Eva, powdercell can be used for the comparison of calculated and experimental powder patterns for compound identification and quantitative phase analysis.

2.4.4. Mercury CSD version 3.11 Development (Build RC7) (Macrae *et al.* 2006)

The Mercury (Macrae *et al.* 2006) interface is used to analyse structural characteristics of both structures reported in literature and novel structures. This allows for visual representation of the packing of the units in a structure, types of hydrogen bonding interactions between cations and anions, thermal ellipsoids and magnetic exchange pathways.

2.4.5. Origin (OriginLab, Northampton, MA)

The Origin software package was used to fit theoretical quantum magnetic models to the experimentally observed magnetic data. From the fit of a suitable magnetic model, values for the parameters defining the model could be determined, including the exchange parameter(s), J.

2.5. References

Allen, F. R. (2002). *Acta Cryst.* B58, 380-388.

Billing D.G. and Lemmerer, A. (2007). *CrystEngComm.* 9, 236-244.

Billing, D.G. and Lemmerer, A. (2009). *CrystEngComm.* 11, 1549-1562.

Bragg, W.L. (1913). *Proceedings of the Cambridge Philosophical Society.* 17, 43-57.

Bruker AXS Inc., Madison, Wisconsin, USA. 2013. 'APEX II'.

Czichos, H., Saito, T. and Smith, L. (2006). *Springer Handbook of Materials Measurements and Methods.* Springer Science+Business Media, Inc.

Fagaly, R. L. (2006). *Superconducting Quantum Interference Device Instruments and Applications, Review of Scientific Instruments.* 77, 101101.

Farrugia, L. J. (2012). *J. Appl. Cryst.* 45, 849-854.

Gramm, K., Lundgren, L. and Beckman, O. (1976). *Physica Scripta.* 13, 93-95.

Josephson, B. D. (1962). "Possible new effects in superconductive tunneling," Phys. Lett. 1, 251-253.

Josephson, B. D. (1974). "The discovery of tunneling supercurrents". Rev. Mod. Phys. 46 (2), 251-254.

Kepler, J. (1611). *Strena seu de Nive Sexangula*. Frankfurt: G. Tampach.

Kraus, W. and Nolze, G. (1996). *J. Appl. Cryst.* 29, 301-303.

Macrae, C. F., Edgington, P. R., McCabe, P., Pidcock, E., Shields, G. P., Taylor, R., Towler, M. and van de Streek, J. (2006). *J. Appl. Cryst.* 39, 453-457.

OriginLab, Northampton, MA.

Pascal, P. (1910). *Ann. Chim. Phys.* 19, 5-70.

Sheldrick, G. M. (2008). *Acta Cryst.* A64, 112-122.

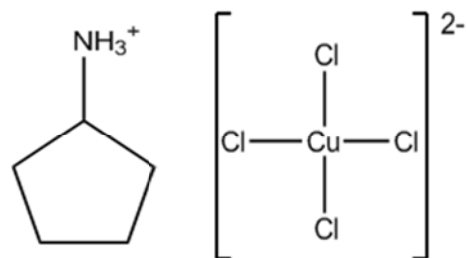
Chapter Three: Experimental Results

The current chapter reports the results obtained in the structure studies, as well as the magnetic investigation of the compounds listed in section 2.1.2.3.

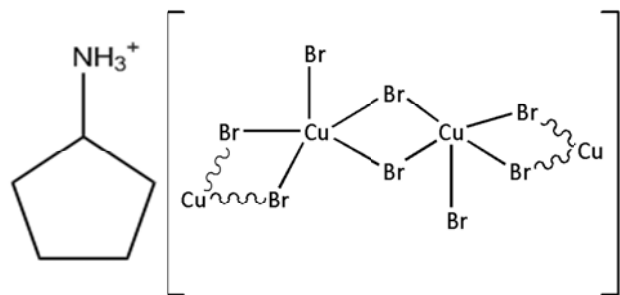
The results are categorised according to the organic cation component of the structure, starting with cyclopentylammonium containing structures, cycloheptylammonium containing structures, piperazinium containing structures and lastly DABCO containing structures.

A total of six novel structures were determined in this study, of which four were characterised magnetically. Two compounds for which the structures have already been published were resynthesised to collect magnetic data for these materials and are referred to by their CSD refcodes indicated in bolded font. Table 3.0.1 lists all the structures analysed in this study, as well as the schematic representations of the components comprising each compound. Table 3.0.2 lists the crystallographic parameters of the novel compounds reported in this chapter.

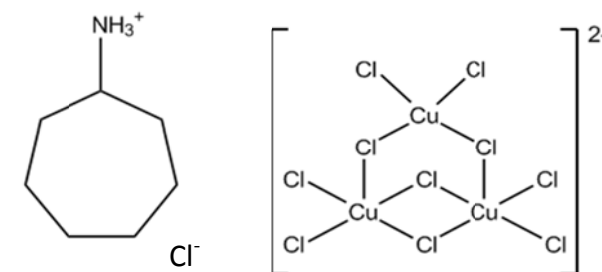
Not all the compounds could be characterised magnetically, due to, among other factors, the difficulty of obtaining samples pure enough for magnetic analysis. If PXRD indicated the presence of an impurity the sample was deemed unfit for magnetic analysis.



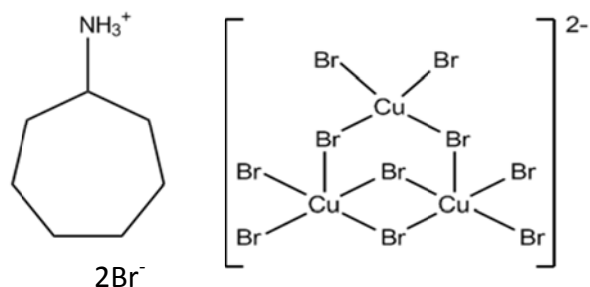
3.1. Bis(cyclopentylammonium) tetrachloridocuprate(II), PENCuCl



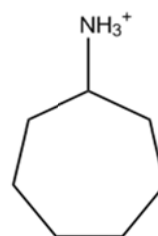
3.2. Cyclopentylammonium catena (μ_2 -bromido) bromidocuprate(II), PENCuBr



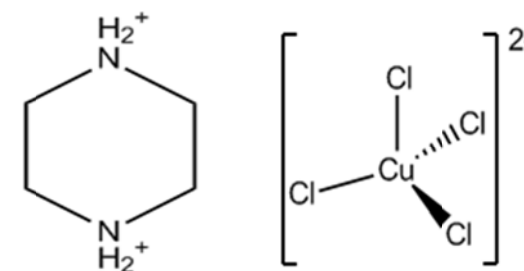
3.3. Hexa(cycloheptylammonium)(μ_2 -chlorido)(μ -chlorido)₂ hexachlorido tricuprate(II) dichloride, HEPCuCl



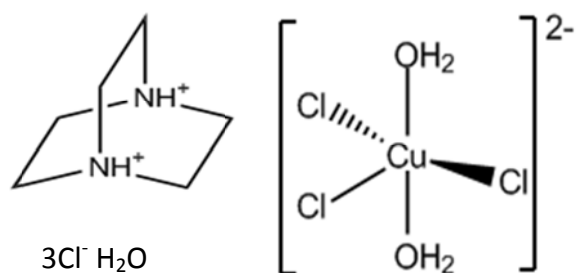
3.4. Hexa(cycloheptylammonium)(μ_2 -bromido)(μ -bromido)₂ hexabromido tricuprate(II) dibromide, HEPCuBr



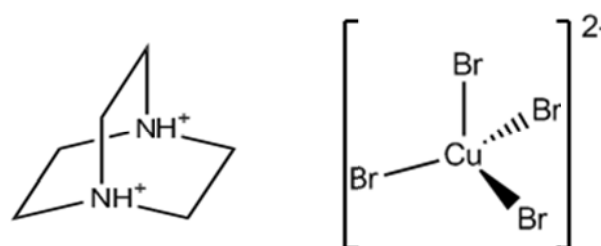
3.5. Cycloheptylammonium Bromide, HEPBr



3.6. Piperazinium tetrachloridocuprate(II), PIPCuCl



3.7. Bis(1,4-diazoniabicyclo[2.2.2]octane) trichloride diaqua trichlorocopper(II) monohydrate, TOZFAP



3.8. 1,4-Diazoniabicyclo[2.2.2]octane tetrabromido copper(II) monohydrate, ULAVAF

**Note that no information with regards to charge balance or stoichiometric ratios is presented.*

Table 3.0.2. The crystallographic parameters of the novel structures determined in this study.

Compound	3.1. PENCuCl	3.2. PENCuBr	3.3. HEPCuCl	3.4. HEPCuBr	3.5. HEPBr	3.6. PIPCuCl
Colour	Bright green	Dark purple/black	Grey	Black	Clear	Yellow
Crystal shape	Block	Needle	Block	Block	Needle	Block
Formula	$2(\text{C}_5\text{H}_{12}\text{N}^+) \text{CuCl}_4^{2-}$	$n(\text{C}_5\text{H}_{12}\text{N}^+) (\text{CuCl}_3)_n$	$6(\text{C}_7\text{H}_{16}\text{N}^+) \text{Cu}_3\text{Cl}_{10}^{4-} \cdot 2\text{Cl}^-$	$6(\text{C}_7\text{H}_{16}\text{N}^+) \text{Cu}_3\text{Br}_{10}^{4-} \cdot 2\text{Br}^-$	$\text{C}_7\text{H}_{16}\text{N}^+ \text{Br}^-$	$\text{C}_4\text{H}_{12}\text{N}_2^{2+} \text{CuCl}_4^{2-}$
M_r (g/mol)	377.66	389.41	1301.30	1834.70	194.11	293.51
Crystal System	Monoclinic	Orthorhombic	Monoclinic	Triclinic	Orthorhombic	Tetragonal
Space group	$P2_1/c$	$Pbca$	$C2/c$	$P\bar{1}$	$Pbca$	$P4_12_12$
Z	2	8	4	2	16	4
$a/\text{\AA}$	13.3881(6)	14.4349(6)	24.621(4)	13.750(4)	16.2840(7)	7.6550(15)
$b/\text{\AA}$	8.2534(4)	6.3843(3)	11.3642(18)	15.838(5)	10.3666(4)	7.6550(15)
$c/\text{\AA}$	7.1892(4)	21.1592(9)	22.673(4)	16.096(5)	21.1323(10)	19.1642(37)
$\alpha/^\circ$	90.00	90.00	90.00	70.570(7)	90.00	90.00
$\beta/^\circ$	97.501(2)	90.00	110.393(8)	78.006(7)	90.00	90.00
$\gamma/^\circ$	90.00	90.00	90.00	78.516(7)	90.00	90.00
$V (\text{\AA}^3)$	787.59(7)	1949.96(15)	5946.3(17)	3201.2(17)	3567.3(3)	1123.0(5)
F (000)	390	1464	2724	1794	1600	588
$D_c (\text{g cm}^{-3})$	1.592	2.653	1.454	1.903	2.276	1.736
$\mu (\text{mm}^{-1})$	2.047	14.468	1.637	8.509	4.535	2.844
Diffractionmeter	Bruker D8 Venture	Bruker D8 Venture	Bruker D8 Venture	Bruker D8 Venture	Bruker D8 Venture	Bruker D8 Venture
T (K)	150(2)	150(2)	150(2)	150(2)	150(2)	150(2)
$\lambda (\text{Mo K}\alpha) (\text{\AA})$	0.71073	0.71073	0.71073	0.71073	0.71073	0.71073
Reflections collected	64779	267699	40721	20280	97419	112515
Unique reflections	5290	8362	3595	7020	4305	3187
Parameters	80	92	288	334	227	51
$R[F^e > 2\sigma(F^e)]$	0.0254	0.0577	0.0455	0.0987	0.0243	0.0238
$wR(F^e)$	0.0614	0.0751	0.1138	0.3038	0.0617	0.0610
Flack parameter	-	-	-	-	-	0.032(9)

3.1. Bis (cyclopentylammonium) tetrachloridocuprate(II)

Moiety Formula: $2(\text{C}_5\text{H}_{12}\text{N}^+) \text{CuCl}_4^{2-}$
Abbreviated as PENCuCl

Compounds consisting of isolated tetrahedral perchloridocuprate(II) anionic units and isolated cyclopentylammonium cationic units have been reported in the literature, with CSD refcodes **NABNEK** and **NABNEK01** (Willet *et al.* 2004) as discussed in section 1.5. A compound that comprises isolated cyclopentylammonium cations and polymeric perchloridocuprate(II) anionic units has also been reported in literature, with CSD refcode, **FAWDAI**, (Geiser *et al.* 1986). Hybrid compounds, which consists of isolated cyclopentylammonium cations and perovskite perchloridocuprate(II) anions were not found in literature.

The novel centrosymmetric structure found in this study, PENCuCl, contains isolated cyclopentylammonium cations and CuCl_4^{2-} anions, but the anionic moieties of the PENCuCl structure differs from the cyclopentylammonium containing compounds in literature, as the PENCuCl structure contains CuCl_4^{2-} anionic units that are connected by semi-coordinate bonds to form perovskite sheets. A compound similar to PENCuCl was reported in the CSD, with refcode, **YATYUP** (Han. 2012). The **YATYUP** structure comprises cyclohexylammonium cations and CuCl_4^{2-} anions that form perovskite sheets.

3.1.1. Structure Analysis

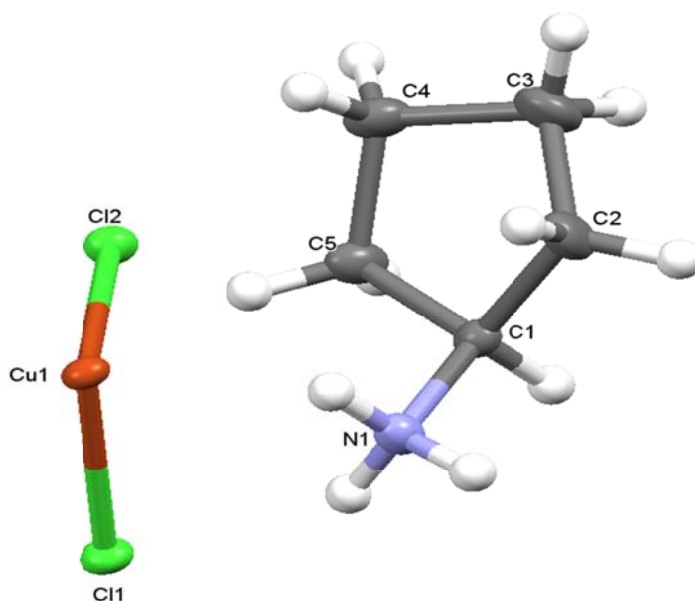


Figure 3.1.1. The asymmetric unit of PENCuCl. Displacement ellipsoids are drawn at the 50% probability level and hydrogen atoms are drawn as spheres of arbitrary radius.

The asymmetric unit of PENCuCl consists of a CuCl_2 unit and an isolated cyclopentylammonium cationic unit. The Cu^{2+} metal ion, labelled, Cu1, as shown in Figure 3.1.1, lies on special position [0, 0, 0] and is coordinated to two chlorido ligands. An inversion centre on the Cu^{2+} ion generates the other half of the CuCl_4^{2-} anion. The CuCl_4^{2-} anionic moiety adopts a square planar geometry, as shown in Figure 3.1.2 (a).

The bond lengths for Cu1-Cl1 and Cu1-Cl2 are 2.296(2) Å and 2.273(2) Å respectively, with Cl1-Cu1-Cl2 bond angles ranging from 89.42(1)° to 90.57(1)°, deviating slightly from the ideal square planar angle of 90°. The isolated cyclopentylammonium cation adopts an envelope conformation, where the nitrogen atom of the cation is singly protonated and the $^+NH_3$ group adopts an axial position on the cation.

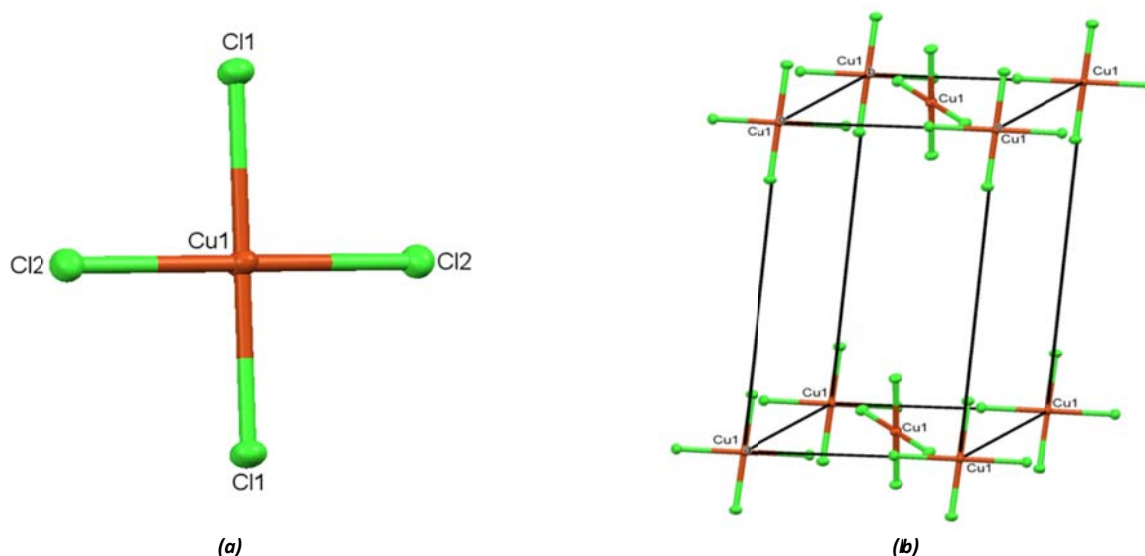


Figure 3.1.2. (a) The anionic moiety of PENCuCl. (b) The positions of the Cu^{2+} ion centres within the unit cell. The cations are omitted for clarity. Displacement ellipsoids are drawn at the 50 % probability level.

The unit cell hosts ten Cu^{2+} metal centres, with one Cu^{2+} ion positioned on all eight corners of the unit cell, while the two opposite faces of the unit cell each contain one Cu^{2+} ion, as seen in Figure 3.1.2 (b). The unit cell also contains four cyclopentylammonium cationic units. Repetition of the unit cell produces two-dimensional inorganic perovskite sheets, which are separated by organic bilayers, as shown in Figure 3.1.3 (a). As illustrated in Figure 3.1.3 (b), long, semi-coordinate bonds form between the Cu^{2+} ion of one $CuCl_4^{2-}$ moiety and the terminal chlorido ligand of a perpendicular $CuCl_4^{2-}$ anion, with semi-coordinate bond lengths of 3.2644(2) Å. When the structure of PENCuCl is viewed down the c -axis, it can be seen that the ammonium tails of the cyclopentylammonium cations point towards inorganic layers as shown in Figure 3.1.3 (a).

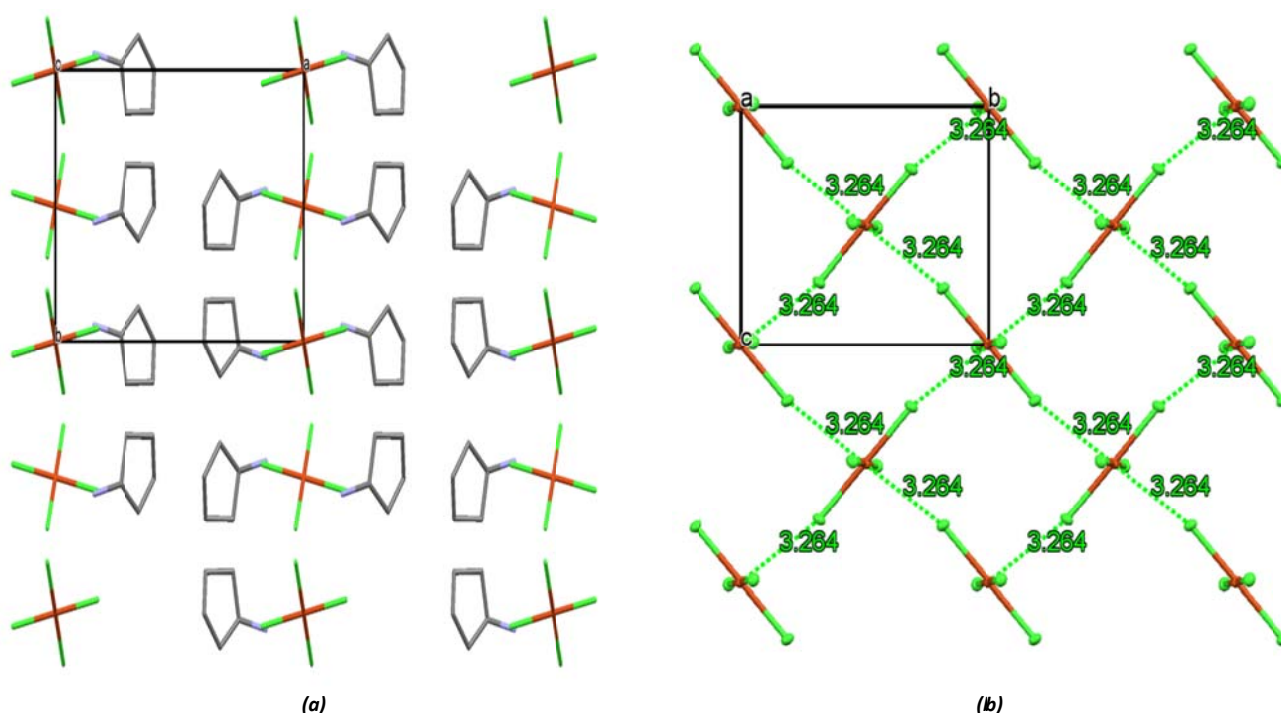


Figure 3.1.3. (a) The packing diagram of PENCuCl as viewed down the c -axis. The hydrogen atoms are omitted for clarity. (b) The two-dimensional perovskite sheet showing long semi-coordinate bonds between Cu1 and Cl1 (green dotted lines). The distances of the semi-coordinate bonds are given in Angstroms (Å).

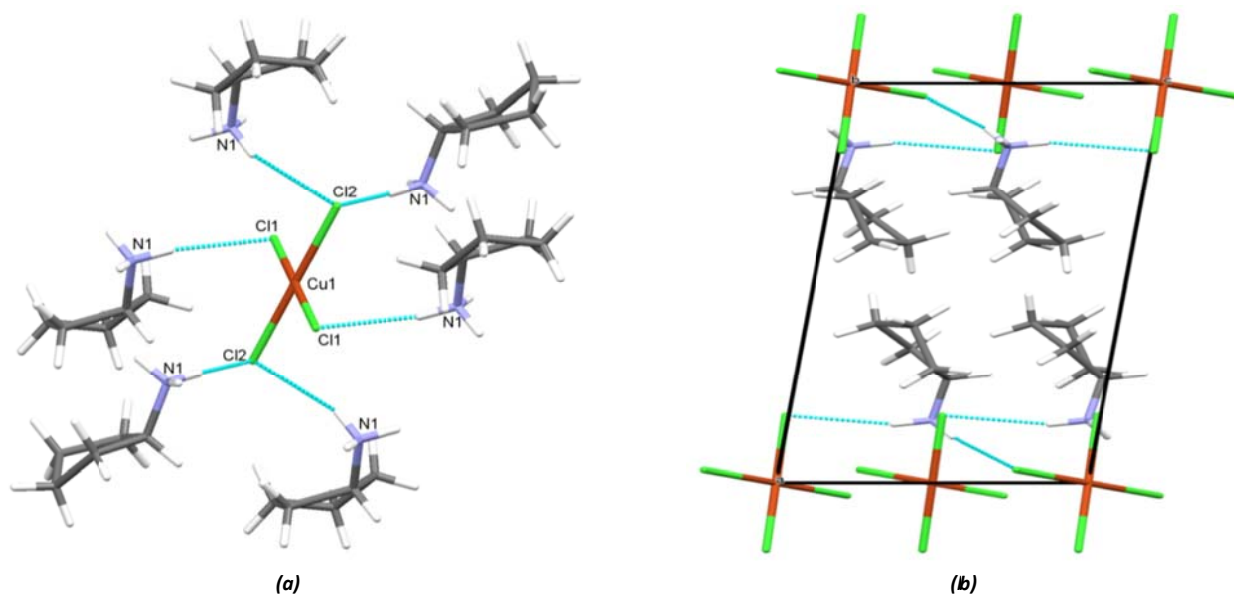


Figure 3.1.4. (a) Classic, charge assisted hydrogen bonding interactions that exist between the anionic and cationic moieties. (b) The hydrogen bonding network.

Each anionic moiety accepts hydrogen bonds from six individual cationic species and this is achieved through classic, charge assisted, ${}^{\delta+}\text{N}-\text{H}\cdots\text{Cl}^{-}-\text{Cu}$ hydrogen bonding interactions. Hydrogen bonding interactions occur between one hydrogen atom of a donor nitrogen atom from each individual cationic species to chlorido acceptor ligands of a CuCl_4^{2-} moiety, as shown in Figure 3.1.4 (a). A two-dimensional hydrogen-bonded sheet is formed, parallel to the *ac*-plane, as shown in Figure 3.1.4 (b). Hydrogen bonding parameters are listed in Table 3.1.

Table 3.1. Hydrogen bonding parameters of *PENCuCl*.

D-H	d(D-H) (Å)	d(H \cdots A) (Å)	<DHA ($^{\circ}$)	d(D \cdots A) (Å)	A
N1-H1A	0.890	2.385	169.56	3.265(7)	Cl1 [-x, -y, -z+1]
N1-H1B	0.890	2.398	156.92	3.236(7)	Cl2 [x, -y+1/2, z+1/2]
N1-H1C	0.890	2.842	114.69	3.313(7)	Cl1
N1-H1C	0.890	2.504	162.09	3.362(7)	Cl2

3.1.2. Magnetic Characterisation

Due to the difficulty of obtaining a pure sample of large enough mass, the magnetic data was not collected for the *PENCuCl* compound.

3.2. Cyclopentylammonium catena (μ_2 -bromido) bromidocuprate(II)

Moiety Formula: $n(\text{C}_5\text{H}_{12}\text{N}^+) (\text{CuBr}_3^-)_n$
Abbreviated as PENCuBr

Two structures that are related to the novel PENCuBr compound could be located in literature, with CSD refcodes **NABNEK** and **NABNEK01** (Willett *et al.* 2004). These two compounds both consist of isolated cyclopentylammonium cations and isolated perbromidocuprate(II) anions, but the structures **NABNEK** and **NABNEK01** were determined at room temperature and at -70°C respectively and differ from each other with regards to the relative orientations of the cyclopentylammonium rings.

A third structure related to PENCuBr was located in the CSD, with refcode **FAWDAI** (Geiser *et al.* 1986). This compound consists of polymeric perchloridocuprate(II) anions as well as isolated cyclopentylammonium cations. The **NABNEK**, **NABNEK01** and **FAWDAI** structures are not isostructural to the PENCuBr structure.

In this study the novel structure of PENCuBr consisting of polymeric perbromidocuprate(II) anions and isolated cyclopentylammonium cations was determined. Magnetic data for this compound were also collected and are discussed in the magnetic characterisation section.

3.2.1. Structure Analysis

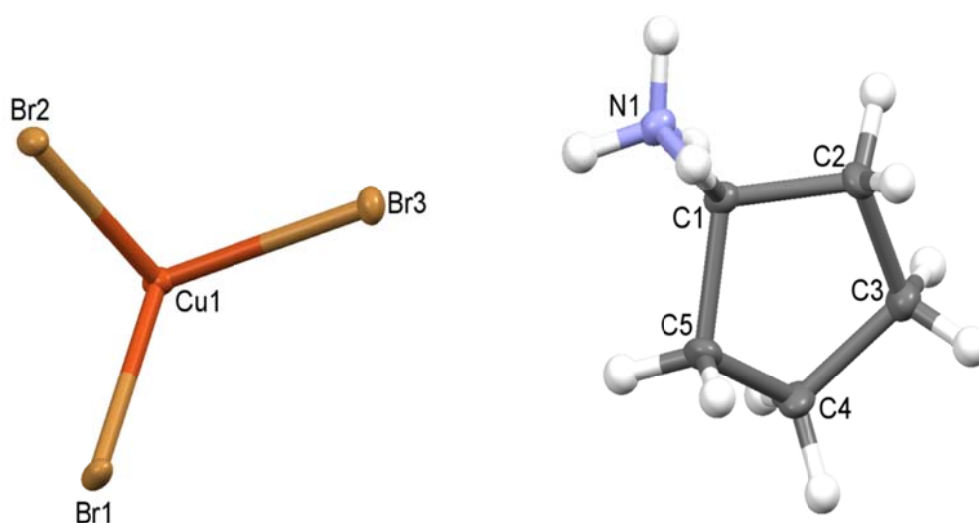


Figure 3.2.1. The asymmetric unit of PENCuBr. The ellipsoids are drawn to encompass 50% of the probability density and hydrogen atoms are drawn as spheres of arbitrary radius.

The asymmetric unit of PENCuBr comprises a Cu^{2+} ion centre with three bromido ligands coordinated to the metal centre, Cu1, as well as an isolated cyclopentylammonium cation, which adopts an envelope conformation. The nitrogen atom of the cation is singly protonated and the $^+\text{NH}_3$ group is located in the axial position, as seen in Figure 3.2.1.

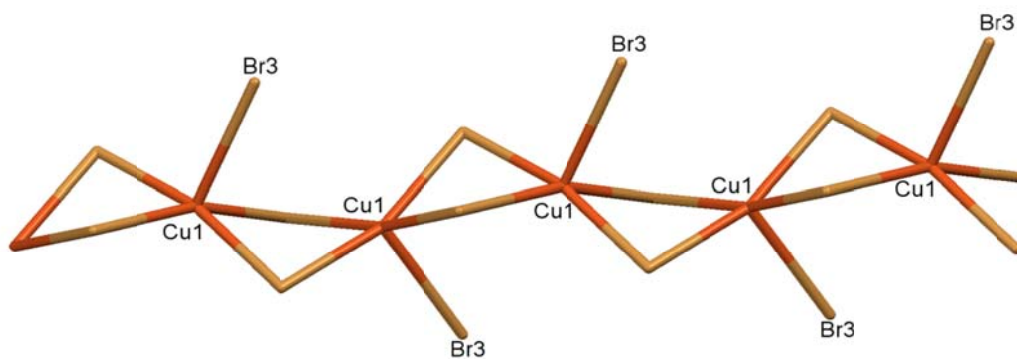


Figure 3.2.2. The polymeric perbromidocuprate(II) anionic chain formed in PENCuBr.

A one-dimensional polymeric perbromidocuprate(II) anionic chain is formed through growth of the CuBr_3^- unit and extends along the b -axis. The polymer contains one terminal bromido ligand, which is located in the axial position and two bridging bromido ligands that fold along the Br-Br line, as illustrated in Figure 3.2.2. The copper coordination sphere, Cu1, of the anionic moiety, adopts a distorted square pyramidal geometry and the polymer is formed *via* edge sharing of the bromido ligands. Adjacent square pyramidal units alternate in their respective orientations. The terminal Cu1-Br3 bond lengths are slightly elongated at 2.676(3) Å, with bridged bromido ligands having shorter Cu-Br bond lengths of 2.432(3) Å to 2.450(3) Å. The bond angles for the Br3-Cu1-Br2 and Br3-Cu1-Br1(-x+3/2, y-1/2, z) angles are 95.76(1)° and 98.61(1)°, respectively, deviating from the ideal square pyramidal bond angle of 90°. *Trans* bond angles for the bridging bromido ligands, Cu1(-x+3/2, y+1/2, z)-Br1-Cu1 and Cu1(-x+3/2, y+1/2, z)-Br2-Cu1 are smaller at 83.87(1)° and 83.29(1)° respectively.

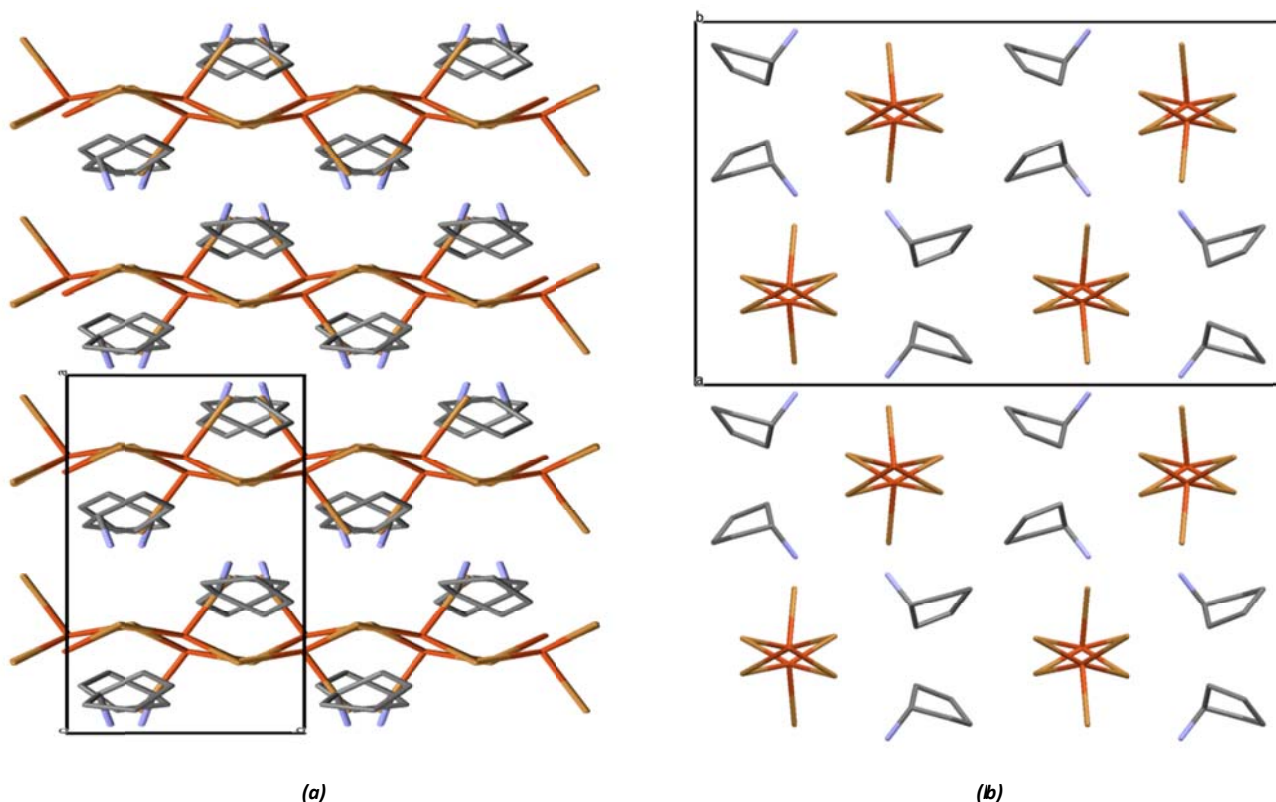


Figure 3.2.3 (a) The packing diagram of PENCuBr as viewed down the b -axis. (b) The packing diagram of PENCuBr as viewed down the c -axis. Hydrogen atoms are omitted for clarity.

The centrosymmetric structure of PENCuBr consists of an organic bilayer sandwiched between single layers of inorganic polymeric moieties, which run parallel to the bc -plane, as seen in Figure 3.2.3 (a). When viewed down the c -axis (Figure 3.2.3 (b)), it can be seen that the neighbouring cationic species alternate in their orientation with respect to each other. The $^+\text{NH}_3$ groups of the cationic species point towards the inorganic layer and are involved in hydrogen bonding. Each polymer, when viewed down the b -axis is surrounded by six cations, as seen in Figure 3.2.3 (b).

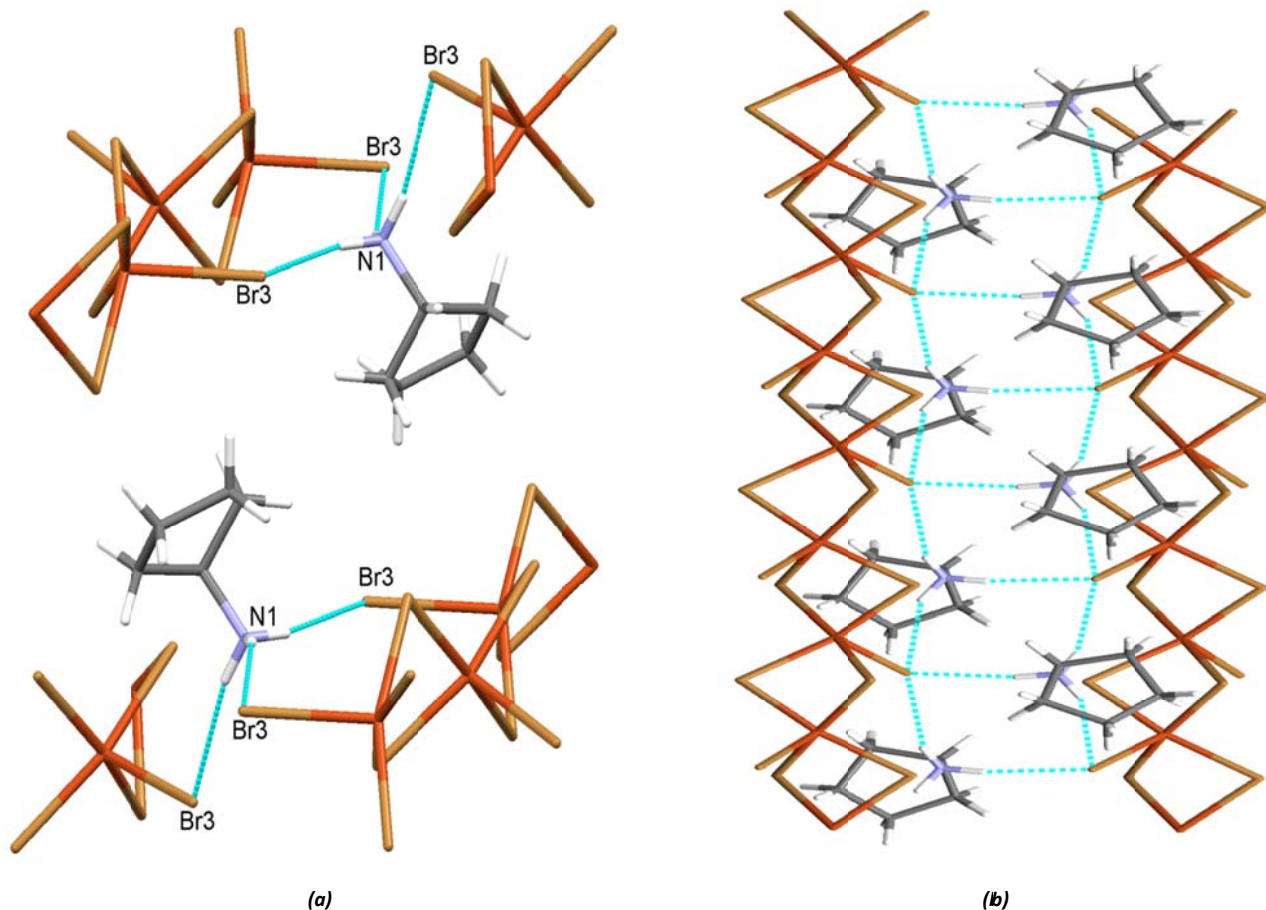


Figure 3.2.4. (a) The hydrogen bonding between the anionic and cationic units. (b) Hydrogen bonding network of PENCuBr.

The hydrogen atoms of the nitrogen donor atom of the cation form two classic, charge assisted, $^+N-H\cdots Br-Cu$ hydrogen bonds to two terminal bromido acceptor ligands on a single polymeric perbromidocuprate(II) anionic chain and to a third terminal bromido ligand of a different polymeric anion, as shown in Figure 3.2.4 (a). In the structure, the polymeric anionic moiety is surrounded by six cationic units, but hydrogen bonding only occurs to four of the six cations. Through hydrogen bonding interactions, the cations are linked to two inorganic polymers, to form a one-dimensional hydrogen bonding ladder, as shown in Figure 3.2.4 (b). The hydrogen bonding parameters are listed in the Table 3.2.

Table 3.2. Hydrogen bonding parameters of PENCuBr.

D-H	d(D-H) (Å)	d(H...A) (Å)	<DHA (°)	d(D...A) (Å)	A
N1-H1A	0.890	2.619	153.94	3.441(18)	Br3 [x, y-1, z]
N1-H1B	0.890	2.555	166.72	3.428(16)	Br3 [-x+1, y-1/2, -z+1/2]
N1-H1C	0.890	2.608	154.26	3.431(18)	Br3

3.2.2. Magnetic Characterisation

Powder X-ray diffraction confirmed that the single crystal structure determined for the compound is representative of the bulk material used in the magnetic study, as shown in appendix one, Figure 1. The rapid increase to saturation point, as seen in the M vs H graph of Figure 3.2.5 is characteristic of a ferromagnet. However, considering the shape of the M vs H plot at low field in the range of 0 Oe to 2000 Oe, a kink in the graph can be seen, thus indicating metamagnetic behaviour implying that PENCuBr exhibits both FM as well as AFM behaviour, with AFM interactions appearing in the low temperature region.

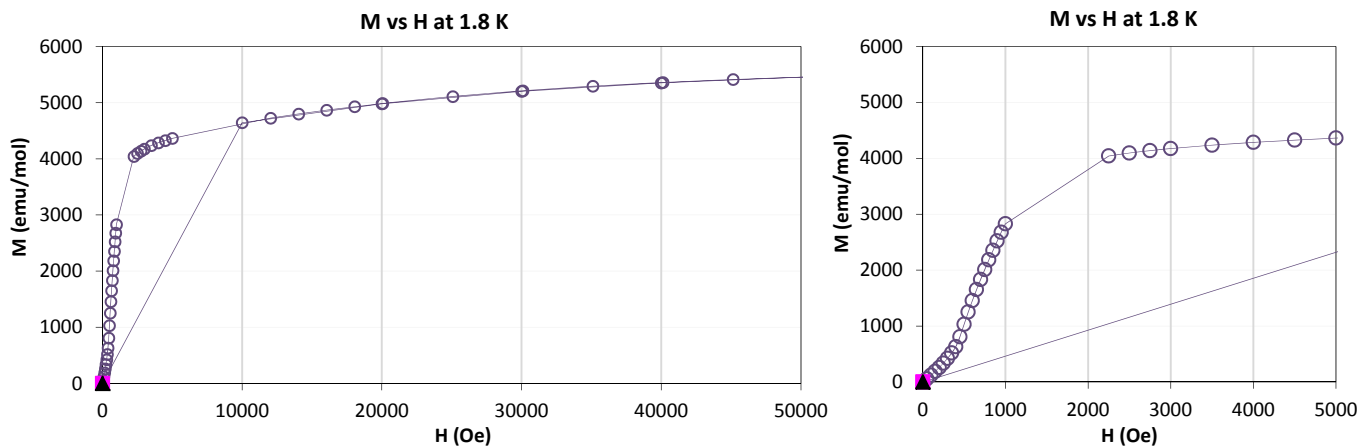


Figure 3.2.5. The M (emu/mol) vs H (Oe) plot of PENCuBr (left) and the plot zoomed in at the low field region (right).

Magnetic susceptibility data was collected over a temperature range of 294 K to 1.8 K in a 0.5 kOe RSO magnetic field. The lower field was selected due to the strong FM interactions observed in the M vs H plot. The χT vs T graph shows a constant χT value of approximately 0.405 emu.K/mol.Oe in the temperature range of 294 K to approximately 70 K, as illustrated in Figure 3.2.6. On cooling below 70 K, a steady increase of χT occurs in a temperature range of between 65.5 K to 5.4 K, with a maximum value of χT of 13.5 emu.K/mol.Oe at 5.4 K, which is characteristic of strong FM interactions between Cu^{2+} ion centres in the polymeric chains. A sudden decrease in χT from 5.4 K to 1.8 K is due to weak AFM interactions occurring between polymer chains at low temperature. The occurrence of both FM and AFM interactions in the material as observed in the χT vs T plot and this agrees with the metamagnetic behaviour observed in the M vs H plot.

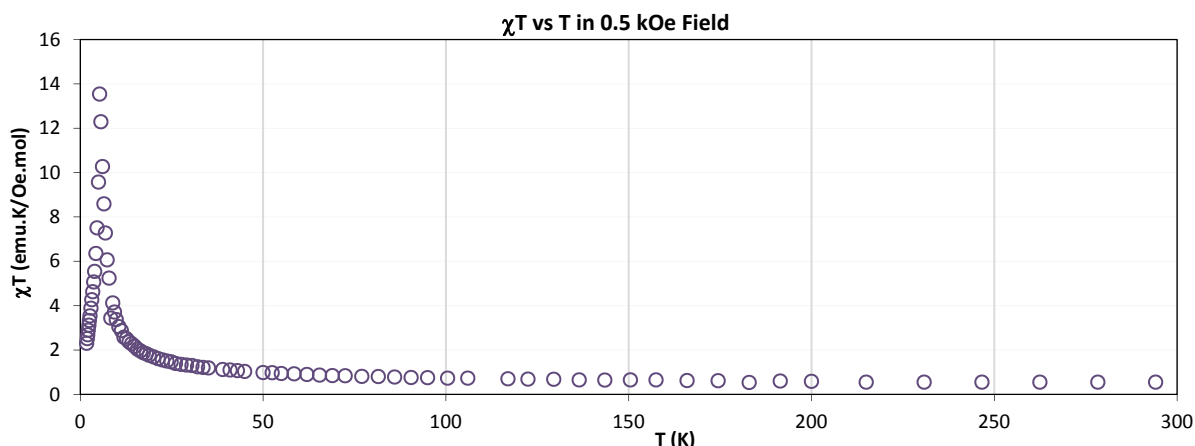


Figure 3.2.6. The graph of χT (emu.K/Oe.mol) vs T (K) for PENCuBr.

The magnetic structure of PENCuBr was determined to identify suitable quantum magnetic models to fit the experimental data. From the orientation of magnetic orbitals along the one-dimensional coordination polymer, strong FM interactions are expected to occur along the one-dimensional polymer chain, which extends along the b -axis. Along the one-dimensional polymer the magnetic orbitals, $d_{x^2-y^2}$, are orientated on the base of the square pyramidal CuX_5^{3-} units, as shown in Figure 3.2.7. Edge sharing square pyramidal units result in the formation of Cu-Br-Cu, through-bond superexchange pathways between neighbouring Cu^{2+} ions *via* bridging bromido ligands, along the b -axis. The exchange pathway consists of magnetic Cu^{2+} ions that are equidistant from each other, forming a uniform chain. Thus, this exchange accounts for the strong FM behaviour observed in the temperature range 294 K to 50 K in the χT vs T plot. Weak AFM interactions are expected to occur between neighbouring polymer chains. This exchange occurs *via* the through space double-halide exchange pathway, $\text{Cu-Br} \cdots \text{Br-Cu}$, specifically between a terminal bromido ligand and the nearest bridging bromido ligand, with the closest $\text{Br} \cdots \text{Br}$ distance of 4.223 Å, as illustrated in Figure 3.2.8.

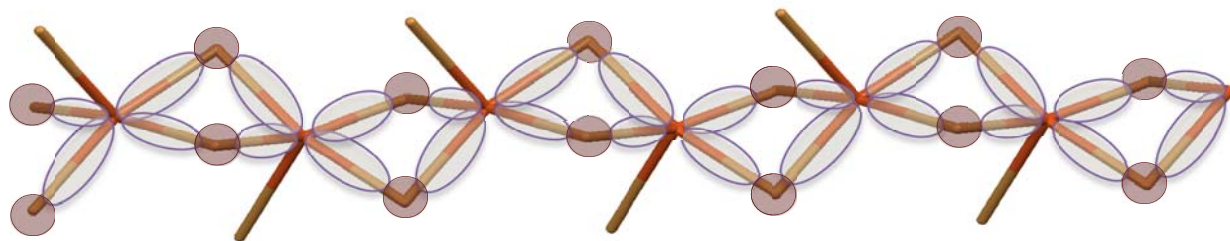


Figure 3.2.7. The magnetic through-bond exchange pathways that exist via the $d_{x^2-y^2}$ orbitals (blue ovals) of the Cu^{2+} ions and the s orbitals of the halogeno ligands (purple circles).

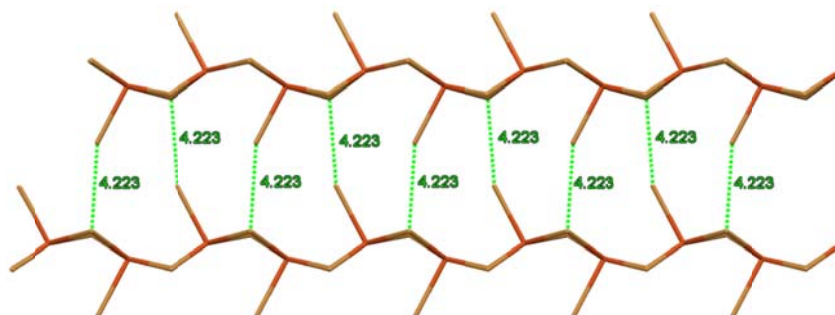


Figure 3.2.8. The distance between neighbouring polymers (green dotted lines). The distance is given in angstrom units (\AA).

The Heisenberg Hamiltonian, $\hat{H} = -\sum_{A,B} J_{AB} \hat{S}_A \cdot \hat{S}_B$, was used to interpret the magnetic data based on the identified exchange pathways in the polymer and between polymers. The data was fitted to the $S = \frac{1}{2}$ uniform ferromagnetic (FM) chain model, with a Curie-Weiss correction. The Curie-Weiss correction takes into account possible magnetic interactions between neighbouring chains. The theoretical model was fitted to the experimental χ vs T data for the high temperature data range of 50 K to 294 K, in the temperature region where FM interactions dominate. Because the model does not take simultaneous FM and AFM interactions into account, the lower temperature data could not be included in the fit.

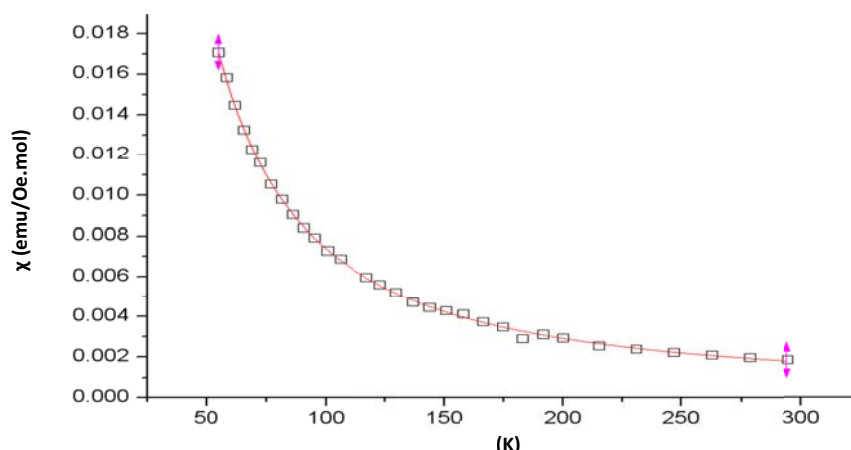


Figure 3.2.9. The fit of experimental magnetic susceptibility data (χ) to a one-dimensional FM model with a CW correction.

When using the uniform FM chain model, the parameters fitted are the Curie constant (CC), the exchange parameter in the chain, J and the Curie-Weiss parameter (CW). A large J value of +192 K was obtained for the FM chain interactions, indicating strong ferromagnetic exchange between Cu^{2+} ions within the chain. Weak antiferromagnetic interactions occur between the polymeric chains, with $\text{CW} = -0.54$. The small value of the Curie-Weiss constant is an indication of the weakness of the AFM exchange, which also explains why these AFM interactions only become significant at low temperatures. The negative sign of the CW constant indicates that the interactions between the chains are AFM, as expected for the double-halide exchange.

It should be mentioned that the uncertainty in the value of J is relatively large due to the fact that not all data points could be fitted.

3.3. Hexa (cycloheptylammonium) (μ_2 -chlorido) (μ -chlorido) $_2$ hexachlorido tricuprate(II) dichloride

Moiety Formula: $6(\text{C}_7\text{H}_{16}\text{N}^+) \text{Cu}_3\text{Cl}_{10}^{4-} \cdot 2\text{Cl}^-$
Abbreviated as HEPCuCl

The structures of many organic-inorganic hybrid materials comprising C_3 - C_6 primary cycloalkylammonium cations and perhalometallate(II) anions have been reported in literature. However not much has been reported on cycloheptylammonium compounds. Only three cycloheptylammonium containing hybrids were located in the CSD, with refcodes **UHAGEQ** (Billing *et al.* 2009), **UHAHIV** (Billing *et al.* 2009) and **VEZPAS** (Billing *et al.* 2007). These compounds consist of primary cycloheptylammonium cations and PbX_n ($\text{X}=\text{Cl}^-$, Br^- or I^-) anions.

The novel structure, HEPCuCl, discussed in this study, is to our knowledge the first cycloheptylammonium compound containing perhalocuprate(II) anions. None of the compounds reported in literature are isostructural to the novel structure discussed here. In addition the structure is of special significance since the type of perhalocuprate(II) anion has never been reported previously.

3.3.1. Structure Analysis

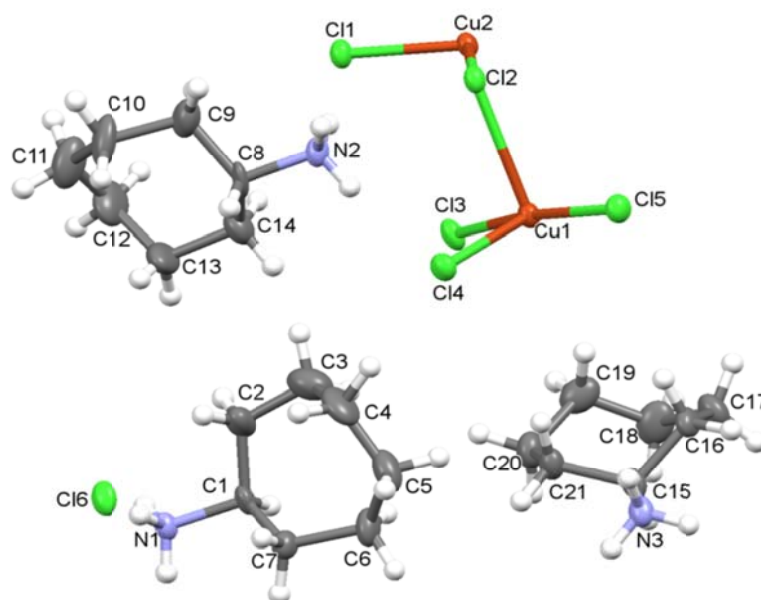


Figure 3.3.1. The asymmetric unit of HEPCuCl. Displacement ellipsoids are drawn the 50% probability level and hydrogen atoms are drawn as spheres of arbitrary radii.

The asymmetric unit of HEPCuCl consists of three crystallographically independent strained primary cycloheptylammonium cations, which all adopt a twist-chair-twist conformation, as well as a Cu_2Cl_5^- anionic moiety. A single isolated chlorido ion is also present in the asymmetric unit, which ensures charge neutrality, as shown in Figure 3.3.1. Four asymmetric units make up the unit cell. The Cu^{2+} ion, Cu2, lies on special position [0.50, 0.02, 0.25].

A two-fold rotation axis completes the anionic moiety resulting in a symmetric $\text{Cu}_3(\mu_2\text{-Cl})(\mu\text{-Cl})_2\text{Cl}_6^{4-}$ trimer, as shown in Figure 3.3.2 (a). The trimeric unit comprises three individual Cu^{2+} ions that are linked by bridging chlorido ligands. Each Cu^{2+} ion is coordinated to two terminal chlorido ligands, while a single bridging chlorido ligand links the Cu1 and Cu2 ions and two bridging chlorido ligands link the two Cu1 metal centres. Cu1 adopts a square pyramidal geometry, with terminal Cl2-Cu1-Cl3 bond angles of $94.26(5)^\circ$, deviating significantly from the ideal square pyramidal geometry of 90° . The bridging Cu1(-x+1,y,-z+1/2)-Cl1-Cu1 and Cu1-Cl5-Cu2 bond angles have an approximate average value of 96° . The Cu2 ion is positioned above the square pyramidal Cu1 ions and adopt a distorted seesaw configuration, with a Cl4-Cu2-Cl4(-x+1,y,-z+1/2) bond angle of $146.90(7)^\circ$. In the trimer, terminal Cu-Cl bond lengths range from $2.257(13) \text{ \AA}$ to $2.274(12) \text{ \AA}$, which are shorter than the bridging Cu-Cl bond lengths, which range from $2.262(13) \text{ \AA}$ to $2.811(14) \text{ \AA}$. The nitrogen atoms are singly protonated and take up the axial position on the cycloheptylammonium cation.

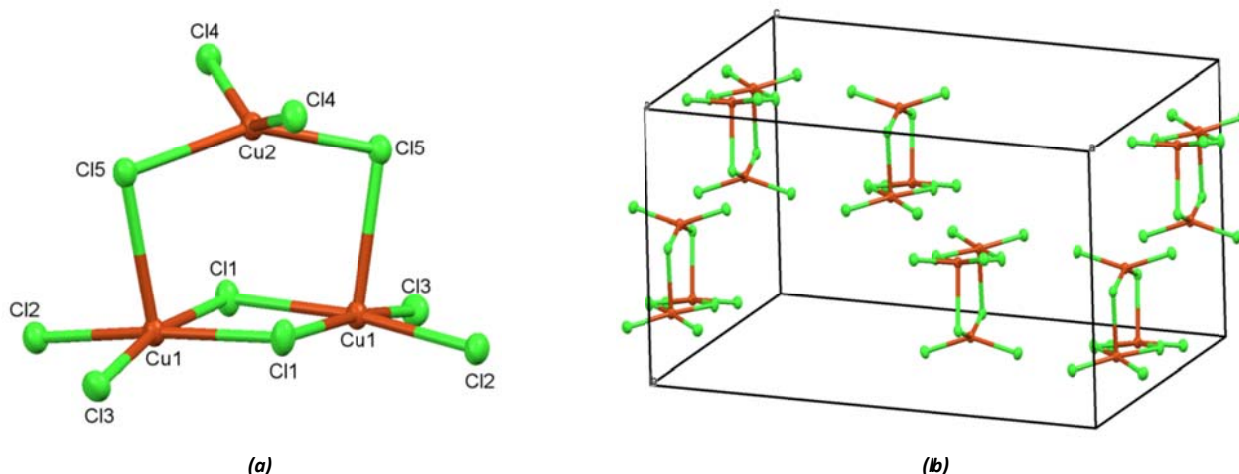


Figure 3.3.2 (a). The complete copper(II) chlorido trimeric unit. (b) The positions of the copper(II) chlorido trimers in the unit cell. The cations are omitted for clarity and displacement ellipsoids are drawn at the 50% probability level.

Figure 3.3.2 (b), illustrates the positions of the anionic copper(II) chlorido trimers within the unit cell. From Figure 3.3.2 (b), it can be seen that the two trimers have all three Cu^{2+} ions positioned on two of the three faces of the unit cell and two trimers have one Cu^{2+} ion positioned in the ac -plane.

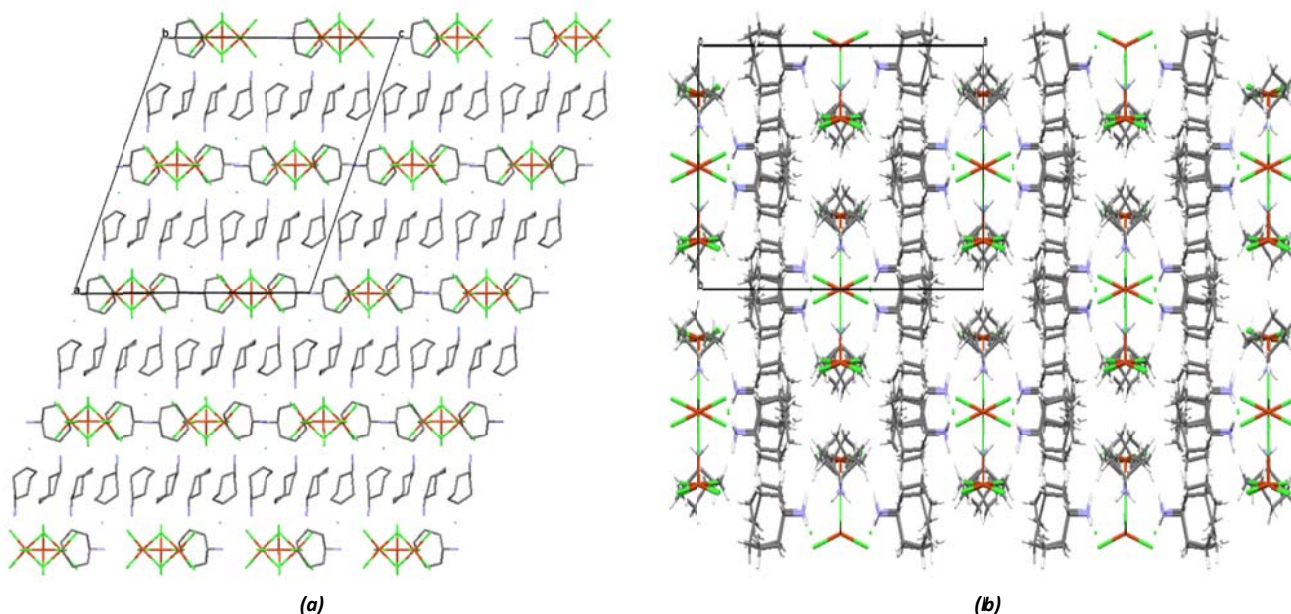


Figure 3.3.3. The packing diagram of cationic and anionic units as viewed down (a) the b-axis and (b) the c-axis respectively.

Through repetition of the unit cell the packing diagram of HEPCuCl can be obtained, as represented in Figure 3.3.3 (a) and (b). The cationic units and anionic trimers pack to form two-dimensional sheets, parallel to the bc -plane. In the HEPCuCl structure, single layers of organic cycloheptylammonium cations alternate with layers

of inorganic copper(II) chlorido trimers, isolated chloride ions and cations, as shown in Figure 3.3.3 (a). In the organic layers, $^+\text{NH}_3$ groups on the cycloheptylammonium cations alternate in orientation and the axial $^+\text{NH}_3$ groups are pointed towards the nearest inorganic unit, as seen in Figure 3.3.3 (b). This orientation of $^+\text{NH}_3$ groups with respect to the inorganic copper(II) chlorido trimers can be explained by strong, charge assisted hydrogen bonding between the cations and anions. Hydrogen bonding parameters are listed in Table 3.3. Figure 3.3.4 shows that six cations are hydrogen-bonded to each anion. The hydrogen bonding capability of all six cations is satisfied, as all three hydrogen atoms of each nitrogen atom are involved in hydrogen bonding, as seen in Figure 3.3.4

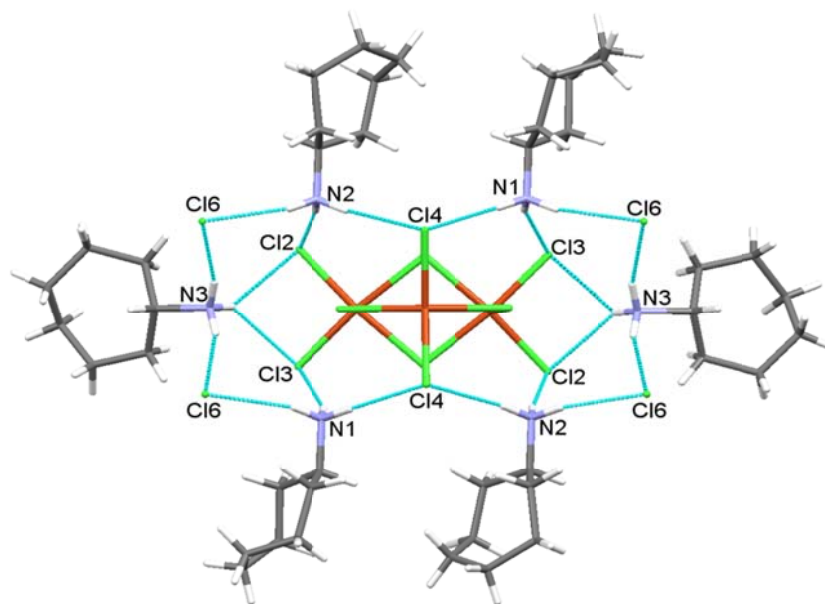


Figure 3.3.4. The hydrogen-bonded unit.

In this network the cations form classic, charge assisted $^+\text{N-H}\cdots\text{Cl-Cu}$ and bifurcated $^+\text{N-H}\cdots(\text{Cl})_2\text{-Cu}$ hydrogen bonds to the trimeric anions and isolated chloride ions. The $^+\text{N1-H}$ and $^+\text{N2-H}$ groups exhibit classic, charge assisted hydrogen bonding interactions to the terminal chlorido ligands of all three Cu^{2+} ions in the trimer. A third classic, charge assisted hydrogen bonding interaction is present between the donor cations and the isolated chloride acceptor ions. Repetition of this hydrogen-bonded motif results in a hydrogen-bonded ribbon, as illustrated in Figure 3.3.5.

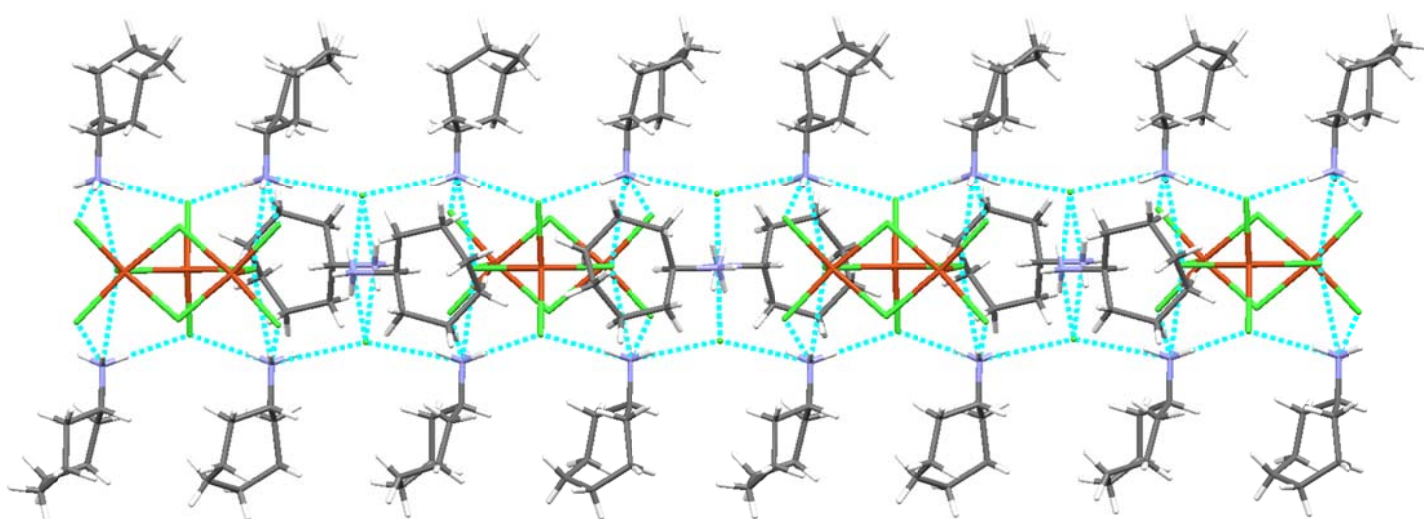


Figure 3.3.5. The one-dimensional hydrogen bonding network between neighbouring cationic and anionic species.

Table 3.3. Hydrogen bonding parameters of HEPCuCl.

D-H	d(D-H) (Å)	d(H...A) (Å)	<DHA (°)	d(D...A) (Å)	A
N3-H3A	0.890	2.341	161.06	3.196(4)	Cl6
N3-H3B	0.890	2.335	163.20	3.198(4)	Cl6 [-x, -y+1, -z]
N3-H3C	0.890	2.588	139.18	3.313(4)	Cl2 [x-1/2, y+1/2, z]
N3-H3C	0.890	2.625	134.51	3.310(4)	Cl3 [x-1/2, y+1/2, z]
N2-H2A	0.890	2.311	168.27	3.188(4)	Cl2
N2-H2B	0.890	2.309	160.76	3.163(4)	Cl6 [-x+1/2, -y+1/2, -z]
N2-H2C	0.890	2.373	173.30	3.259(4)	Cl4
N1-H1A	0.890	2.397	158.17	3.240(4)	Cl3 [x-1/2, y+1/2, z]
N1-H1B	0.890	2.373	178.36	3.263(4)	Cl4 [-x+1/2, y+1/2, -z+1/2]
N1-H1C	0.890	2.360	162.57	3.220(4)	Cl6

3.3.2. Magnetic Characterisation

Due to difficulties experienced in obtaining a large enough pure sample of HEPCuCl, the magnetic characterisation could not be done for this compound. Preliminary studies were done indicating AFM behaviour but due to the sample problems the data could not be fitted to a magnetic model.

3.4. Hexa (cycloheptylammonium) (μ_2 -bromido) (μ -bromido) $_2$ hexabromido tricuprate(II) dibromide

Moiety Formula: $6(\text{C}_7\text{H}_{16}\text{N}^+) \text{Cu}_3\text{Br}_{10}^{4-} \cdot 2\text{Br}^-$
Abbreviated as HEPCuBr

As stated in the structural discussion of HEPCuCl, only three cycloheptylammonium containing hybrid structures have been reported in the literature, namely the PbX_n ($X = \text{Cl}^-$, Br^- or I^-) cycloheptylammonium hybrids, with refcodes **UHAGEQ** (Billing *et al.* 2009), **UHAHIV** (Billing *et al.* 2009) and **VEZPAS** (Billing *et al.* 2007).

The novel structure discussed in this section is the copper(II) bromido version of the HEPCuCl structure reported in the previous section. To our knowledge, there are no known compounds in literature comprising cycloheptylammonium cations and perbromidocuprate(II) anions. The novel structure, HEPCuBr is not isostructural to the HEPCuCl structure. However, it also contains the unexpected, unprecedented, cluster type anion found in the HEPCuCl structure.

3.4.1. Structure Analysis

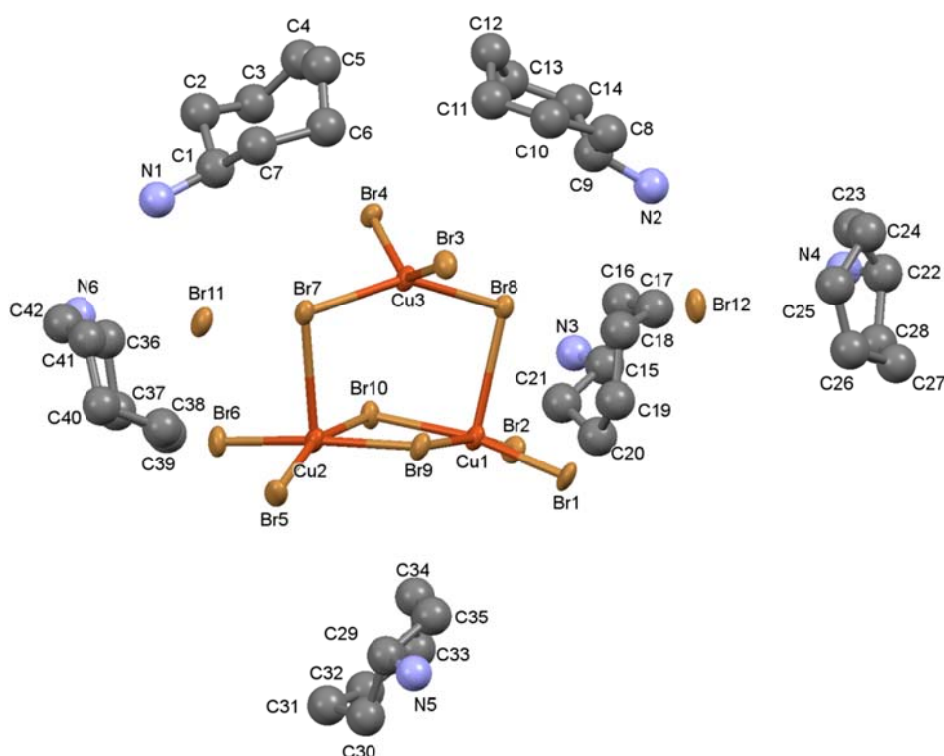


Figure 3.4.1. The asymmetric unit of HEPCuBr. Displacement ellipsoids are drawn at the 50 % probability level. The carbon atoms are drawn as spheres of arbitrary radius and hydrogen atoms are omitted for clarity.

Before commencing the structural discussion, it should be pointed out that the crystallographic data collected for the HEPCuBr crystal is not of a very good quality and crystals of better quality could not be obtained. Due to the uniqueness of the structure, it was decided to still include the structure in the dissertation. In the

structure, the inorganic component could be refined anisotropically, but the carbon and nitrogen atoms were refined isotropically.

The asymmetric unit of HEPCuBr comprises six crystallographically independent cycloheptylammonium cations, a $\text{Cu}_3(\mu_2\text{-Br})(\mu\text{-Br})_2\text{Br}_6^{4-}$ anionic moiety and two isolated bromide ions, which ensures charge neutrality, as shown in Figure 3.4.1. The unit cell contains two asymmetric units.

The cycloheptylammonium cations adopt a twist-chair-twist conformation and the nitrogen atoms on all six cations in the asymmetric unit are singly protonated. The positively charged $^+\text{NH}_3$ groups adopt the axial position on the C_7 ring of the cations.

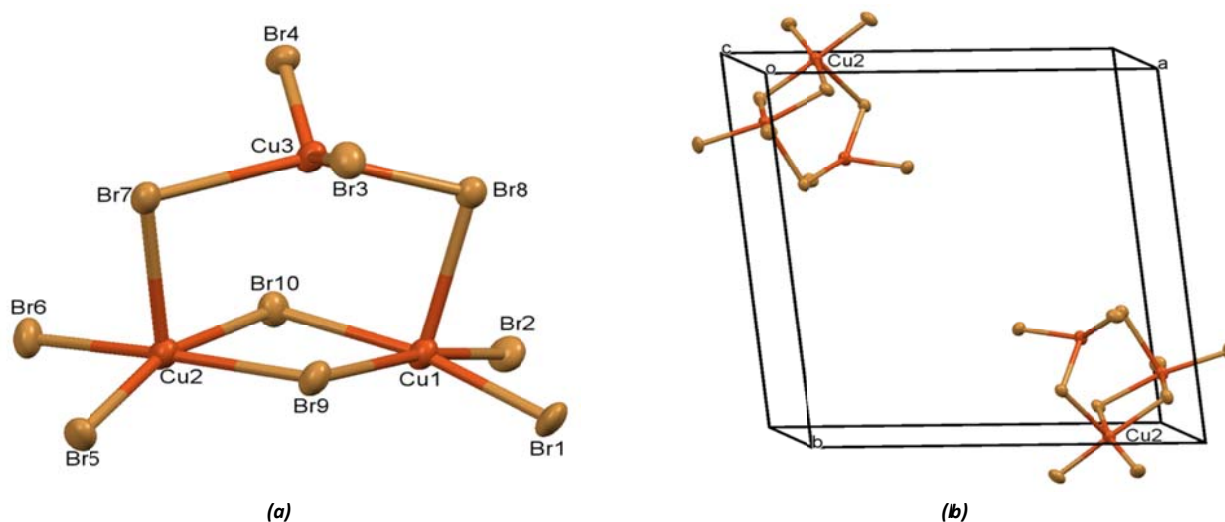


Figure 3.4.2. (a) The copper(II) bromido trimer. (b) The unit cell showing only the trimer anions as viewed down the c -axis. The cationic units and isolated bromide ions are omitted for clarity and displacement ellipsoids are drawn at the 50% probability level.

The asymmetric copper(II) bromido trimeric anion, as shown in Figure 3.4.2 (a), contains three individual Cu^{2+} metal centres. Each metal centre is coordinated to bridging and two terminal bromido ligands. The Cu1 and Cu2 copper(II) coordination spheres adopt square pyramidal geometries, while the trimer has Br-Cu1-Br and Br-Cu2-Br bond angles averaging 91.98° and 89.59° , respectively and terminal Cu-Br bond lengths of approximately 2.3 Å. The doubly bridged part of the trimer has Cu2-Br10 and Cu1-Br10 bond lengths that are slightly longer than the Cu1-Br9 and Cu2-Br9 bonds, with Cu2-Br10-Cu1 and Cu2-Br9-Cu1 bridging angles of $95.11(14)^\circ$ and $95.27(14)^\circ$, respectively. Single bromido ligands bridge the Cu1 and Cu2 ions to the Cu3 metal centre *via* long Cu-Br bond lengths of 2.8858(41) Å and 2.8887(41) Å and bond angles of $96.75(13)^\circ$ and $97.52(13)^\circ$, while the Cu3 ion adopts a distorted see-saw configuration.

Two trimers are positioned at the opposite corners of the unit cell related by an inversion centre. One Cu^{2+} ion, Cu2, from each trimer is positioned on the ac -plane of the unit cell, as shown in Figure 3.4.2 (b).

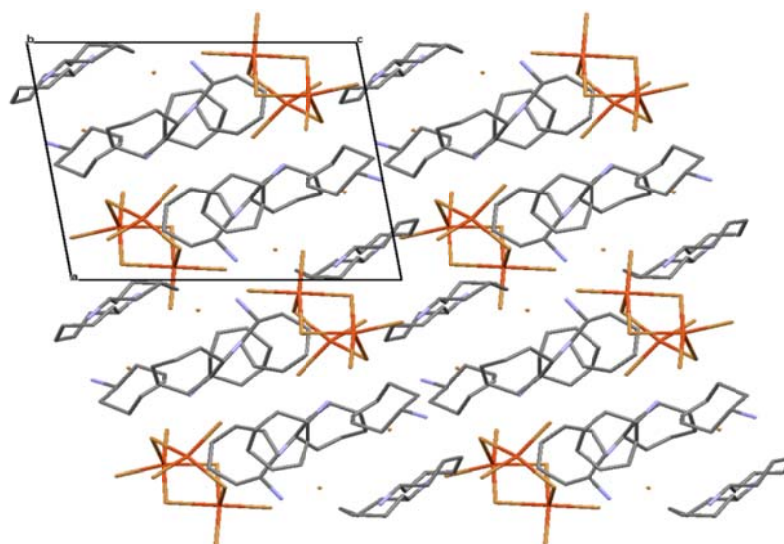


Figure 3.4.3. The packing diagram of cationic and anionic species, as viewed down the *b*-axis. The hydrogen atoms are omitted for clarity.

The anionic and cationic moieties pack in two-dimensional sheets, as shown in Figure 3.4.3. The inorganic layers contain individual trimers, which are separated by layers of cycloheptylammonium cations. The inorganic layers alternate with organic layers of cycloheptylammonium cations. The $^+\text{NH}_3$ groups are oriented towards the nearest inorganic trimer and this orientation can be explained by strong, charge assisted hydrogen bonds between cations and anions, as shown in Figure 3.4.4. It is interesting to note that exactly the same hydrogen bonding interactions are present in this structure and in the HEPCuCl structure, even though the compounds are not isostructural. The hydrogen bonding parameters are listed in Table 3.4.

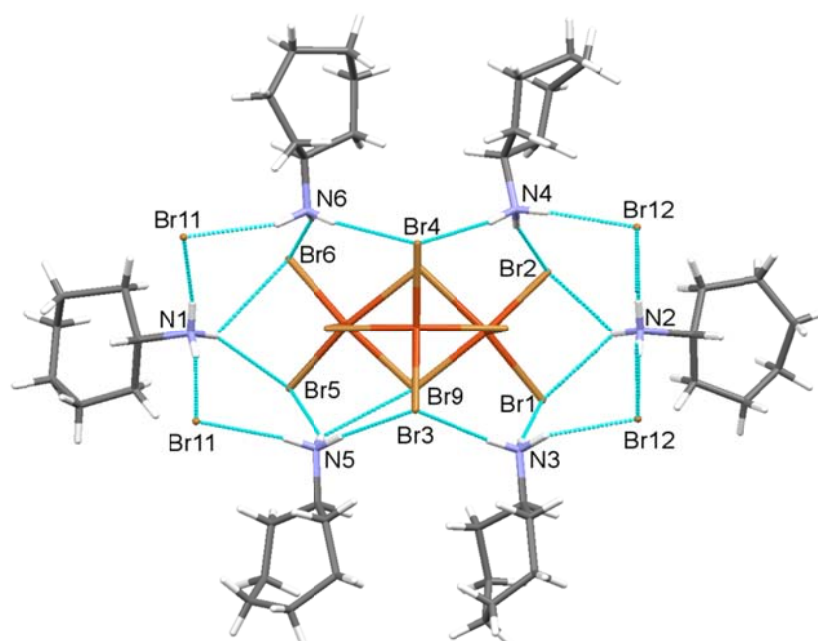


Figure 3.4.4. The hydrogen-bonded motif.

In this hydrogen-bonded network, two types of hydrogen bonding interactions exist, firstly $^+\text{N-H}\cdots\text{Br}^-$, in which hydrogen bonding occurs to isolated bromide acceptor ions and secondly, $^+\text{N-H}\cdots\text{Br-Cu}$, where hydrogen bonding occurs to coordinated bromido acceptor ligands, as shown in Figure 3.4.4. Six cations, four bromide anions and a cluster anion form a hydrogen-bonded motif. In this motif, the hydrogen bonding capability is satisfied for all six cations, as all three hydrogen atoms of each nitrogen atom partake in hydrogen bonding. Each trimer is hydrogen-bonded to six individual cations *via* classic, charge assisted $^+\text{N-H}\cdots\text{Br-Cu}$ and bifurcated hydrogen bonds, $^+\text{N-H}\cdots(\text{Br}^-)_2\text{-Cu}$. Classic hydrogen bonding interactions occur between cations and the terminal bromido ligands, as well as to the isolated bromide ions. Bifurcated hydrogen bonding occur between the hydrogen atom on a donor nitrogen atom of three individual cationic species and the terminal

bromido ligands on the two sides of the trimer, as well to a bridging bromido ligand, Br9. Repetition of the hydrogen-bonded motif results in a one-dimensional hydrogen-bonded ribbon, as shown in Figure 3.4.5.

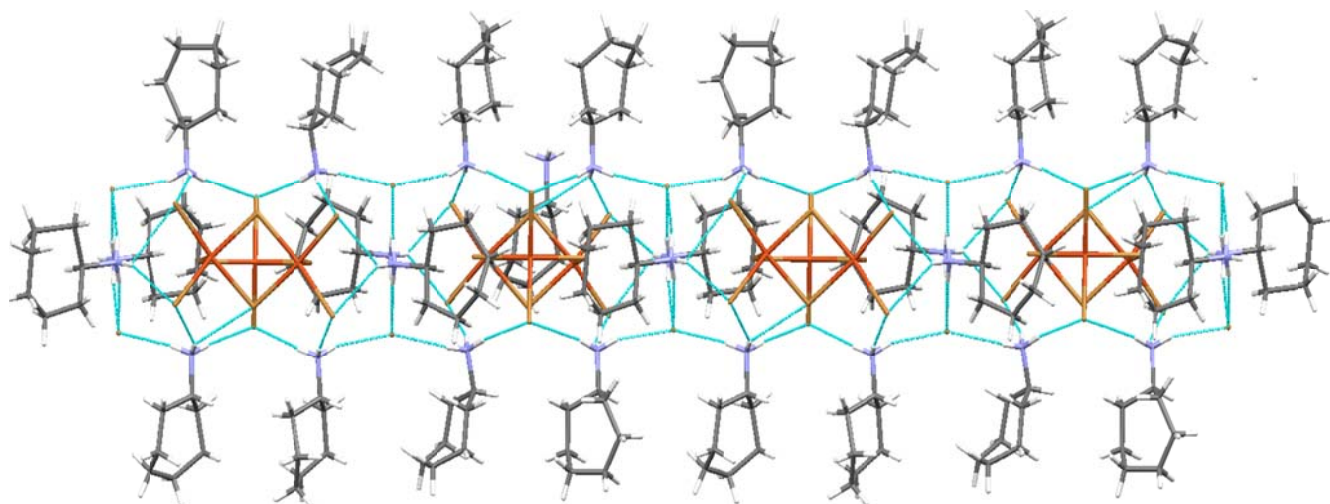


Figure 3.4.5. The one-dimensional hydrogen-bonded ribbon.

Table 3.4. Hydrogen bonding parameters of HEPCuBr.

D-H	d(D-H) (Å)	d(H...A) (Å)	<DHA (°)	d(D...A) (Å)	A
N1-H1A	0.890	2.618	148.91	3.411(2)	Br5 [-x+1, -y+2, -z]
N1-H1A	0.890	2.958	125.85	3.553(2)	Br6 [-x+1, -y+2, -z]
N1-H1B	0.890	2.460	159.49	3.308(2)	Br11
N1-H1C	0.890	2.463	171.33	3.346(2)	Br11 [-x+1, -y+2, -z]
N2-H2C	0.890	2.449	176.18	3.338(2)	Br12 [-x+2, -y+1, -z+1]
N2-H2D	0.890	2.528	169.53	3.407(2)	Br12
N2-H2E	0.890	2.714	135.97	3.411(2)	Br2 [-x+2, -y+1, -z+1]
N2-H2E	0.890	2.771	142.41	3.519(2)	Br1 [-x+2, -y+1, -z+1]
N3-H3C	0.890	2.548	165.48	3.417(2)	Br1
N3-H3D	0.890	2.474	150.70	3.279(2)	Br12
N3-H3E	0.890	2.513	167.68	3.388(2)	Br3
N4-H4C	0.890	2.444	162.56	3.304(2)	Br12
N4-H4D	0.890	2.587	170.78	3.468(2)	Br4 [-x+2, -y+1, -z+1]
N4-H4E	0.890	2.572	163.44	3.434(2)	Br2 [-x+2, -y+1, -z+1]
N4-H4E	0.890	3.051	121.76	3.600(2)	Br10 [-x+2, -y+1, -z+1]
N5-H5C	0.890	2.480	173.08	3.366(2)	Br11 [-x+2, -y+2, -z]
N5-H5D	0.890	2.656	174.79	3.543(2)	Br3 [-x+2, -y+2, -z]
N5-H5E	0.890	2.609	150.50	3.412(2)	Br5 [-x+2, -y+2, -z]
N5-H5E	0.890	2.960	128.40	3.581(2)	Br9 [-x+2, -y+2, -z]
N6-H6C	0.890	2.425	156.73	3.261(2)	Br11
N6-H6D	0.890	2.595	154.95	3.422(2)	Br6 [-x+1, -y+2, -z]
N6-H6E	0.890	2.557	170.27	3.438(2)	Br4 [-x+1, -y+2, -z]

3.4.2. Magnetic Characterisation

Preliminary magnetic studies indicated that the HEPCuBr compound exhibits AFM interactions at low temperatures. However, due to the difficulty of crystallising a pure sample, the magnetic data could not be analysed further.

3.5. Cycloheptylammonium bromide

Moiety Formula: $(C_7H_{16}N^+) \cdot Br^-$

Abbreviated as HEPBr

In the literature, cyclohexylammonium, DABCO and piperazinium halide salt structures have been reported and the majority of these structures are chloride salts, as bromide salts seem to be more scarce. However, to our knowledge, no halide salt structures of cyclopentylammonium and cycloheptylammonium have been reported in the CSD.

Even though the aim of the current study is the combination of metal(II) halide and cycloalkylammonium units, the formation of the novel cycloheptylammonium bromide, HEPBr happened by role of chance. The cycloheptylammonium bromide salt, is to our knowledge, the first cycloheptylammonium salt structure determined. No magnetic data was collected on HEPBr, as there are no metal ions present to impart magnetic properties. The crystal structure was determined and is discussed in this section.

3.5.1. Structure Analysis

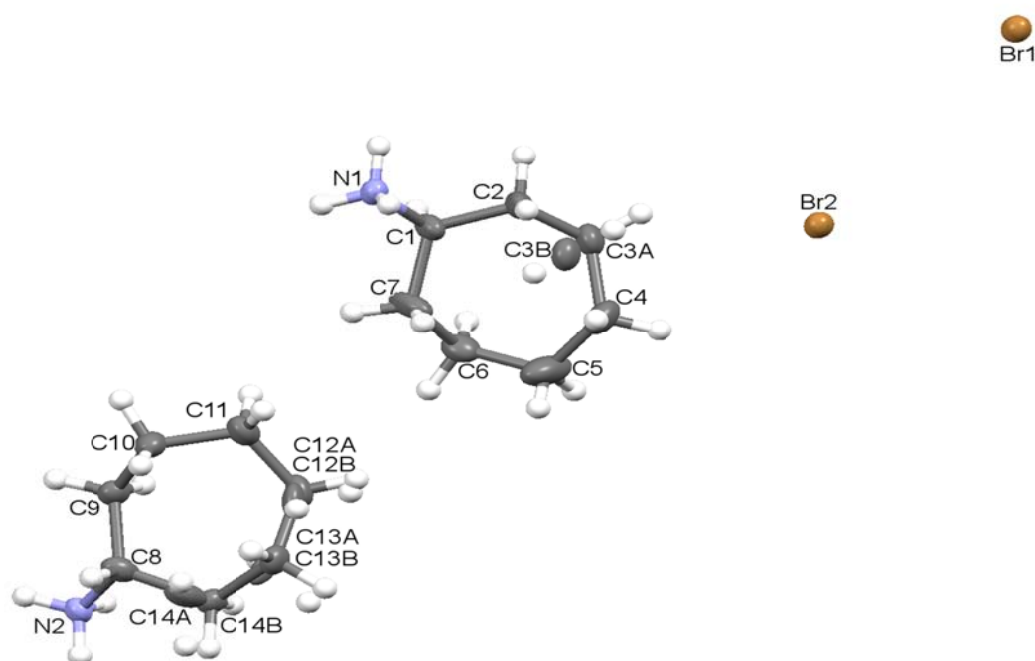


Figure 3.5.1. The asymmetric unit of HEPBr. Displacement ellipsoids are drawn at the 50% probability level and hydrogen atoms are drawn as spheres of arbitrary radius.

The asymmetric unit comprises two crystallographically independent, isolated cycloheptylammonium cations and two isolated bromide ions, as shown in Figure 3.5.1. Both cycloheptylammonium rings are disordered, with atom C3 disordered over two positions (0.68 : 0.32) in the cation containing atom N1, while atoms C12, C13 and C14 are disordered over two positions (0.74 : 0.26) in the cation containing atom N2. The cycloheptylammonium cations are both singly protonated and each individual cation contains one $^+NH_3$ group which adopts the axial position on the cycloheptylammonium ring and conforms to a twist chair-twist conformation. The packing diagram, Figure 3.5.2, shows that each individual cycloheptylammonium cation packs in a separate layer, such that the cycloheptylammonium cation with nitrogen atom N1 forms one layer and the cycloheptylammonium cation containing the N2 nitrogen atom forms another layer. From here on, the individual layers will be referred to as the N1 layer and the N2 layer.

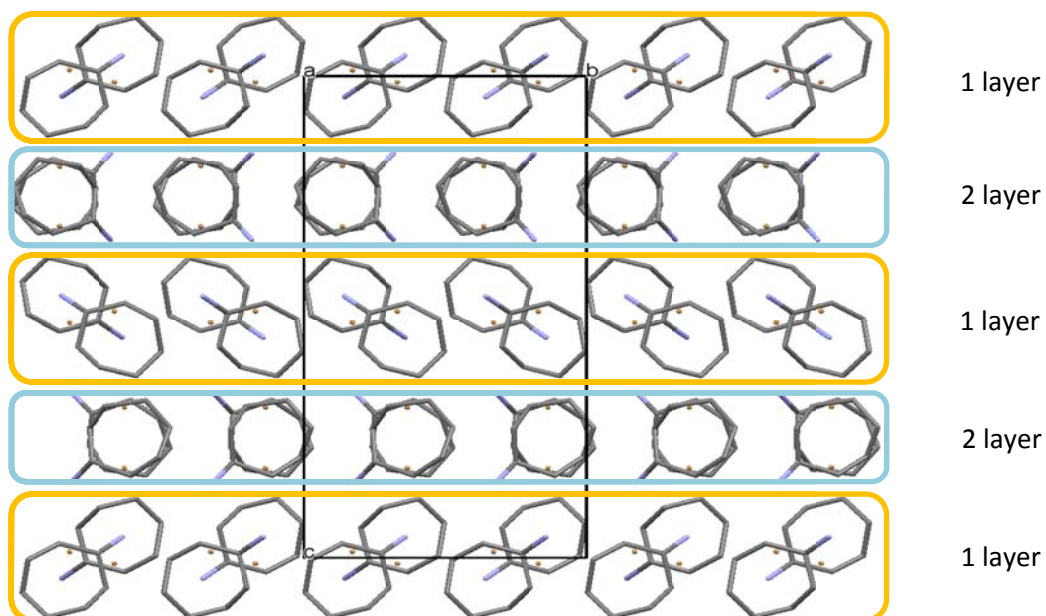


Figure 3.5.2. The packing diagram of HEPBr as viewed down the a -axis. Only the major cations are shown.

The alternating N1 and N2 layers extend along the bc -plane. In the N1 layer, the cations adopt opposite orientations relative to each other. In the N2 layer, the cycloheptylammonium cations overlap when viewed down the a -axis and the $^+NH_3$ groups are positioned at an angle to each other. In both layers a single bromide ion lies close to the $^+NH_3$ groups.

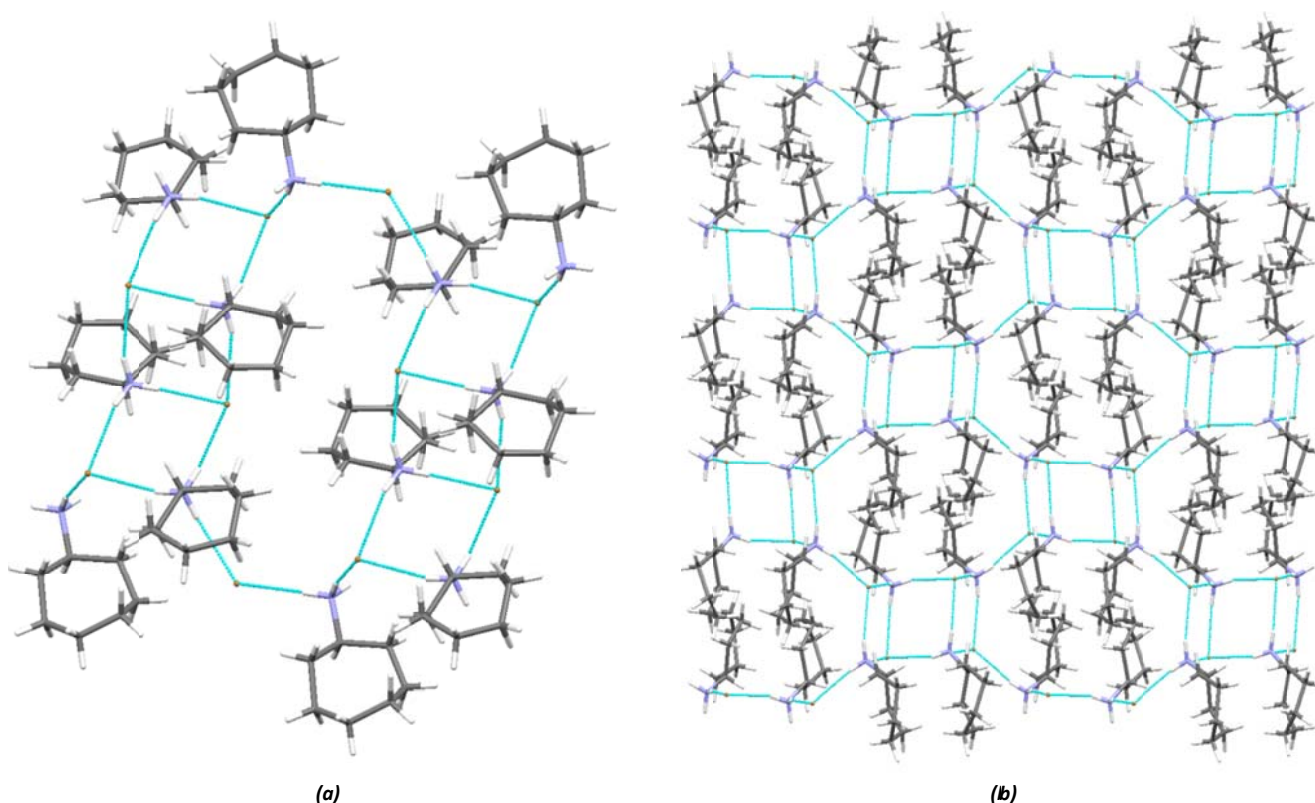


Figure 3.5.3. (a) The hydrogen-bonded unit and (b) The two-dimensional hydrogen-bonded sheet.

The hydrogen bonding interactions that occur between cycloheptylammonium cations and bromide ions can be described as classic, charge assisted $^+N-H \cdots Br$ hydrogen bonding interactions. Rows of hydrogen-bonded ladders form and are linked by hydrogen bonds to isolated bromide ions, as shown in Figure 3.5.3 (a), to form two-dimensional hydrogen-bonded sheets, as illustrated in Figure 3.5.3 (b). All three hydrogen atoms of

individual cations partake in hydrogen bonding and as a result the hydrogen bonding capability of all cationic species is fully satisfied. The hydrogen bonding parameters are listed in Table 3.5.

Table 3.5. Hydrogen bonding parameters of HEPBr.

D-H	d(D-H) (Å)	d(H...A) (Å)	<DHA (°)	d(D...A) (Å)	A
N1-H1A	0.890	2.431	170.96	3.312(3)	Br2 [x, y-1, z]
N1-H1B	0.890	2.432	160.89	3.286(3)	Br1 [x, y-1, z]
N1-H1C	0.890	2.482	161.83	3.339(3)	Br2 [-x, -y, -z+1]
N2-H2A	0.890	2.478	166.38	3.350(3)	Br1 [x, -y-1/2, z+1/2]
N2-H2B	0.890	2.429	171.96	3.312(3)	Br2 [x, -y-1/2, z+1/2]
N2-H2C	0.890	2.477	170.02	3.357(3)	Br1 [-x+1/2, -y, z+1/2]

3.6. Piperazinium tetrachloridocuprate(II)

Moiety Formula: $(C_4H_{12}N_2^{2+}) CuCl_4^{2-}$
Abbreviated as PIPCuCl

A number of studies have previously been conducted on compounds which consist of isolated piperazinium dications and either isolated distorted tetrahedral, polymeric or perovskite perchloridocuprate(II) anionic moieties. These compounds have been reported in the CSD, namely structures with the following refcodes: **COPDOA** (Daoud *et al.* 1984), **COPDOA01** (Battaglia *et al.* 1988), **COPDOA10** (Daoud *et al.* 1986) and **NUTDOV** (Riley *et al.* 1998).

A novel structure, consisting of tetrahedral $CuCl_4^{2-}$ anions and isolated piperazinium dications, has been prepared in this study. However, during the course of this investigation it came to our attention that the structure has been reported recently by another group, Tuikka *et al.* 2013, with CSD refcode **BICPEK**. Due to the fact that magnetic studies were also conducted on this compound in the current study, its inclusion in the results section is warranted.

The PIPCuCl structure was found to be non-centrosymmetric, crystallising in space group $P4_12_12$, but both of the ions comprising the structure are achiral. The absolute configuration was determined, with a Flack parameter of 0.0390(9). The hydrated form of this tetrachloridocuprate(II) compound, **NUTDUB** (Riley *et al.* 1998), has already been reported in the CSD. As mentioned previously, magnetic data were collected for the PIPCuCl compound and are discussed in the magnetic characterisation section.

3.6.1. Structure Analysis

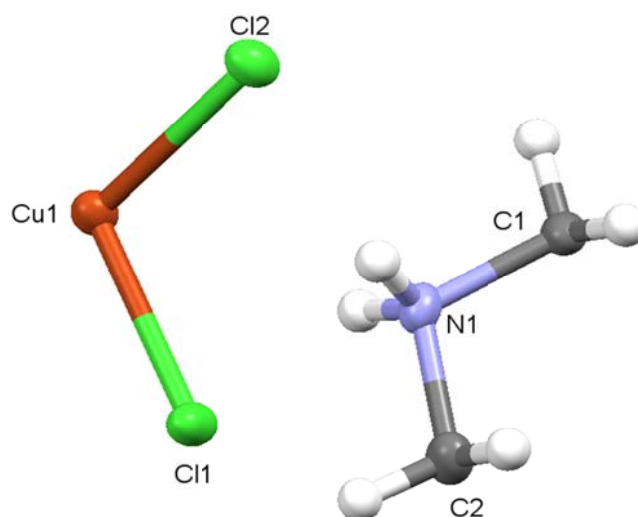


Figure 3.6.1. The asymmetric unit of PIPCuCl. Displacement ellipsoids are drawn at the 50% probability level and hydrogen atoms are drawn as spheres of arbitrary radius.

The asymmetric unit of PIPCuCl consists of an isolated $CuCl_2$ unit and half an isolated piperazinium dication, as shown in Figure 3.6.1. The cuprate(II) ion, Cu1, lies on a special position, [0.4056, 0.4056, 0], with a 2-fold rotation axis running through the Cu^{2+} ion. The isolated piperazinium dication is bisected by a 2-fold rotation axis, which passes through the C2-C2 and C1-C1 bonds.

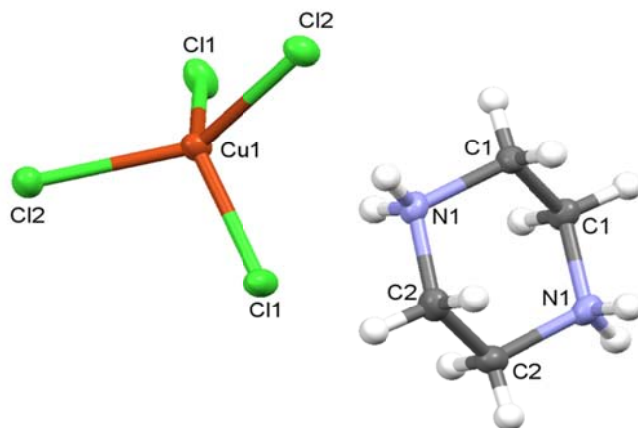


Figure 3.6.2. The cationic and anionic units comprising the PIPCuCl structure. Displacements of ellipsoids are drawn at the 50% probability level and hydrogen atoms are drawn as spheres of arbitrary radius.

Growing the asymmetric unit gives an isolated CuCl_4^{2-} anion and an isolated piperazinium dication, as shown in Figure 3.6.2. The isolated anion is comprised of a Cu^{2+} ion centre, with four chlorido ligands coordinated to the metal ion. The isolated CuCl_4^{2-} anion adopts a flattened tetrahedral geometry, with Cl1-Cu1-Cl1 and Cl2-Cu1-Cl2 bond angles of $131.44(2)^\circ$ and $136.62(2)^\circ$ respectively, deviating significantly from the ideal tetrahedral angle of 109.5° . All four Cu-Cl bond distances are reasonably similar in length. The isolated dication adopts a chair conformation, with both nitrogen atoms of the piperazinium dication being singly protonated.

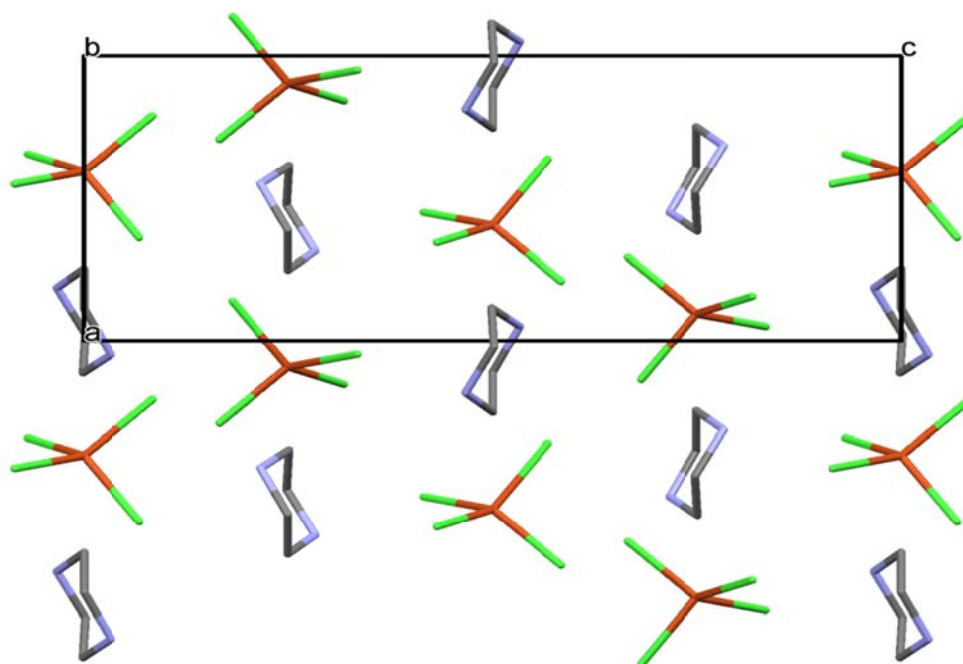


Figure 3.6.3. The packing diagram of PIPCuCl as viewed down the *b*-axis. The hydrogen atoms are omitted for clarity.

Alternating isolated anions and dications pack in sigmoidal rows of dications and anions extending along the *ac*-plane, as shown in Figure 3.6.3. Bifurcated, charge assisted, $^+\text{N}-\text{H}\cdots(\text{Cl})_2-\text{Cu}$, hydrogen bonding interactions exist between the hydrogen atoms of the nitrogen donor atoms of the dication and the acceptor chlorido ligands of the anions.

Each $^+\text{NH}_2$ group is bifurcately hydrogen-bonded to two adjacent chlorido acceptor ligands of two different anions. As a result, each $\text{C}_4\text{H}_{12}\text{N}_2^{2+}$ dication is hydrogen-bonded to four separate CuCl_4^{2-} anions, as illustrated in Figure 3.6.4 (a). A three-dimensional hydrogen bonding network, which links cations and anions, is formed, as shown in Figure 3.6.4 (b). Hydrogen bonding parameters are listed in Table 3.6.

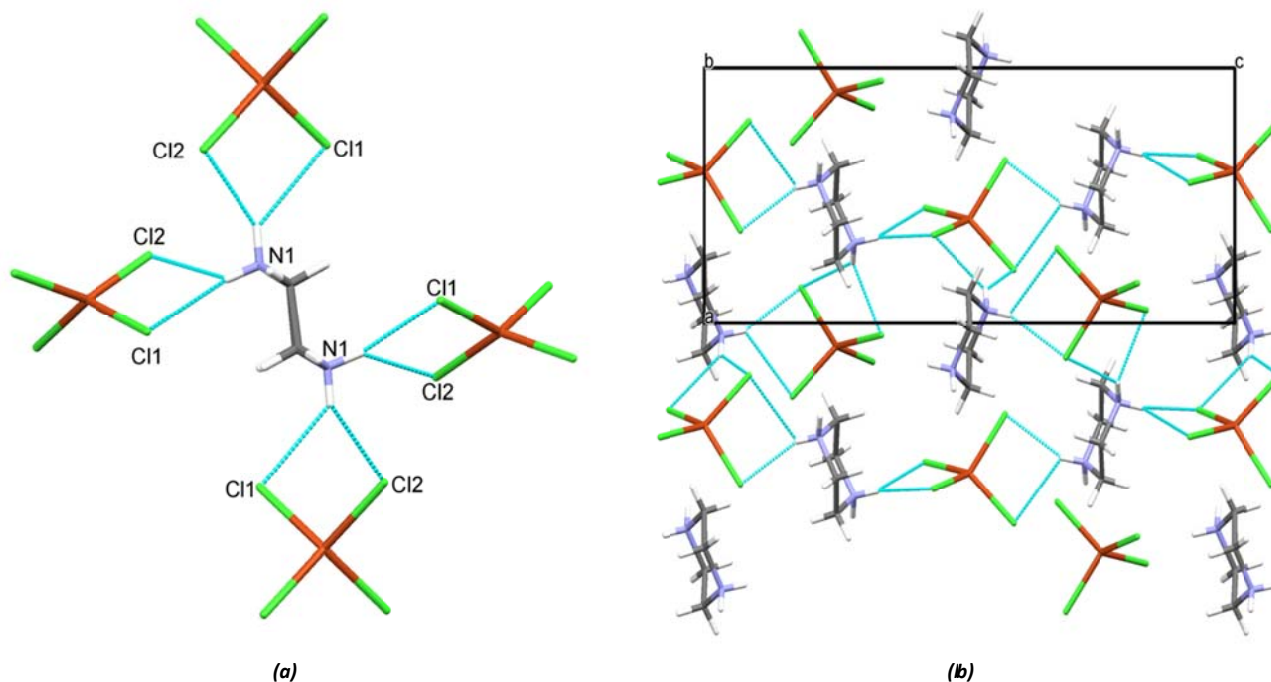


Figure 3.6.4. (a) The hydrogen bonding interactions between a dication and four different anions. (b) The hydrogen bonding network formed between anions and dications.

Table 3.6. Hydrogen bonding parameters of PIPCuCl

D-H	d(D-H) (Å)	d(H...A) (Å)	<DHA (°)	d(D...A) (Å)	A
N1-H1	0.830	2.508	140.38	3.191(12)	Cl2 [-x+1/2, y-1/2, -z+1/4]
N1-H1	0.830	2.629	133.64	3.258(12)	Cl1 [-y+1/2, x-1/2, z+1/4]
N1-H2	0.840	2.778	122.90	3.311(11)	Cl2
N1-H2	0.840	2.426	155.59	3.209(11)	Cl1

3.6.2. Magnetic Property Analysis

Powder X-ray diffraction confirmed that the single crystal is representative of the bulk of the PIPCuCl compound (Appendix one, Figure 2).

Figure 3.6.5. The plot of χT (emu.K/Oe.mol) vs T (K).

As illustrated in Figure 3.6.5, the graph of χT vs T indicates a constant χT value of approximately 0.443 emu.K/Oe.mol from a temperature range of 300 K to 80 K. A sudden decrease in χT in the low temperature range from approximately 80 K indicates antiferromagnetic behaviour between Cu^{2+} ions. These results correspond to the χ vs T plot of Figure 3.6.6 as a steady increase is seen in χ from about 80 K. However a maximum is not observed for χ , which suggests that the antiferromagnetic interactions in the double-halide

Cu-Br⁻...Br-Cu exchange pathways are weak. This exchange is typical for the double-halide exchange between isolated CuCl₄²⁻ units.

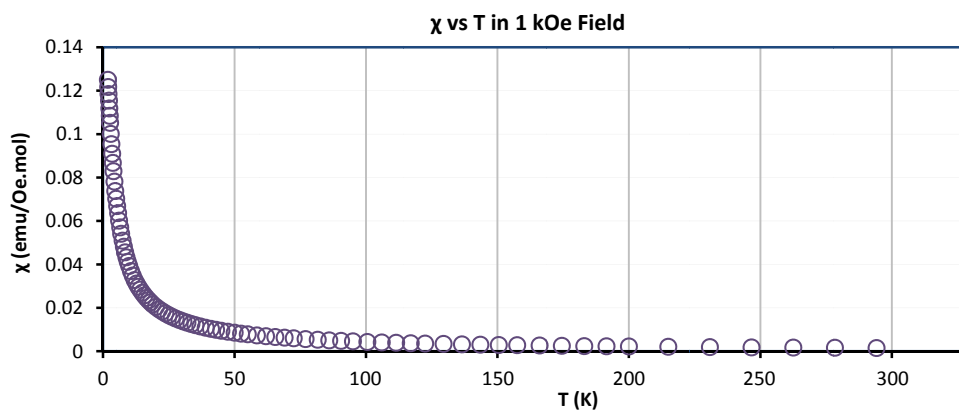


Figure 3.6.6. The plot of χ (emu./Oe.mol) vs T (K).

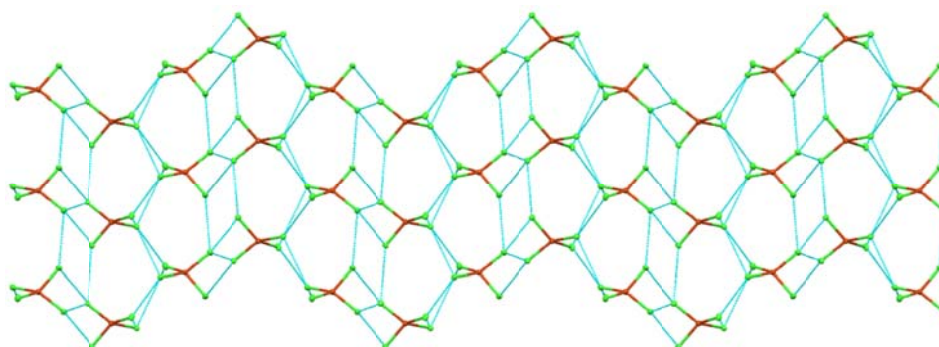


Figure 3.6.7. The double-halide exchange pathway that links anions to form a three-dimensional network.

An analysis of the Cu-Cl⁻...Cl-Cu close contacts in the structure showed that a three-dimensional exchange pathway exists in the structure, as illustrated in Figure 3.6.7. Unfortunately, due to the complexity of this three-dimensional exchange, no quantum mechanical model is available to fit the magnetic data, in order to obtain information on the exchange parameter, J. Suffice to say at this point that AFM exchange interactions are present between the inorganic CuCl₄²⁻ units in the structure.

3.7. Bis (1,4-diazoniabicyclo[2.2.2]octane) trichloride diaqua trichloridocuprate(II) monohydrate

Moiety Formula: $2(\text{C}_6\text{H}_{14}\text{N}_2^{2+}) \text{CuCl}_3(\text{H}_2\text{O})_2 \cdot 3\text{Cl}^- \cdot \text{H}_2\text{O}$
Abbreviated as TOZFAP

Four crystal structures of the title compound have been reported in the literature, with CSD refcodes **TOZFAP** (Wei and Willet. 1996), **TOZFAP01** (Zhang *et al.* 2010), **TOZFAP02** (Zhang *et al.* 2010) and **TOZFAP03** (Zhang *et al.* 2010). The crystal structures were determined at three different temperatures, with **TOZFAP** and **TOZFAP03** determined at room temperature (R.T), **TOZFAP01** at 193 K and **TOZFAP02** at 93K.

Three of the four structures were determined as part of a study of the ferroelectric properties of materials, as well as DSC studies revealed that a phase transition occurs on cooling. The DSC scan showed that a phase transition from the room temperature (**TOZFAP03**) to a low temperature crystal structure (**TOZFAP01**) occurs at 234 K (Zhang *et al.* 2010), while a transition from the low temperature form to the high temperature form occurs at 235 K. The hysteresis of 5 K indicates that the phase transition is reversible (Zhang *et al.* 2010).

An interesting feature of this structure is that the anions adopt trigonal bipyramidal geometries and this is the only example of such an anion in the CSD. To study the magnetic exchange occurring between these unique anions, it was decided to resynthesise the material and conduct magnetic studies.

3.7.1. Structure Description

Because the **TOZFAP** structure was already discussed in detail in section 1.5, only the magnetic results are reported here.

3.7.2. Magnetic Characterisation

Powder X-ray diffraction showed that the powder pattern of the powder sample used for magnetic characterisation corresponded to the calculated powder pattern of the room temperature structures, **TOZFAP** and **TOZFAP03** (Appendix one, Figure 3). However, since the magnetic susceptibility data was collected over a temperature range of 310 K to 1.8 K, it was expected that the compound underwent a phase transition to the **TOZFAP01** and **TOZFAP02** structures. Magnetic interactions are known to exist at low temperatures, as a result the magnetic susceptibility data is modelled according to the **TOZFAP02** structure.

The graph of χT vs T , illustrated in Figure 3.7.1, shows a constant value of χT of approximately of 0.485 emu.K/mol.Oe in the temperature range 80 K to 310 K. On cooling below 80 K the value of χT starts to decrease, which indicates the presence of antiferromagnetic interactions between Cu^{2+} ions. When considering the plot of χ vs T , as shown in Figure 3.7.2, an increase in the value of χ is observed at lower temperatures, as expected for an antiferromagnetic material, however, a maximum is not observed for χ and this suggests that the antiferromagnetic interactions are weak.

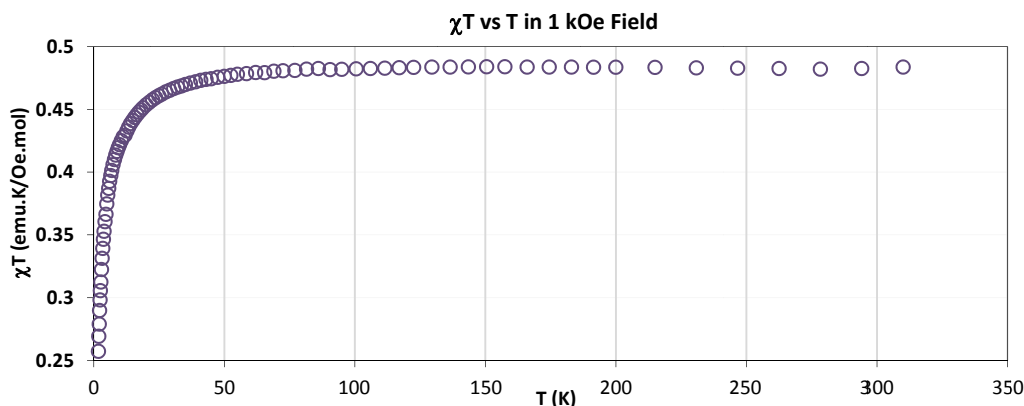


Figure 3.7.1. The χT (emu.K/Oe.mol) vs T (K) plot of TOZFAP02 in 1 kOe field.

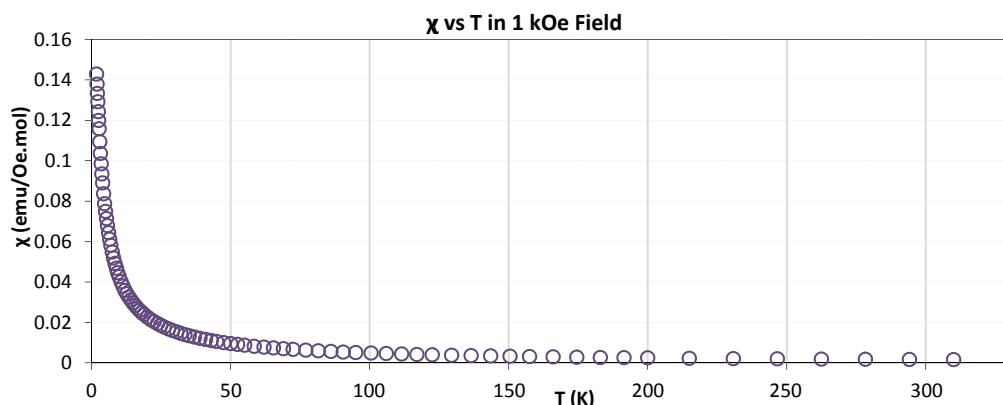


Figure 3.7.2. The χ (emu/Oe.mol) vs T (K) plot of TOZFAP02 in 1 kOe field.

The magnetic structure of the compound was analysed to identify a suitable magnetic model to fit the experimental data. For this interpretation the structure of the title compound collected at the lowest temperature was considered, namely **TOZFAP02** (Zhang *et al.* 2010), for which crystallographic data were collected at 93 K. It is assumed that the compound retains this crystal structure, as well as the corresponding magnetic structure, down to 1.8 K.

In the **TOZFAP02** structure, a close Cu-Cl \cdots Cl-Cu contact is observed between neighbouring tetrachloridocuprate anions, as shown in Figure 3.7.3 (a), which provides a double-halide exchange pathway. In this pathway the Cu-Cl \cdots Cl-Cu distance is 4.072 Å. All other Cu-Cl \cdots Cl-Cu contact distances in the structure exceed the cut-off value of 4.5 Å.

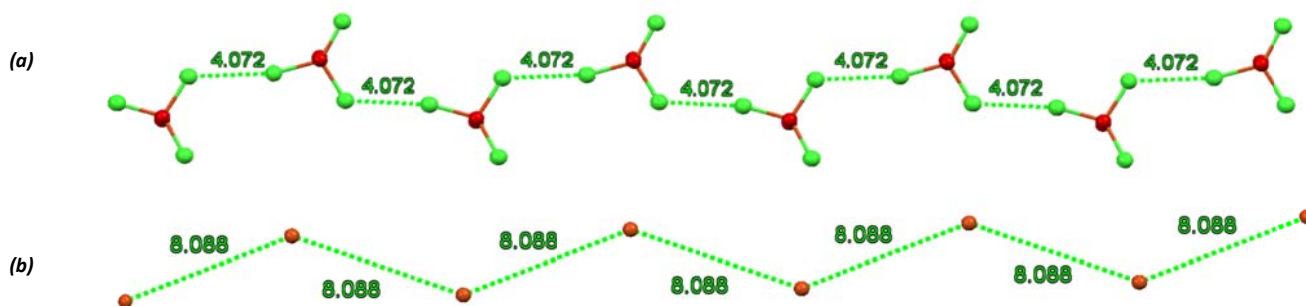


Figure 3.7.3. (a) The double-halide exchange pathway that links anions to form a one-dimensional chain (green dotted line). (b) The distance between magnetic atoms in the one-dimensional chain (green dotted line), distances are given in Å.

In the linear exchange pathway, the magnetic copper ions are at equal distances from each other, forming a uniform chain, as illustrated in Figure 3.7.3 (b). The Heisenberg Hamiltonian, $\hat{H} = -\sum_{A,B} J_{AB} \hat{S}_A \cdot \hat{S}_B$, was used to interpret the magnetic data. The data were fitted to two quantum mechanical magnetic models, firstly the $S = \frac{1}{2}$ uniform antiferromagnetic (AFM) chain model and secondly the $S = \frac{1}{2}$ antiferromagnetic chain model with a

Curie-Weiss correction. The Curie-Weiss correction takes into account possible magnetic interactions between neighbouring chains.

When using the uniform chain model the parameters fitted are the Curie constant (CC) and the exchange parameter in the chain, J_K . A third parameter, the percentage impurity (xx), was fixed at 1%. An additional Curie-Weiss parameter (CW) was fitted for the uniform chain model with a Curie-Weiss correction. The parameters obtained for the two models are listed in Table 3.7.

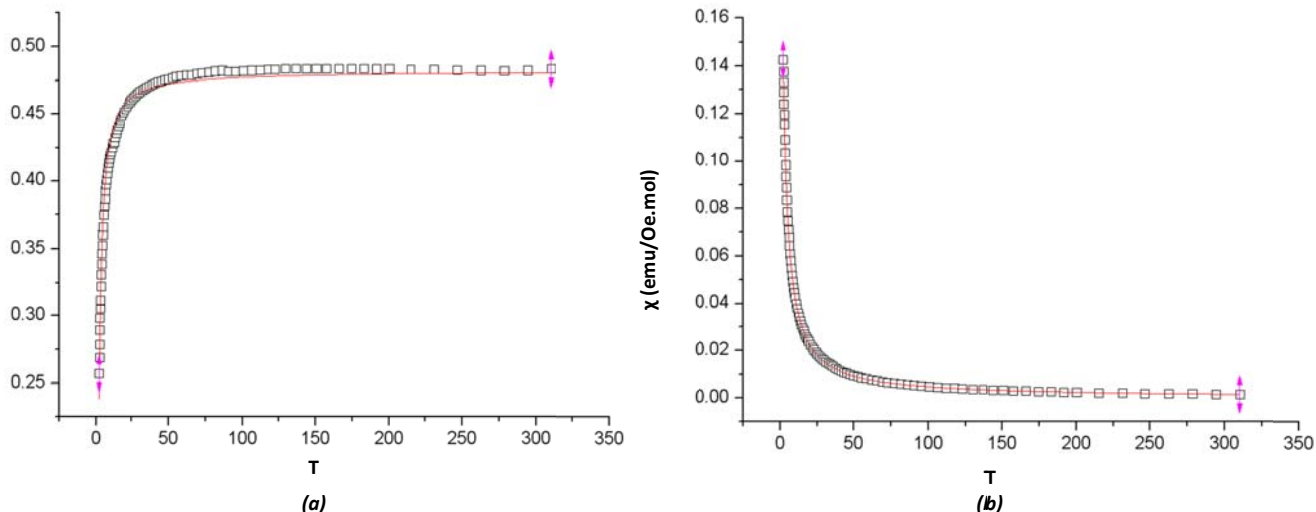


Figure 3.7.4. (a) The χT (emu.K/Oe.mol) vs T (K) data fit to the AFM chain model. (b) The χ (emu/Oe.mol) vs T (K) data fit to the AFM chain model with CW correction.

Table 3.7. The parameters obtained for the AFM chain and AFM chain with CW models employed.

Model	Curie Constant	J (K)	CW	R ²
AFM Chain	0.486	-2.09	-	0.98746
AFM Chain with CW	0.463	-3.05	+0.68	0.99985

A better fit was achieved with the uniform chain model with a Curie-Weiss correction than the chain model without the Curie-Weiss correction, as shown in Figure 3.7.4 (a) and (b). It can be concluded that weak antiferromagnetic interactions occur in the chains, with $J = -3.05$ K. The J value obtained for the AFM chain with CW correction is slightly higher than that obtained for the fit to the AFM chain. In addition weak magnetic interactions are present between neighbouring chains, however, due to the weakness of these interactions, as indicated by the small value of the CW constant, more information cannot be obtained.

3.8. 1,4-Diazoniabicyclo[2.2.2]octane tetrabromidocuprate(II) monohydrate

Moiety Formula: $C_6H_{14}N_2^{2+}CuBr_4^{2-}\cdot H_2O$
Abbreviated as ULAVAF

The compound, reported in the CSD as **ULAVAF**, was resynthesised in order to study its magnetic properties. In the literature, three compounds related to the title compound exist, with CSD refcodes **AGAWIO** (Brammer *et al.* 2002), **AGAWIO01** (Wei and Willet. 2002) and **LURTAT** (Wei and Willet. 2002). The **AGAWIO** and **AGAWIO01** are structurally equivalent and are the anhydrous form of the **LURTAT** compound. Both structures comprise DABCO cations and flattened tetrahedral $CuCl_4^{2-}$ anions. Structural studies of the anionic components of **AGAWIO01** and **LURTAT**, reveal a further distortion from the tetrahedral geometry of the $CuCl_4^{2-}$ anionic unit in the **LURTAT** compound, this is due to an increase in hydrogen bonding interactions in the monohydrated (**LURTAT**) structure (Wei and Willet. 2002). These results agreed with the review of $CuCl_4^{2-}$ geometries by Halvorson (Halvorson *et al.* 1990), where an increase in hydrogen bonding interactions increased the distortion of the anions from tetrahedral to square planar. The **AGAWIO01** and **LURTAT** compounds are isostructural, with the **LURTAT** compound being a $CuCl_2$ analogue of the title compound.

The resynthesis of the title compound, with CSD refcode, **ULAVAF** (Zhang. 2011) was proven successful by PXRD analysis, as shown in appendix one, Figure 4. The **ULAVAF** and **LURTAT** structures are isostructural and both crystallise in the monoclinic space group $P2_1/c$. The magnetic susceptibility data was collected and interpreted for the **ULAVAF** structure.

3.8.1. Structure Description

The structure of the **ULAVAF** compound has been reported in the literature, as discussed in section 1.5, but the magnetic properties have not been investigated. In this study the material was resynthesised in order to analyse its magnetic characteristics. The reader is referred to Chapter One for a detailed discussion of the structure.

3.8.2. Magnetic Property Analysis

As illustrated in Figure 3.8.1, the graph of χT vs T indicates a constant χT value of approximately 0.4075 emu.K/Oe.mol from a temperature range of 310 K to approximately 62 K. A sudden increase in χT in the low temperature range from about 62 K indicates ferromagnetic behaviour between Cu^{2+} ions. This behaviour is unexpected, since AFM interactions typically occur between isolated tetrahedral $CuBr_4^{2-}$ units. Two examples of FM exchange between these anions have been reported previously (Turnbull *et al.* 2005).

Figure 3.8.1. The plot of χT (emu/Oe.mol) vs T (K).

Analysis of the close Cu-Br \cdots Br-Cu contacts in the structure indicate that the magnetic structure of the compound can be described as three-dimensional, with possible double-halide exchange pathways indicated by blue dotted lines, Figure 3.8.2. To our knowledge there are no three-dimensional quantum models available to fit the magnetic data of **ULAVAF**, hence it is impossible to determine the value of the exchange parameter, J . It can however, be emphasised that the observed FM exchange is unique and uncommon.

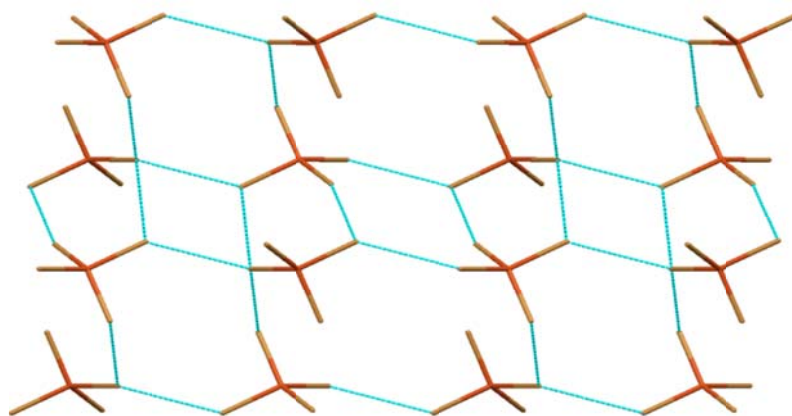


Figure 3.8.2. The double-halide exchange pathway that links anions to form a three-dimensional network.

3.9. References

- Battaglia, L.P., Corradi, A.B., Geiser, U., Willett, R.D., Motori, A., Sandrolini, F., Antolini, L., Fredini Man, T., Menabae, L. and Pellacani, G.C. (1988). *J. Chem. Soc, Dalton Trans*, 265-271.
- Billing, D.G. and Lemmerer, A. (2007). *CrystEngComm*. 9, 236-244.
- Billing, D.G. and Lemmerer, A. (2009). *CrystEngComm*. 11, 1549-1562.
- Brammer, L., Swearingen, J.K., Bruton, E.A. and Sherwood, P. (2002). *Proc. Nat. Acad. Sci. USA*. 99, 4956-4961.
- Daoud, A. and Qui, D.T. (1984). *Acta Cryst., Sect A: Found Cryst.* 40, C234.
- Daoud, A., Salah, A.B., Chappert, C., Renard, J.P., Cheikhrouhal, T.D. and Verdaguer., M. (1986). *Phys. Rev. B, Condens. Mat.* 33, 6253-6260.
- Geiser, U., Gaura, R.M., Willett, R.D. and West, D.X. (1986). *Inorg. Chem.* 25, 4203-4212.
- Halvorson, K., Patterson, C. and Willett, R.D. (1990). *Acta Cryst. Sect.B.* 46, 508-519.
- Han, M.T. (2012). *Acta Cryst., Sect. E: Struct. Rep. Online.* 68, m448.

- Riley, M.J., Neill, D., Berhardt, P.V., Byriel, K.A. and Kennard, C.H.L. (1998). *Inorg. Chem.* 37, 3635-3639.
- Tuikka, M., Kersen, U. and Haukka, M. (2013). *CrystEngComm.* 15, 6177-6183.
- Turnbull, M.M, Landee, C.P and Wells, B.M. (2005). *Coord. Chem. Rev.* 249, 2567-2576.
- Wei, M. and Willett, R.D. (1996). *Inorg. Chem.* 35, 6381-6385.
- Wei, M. and Willett, R.D. (2002). *J. Chem. Cryst.* 32, 439-445.
- Willett, R.D., Galeri, C., Landee, C.P., Turnbull, M.M. and Twamley, B. (2004). *Inorg. Chem.* 43, 3804-3811.
- Zhang, W., Ye, H-Y., Cai, H-L., Ge, J-Z., Xiong, R-G. and Huang, S.D. (2010). *J. Am. Chem. Soc.* 132, 7300-7302.
- Zhang, Y. and Wang, B. (2011). *Acta Cryst., Sect E: Struct. Rep. Online.* 67, m371.

Chapter Four: Discussion

In this chapter, the structural and magnetic results reported in Chapter Three are compared with related results from this study and/or from the literature, with the aim of gaining insight in the structural and magnetic behaviour of the sub-families of related materials.

4.1. Structural Comparisons

4.1.1. Perhalometallate Anion Diversity

By considering the structures reported in the literature, as summarised in section 1.5, as well as the novel structures determined in the current study, the structural diversity exhibited by the perhalocuprate(II) anions in the hybrid compounds under investigation is again confirmed. Anions observed include polymeric, one-dimensional, isolated tetrahedral, as well as cluster type anions.

A number of structures were observed and/or reported, in which the same cycloalkylammonium cation is combined with different forms of perhalocuprate(II) anions, for example the cyclopentylammonium cations, which are combined with one-dimensional perbromidocuprate(II) polymeric anions in the novel PENCuBr structure and with isolated, distorted tetrahedral CuBr_4^{2-} anions in the **NABNEK** (Willet. 2004) structure. Another example is the piperazinium cation which crystallises with two-dimensional perovskite perchloridocuprate(II) anions in the **NUTDOV** (Riley *et al.* 1998) structure and with zero-dimensional tetrahedral perchloridocuprate(II) anions in the novel PIPCuCl structure.

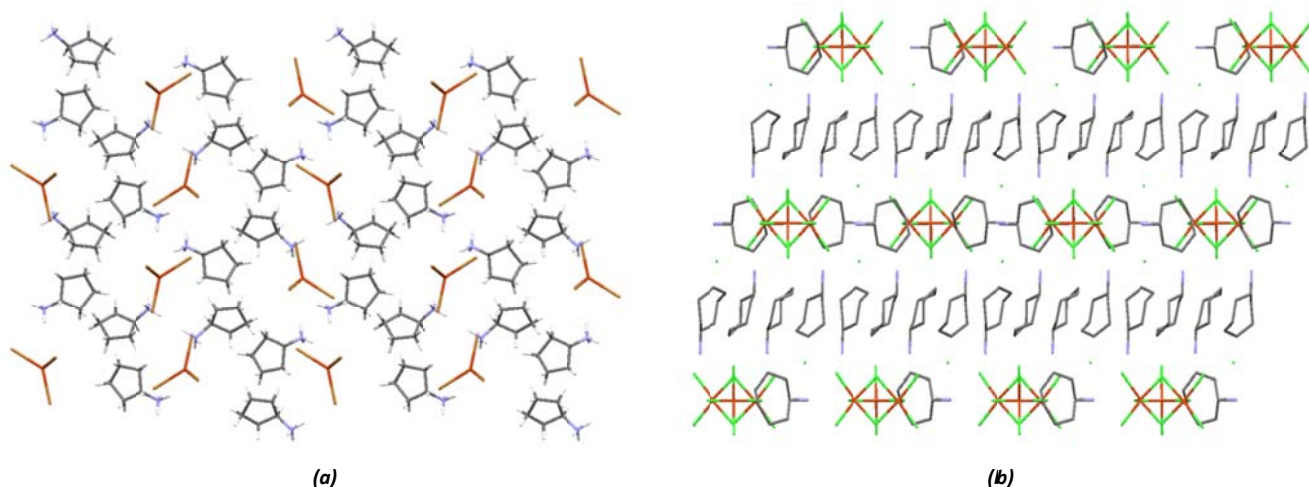
McCrone (McCrone. 1965) famously said that the number of polymorphs of a specific compound that are known is directly proportional to the amount of time and money spent on investigating the specific compound. Perhaps the same can be said for the perhalocuprate hybrid compounds and that under the right synthetic conditions, a range of anionic forms can be obtained for each combination of the organic component and metal(II) halide.

An understanding of the factors determining the specific type of perhalocuprate anion present in a structure would be required in order to exert full control over the type of inorganic sub-structure that is formed. Since an inorganic sub-structure carries both the magnetic moment carriers as well as the halogeno ligands responsible for magnetic exchange between the metal ions, this sub-structure would certainly influence the magnetic properties of the material. It should be kept in mind that compounds with the same inorganic anion can display very different magnetic properties due to effect of the cations separating the inorganic units and hence influencing the magnetic exchange between Cu^{2+} metal centres.

Even though a detailed understanding of the specific synthetic conditions required to form a specific perhalocuprate anion is beyond the scope of the current project, it can be suggested that a large number of parameters would have to be taken into account, including the counter cation, stoichiometric ratio between organic and inorganic reagents, solvents used and the temperature of the reaction (Arnby *et al.* 2004). It is suggested that further studies are carried out on the current system in order to obtain a better understanding of the role of these and other parameters on the structures and the magnetic properties of the hybrid compounds.

Even though a detailed study on all the parameters affecting the structures obtained was not carried out, it is still informative to consider the available structures, both from the literature and the current study, with the aim of identifying structural trends.

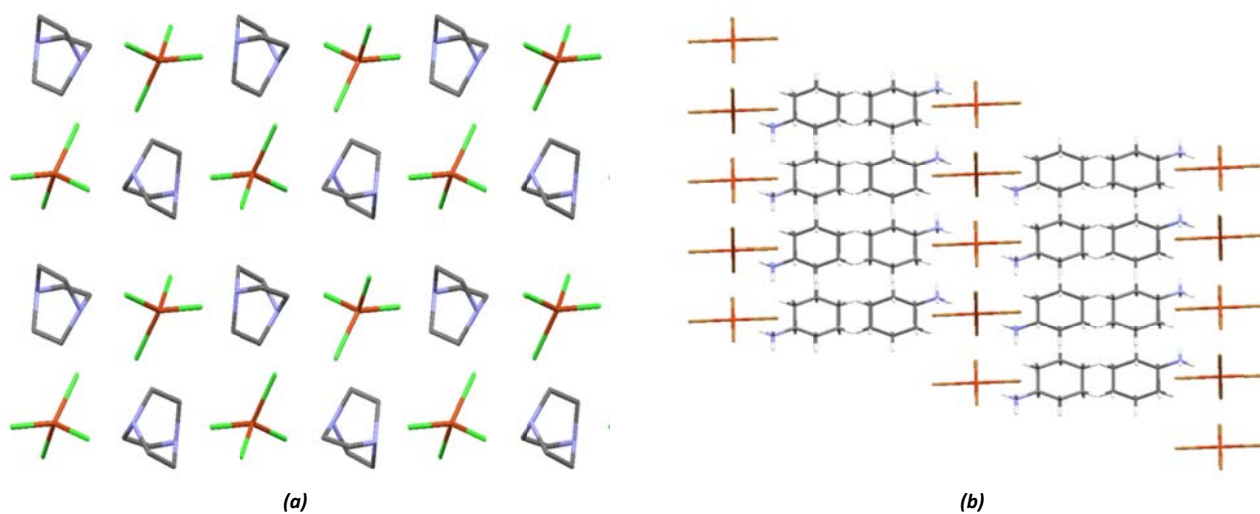
4.2. Layered Structures



(a) (b)
Figure 4.2.1. The packing diagrams of (a) NABNEK01 and (b) HEPCuCl respectively.

By considering the structures in the current series, i.e., those containing saturated cations, the tendency to form layered structures can be seen. The organic layers may be sigmoidal, for example in the **NABNEK01** structure, shown in Figure 4.2.1 (a). The layered packing in HEPCuCl (Figure 4.2.1 (b)) is unique in that a purely organic layer is formed by the cations, while the second type of layer contains both cations and anions. To our knowledge, this is the first example of a hybrid compound showing a “mixed” layer instead of a purely inorganic layer.

In the **AGAWIO** structure, which contains the DABCO dication, the packing diagram shown in Figure 4.2.2 (a) illustrates the alternating orientation of the anions in the inorganic layer, while in the cationic layer the DABCO cations alternate in orientation with respect to each other. In the **YATYUP** structure (Figure 4.2.2 (b)), the cations are orientated such that the $^+\text{NH}_3$ groups of each cation are pointed towards the nearest inorganic perovskite sheet, with the anions adopting the same orientation within the inorganic sheets.



(a) (b)
Figure 4.2.2. The packing diagram of (a) AGAWIO and (b) YATYUP.

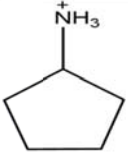
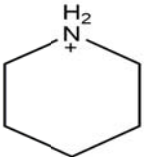
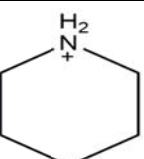
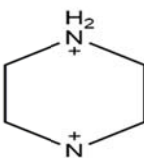
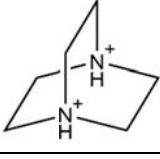
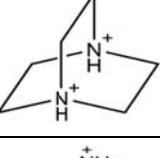
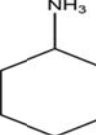
4.3. Cation Effects

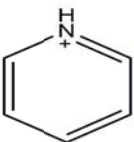
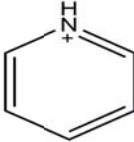
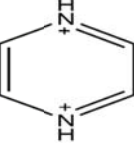
It has been reported (Mitzi *et al.* 2001) that the cation often has a templating effect on the structure obtained for a hybrid compound. In the next section the effect of the cation characteristics on the hybrid structures are considered.

4.3.1. Aromatic vs Saturated Cations

As mentioned in Chapter One, not many perhalocuprate(II) hybrid structures containing saturated cations are available in the literature, hence the choice of saturated cations in the current study. To consider the effect of a change from an aromatic cation to a saturated cation, a CSD search was conducted to find related structures containing aromatic cations analogous to the saturated cations employed in this study and these are listed in Table 4.1. In order to keep as many parameters as possible constant, only zero-dimensional structures containing isolated tetrahedral CuX_4^{2-} anions are considered.

Table 4.1. The structures containing CuX_4^{2-} anions and saturated or aromatic cations used in the current study.

Saturated Cations				
Refcode	Cation	Scheme of Cation	Anion	Reference
NABNEK	cyclopentylammonium		CuBr_4^{2-}	Willet. 2004
PNLCU01	piperidinium		CuCl_4^{2-}	Emerson & Drumheller. 1980
PAFYUR	piperidinium		CuBr_4^{2-}	Patyal <i>et al.</i> 1990
PIPCuCl/BICPEK	piperazinium		CuCl_4^{2-}	Tuikka <i>et al.</i> 2013
AGAWIO	DABCO		CuCl_4^{2-}	Brammer <i>et al.</i> 2002
ULAVAF	DABCO		CuBr_4^{2-}	Zhang & Wang. 2011
YATYUP	cyclohexylammonium		CuBr_4^{2-}	Han. 2012

Related Aromatic Cations				
HUPVIX	pyridinium		CuCl_4^{2-}	Czugler <i>et al.</i> 2002
BACHIX	pyridinium		CuBr_4^{2-}	Luque <i>et al.</i> 2001
ANILCP	anilinium		$\text{Cu}_2\text{Cl}_8^{4-}$	Larsen. 1974

Even though not many structures are available to assess the effect of a change from aromatic to saturated cation, past experience with aromatic cation containing structures in our research group (Rademeyer *et al.* 2010), indicates that aromatic cations typically pack with the aromatic rings parallel and slipped relative to each other, to allow for the formation of attractive aromatic π - π interactions (Janiak. 2000) between the rings. In aromatic containing hybrid compounds, the π - π interactions are strong enough to significantly affect the structure and they play an important structural directing role, in addition to hydrogen bonding interactions. This results in the formation of hybrid structures that consist of clearly defined layers, with an organic layer containing the organic cation and an inorganic layer containing the inorganic anions.

From Table 4.1, the comparison of the aromatic piperidinium containing structures **HUPVIX** and **BACHIX** with their saturated analogues **PNCLCU01** and **PAFYUR** allows for the investigation of the effect of aromatic vs saturated cations on the structures, since all the other parameters remain unchanged.

The isostructural compounds, **HUPVIX** (Czugler *et al.* 2002) and **BACHIX** (Luque *et al.* 2001) show layered structures consisting of single organic layers alternating with inorganic layers, as shown in Figure 4.3.1 (a) and (b). In the organic layer, the cations pack in a parallel, head-to-tail fashion that allows for the formation of stable aromatic interactions (Janiak. 2000). The head-to-tail packing of the aromatic rings is due to the heteroatom, nitrogen, that is present on the ring and orientating the heteroatom on opposite sides of the cation helps stabilise the aromatic attraction between rings (Janiak. 2000).

The saturated analogues of **HUPVIX** and **BACHIX**, are the isostructural compounds **PNCLCU01** (Emerson & Drumheller. 1980) and **PAFYUR** (Patyal *et al.* 1990), that also display layered structures, as shown in Figure 4.3.1 (c) and (d), respectively. The layers are, however, less clearly defined and the organic layer is a bilayer, consisting of two rows of cations instead of the single row of aromatic cations displayed in **HUPVIX** and **BACHIX**. Thus, without the aromatic interactions in the organic layer, a bilayer is formed, with the orientation of the $-\text{NH}_3^+$ groups of the cations dictated by hydrogen bonding interactions between cations and anions. It is interesting to note that “pairs” of cations can be identified which still show head-to-tail packing. Clearly the head-to-tail orientation and placement of nitrogen atoms favour hydrogen bonding in this case. It can be imagined that in going from the aromatic compound to the saturated compound, the head-to-tail packed cationic pair in the saturated compounds separates laterally into a bilayer due to the absence of aromatic interactions and the bulkiness (planar aromatic ring vs chair conformation of the saturated species) of the cation, but retaining the orientation of the NH_3 groups. It should be mentioned that the anions in the saturated cation containing structures **PNCLCU01** and **PAFYUR** are more distorted from ideal tetrahedral geometry than those in the aromatic cation containing structures **HUPVIX** and **BACHIX**. This is most probably

ascribed to the hydrogen bonding requirements of the saturated cations forcing the anions to be “stretched” open.

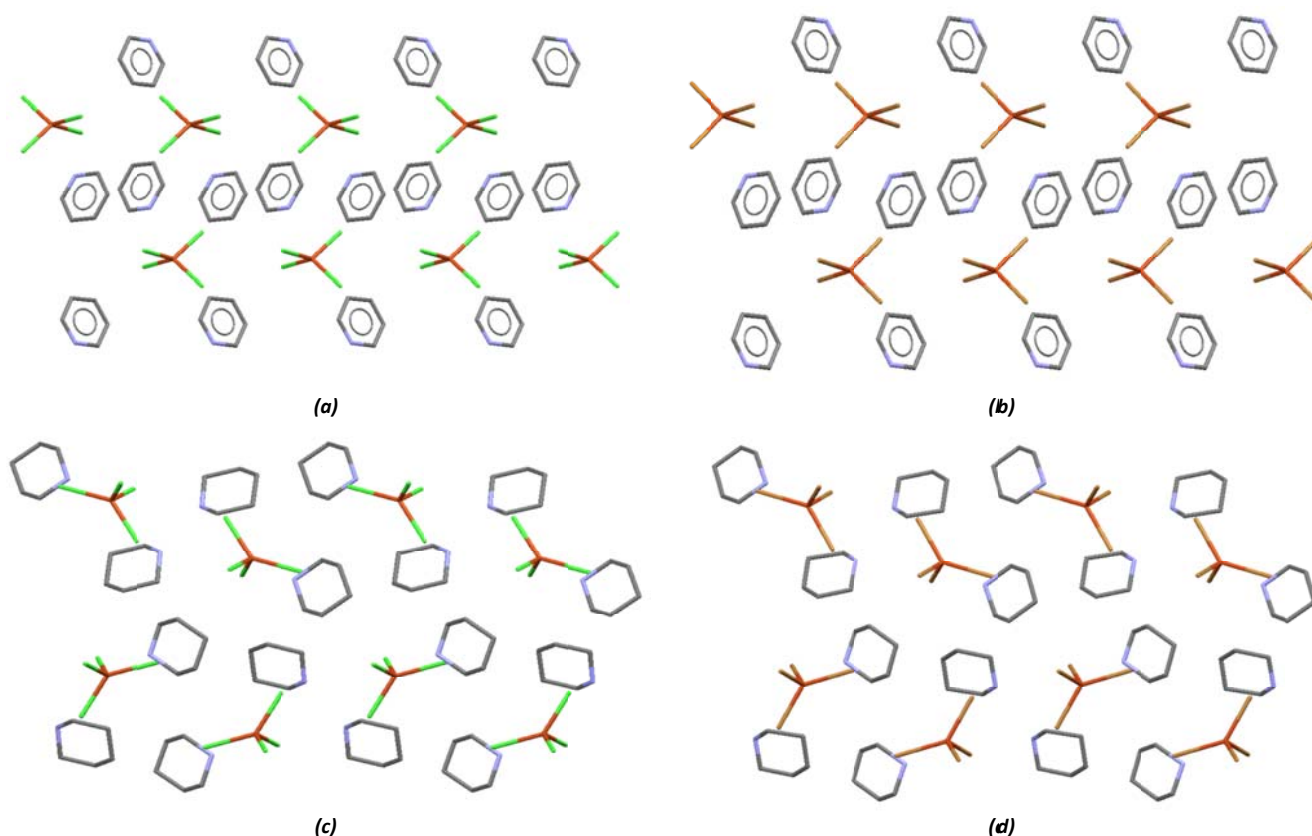


Figure 4.3.1. The packing diagrams of aromatic systems such as (a) HUPVIX, (b) BACHIX and saturated systems (c) PNLCU01 and (d) PAFYUR.

Despite aromatic interactions not being present in the hybrid structures containing saturated cations, layered structures are still formed, even though the layers are not as clearly defined as in the case of the aromatic cation containing hybrids. Layered structures are formed in the case of the zero-dimensional structures **NABNEK**, **PNLCU01** and **PAFYUR**, one-dimensional structures **FAWDAI**, **PENCuBr**, **BAPYUM**, **FUTBUR** and two-dimensional structures, **YATYUP** and **PENCuCl**.

4.3.2. Monocations vs Dications

The structures containing the singly protonated cycloalkylammonium cations typically crystallise in an organic to inorganic ratio of 2:1 to ensure charge neutrality, while this ratio is 1:1 for the dications **DABCO** and piperazine.

The effect of this cation:anion ratio is evident in the types of structures obtained. In the 1:1 structures containing the secondary and tertiary cations piperazinium and **DABCO**, for example **AGAWIO**, **LURTAT**, **ULAVAF** and **PIPCuCl/BICPEK**, the organic layers contain only a single row of molecules, due to the ability of the cation to hydrogen bond *via* the nitrogen atoms on both sides of the cation. The packing of the dications and anions allows for the formation of the optimum number of hydrogen bonding interactions between the dications and the anions in these structures. The packing diagrams of these structures are shown in Figure 4.3.2 (a) to (d). Even though the structures can be considered as layered structures, an important difference becomes evident when considering the types of neighbours in these structure types. In the 1:1 structures, each cation is surrounded by four anions, when viewed down a row of cations and each anion is surrounded by four cations, this packing reminds one of a checkerboard type packing, which is not seen for the monocationic compounds.

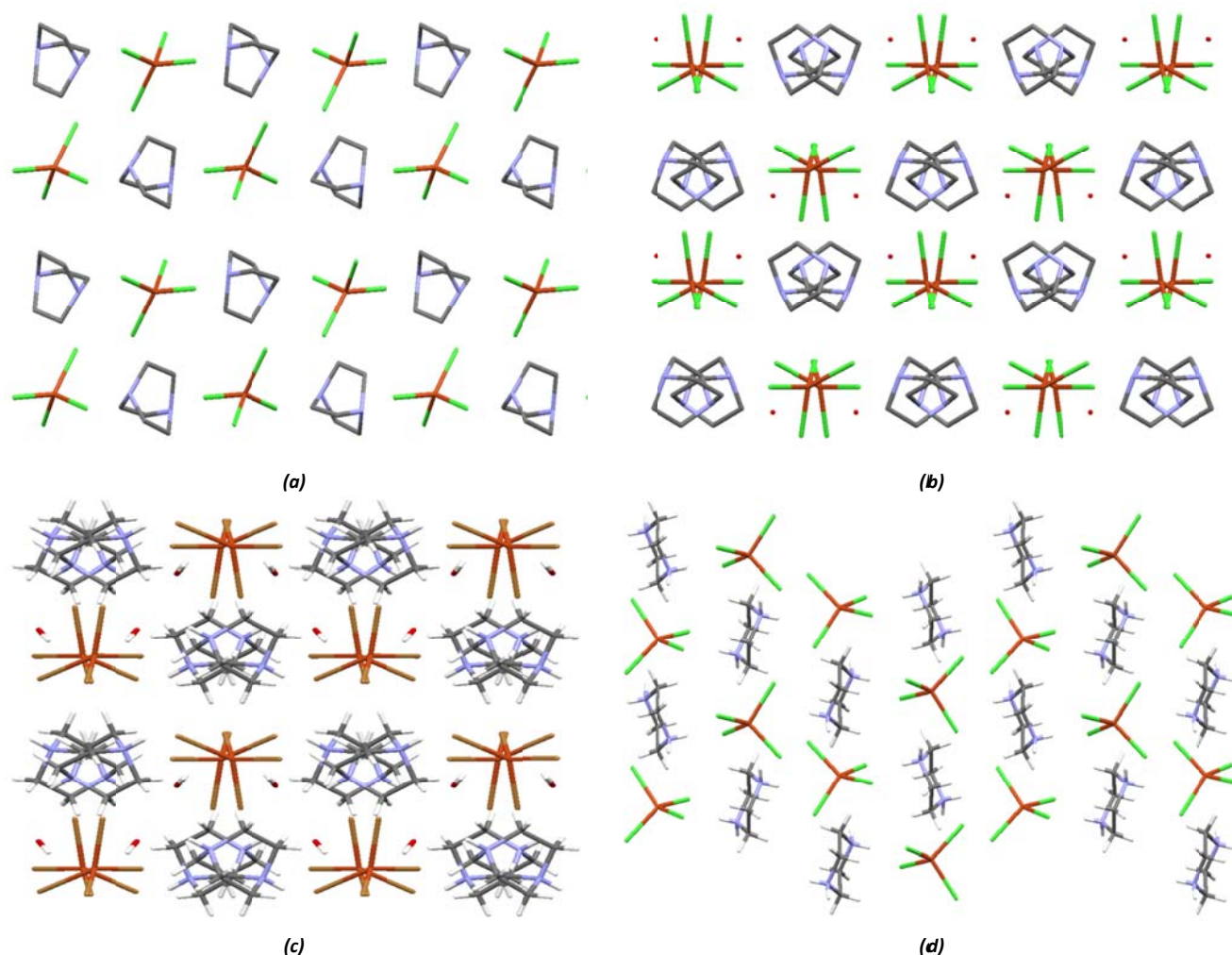


Figure 4.3.2. Monolayer type packing of secondary/ tertiary cations observed in (a) AGAWIO (b) LURTAT (c) ULAVAF (d) PIPCuCl/BICPEK.

In the primary cycloalkylammonium structures, hydrogen bonding is only possible on one side of the cation and this typically results in the formation of organic bilayers, as can be seen in Figure 4.3.3 (a)-(f).

It is interesting to note the structural similarity between the cyclopentylammonium containing **NABNEK01** structure and the piperidinium containing **PAFYUR** and **PNCLCU01** structures. In the cyclopentylammonium cation the nitrogen atom is a substituent on the C₅ ring, whereas the piperidinium cation contains the nitrogen atom as a heteroatom in the six-membered ring. In both structures, the cations are orientated such that the nitrogen atoms occupy approximately the same positions allowing for the formation of hydrogen bonds.

By visual inspection of these structures it can be deduced that the bulkiness of the DABCO cation and the flexibility of the five-/six-membered rings do not have much influence on the assembly of these structures. However, the number of nitrogen atoms present on the cations plays a more significant role in structure assembly.

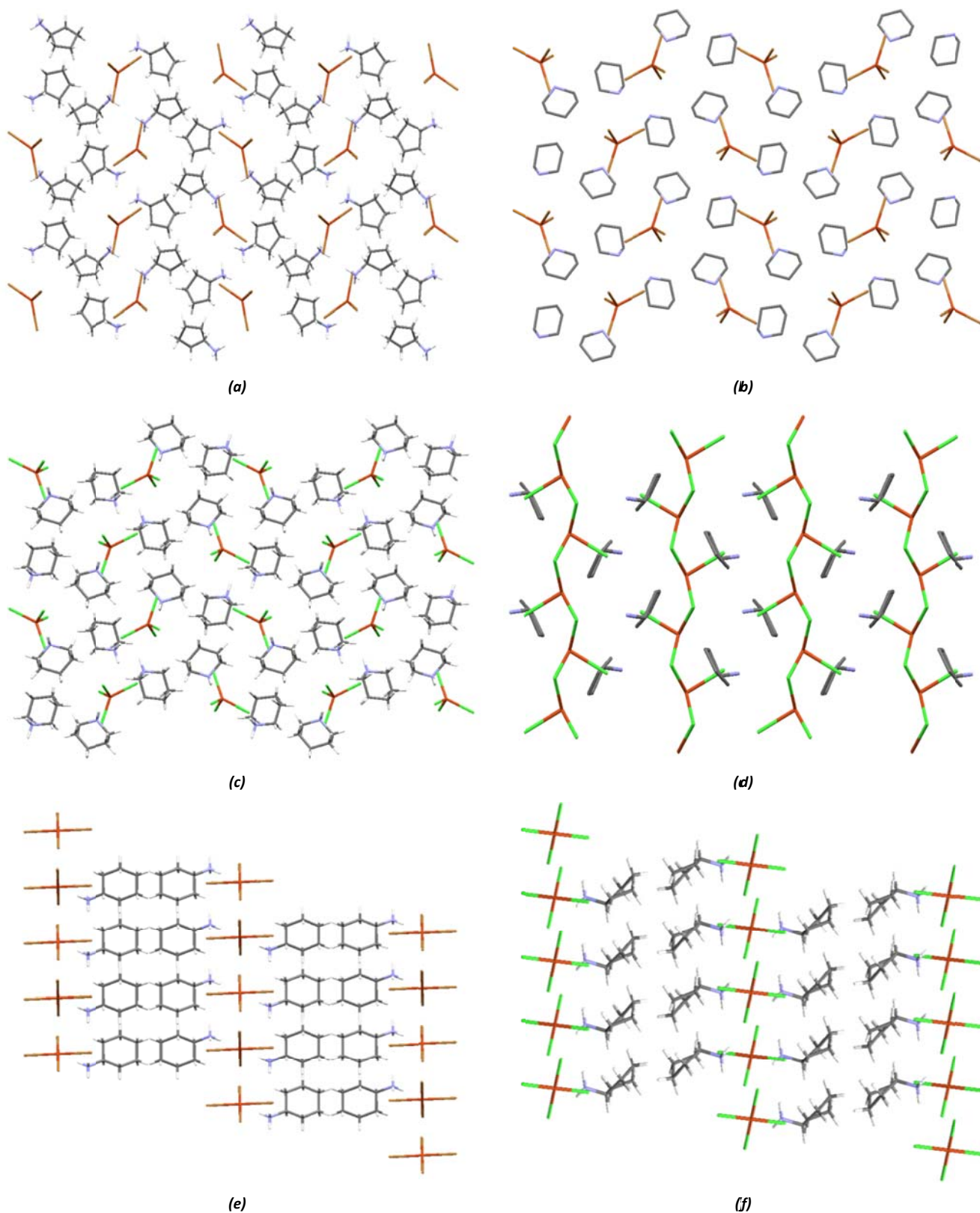


Figure 4.3.3. Layered packing of cations and anions in (a) NABNEK01, (b) PAFYUR (no hydrogen atoms were reported in the cif file), (c) PNLCU01, (d) FAWDAI, (e) YATYUP and (f) PENCuCl.

4.4. Comparisons of Families of Structures

4.4.1 Cycloheptylammonium (HEP) Clusters

Both the cycloheptylammonium containing perhalocuprate(II) structures exhibit the novel, unique, anionic cluster, however, they are not isostructural. The HEP₂CuCl structure shows higher symmetry and crystallises in

the space group $C2/c$, while HEPCuBr crystallises in $P\bar{1}$. The higher symmetry in the HEPCuCl structure is also evident from the fact that its asymmetric unit is half that of HEPCuBr.

Despite the difference in space group, the structures are still very similar in that the same hydrogen-bonded 'tube' is formed in both structures, as illustrated in Figure 4.4.1 (a) and (b). In both structures the same hydrogen bonding interactions link the cycloheptylammonium cations, halogeno anions and perhalocuprate(II) anions in the hydrogen-bonded tube.

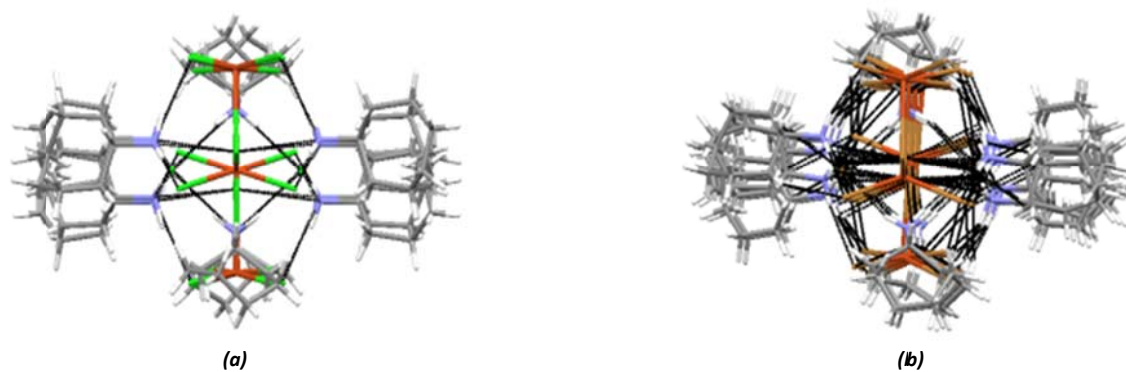


Figure 4.4.1. The hydrogen-bonded tube in (a) HEPCuCl and (b) HEPCuBr

The hydrogen-bonded tubes may be seen as pre-formed, supramolecular building blocks. It can be seen that the cycloheptylammonium cations in the hydrogen-bonded tube of HEPCuBr are spread over more positions than in the HEPCuCl hydrogen-bonded tube. In the HEPCuBr structure, the larger bromido ligands and bromide anions result in slightly longer hydrogen bonding distances and this may require different orientations of the cations to achieve optimal hydrogen bonding compared to the HEPCuCl case.

Figure 4.4.2 (a) and (b) shows the packing diagrams of the hydrogen-bonded tubes along the direction of the tubes for the HEPCuCl and HEPCuBr structures, respectively. The HEPCuCl and HEPCuBr structures differ in the way the hydrogen-bonded tubes pack relative to each other. In the HEPCuCl structure, the tubes pack on top of each other, with neighbouring layers of tubes slipped relative to each other, to allow the protrusions of one tube to pack in a space-filled manner with a neighbouring tube. In the HEPCuBr structure, the hydrogen-bonded tubes pack diagonally relative to each other.

The difference in packing of the hydrogen-bonded tubes is possibly the result of a better space fill packing due to the increased size of the bromido ligands and bromide anions in HEPCuBr compared to HEPCuCl, as well as the slightly different shape of the hydrogen-bonded tube found in HEPCuBr due to the positions occupied by the cations.

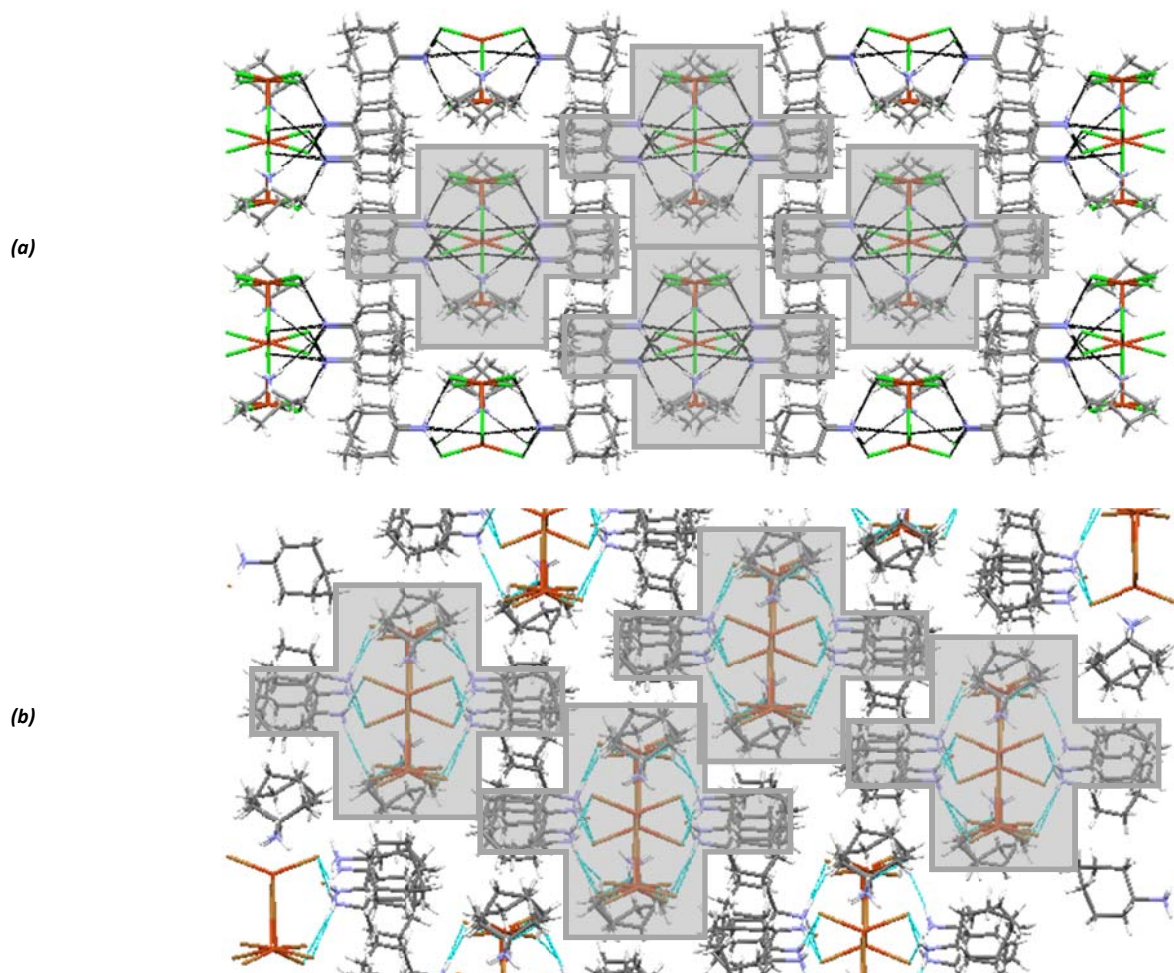


Figure 4.4.2. The packing of the hydrogen bonding tubes in (a) HEPCuCl and (b) HEPCuBr.

4.5. Comparison of Perovskite Compounds

Only two structures in the series under investigation adopt a perovskite structure, namely the novel cyclopentylammonium containing compound, PENCuCl and the literature structure, **YATYUP** (Han. 2012), which contains cyclohexylammonium cations. Despite the fact that the two structures differ in terms of the halogeno ligands linking the Cu^{2+} ions, as well as their cations, a comparison can still be done in order to note the effect of these changes on the structures. In addition, the structures can be compared to the structure **ANILCP** (Larsen. 1974), a perovskite structure containing the aromatic analogue of the cyclohexylammonium cation, namely the anilinium cation.

All three compounds comprise layered structures, with the cations packing in organic bilayers between layers of anions, as shown in Figure 4.5.1.

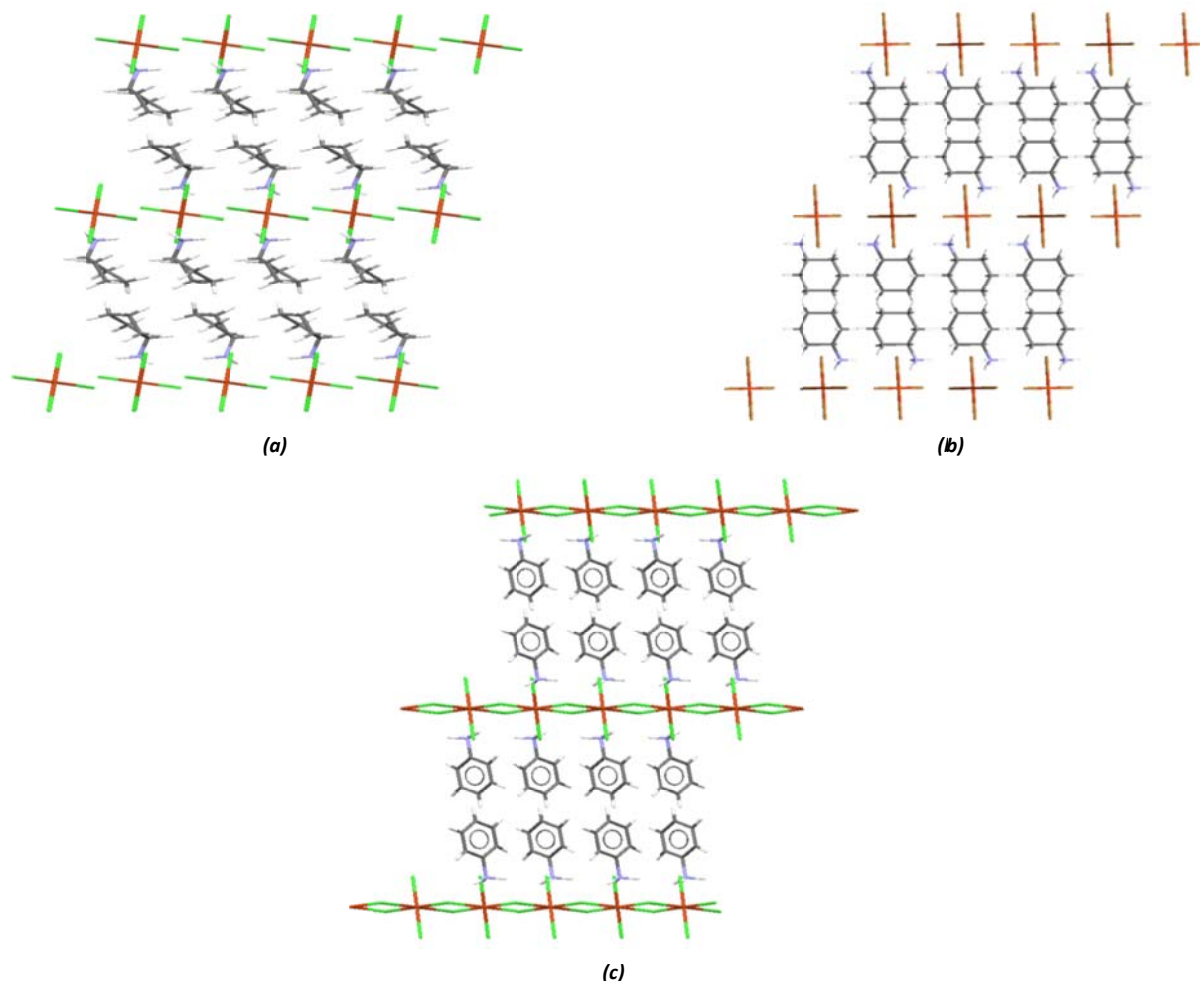


Figure 4.5.1. Layered packing in (a) PENCuCl, (b) YATYUP and (c) ANILCP as viewed down the *b*-axis. Note that semi-coordinate bonds are present between halogeno ligands and metal ions in the inorganic layer. However, since this interaction distance exceeds the distance of an interaction definition in Mercury (Macrae et al. 2006), the bonds are not shown in structures (a) and (b).

In all three structures, the cations are hydrogen-bonded to both sides of the perovskite sheets, with two cations per gap, one above and one below, as illustrated in Figure 4.5.1.

In order to assess the effect of the change in cation geometry and size in going from anilinium to cyclopentylammonium to cyclohexylammonium cations on the structures, the perovskite sheet geometries were compared.

A corrugated inorganic perovskite sheet is formed in the **ANILCP** (Figure 4.5.2 (c)) structure, with Cu...Cu distances of approximately 5.17 Å. In the PENCuCl structure (Figure 4.5.2 (a)) the bulkier saturated cyclopentylammonium cation causes a lengthening of the Cu...Cu distances to approximately 5.47 Å. In the **YATYUP** structure (Figure 4.5.2 (b)) the larger bromido ligands and cyclohexylammonium cations cause the Cu...Cu distances to further increase to 5.96 Å.

An increase in the interlayer distances between sheets of perovskite units is seen when moving from PENCuCl to **YATYUP** to **ANILCP**, with interlayer distances of 13.27 Å, 13.75 Å and 14.79 Å, respectively. The shortest interlayer distance was expected for the PENCuCl structure due to the structure containing the smallest cation (C₅). The C₅ cations adopt an envelope conformation and are tilted in a parallel arrangement to each other. This arrangement of the cations in PENCuCl allows for the shortest inter perovskite sheet distance. In the **YATYUP** structure a slightly larger inter sheet distance is observed due to slightly larger cations (C₆) present between perovskite layers. The **ANILCP** structure exhibits the largest distance between perovskite sheets due to the small tilt angle of the aromatic cations and the presence of parallel and T-shaped aromatic interactions. These result in a larger separation of the perovskite sheets.

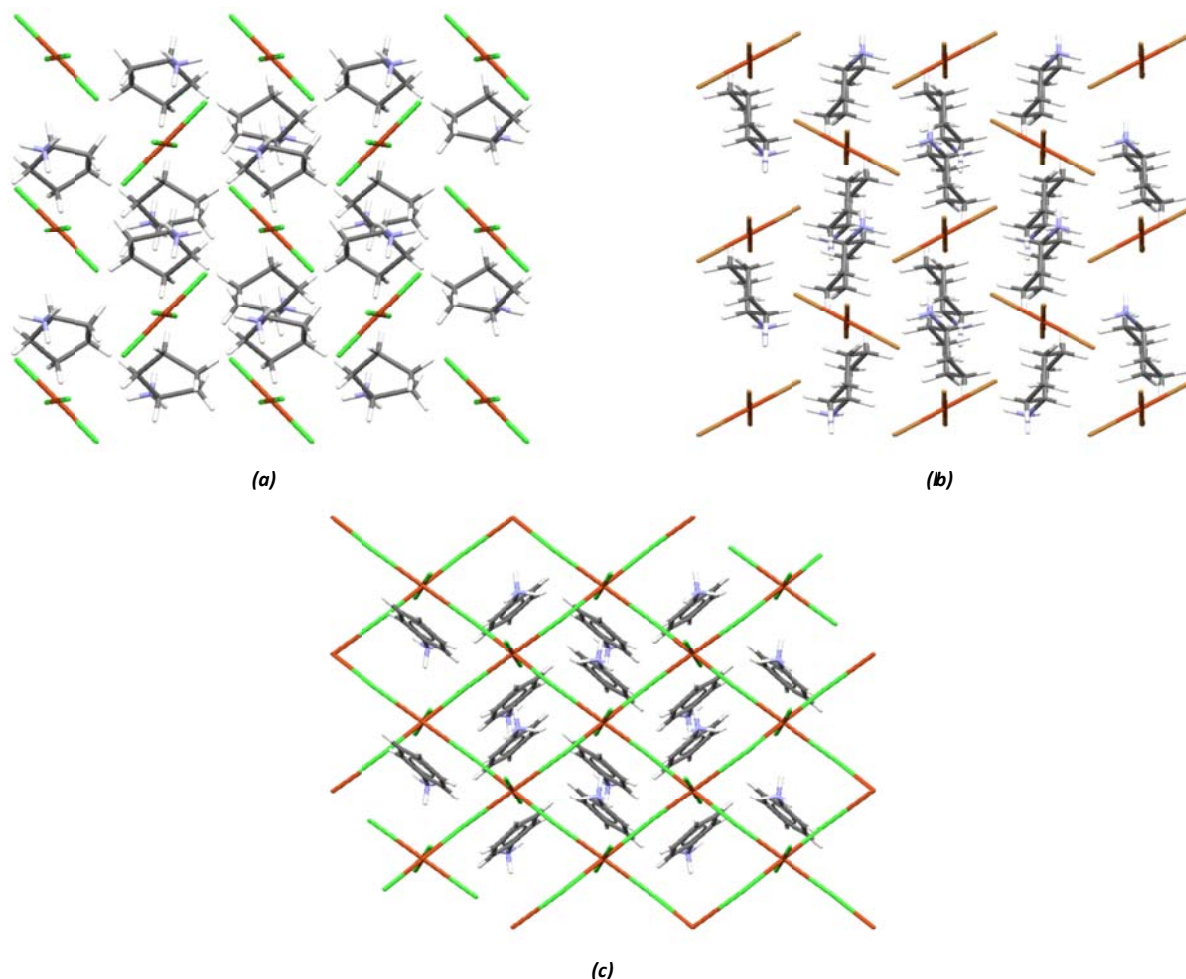


Figure 4.5.2. The packing diagrams in (a) PENCuCl, (b) YATYUP and (c) ANILCP as viewed down the *a*-axis. Note that semi-coordinate bonds are present between halogeno ligands and metal ions in the inorganic layer. However, since this interaction distance exceeds the distance of an interaction definition in Mercury (Macrae et al. 2006), the bonds are not shown in structures (a) and (b).

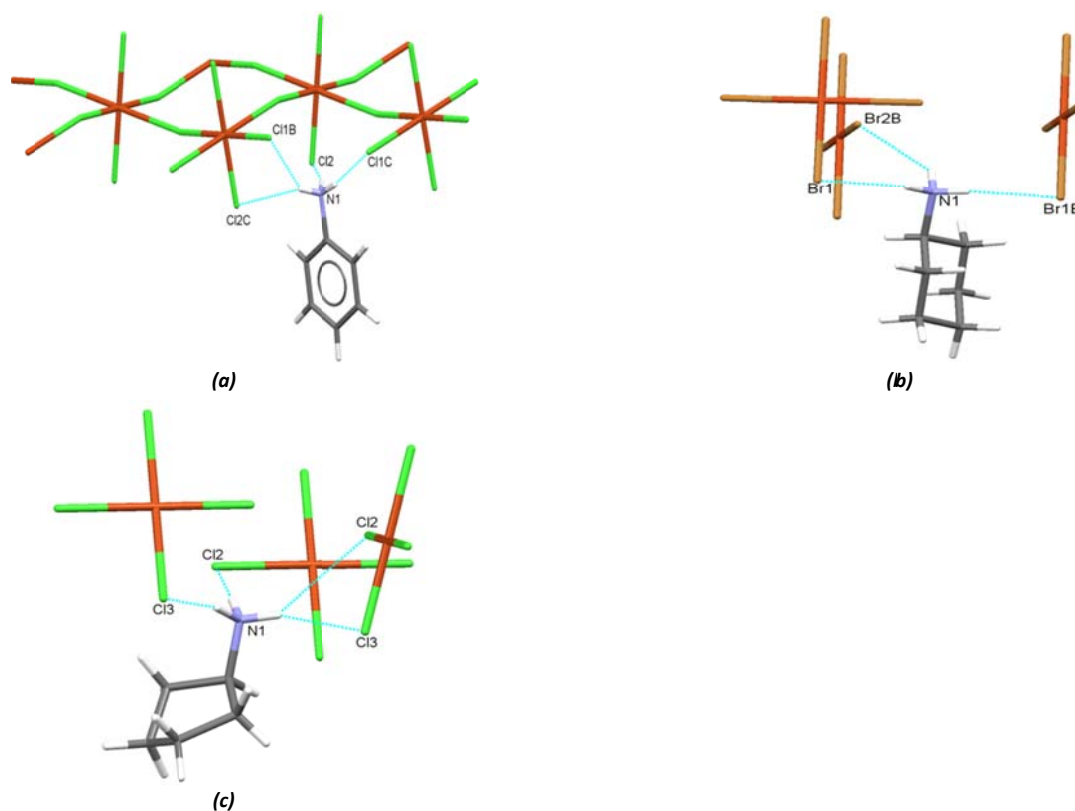


Figure 4.5.3. The hydrogen bonding interactions of (a) ANILCP, (b) YATYUP and (c) PENCuCl.

Table 4.2. The hydrogen bonding parameters of ANILCP, YATYUP and PENCuCl.

ANILCP		
D-H	D(H...A)	A
N1-H8	2.302	Cl2 [x, y, z]
N1-H6	2.382	Cl1C [x, ½-y, ½+z]
N1-H7	3.008	Cl1B [-x, -y, 1-z]
N1-H7	2.457	Cl2C [x, ½-y, ½+z]
YATYUP		
D-H	D(H...A)	A
N1-H3	2.604	Br1 [x, 1+y, -1+z]
N1-H2	2.559	Br1B [x, ½-y, +z]
N1-H1	2.623	Br2B [x, 1.5-y, -1/2+z]
PENCuCl		
D-H	D(H...A)	A
N1-H1C	2.499	Cl3 [x, y, z]
N1-H1A	2.387	Cl2 [-x, ½-y, ½+z]
N1-H1B	2.99	Cl2 [x, ½-y, ½+z]
N1-H1B	2.405	Cl3 [x, ½-y, ½+z]

**Standard deviations for the CSD entries are not available*

In the **ANILCP** compound, bifurcated as well as classic, charge assisted, $^+N-H\cdots Cl^-Cu$ hydrogen bonding interactions occur, the same can be said for the PENCuCl structure, as shown in Figure 4.5.3 (a) and (c) respectively. In the chlorido containing compounds (**ANILCP** and PENCuCl), the hydrogen bond distances between the hydrogen atoms of the nitrogen atom and the acceptor chlorido ligands are similar, with values ranging between 2.3 Å and 3.00 Å. In the **YATYUP** structure only classic, charge assisted $^+N-H\cdots Br^-Cu$ hydrogen bonds are formed, as shown in Figure 4.5.3 (b), with hydrogen bond distance slightly longer than the related chlorido structures. The hydrogen bonding interactions occur between the hydrogen atoms of a donor nitrogen atom to the acceptor bromido ligand of three individual $CuBr_4^{2-}$ anions, with hydrogen bond distances ranging from 2.5 Å to 2.6 Å. The hydrogen bonding parameters are listed in Table 4.2.

4.6. Polymeric Structure and Magnetic Comparison

In this section the three related polymeric structures reported in the literature are structurally and magnetically compared to the novel PENCuBr structure characterised in this study. As mentioned previously in section 1.5, related polymeric structures were reported for cyclopentylammonium trichloridocuprate(II), **FAWDAI** (Geiser *et al.* 1986), cyclohexylammonium trichloridocuprate(II), **BAPYUM** (Groenendijk *et al.* 1981) and the isostructural bromido analogue of **BAPYUM**, cyclohexylammonium tribromidocuprate(II), **FUTBUR** (de Vries *et al.* 1987).

The three crystal structures reported in the literature, namely **FAWDAI**, **BAPYUM** and **FUTBUR**, as well as the novel compound structure PENCuBr found in this study, all contain the same polymer perhalometallate chains. To our knowledge, these are the only four structures that display these chains with *cis* edge-sharing of halogeno ligands, resulting in the formation of uniform, bridged, non-planar polymer chains of the formula $(CuX_3)_n^{n-}$. In these polymer chains the terminal $Cu-X_{ax}$ bond lengths are slightly longer than the bridging $Cu-X_{eq}$ bond lengths and the Cu^{2+} ions adopt square pyramidal geometries and are positioned out of the halogeno plane. The polymers are separated by bilayers of organic cations to form layered structures, as shown in Figure 4.6.1 (a) to (d). All four structures contain similar saturated cations, either cyclohexylammonium or

cyclopentylammonium, with disorder occurring in one of the cations of the **FAWDAI** structure (Geiser *et al.* 1986).

In this series the **BAPYUM** and **FUTBUR** structures are isostructural and crystallise in space group, $P2_12_12_1$, but the cyclopentylammonium analogues **FAWDAI** and **PENCuBr** are not isostructural and crystallise in space groups $P2_1/n$ and $Pbca$ respectively. The structural similarities and differences will be discussed in the next section followed by the comparison of the magnetic properties.

A detailed analysis of the polymer geometry and comparison of the magnetic properties of two of the structures **FAWDAI** and **BAPYUM** was done by Geiser (Geiser *et al.* 1986) and the geometrical parameters defined in this reference will also be used in the current discussion.

In the **FAWDAI** structure, the polymeric chains are related by inversion centres. However, in the **BAPYUM** and **FUTBUR** structures, the chains are related by two-fold screw axes, as given by the $P2_12_12_1$ space group. In the novel **PENCuBr** structure, the polymer chains are related by both inversion centres as well as two-fold screw axes.

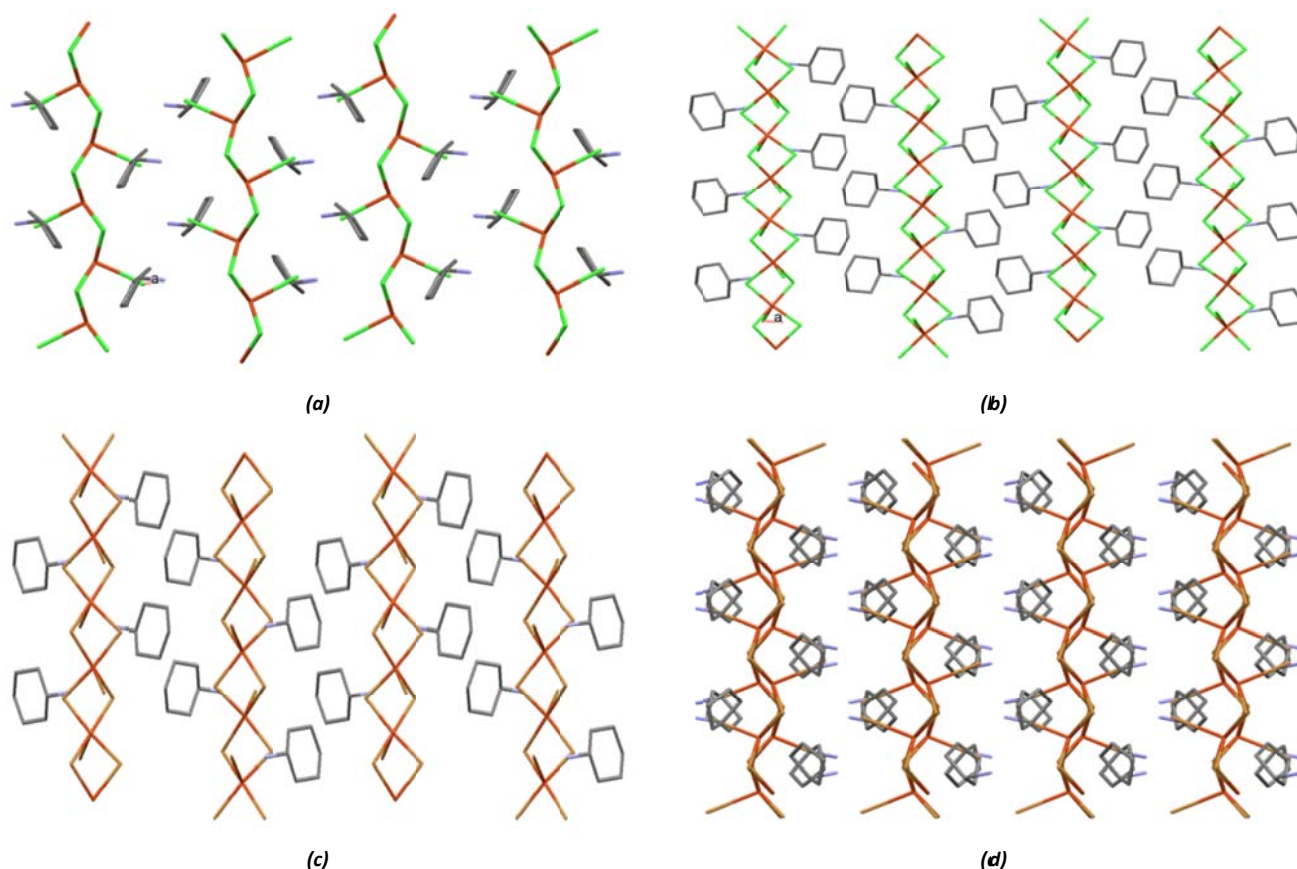


Figure 4.6.1. The packing diagrams of (a) **FAWDAI**, (b) **BAPYUM** (c) **FUTBUR** and (d) **PENCuBr** respectively. The hydrogen atoms are omitted for clarity.

In each of the four structures, the Cu-X-Cu angles of the bridging halogeno ligands are not co-planar with the Cu^{2+} ion, but bent along the X-X line in the bridge, as shown in Figure 4.6.2. The effect of this bending is to bring the neighbouring Cu^{2+} ions closer together than they would have been if a planar geometry was adopted and also to bring the terminal halogeno ligand closer to the coordination sphere of the neighbouring Cu^{2+} ion. The $\text{Cu}\cdots\text{X}_{\text{ax}}$ distances, where X_{ax} refers to the terminal or axial halogeno ligand, are listed in Table 4.2. Further bending would result in the formation of a tribridged chain (Kenneth *et al.* 1990, Wei and Willet. 1996). Geiser introduced a parameter, δ , to quantify the degree of bending in the chain. The angle between the planes formed by the CuX_2 units gives the value of δ for a chain. On bending, the Cu-X-Cu angle is reduced. The folding leads to a shortening of the intrachain Cu-Cu and Cu-X_{eq} distances, as well as to a longer Cu-X_{ax}

distance, where X_{eq} refers to an equatorial ligand. The geometrical parameters describing the polymers of the four structures are listed in Table 4.2.

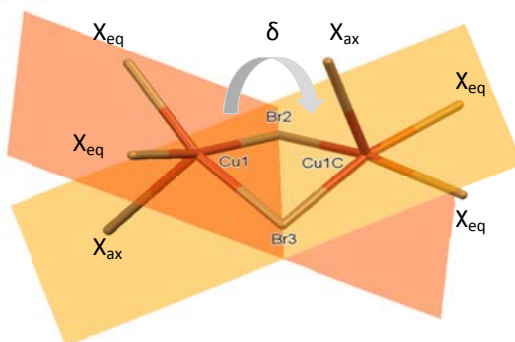


Figure 4.6.2. The dihedral angle, δ , measured between the X-Cu-X planes, in this example, $X = Br^-$.

Despite the fact that three different types of structures are formed, as indicated by three different space groups, it is interesting to note that the same hydrogen bonding network is formed in all four compounds, irrespective of the specific halogeno ligand or cation present. Strong charge assisted $^+N-H \cdots X-M$ hydrogen bonds link the cations to the polymeric anions in all four structures, as illustrated in Figure 4.6.3 (a) to (c). Each R^+NH_3 group forms three hydrogen bonds to two terminal hydrogen bonding acceptors in one polymer and a third hydrogen bond forms between a halogeno acceptor in a second polymer. These interactions result in the formation of one-dimensional hydrogen-bonded ladders between polymers, with hydrogen bonds forming the ladder rails and rungs. Even though the same hydrogen-bonded ladder is formed, the cation orientations differ in the three types of structures, as shown in Figure 4.6.3 (a) to (c). Figure 4.6.3 (d) shows the side-view of the hydrogen-bonded ladders, which also illustrates the difference in cation orientation.

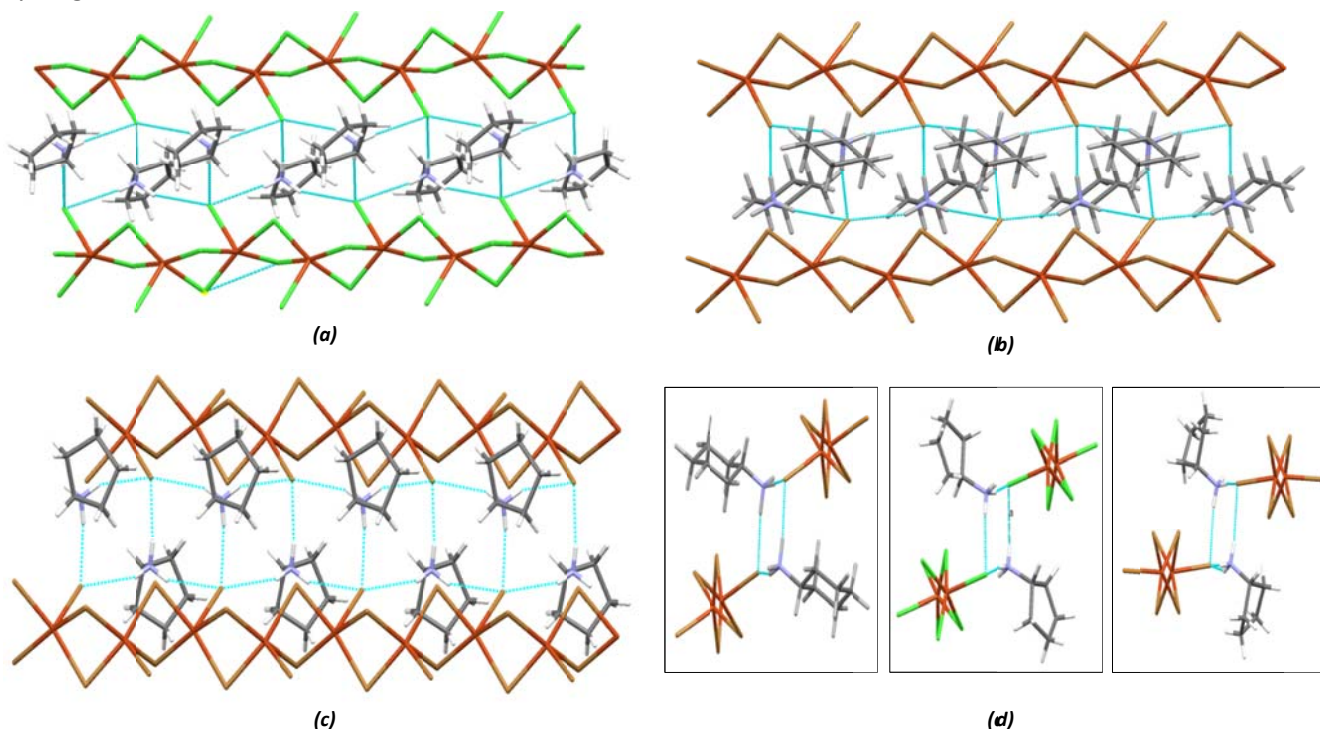


Figure 4.6.3. The hydrogen bonding network formed in (a) FAWDAI, (b) FUTBUR and (c) PENCuBr structures and (d) the side-view of the hydrogen bonding ladders in FAWDAI, FUTBUR and PENCuBr respectively.

Even though the structures display the same hydrogen-bonded ladders, they differ in how the polymeric anions are linked by cations to form the two-dimensional hydrogen-bonded sheets. In the **FAWDAI** structure, the polymers in the hydrogen-bonded sheets lie on the same plane and neighbouring hydrogen-bonded sheets pack in an interdigitated, close packing arrangement, as shown in Figure 4.6.4.

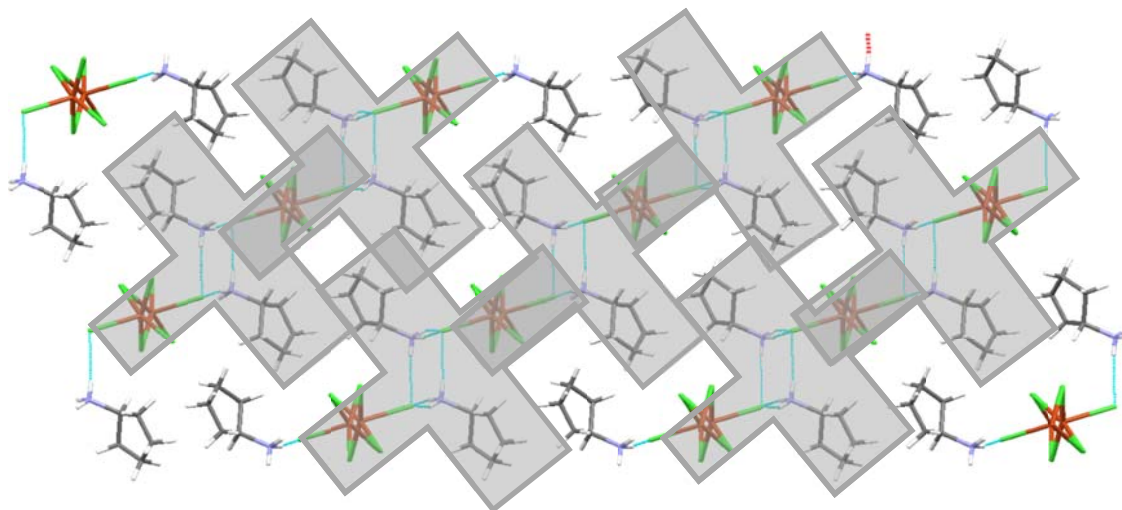


Figure 4.6.4. The arrangement of the hydrogen-bonded sheets, (grey highlight) and the orientation of the polymer units in the FAWDAI structure as viewed down the b-axis.

In the **FUTBUR** structure the polymers in the hydrogen-bonded sheets also lie in the plane and close packing by interdigitation of the cations, as shown in Figure 4.6.5.

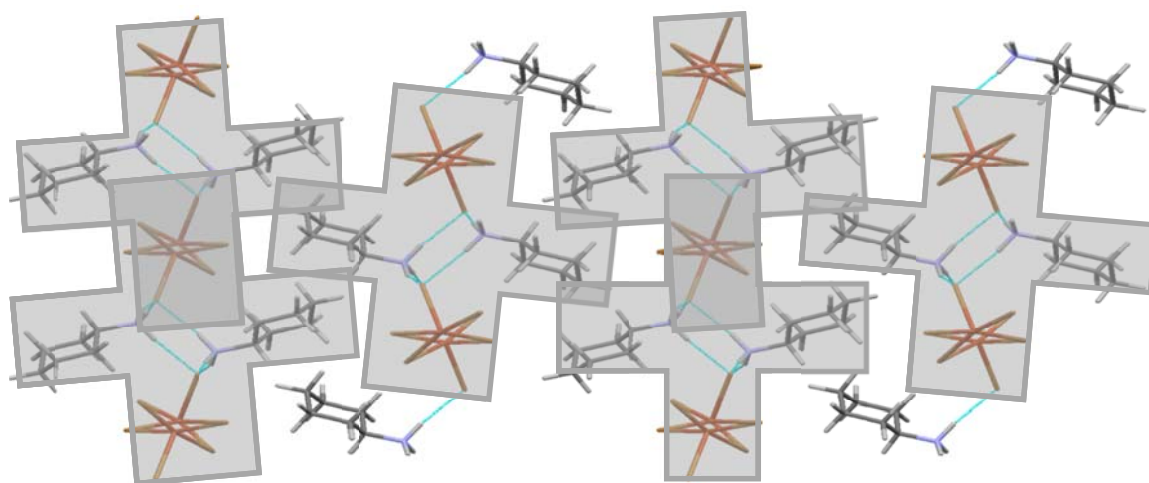


Figure 4.6.5. The arrangement of the hydrogen-bonded sheets (grey highlight) and the orientation of the polymer units in FUTBUR as viewed down the c-axis.

In the novel structure, **PENCuBr**, the polymers no longer lie in the same plane in the hydrogen-bonded sheet, instead they form a zig-zag arrangement when the sheet is viewed side-on and neighbouring sheets pack next to each other, as shown in Figure 4.6.6. Here the cations are no longer interdigitated.

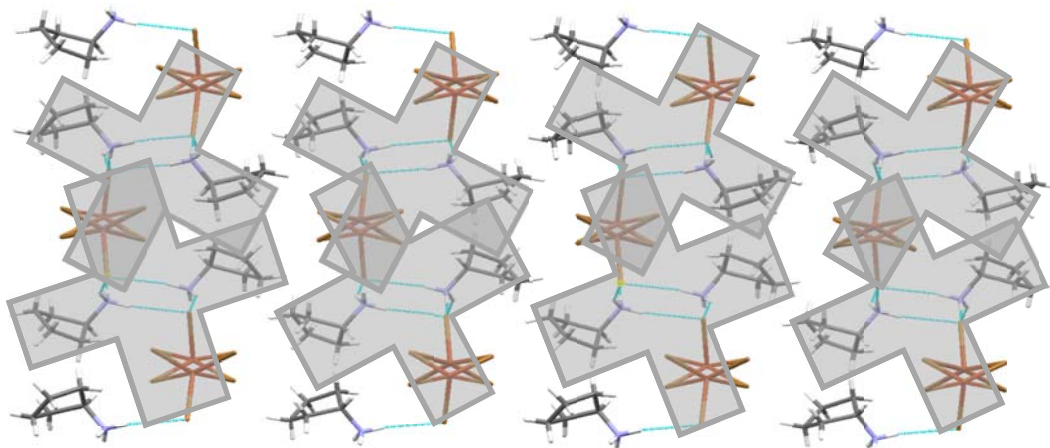


Figure 4.6.6. The arrangement of the hydrogen-bonded sheets (grey highlight) and the orientation of the polymer units in PENCuBr as viewed down the b-axis.

Because the magnetic properties of the compounds **FAWDAL** (Geiser *et al.* 1986), **BAPYUM** (Groenedijk *et al.* 1981) and **FUTBUR** (de Vries *et al.* 1987) have been reported in the literature and the magnetic properties of the novel **PENCuBr** have been determined in the current study, the magnetic behaviour of the compounds can be compared, with consideration of the structural aspects.

The **FAWDAL**, **BAPYUM** and **FUTBUR** structures were reported to be one-dimensional ferromagnets with additional magnetic interactions occurring at low temperatures. FM interactions between Cu^{2+} metal centres were expected for the three structures, as they all contain Cu-X-Cu bond angle less than 85° (Geiser *et al.* 1986). Strong FM intrachain interactions were reported for the three literature structures (de Vries *et al.* 1987 and Geiser *et al.* 1986), as well as very weak AFM exchange interactions occurring between the polymer chains at low temperature.

In these structures the strongest magnetic exchange pathway is expected to occur within the polymer, *via* through-bond Cu-X-Cu superexchange employing the two bridging, non-magnetic halogeno ligand orbitals, which overlap with the magnetic orbitals of the Cu^{2+} ions in the polymer chain. This pathway is assigned the exchange parameter, J_1 . Another possible, much weaker exchange pathway is a double-halide exchange pathway through close M-X...X-M contacts in the hydrogen-bonded sheet, with exchange parameter, J_2 . Lastly a double-halide exchange pathway may be present between polymers in neighbouring sheets, but again this exchange, denoted J_3 , is expected to be weak. The structural parameters, as well as the values of J_1 are listed in Table 4.3.

Table 4.3. The average intrachain structural parameters and exchange constants.

Compound	Space group	J_1 (K)	δ ($^\circ$)	Cu...Cu (\AA)	Cu...X _{ax} (\AA)	Cu-X _{ax} (\AA)	X _{ax} -Cu-X _{eq} ($^\circ$)	X _{eq} -Cu-X _{eq} ($^\circ$)	Cu-X _{eq} (\AA)	Cu-X-Cu ($^\circ$)
FAWDAL ^a (C ₅ CuCl)	<i>P2₁/n</i>	+45-+50	131.6	3.084	3.370	2.576	96.62(5)	85.49	2.302	84.12
BAPYUM ^a (C ₆ CuCl)	<i>P2₁2₁2₁</i>	+50	135.2	3.138	3.477	2.564	96.87(7)	85.38	2.307	85.62
FUTBUR ^b (C ₆ CuBr)	<i>P2₁2₁2₁</i>	+55	130.31	3.234	2.678	2.678	96.82(14)	86.34	2.443	82.88
PENCuBr (C ₅ CuBr)	<i>Pbca</i>	+96	130.31	3.254	2.676	2.676	98.17(10)	85.49	2.441	83.59

^a Geiser *et al.* 1986.

* CuBr containing structures are highlighted

^b de Vries. 1987.

In the cyclohexylammonium chlorido containing structure **BAPYUM**, an exchange parameter of +50 K was determined by heat capacity measurements indicating FM intrachain interactions, the magnetic ordering temperature (T_N) is 2.17 K, with weak AFM interactions occurring between sheets with exchange strength of -1.44×10^{-2} K.

For the bromido containing structure **FUTBUR**, a strong intrachain exchange parameters, J_1 , of +55 K was determined from heat capacity measurements indicating strong FM exchange interactions within the polymer chains. The magnetic exchange interactions occurring within sheets of polymers, J_2 , in the **FUTBUR** structure are weakly AFM.

In the **FAWDAL** structure, Geiser reported that the data in the temperature range of 4.2 K to 300 K was compared to the **BAPYUM** and **FAWDAL** data, yielding a J value of +45 to +50 K. A maximum was observed in the χT plot at approximately 2.8 K, which indicates AFM interactions between polymer chains at low temperature with an exchange of -3.00×10^{-2} K.

In the current study, the PENCuBr data was modelled as a one-dimensional FM chain with CW correction. Only the high temperature data was taken into account (50 K to 294 K) and a J_1 value of +192 K was obtained. This value has to be divided by two, to allow for the comparison with the literature values, since our model employs the single J Hamiltonian. Metamagnetic behaviour was exhibited by both perbromidocuprate(II) containing structures and this was evident in the low field region of the M vs T plot of both PENCuBr (Figure 3.2.5).

The two chlorido containing compounds in the family, **FAWDAl** and **BAPYUM**, both exhibit a value of +45 K for the exchange parameter J_1 , despite a difference of approximately 3° in their δ values. The rest of the geometrical parameters are similar, explaining the similarity in the exchange constant.

When the bromido analogues, **FUTBUR** and PENCuBr are considered, the exchange constants for the PENCuBr, $J_1 = +96$ K, structure is higher than that reported for the **FUTBUR** structure, with $J_1 = +55$ K. The main difference between the PENCuBr polymer chain and the other three chains are an increase in the $X_{\text{eq}}\text{-Cu-}X_{\text{ax}}$ angle, which is close to 98.2° in the PENCuBr structure, but averages 96.8° in others. The uncertainty in the value of J_1 for the PENCuBr compound as explained in Chapter Three, makes it difficult to say whether the difference in exchange parameters of the bromido containing compounds is due to this geometrical difference. It should be noted that the exchange parameters of **BAPYUM** and **FUTBUR** were obtained by heat capacity measurements (Kopinga *et al.* 1982) not by fitting the susceptibility data to a model. The exchange value for **FAWDAl** was obtained by comparing the susceptibility data of this compound with that of **BAPYUM** and **FUTBUR** (Geiser *et al.* 1986). In the paper by Geiser *et al.* (1986) it is mentioned that fitting of the high temperature data was not done due to the correlation between J_1 and other parameters that affect the magnitude of the high temperature data, which makes the values obtained *via* fitting very unreliable. The experimental data for the **BAPYUM**, **FUTBUR** and **FAWDAl** is not available from the literature. Hence a direct comparison of the values could not be done in this study. Suffice to say that the value of +96 K can be assumed to not be very accurate.

Table 4.4. The average interchain parameters of polymeric containing structures.

Compound	Space group	Cu...Cu (Å)	$X_{\text{ax}}\cdots X_{\text{ax}}$ (Å)	$X_{\text{eq}}\cdots X_{\text{eq}}$ (Å)	$X_{\text{ax}}\cdots X_{\text{eq}}$ (Å)	T_N (K)
FAWDAl ^a (C ₅ CuCl)	<i>P2₁/n</i>	8.284	4.936	7.036	4.406	2.78
BAPYUM ^a (C ₆ CuCl)	<i>P2₁2₁2₁</i>	8.549	4.935	7.042	5.066	2.17
FUTBUR ^b (C ₆ CuBr)	<i>P2₁2₁2₁</i>	8.678	5.055	7.247	4.977	1.50
PENCuBr (C ₅ CuBr)	<i>Pbca</i>	8.157	5.016	7.277	4.223	5.35

^a Geiser *et al.* 1986.

^b de Vries. 1987.

* CuBr containing structures are highlighted in grey

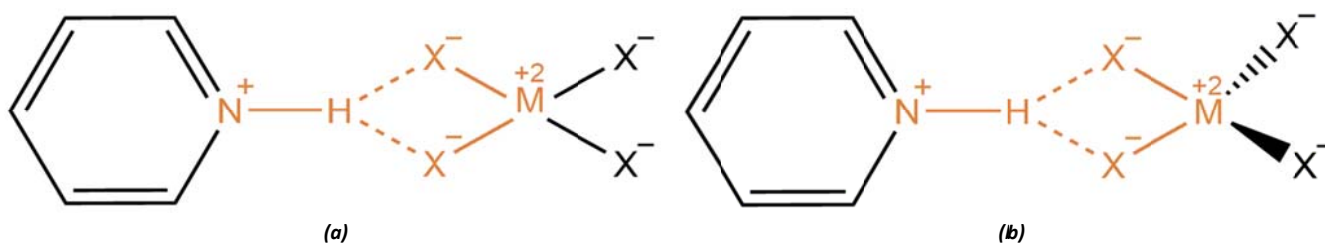
The AFM magnetic ordering temperature (T_N) for **FUTBUR** is 1.50 K and a higher ordering temperature of $T_N = 5.35$ K was obtained for the novel PENCuBr compound. AFM exchange (J_2) occurs in the sheet of anions *via* through-space halide-halide interactions, with the shortest interchain pathway between Cu- $X_{\text{ax}}\cdots X_{\text{eq}}$ -Cu contacts, at a distance of 4.223 Å for PENCuBr and 4.977 Å for **FUTBUR**. The shorter interchain distance between polymers in PENCuBr is responsible for the higher Néel temperature, T_N , of 5.35 K for PENCuBr. Thus, in the PENCuBr structure, the polymer anions are less isolated than the polymeric units in **FUTBUR**. This is due to an increase in ring size, as the cation, (C₆) present in **FUTBUR** is larger than the cation (C₅) of PENCuBr and therefore has more steric influence in the separation of the polymer units, as well as a difference in the way hydrogen-bonded ladders pack in the PENCuBr structure. As a result, the polymeric anions in the **FUTBUR** structure have longer interchain contacts than the polymeric units of PENCuBr, as listed in Table 4.4.

4.7. Crystal Engineering Synthons

Arnby *et al* (2004) commented on the difficulty of applying crystal engineering principles of the perhalocuprate systems due to the structural diversity of this system, as well as the fact that species in solution are not representative of species in the solid-state. In the current system, the subtle changes in cations allows for an investigation of the effect of these changes on the crystal engineering synthons in these compounds.

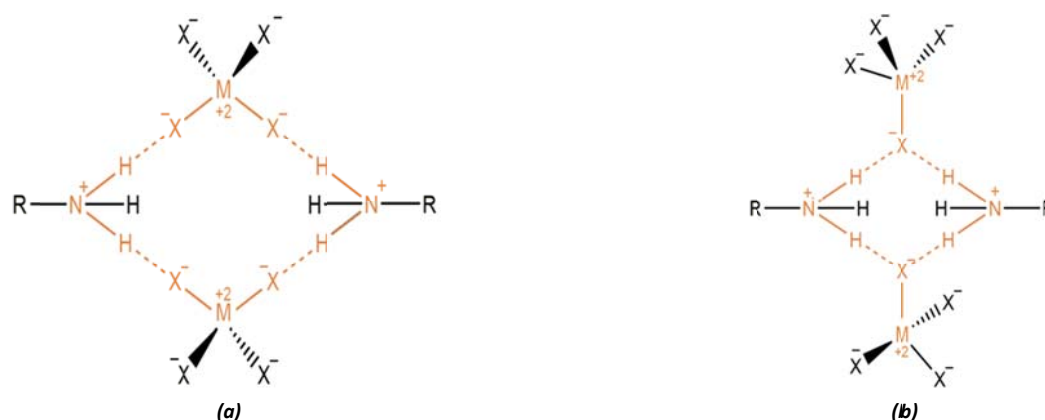
Crystal engineering synthons have been identified for hybrid materials containing isolated square planar (Gillon *et al.* 2000, Angeloni and Orpen. 2001) and tetrahedral (Luque *et al.* 2001) anions and primary or secondary organic cations for a range of metal ions and these are summarised below.

The secondary cation used in the study by Angeloni (2001) and Gillon (2000) revealed the formation of similar hydrogen-bonded motifs in structures containing both square planar or tetrahedral isolated anions. The bifurcated $^+N-H\cdots(Cl)_2-M$ hydrogen-bonded synthon, shown in Scheme 4.7.1 was reported for pyridinium type cations and square planar $PtCl_4^{2-}$ anions (Gillon *et al.* 2000), as well as tetrahedral $CuBr_4^{2-}$ anions (Angeloni *et al.* 2001), where one hydrogen atom present on the donor nitrogen atom forms hydrogen bonding interactions to two independent halogeno ligands that are part of a single square planar or tetrahedral anionic moiety.



Scheme 4.7.1. The schematic representation of the hydrogen bonding motif found in compounds containing secondary cations and (a) square pyramidal anions or (b) tetrahedral anionic units. (The hydrogen bonding synthons are coloured in orange).

Rademeyer *et al.* (2011) reported the synthons shown in Scheme 4.7.2 in structures containing primary ammonium cations and isolated, tetrahedral MX_4^{2-} anions, with $M = Zn^{2+}$, Cd^{2+} , Hg^{2+} and $X = Cl^-$, Br^- and I^- . Both types of synthons consist of two anions and two cations, but differ in the number of anion halogeno ligands that accept hydrogen bonds. In these synthons, two hydrogen atoms on each ammonium group may form classic, charge assisted hydrogen bonds to either four or two halogeno ligands on two different anions.



Scheme 4.7.2. The schematic representation of the two types of hydrogen bonding motifs present in primary cation containing compounds. (a) Type one and (b) type two. (The hydrogen bonding synthons are coloured in orange).

4.7.1. Zero-dimensional Systems (DABCO vs Piperizinium Cations)

In the current study the PIPCuCl/**BICPEK** structure allows for the study of the effect of additional hydrogen bonding capability compared to the DABCO containing structure, **AGAWIO**. Both structures contain isolated tetrahedral CuCl_4^{2-} anions.

In the DABCO containing structure, **AGAWIO**, a one-dimensional hydrogen-bonded ribbon is formed, as shown in Figure 4.7.1. In this ribbon, the hydrogen bonding capacity of the DABCO dication is satisfied through the formation of a bifurcated $^+\text{N-H}\cdots(\text{Cl})_2\text{-M}$ hydrogen bond (Brammer *et al.* 2002). This synthon corresponds to the synthon shown in Scheme 4.7.1 (b).

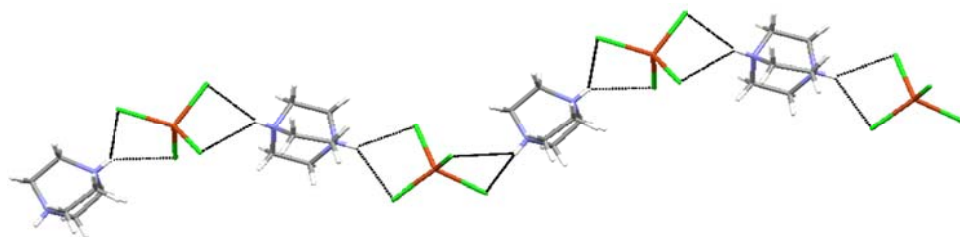


Figure 4.7.1. The bifurcated, one-dimensional hydrogen bonding capability of **AGAWIO**.

In the PIPCuCl/**BICPEK** structure a hydrogen-bonded ribbon, which contains the same synthon as observed in **AGAWIO** structure, is formed, as shown in Figure 4.7.2. However, an additional $^+\text{N-H}\cdots\text{Cl}$ hydrogen bond is formed by the second hydrogen atom on each nitrogen atom, as shown in Figure 4.7.3 (a)

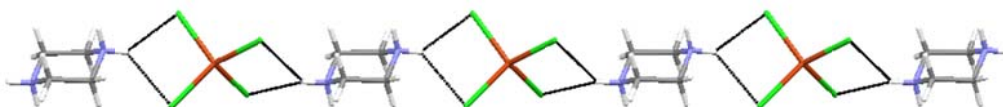


Figure 4.7.2. The hydrogen-bonded motif present in the **BICPEK** structure.

The piperizinium dication is thus able to form additional bifurcated hydrogen bonds perpendicular to the ribbon, to two individual anions, with each cation forming four $^+\text{N-H}\cdots(\text{Cl})_2\text{-M}$ synthons, each corresponding to the synthon shown in Scheme 4.7.1 (b), as shown in Figure 4.7.3 (a), while in the **AGAWIO** structure only two such synthons are formed per cation. Neighbouring one-dimensional ribbons are thus linked by alternating cations and anions to form two-dimensional hydrogen-bonded sheets, as shown in Figure 4.7.3 (b).

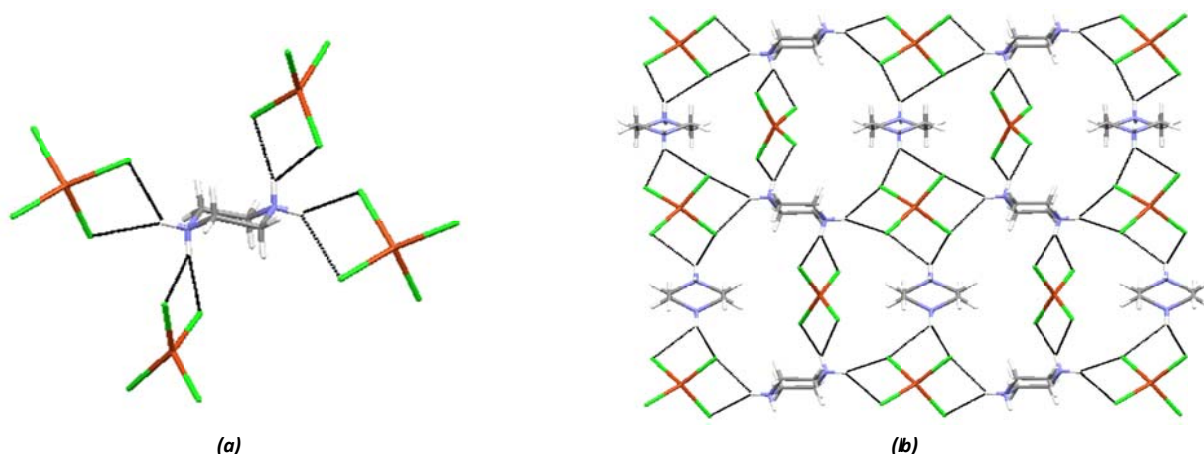


Figure 4.7.3. (a) The hydrogen-bonded motif of **BICPEK**. (b) The two-dimensional hydrogen bonding network of **BICPEK**.

Thus, the change from a tertiary dication to a secondary dication in going from the **AGAWIO** structure to the PIPCuCl/**BICPEK** structure introduces additional hydrogen bonding interactions, but the same synthon is formed, indicating the robustness of the bifurcated $^+\text{N-H}\cdots(\text{Cl})_2\text{-M}$ synthon.

4.7.2. One-dimensional Systems

As reported in section 4.6, the same hydrogen-bonded ladder is formed in the **FUTBUR**, **FAWDAL** and **PENCuBr** structures, as shown in Figure 4.7.4. The hydrogen bonding motif corresponds to the synthon shown in Scheme 4.7.3, which is in effect the same synthon as shown in Scheme 4.7.2 (b) except that the acceptor halogeno ligands are no longer part of the isolated anions but form part of the polymers. In each structure the repeated motif consists of two cations hydrogen-bonded to two terminal halogeno ligands in two different polymers *via* four hydrogen bonds, as shown in Figure 4.7.4. This motif is repeated along the length of the polymer. Neighbouring hydrogen-bonded polymers are connected *via* $^+\text{N-H}\cdots\text{Br-M}$ hydrogen bonds to form hydrogen-bonded sheets.

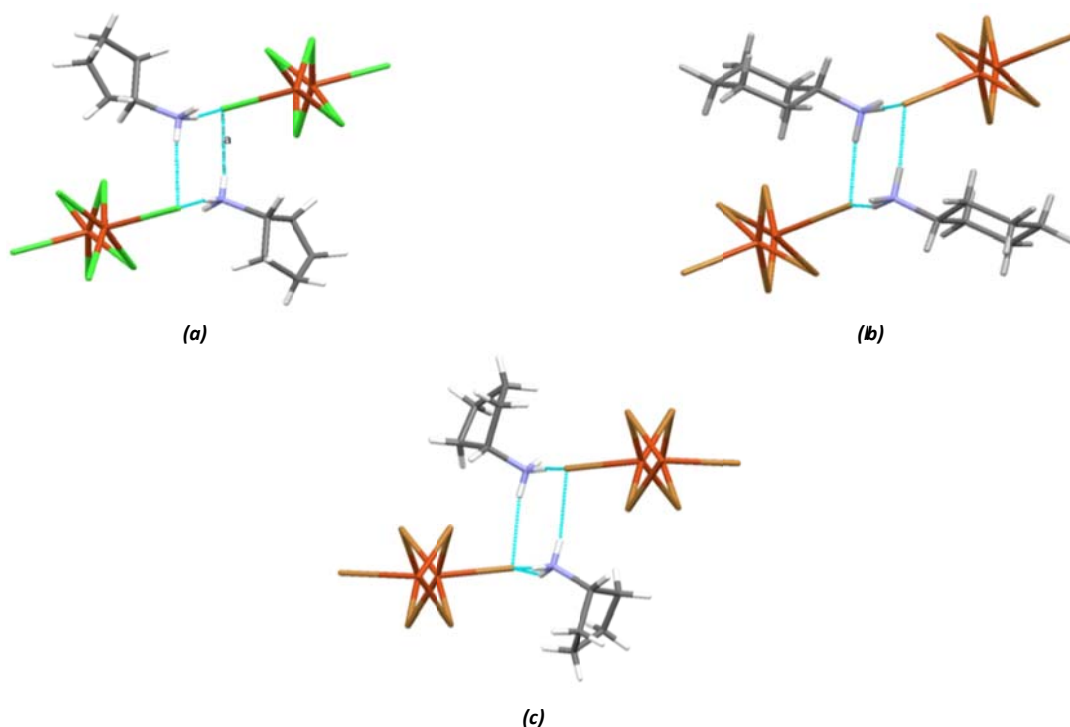
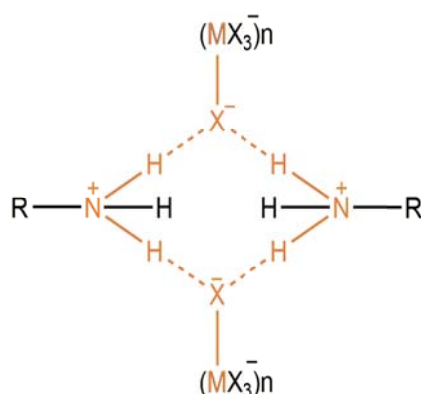


Figure 4.7.4. The hydrogen-bonded motifs in (a) FAWDAI, (b) FUTBUR and (c) PENCuBr.

The fact that this motif, which has been reported previously for hybrid structures containing isolated tetrahedral anions and 2-phenylethylammonium cations (Rademeyer *et al.* 2011), is also present in the current three structure types, containing very different anions, indicates the robustness of this motif.



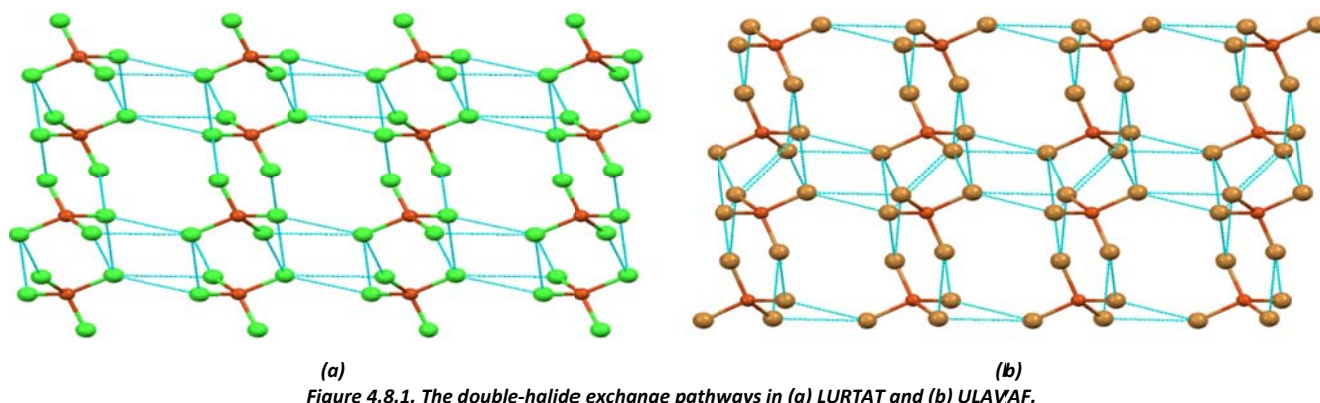
Scheme 4.7.3. The schematic representation of the hydrogen-bonded motif that forms between anions and cations.

4.8. Diversity and Trends in Magnetic Behaviour

The structural diversity observed in the perhalocuprate(II) hybrids of interest is also reflected in the range of magnetic characteristics observed for these compounds. Since the metal ions, as well as the halogeno ligands

providing magnetic exchange pathways, are contained in the perhalocuprate(II) anions, the structural characteristics of the anions significantly affect the magnetic properties. In the materials of interest, the anions include isolated tetrahedral perhalocuprate(II) anions (**LURTAT** and **ULAVAF**), trigonal bipyramidal perhalocuprate(II) anions (**TOZFAP**), polymeric perhalocuprate(II) anions (**FAWDAI**, **FUTBUR**, **BAPYUM** and **PENCuBr**), cluster type anions (**HEPCuCl** and **HEPCuBr**) and perovskite layer type anions (**YATYUP** and **PENCuCl**). Due to the difficulty of obtaining large enough samples of adequate purity, not all the compounds could be characterised magnetically. The following section highlights the trends in magnetic behaviour, as well as magnetostructural relationships, observed in the compounds for which magnetic data were collected, or reported in the literature.

A number of structures were found to contain isolated tetrachloridocuprate(II) or tetrabromidocuprate(II) anions, with the anions typically displaying a distorted tetrahedral geometry. Even though the double-halide exchange pathway between these anions is expected to result in AFM exchange, FM behaviour was observed for the **ULAVAF** compound (Figure 4.8.1 (b)). This result is of interest since only two other examples have been reported in the literature (Turnbull *et al.* 2005). Unfortunately, due to the unavailability of three-dimensional quantum mechanical models, the magnetic data for the **ULAVAF** compound could not be fitted to a model and the strength of the exchange could not be determined. Due to the unexpected and interesting FM behaviour of the **ULAVAF** compound, there was significant interest in the experimental study of the magnetic behaviour of the isostructural chlorido analogue, **LURTAT**, (Figure 4.8.1 (a)). Unfortunately, all attempts to obtain a pure sample of **LURTAT** were unsuccessful, as all the samples were found to contain the anhydrous phase, **AGAWIO**, in addition to **LURTAT**. Hence the magnetic behaviour of **LURTAT** could not be studied experimentally. Based on the results obtained for the **ULAVAF** compound, it can be proposed that the magnetic exchange in the isostructural chlorido analogue, **LURTAT**, would also be FM, however, the exchange is expected to be weaker due to the exchange pathway involving chlorido ligands, which result in less overlap of magnetic orbitals. The exchange pathways in **LURTAT** and **ULAVAF** are shown in Figure 4.8.1.



The **PIPCuCl/BICPEK** compound, which contains isolated tetrahedral tetrachloridocuprate(II) anions, shows AFM exchange. However, since the exchange pathway is three-dimensional, the magnetic data could not be fitted to a model to obtain the value of the exchange constant(s).

The **PENCuBr** structure, which contains a bi-bridged perbromidocuprate(II) polymeric chain, exhibits FM ordering *via* superexchange in the polymeric chain, with a J_1 value of approximately +96 K. Weak AFM interactions are present between FM chains and occur through a double-halide exchange mechanism. The behaviour agrees with what was reported for the related structures **FAWDAI** and **FUTBUR**.

AFM behaviour was found for both the **HEPCuCl** and **HEPCuBr** compounds, however due to problems experienced with both the samples more detailed information on the exchange parameters could not be obtained.

AFM exchange occurs between the trigonal bipyramidal $\text{Cu}(\text{H}_2\text{O})_2\text{Cl}_3^-$ anions in the **TOZFAP** structure, as shown in Figure 4.8.2, which is unique in that it is the only structure in the CSD containing this anion. Consideration of the close $\text{M}-\text{Cl} \cdots \text{Cl}-\text{M}$ contacts in the structure revealed the existence of a one-dimensional double-halide exchange pathway. The magnetic susceptibility data were fitted to an $S = \frac{1}{2}$ uniform chain model with a Curie-Weiss correction and an exchange parameter, $J = -3.05$ K and a Curie-Weiss constant of $+0.68$ were obtained.

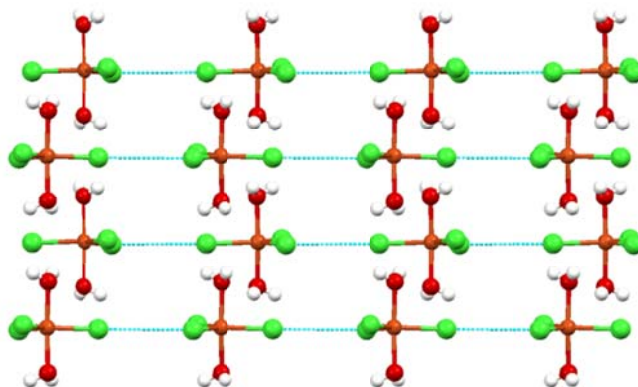


Figure 4.8.2. The double-halide exchange pathways in the TOZFAP structure.

4.9. References

- Angeloni, A. and Orpen, A.G. (2001). *Chem. Commun.*, 343-344.
- Arnby, C.H., Jagner, S. and Dance, I. (2004). *CrystEngComm*. 6 (46), 257-275.
- Brammer, L., Swearingen, J.K., Bruton, E.A. and Sherwood, P. (2002). *PNAS*. 99. 8, 4956-4961.
- Czugler, M., Kotai, L., Sreedhar, B., Rockenbauer, A., Gacs, I. and Holly, S. (2002). *Eur. J. Inorg. Chem.*, 3298-3304.
- de Vries, G.C., Helmholtz, R.B., Frikkee, E., Kopinga, K., de Jonge, W.J.M. and Godefroi, E.F. (1987). *J. Phys. Chem. Solids*. 48, 803-811.
- Emmerson, K. and Drumheller, J.E. (1980). *ACA, Ser. 2*. 8, 24 a.
- Geiser, U., Gaura, R.M., Willet, R.D. and West, D.X. (1986). *Inorg. Chem.* 25, 4203-4212.
- Gillon, A.L., Lewis, G.R., Orpen, A.G., Rotter, S., Starbuck, J., Wang, X-M., Rodriguez-Martin, Y. and Ruiz-Perez, C. (2000). *J. Chem. Soc. Dalton. Trans*, 3897-3905.
- Groenendijk, H.A., Blote, H.W.J., van Duynveldt, A.J., Gaura, R.M., Landee, C.P. and Willett, R.D. (1981). *Physica, Pays-Bas*. 106, 47-58.
- Han, M.T. (2012). *Acta Cryst. Sect E: Struct. Rep. Online*. 68, m448.
- Janiak, C. (2000). *J. Chem. Soc. Dalton. Trans*, 3885-3896.
- Kenneth, E.L., Atta, M.A. and Gladysz, J.A. (1990). *Inorg. Chem.* 29, 2887-2888.
- Kopinga, K., Tinus, A. M. C. and de Jonge, W. J. M. (1982). *Phys. Rev. B*. 25, 7, 4685-4690.
- Larson, K.P. (1974). *Acta. Chem. Scand.* A28, 194-200.

- Luque, A., Sertucha, J., Castillo, O. and Roman, P. (2001). *New J. Chem.* 25, 1208-1214.
- Macrae, C. F., Edgington, P. R., McCabe, P., Pidcock, E., Shields, G. P., Taylor, R., Towler, M. and van de Streek, J. (2006). *J. Appl. Cryst.* 39, 453-457.
- McCrone, W.C. (1965). *Physics and Chemistry of the Organic Solid State*, eds. D. Fox, M. M. Labes and A. Weissberger, Interscience Publishers, London. 2, 725-767.
- Mitzi, D.B. (2001). *J. Chem. Soc. Dalton Trans*, 1-12.
- Patyal, B.R., Scott, B.L. and Willett, R.D. (1990). *Phys. Rev. B.* 41, 1657-1663.
- Rademeyer, M., Overbreek, G.E. and Liles, D. (2010). *Acta Cryst.* E66, m1634.
- Rademeyer, M., Tsouris, C., Billing, D. G., Lemmerer, A. and Charmant, J. (2011). *CrystEngCom.* 13, 3485-3497.
- Riley, M.J., Neill, D., Berhardt, P.V., Byriel, K.A. and Kennard, C.H.L. (1998). *Inorg. Chem.* 37, 3635-3639.
- Tuikka, M., Kersen, U. and Haukka, M. (2013). *CrystEngComm.* 15, 6177-6183.
- Turnbull, M.M. et al. (2005). *Coord. Chem. Rev.* 249, 2567-2576.
- Wei, M. and Willett, R.D. (1996). *Inorg. Chem.* 35, 6381-6385.
- Willett, R.D. (2004). *Inorg. Chem.* 43, 3804-3811.
- Zhang, Y. and Wang, B. (2011). *Acta. Cryst. Sect E: Struct. Rep. Online.* 67, m371.

Chapter Five: Conclusion and Future Work

5.1. Conclusion

Ionic hybrid materials containing amine-based cations and perhalocuprate(II) anions are of interest due to the tendency of these materials to combine the properties of the organic and inorganic components in the same materials. Of specific interest in the Cu^{2+} containing hybrid is the magnetic properties imparted to the material due to the unpaired electron on the metal ion. The structural diversity displayed by the perhalocuprate(II) anions make the magnetic properties of these compounds even more interesting, but also more challenging. Before the ultimate aim of designing these hybrid materials with specific magnetic properties can be achieved, the effect of the crystal structure on the magnetic properties needs to be fundamentally understood.

In the current study a range of saturated cycloalkylammonium cations were chosen with perhalocuprate(II) anions. The cations systematically increase in size and include monocations of primary and dications of secondary and tertiary amines. Compounds from the matrix were synthesised and characterised structurally and magnetically and an important observation is that the same cation can crystallise with different perhalocuprate(II) anions consisting of the same metal and halogeno ligand, under different experimental conditions. In addition, a wide range of anions were found. An interesting cluster-type anion was obtained for the HEPCuCl and HEPCuBr structures in this study. This type of anion has never been reported before in the literature for any compound.

It was found that the hybrid materials typically form layered structures consisting of exclusively organic or inorganic layers, with the HEPCuCl and HEPCuBr structures the only exceptions. Organic bilayers are typically formed in structures containing monocations, while structures containing dications exhibit single organic layers. Strong, charge assisted $^+\text{N-H}\cdots\text{X-M}$ hydrogen bonds link cations to perhalocuprate(II) anions.

In the cycloheptylammonium-containing family HEPCuCl and HEPCuBr structures, as well as the perhalocuprate(II) polymer containing family **FUTBUR**, **FAWDAL**, **BAPYUM** and PENCuBr, the structural differences are ascribed to a different way of packing the hydrogen-bonded sub-units in the structures.

Crystal engineering synthons could be identified for a number of compounds in this series. These synthons were found to display similarities to synthons reported previously in the literature for related compounds, indicating the robustness and usefulness of the synthons.

Due to the diverse structural properties exhibited by the amine containing perhalocuprate(II) compounds in this study, the same can be concluded for the magnetic characteristics of these hybrid materials. The ability to predict the outcome of the magnetic behaviour of these compounds is not possible, due to unpredictable magnetic behaviour exhibited by these compounds. The diverse magnetic characteristic is seen over the range of compounds selected in this study for magnetic characterisation, such as the mixed magnetic behaviour of AFM and FM observed in the polymeric PENCuCl structure to the weak AFM exchange existing in the isolated anionic containing **TOZFAP02** structure.

5.2. Future Work

The structural diversity, as well as the magnetic properties exhibited by the perhalocuprate(II) hybrid compounds under investigation are clearly determined by the type of perhalocuprate(II) anion present in the structure, which illustrates the need for the ability to control the specific anion formed, as well as the dimensionality of the structure. This aspect was not part of the current investigation, but before the ultimate goal of designing perhalocuprate(II) hybrid materials with specific magnetic properties can be achieved, more studies on the factors determining the type of anion obtained are required.

Crystals could not be obtained for certain combinations of cations and perhalocuprate(II) anions and alternative synthetic strategies can be explored to complete the series of structures. In addition, alternative synthetic techniques may also prove useful in obtaining samples of high purity required for the magnetic characterisation of the materials for which this component is still outstanding.

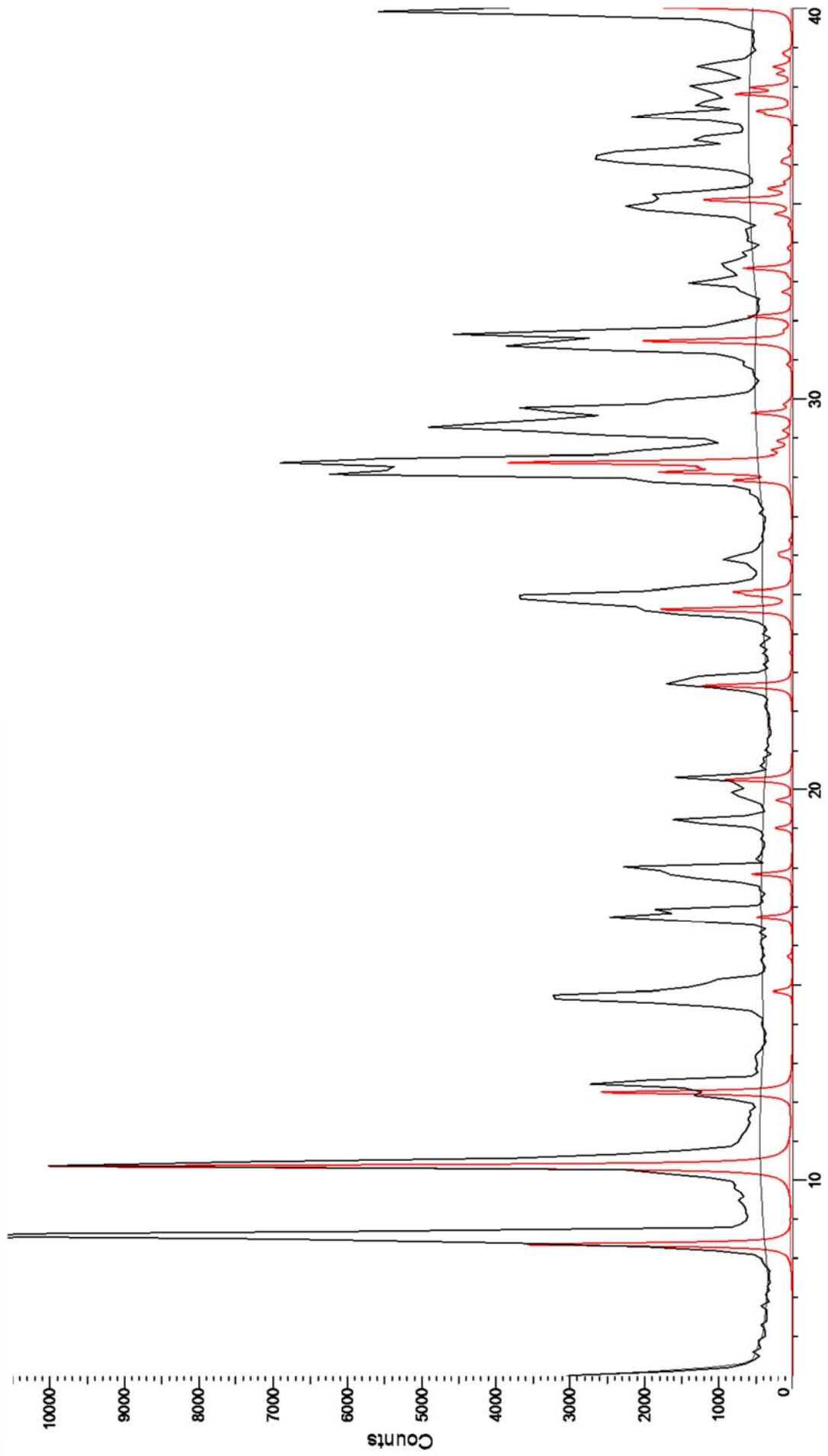
Since the current study focussed on the ionic materials obtained through the combination of the saturated amine cations and perhalocuprate anions, the coordination compounds have not been investigated in detail and this can form the focus of a future study.

When three-dimensional quantum mechanical models become available, the magnetic data obtained for the **ULAVAF** as well as the PIPCuCl/**BICPEK** structures can be modelled. This will also allow for a better understanding of the factors leading to the interesting ferromagnetic exchange observed in the **ULAVAF** compound.

Appendix One

In this appendix, the experimental and calculated powder patterns of the compounds for which magnetic characterisation was carried out are compared, to confirm the purity of the powder samples. The powder patterns of the PENCuBr, PIPCuCl/**BICPEK**, **TOZFAPO3** and **ULAVAF** compounds are shown in Figures 1 to 4.

Commander Sample ID (Coupled TwoTheta/Theta)



2Theta (Coupled TwoTheta/Theta) WL=1.54056

Figure 1. The experimental and calculated powder patterns of PENCuBr.

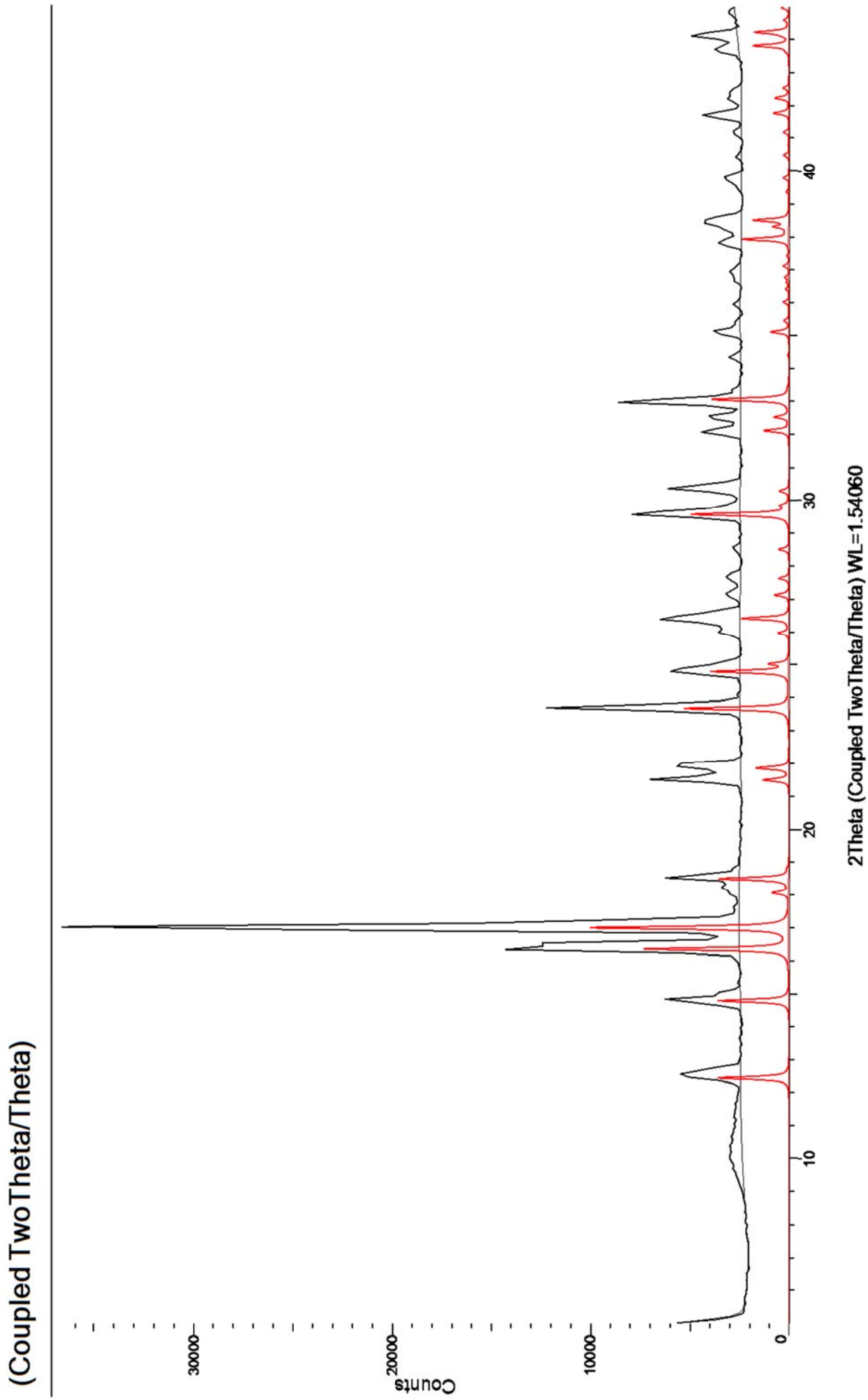
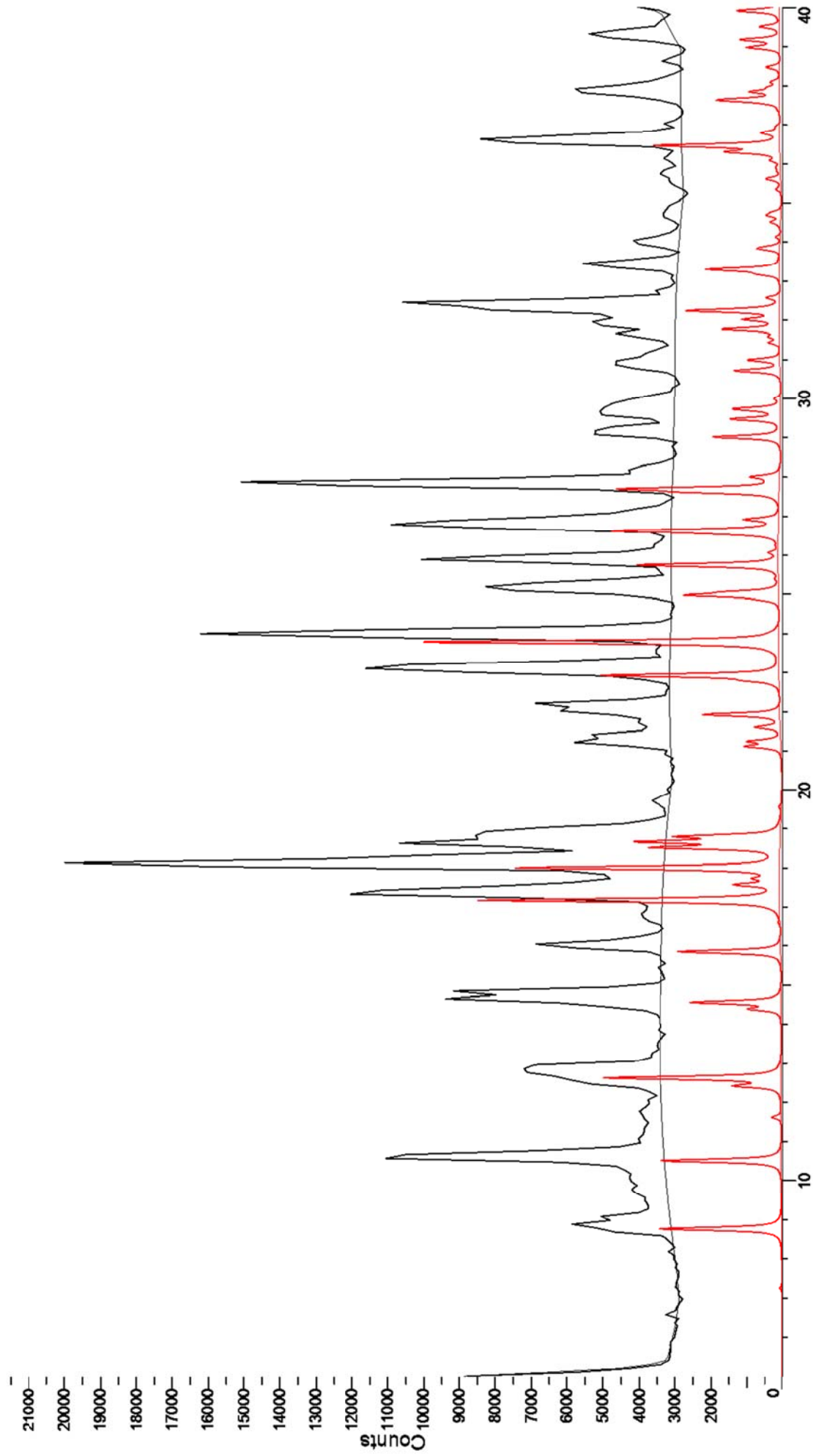


Figure 2. The experimental and calculated powder patterns of PIPCuCl/BICPEK.

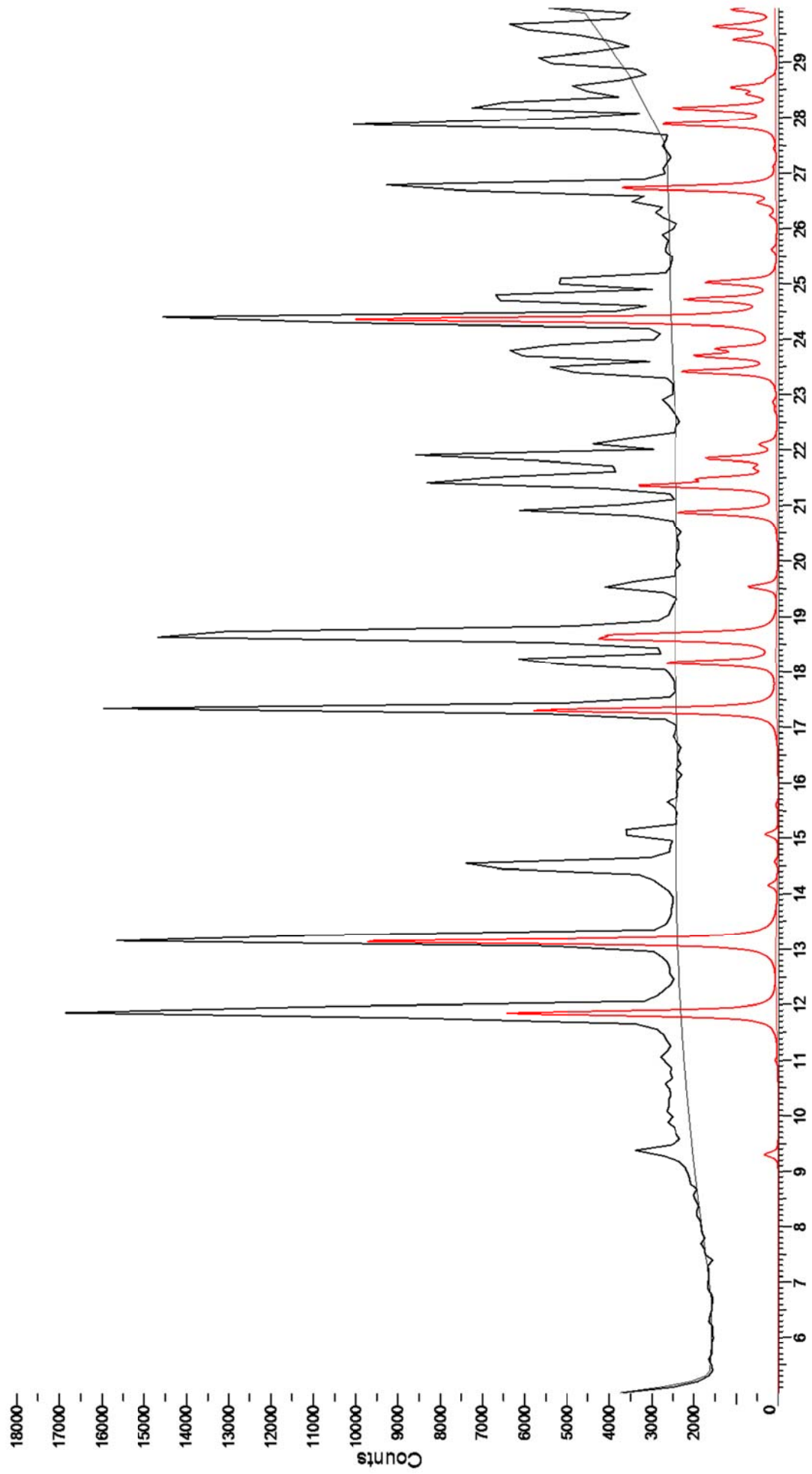
(Coupled TwoTheta/Theta)



2Theta (Coupled TwoTheta/Theta) WL=1.54060

Figure 3. The experimental and calculated powder patterns of TOZFAP03.

(Coupled TwoTheta/Theta)



2Theta (Coupled TwoTheta/Theta) WL=1.54060

Figure 4. The experimental and calculated powder patterns of ULAVAF.

Appendix Two

Crystallographic information files (cif), as well as cif check reports for all the novel structures determined in the study are included on the attached compact disc.